Activation Mechanisms of RIG-I

Dissertation

zur

Erlangung des Doktorgrades (Dr. rer. nat.)

der

Mathematisch-Naturwissenschaftlichen Fakultät

der

Rheinischen Friedrich-Wilhelms-Universität Bonn

vorgelegt von

Ann Kristin de Regt, geb. Bruder

aus Schwäbisch Hall

Bonn, 2019

Angefertigt mit Genehmigung der Mathematisch-Naturwissenschaftlichen Fakultät der Rheinischen Friedrich-Wilhelms-Universität Bonn.

Gutachter: Prof. Dr. rer. nat. Martin Schlee
 Gutachter: Prof. Dr. rer. nat. Sven Burgdorf

Tag der Promotion: 23.01.2020

Erscheinungsjahr: 2020

Table of content

1.	Sum	mary	/	. 1
2.	Zusa	mm	enfassung	. 3
3.	Intro	duc	tion	. 5
3.1.	The	inna	ite immune system	. 5
3.2.	PRF	₹s		. 6
3.3.	The	RIG-	-I like receptors	. 8
3.4.	RIG	i-I sig	naling pathways	. 9
3.5.	RIG	i-I liga	ands	11
3	.5.1.	Opti	mal RIG-I ligand	12
3	.5.2.	Subc	ptimal RIG-I ligands	12
3	.5.3.	Viral	ligands	14
	3.5.3	.1.	dsRNA viruses/(+)ssRNA viruses	14
	3.5.3	.2.	(-)ssRNA viruses	15
3.6.	Vira	al esc	ape strategies	16
3.7.	RIG	i-l str	ucture	18
3.8.	Enc	loger	nous RNA	20
3	.8.1.	mRN	As	21
3	.8.2.	rRNA	Ns	22
3	.8.3.	tRNA	Ns	23
3	.8.4.	mtRI	NAs	23
3.9.	RN	A-ser	sing receptors with direct antiviral activity	24
3.10). Ain	n of t	he study	26
4.	Mate	erial	and methods	27
4.1.	Ma	teria		27
4	.1.1.	Oligo	onucleotides	33
4	.1.2.	Plasr	nids	34
4	.1.3.	Buffe	ers and solutions	35
	4.1.3	.1.	General buffers	35
	4.1.3	.2.	Western Blot buffers	36
	4.1.3	.3.	ELISA buffers	36
	4.1.3	.4.	Acrylamide gels	37
4.2.	Me	thod	S	37
4	.2.1.	Mole	ecular biology	37
	4.2.1	.1.	Production of chemocompetent bacteria	37
	4.2.1	.2.	Plasmid DNA purification	38

4.2.1	1.3.	Polymerase chain reaction (PCR)	39
4.2.2.	Clor	ing	40
4.2.2	2.1.	Preparation of the vector backbone	40
4.2.2	2.2.	Preparation of the insert	40
4.2.2	2.3.	Assembly of the backbone and the insert	40
4.2.2	2.4.	Transformation of chemocompetent bacteria	41
4.2.3.	Nuc	leic acid preparation	41
4.2.3	3.1.	RNA extraction using spin columns	41
4.2.3	3.2.	RNA extraction using TRIzol reagent	41
4.2.3	3.3.	RNA extraction from polyacrylamide gels	42
4.2.3	3.4.	polyA RNA extraction	42
4.2.3	3.5.	rRNA extraction	42
4.2.3	3.6.	cDNA synthesis	43
4.2.3	3.7.	Quantitative polymerase chain reaction (qPCR)	43
4.2.3	3.8.	IVT	44
4.2.3	3.9.	Enzyme treatment	45
4.2.3	3.10.	Annealing of two single-stranded nucleic acids	46
4.2.4.	Poly	acrylamide gel electrophoresis (PAGE) of nucleic acids	46
4.2.5.	Prot	ein based assays	46
4.2.5	5.1.	Enzyme-linked immunosorbent assay (ELISA)	46
4.2.5	5.2.	Cell based measurement of cytokines	47
4.2.5	5.3.	Sodium dodecyl sulfate (SDS)-PAGE and Western Blot	47
4.2.5	5.4.	Electrophoretic mobility shift assay (EMSA)	48
4.2.6.	Cell	culture	48
4.2.6	6.1.	Splitting of cells	48
4.2.6	6.2.	Freezing of cells	49
4.2.6	6.3.	Cell seeding	49
4.2.6	6.4.	Isolation of peripheral blood mononuclear cells (PBMCs)	50
4.2.6	6.5.	Transfection and stimulation of cells	50
4.2.6	6.6.	siRNA knockdown	50
4.2.6	6.7.	KO generation using CRISPR-Cas9	50
4.2.6	6.8.	MTT Assay	51
4.2.6	6.9.	Luciferase Dual Assay	52
4.2.6	6.10.	Transient protein overexpression	52
4.2.6	6.11.	Generation of stable Flp-In [™] Expression Cell Lines	52
4.2.6	6.12.	Generation of mtDNA depleted cells	53
4.2.7.	Viro	logical methods	53
4.2.7	7.1.	Viral infection	53
4.2.7	7.2.	Plaque assay	53

4	.2.8.	Soft	ware	53
4	.2.9.	Stat	istical Analysis	54
5.	Res	sults .		55
5.1.	N:	1-2′0-	methylation mediates immunotolerance towards endogenous RNA	55
5	.1.1.	CM	TR1 knockdown induces RIG-I-dependent immune stimulation	56
5	.1.2.	YFV	escapes RIG-I recognition by N1-methylation of viral RNA	57
5.2.	Im	npact	of RNA modifications on RIG-I activation	58
5	.2.1.	Cha	racterization of RIG-I activation by 3p-dsRNA and OH-dsRNA	59
5	.2.2.	RIG-	l activation by 3p- and OH-dsRNA with overhangs	60
5	.2.3.	Min	imal RNA length for RIG-I activation	61
5	.2.4.	Vira	l recognition by RIG-I CTD mutants	62
5	.2.5.	RNA	RIG-I recognition does not occur end-independently	64
5.3.	5′	p med	diates immunotolerance towards endogenous RNA	66
5	.3.1.	5′p	inhibits RIG-I-dependent immune stimulation	66
5	.3.2.	5′p	prevents RIG-I CTD binding	69
5	.3.3.	Ider	tification of a conserved amino acid in the RIG-I CTD that mediates tolerances to p-dsRNA	
	5.3	.3.1.	Mutation of I875 restores RIG-I activation by p-dsRNA	
		.3.2.	Mutation of I875 restores binding to p-dsRNA	
	.3.4.		g-term expression of RIG-I 1875A leads to immune stimulation	
5	.3.5.		tification of endogenous ligands activating RIG-I I875A	
		.5.1.	Immune stimulation with whole cell RNA extracts	
		.5.2.	Investigation of tRNA and rRNA as possible I875A activators	
		.5.3.	polyA RNA is the activating RNA species in the whole cell RNA extracts	
		.5.4.	mtRNA is the stimulating species for I875A	
5.4.			ivation by long RNAs inhibits the RIG-I mediated antiviral response	
5.5.	Cł	naract	erization of a highly potent RIG-I ligand	91
6.	Dis	cussi	on	94
6.1.	CI	MTR1	is indispensable to prevent RIG-I-dependent activation by endogenous RNA	94
6.2.	YF	V use	s RNA N1-2´O-methylation to avoid RIG-I recognition	96
6.3.	In	teract	ion of the RIG-I CTD with non-optimal ligands	97
6.4.	RI	G-I lig	ands during viral infection	100
6.5.	RI	G-I is	not activated by RNA in a 5´end independent mechanism	102
6.6.	5′	p ren	ders dsRNA non-immunogenic via steric exclusion by the I875 side chain	104
6.7.	Er	ndoge	nous RNA ligands activate RIG-I 1875A	108
6.8.	Pk	<r act<="" td=""><td>ivation by long RNAs inhibits RIG-I-dependent immune activation</td><td> 113</td></r>	ivation by long RNAs inhibits RIG-I-dependent immune activation	113
6.9.			erization of a new potent RIG-I ligand	
7.			ces	
		C. C.II		

8.	Appendix	131
8.1.	RNA Oligonucleotides	131
8.2.	List of Figures	133
8.3.	List of Tables	134
8.4.	Abbreviations	136
9.	Acknowledgments	140

1. Summary

Reliable and rapid elimination of viral infections is essential for all living organisms. RIG-I is a ubiquitously expressed innate immune receptor that is crucial for the detection of most RNA viruses. Upon binding of double-stranded (ds) RNA, RIG-I triggers an interferon (IFN) dominated antiviral immune response. Located in the cytoplasm, RIG-I is faced with the challenge of efficiently recognizing viral RNA without being activated by an excess of endogenous RNA. This thesis identified and investigated molecular interactions of the RIG-I C-terminal domain (CTD) with 5'end RNA modifications that render endogenous RNA non-immunogenic. Furthermore, immune activation by suboptimal, long and viral RNA ligands were studied to gain insights into RIG-I activation mechanisms.

The optimal RIG-I ligand is 5'triphosphorylated, blunt-ended dsRNA. Previously it was identified that RNA N1-2'O-methylation abrogates RIG-I activation. Indeed, this thesis showed that knockdown of endogenous cap-specific mRNA nucleoside-2'-Omethyltransferase 1 (CMTR1), which represses RNA N1-2'O-methylation, causes RIG-I activation. Furthermore, it was demonstrated that the (+)ssRNA yellow fever virus (YFV) exploits this mechanism to escape RIG-I recognition. Another mechanism of 5'end RNA modification mediated suppression of RIG-I activation could be resolved: while OH-dsRNA binds and activates RIG-I substantially, 5'monophosphorylation (p) nearly abrogates binding and immunostimulation. A highly conserved amino acid (1875) in the CTD of RIG-I was identified that blocks p-dsRNA binding by sterical exclusion. Mutation of 1875 to A restored RIG-I binding and activation by p-dsRNA to a similar level as OH-dsRNA. Long-term expression of RIG-I 1875A induced an IFN response, indicating that endogenous RNA species could activate RIG-I if it was not able to differentiate between OH- and p-dsRNA. Polyadenylated (polyA) RNA, and in particular mitochondrial (mt) RNA, was identified to be the main RIG-I 1875A stimulating RNA species.

A system of RIG-I CTD mutants with different ligand specificities was developed to determine essential RIG-I ligand modifications and structures responsible for virus detection. It was found that 5'3p independent RIG-I activation did not play a role during the infection with a panel of tested viruses (Indiana vesiculovirus (VSV), Sendai virus (SeV), influenza A virus (IAV), Herpes simplex virus (HSV)). In addition, using this system, 5'end-independent recognition of long dsRNA by RIG-I, that has been proposed previously, could be rebutted. By testing dsRNAs with different lengths, it was confirmed that long dsRNAs induce more IFN-β and

Summary

CXCL10 than short RNAs at low concentrations. However, at higher concentrations long dsRNAs also activated the translation repressor protein kinase R (PKR), which inhibited RIG-I induced IFN production. This RIG-I/PKR competition based biphasic antiviral response limits RIG-I ligand enhancement by dsRNA length extension. Here, an improved highly potent ligand system was developed that circumvents PKR activation.

This thesis discovered fundamental and within vertebrates highly conserved RNA modification-based mechanisms of immunotolerance towards potential endogenous RIG-I ligands. It therefore highlights the fine tuned balance between RIG-I sensitivity and selectivity for pathogenic RNA: Obviously, vertebrate organisms are not able to completely avoid the occurrence of endogenous RNA structures with short base-paired stretches leading to the requirement of additional immune regulatory RNA modifications.

The impairment of the RIG-I signaling pathway by PKR at high concentrations of long dsRNA indicates alternative and competing antiviral responses depending on the progression of an infection. Competing pathways have to be considered and, as shown in this thesis, can be avoided when designing synthetic RIG-I ligands for immune therapeutic applications.

2. Zusammenfassung

Die zuverlässige und schnelle Elimination einer Virusinfektion ist für jeden Organismus lebenswichtig. RIG-I ist ein ubiquitär exprimierter Rezeptor der angeborenen Immunantwort, der für die Erkennung der meisten RNA Viren essenziell ist. Die Bindung von Doppelstrang (ds) RNA an RIG-I induziert eine Interferon (IFN) dominierte antivirale Immunantwort. Da RIG-I überwiegend im Zytoplasma lokalisiert ist, muss es die Aufgabe bewältigen effizient virale RNA in einem Überfluss von endogener RNA zu erkennen.

Der optimale RIG-I Ligand ist 5'triphosphorylierte, basengepaarte dsRNA (3p-dsRNA). Diese Arbeit identifizierte und untersuchte molekulare Interaktionen der C-terminalen Domäne (CTD) von RIG-I mit 5'End RNA Modifikationen, die Toleranz gegenüber endogener RNA vermitteln. Des Weiteren wurden suboptimale, lange und virale RNA Liganden untersucht um Einblicke in RIG-I Aktivierungsmechanismen zu erhalten.

Zuvor wurde bewiesen, dass N1-2'O-Methylierung einer RNA die RIG-I Aktivierung verhindert. In dieser Arbeit wurde gezeigt, dass der Knockdown der endogenen Capspezifischen mRNA Nucleosid-2´-O-Methyltransferase 1 (CMTR1), welcher die RNA N1-2´O-Methylierung verhindert, zu einer Aktivierung von RIG-I führt. Außerdem wurde bewiesen, dass das (+)ssRNA Gelbfiebervirus (YFV) diesen Mechanismus ausnutzt um einer RIG-I Erkennung zu entgehen. Ein weiterer Mechanismus der 5'End Modifikation vermittelten Unterdrückung der RIG-I Aktivierung wurde in dieser Arbeit aufgeschlüsselt: Während OHdsRNA an RIG-I bindet und zu einer substanziellen RIG-I Aktivierung führt, verhindert eine 5'Monophosphorylierung der RNA die RIG-I Bindung und Aktivierung fast vollständig. Eine hoch konservierte Aminosäure (1875) in der CTD von RIG-I, die die Bindung von p-dsRNA durch sterische Interferenz verhindert, wurde identifiziert. Die Mutation von 1875 zu A konnte die Bindung und Aktivierung durch p-dsRNA zu einem ähnlichen Level wie OH-dsRNA wiederherstellen. Die Langzeit-Expression von RIG-I 1875A verursachte eine IFN-Induktion. Dies verdeutlicht, dass endogene Liganden RIG-I aktivieren würden, wenn es nicht zwischen OH-dsRNA und p-dsRNA unterscheiden könnte. Polyadenylierte (polyA) RNA und insbesondere mitochondriale (mt) RNA konnte als die RIG-I 1875A stimulierende Spezies identifiziert werden.

Um die tatsächlichen Modifikationen und Strukturen eines Liganden zu charakterisieren, die für die Erkennung eines Virus essenziell sind, wurde ein System von RIG-I CTD Mutanten mit verschiedenen Liganden-Spezifitäten entwickelt. Es konnte gezeigt werden, dass 5'3p

Zusammenfassung

unabhängige RIG-I Aktivierung während der Infektion mit dem Panel an gestesteten Viren (Sendaivirus (SeV), Indiana vesiculovirus (VSV), Influenza-A-Virus (IAV), Herpes-simplex-Virus (HSV)) keine Rolle spielt. Außerdem konnte ein zuvor vorgeschlagener 5'End-unabhängiger Mechanismus der Erkennung von langer RNA widerlegt werden. Durch die Untersuchung von verschieden langen 3p-dsRNAs wurde bestätigt, dass lange RNAs bei niedrigen Konzentrationen mehr IFN-β und CxCL10 als kurze RNAs induzieren. Lange RNAs aktivierten bei höheren Konzentrationen jedoch den Translationsrepressor Protein Kinase R (PKR), was zu einer Inhibition der RIG-I induzierten IFN-Produktion führt. Diese biphasische RIG-I/PKR antivirale Antwort limitiert die Verbesserung der RIG-I Ligandenaktivität durch Verlängerung der dsRNA. In dieser Arbeit wurde ein verbessertes hochwirksames Ligandensystem entwickelt, das die PKR Aktivierung umgeht.

Zusammenfassend konnten in dieser Arbeit grundsätzliche und bei Vertebraten hochkonservierte auf RNA Modifikationen basierende Mechanismen der Immuntoleranz gegen potenzielle endogene RIG-I Liganden aufgeschlüsselt werden. Dies unterstreicht das genau abgestimmte Gleichgewicht zwischen RIG-I Selektivität und Sensitivität für pathogene RNA: Vertebraten können das Vorkommen von endogenen RNAs mit kurzen basengepaarten Bereichen nicht vollständig verhindern und benötigen zusätzliche immunregulierende RNA Modifikationen.

Die Beeinträchtigung der RIG-I Signalkaskade durch PKR bei hohen Konzentrationen an langen RNAs weist auf alternative und konkurrierende antivirale Antworten hin, die vom Fortschritt der Infektion abhängen. Diese konkurrierenden Mechanismen sollten bei der Entwicklung von synthetischen RIG-I Liganden berücksichtigt werden und können, wie in dieser Arbeit gezeigt, umgangen werden.

3. Introduction

3.1. The innate immune system

In daily life the human body faces the threat of infections with possibly harmful structures and microorganisms such as viruses, bacteria, fungi and parasites. To protect against and deal with these infections, vertebrates are equipped with an innate and an adaptive immune system.

The innate immune system – consisting of physical and chemical barriers (e.g. the skin), the complement system and the cellular system (e.g. natural killer cells (NKs), dendritic cells (DCs), Macrophages and Neutrophils) – is the first defense and a pre-requisite for initiating the adaptive immune response. While the innate immune system performs an immediate response upon detection of evolutionary highly conserved pathogen-associated molecular patterns (PAMPs) through germ-line encoded pattern recognition receptors (PRRs), the adaptive immune response takes longer to develop as it is based on clonal selection, expansion and differentiation of B and T cells (Rajewsky 1996). To achieve an efficient elimination of the pathogen, the two systems have to be finely tuned and work hand-in-hand (Parkin et al. 2001, Dempsey et al. 2003).

The innate immune response consists of humoral and cell-mediated defense mechanisms. Humoral defense mechanisms include circulating soluble protein components that aim to opsonize and destroy the pathogen. Cell-mediated immunity consists of antigen-presenting cells (monocytes, DCs and macrophages) and NK cells. Upon activation of the PRRs through PAMPs, the infected cells release cytokines which induce an antiviral state in the infected and neighboring cells, and chemokines - chemotactic cytokines - that attract effector cells from the innate as well as the adaptive immune systems. Cells of the innate immune system phagocyte the pathogen, digest it and present pathogen specific protein degradation products on the major histocompatibility complex (MHC) to T cells which, together with the secreted cytokines and chemokines, initiates the activation of the adaptive immune system. While MHC class II molecules are mainly expressed on immune cells and are usually loaded with peptides derived from extracellular pathogens, MHC class I molecules are expressed on all nucleated cells and present intracellularly generated peptides from, for example, viruses, but also peptides specific for tumor cells. A mechanism called cross-presentation allows MHC class I molecules to present peptides from extracellular pathogens. Antigens presented on MHC class II and MHC class I molecules are recognized by receptors on CD4+ and CD8+ T cells respectively. Activated T cells perform their effector and regulatory functions through the secretion of cytokines and cytotoxic molecules (Fung-Leung et al. 1991) and assist driving the B cell response that produces specific antibodies (Stevens et al. 1988, Meffre et al. 2000). Secreted antibodies subsequently opsonize and neutralize the pathogen. After a successful immune response, memory T and B cells remain in the body. In case of a second infection and contact with the same antigen, these memory cells are responsible for an accelerated adaptive immune response and a higher probability of successfully eliminating the pathogen. To summarize, the innate immune system is able to immediately detect a limited number of PAMPs through germline encoded PRRs and initiates the adaptive immune system, while the adaptive immune system, due to genetic recombination-based adaption of its receptors, is able to detect virtually all presented peptides. The functionality, regulation and interplay of both immune systems are necessary to raise an appropriate and successful reaction to an infection. This thesis mainly focuses on the innate immune system and its PRRs, which will be discussed in more detail in the following sections.

3.2. PRRs

PRRs recognize structures and chemical modifications that are endogenously absent or present at an unusual location. These foreign molecules and structures — such as carbohydrates, lipids, proteins or nucleic acids of bacteria, fungi or viruses — are often highly conserved and essential for the growth and viability of the pathogen. Their presence therefore cannot be avoided by the pathogen. PRR stimulation by these structures triggers the induction and secretion of cytokines and chemokines. This leads to the upregulation of defense and alarming mechanisms in the infected and neighboring cells, and to the attraction of immune cells as described in the previous and following sections.

To monitor as much of the body as possible, PRRs are present in the cytoplasm, membrane-associated or as soluble receptors (Figure 3.1). One example for the latter is mannose-binding lectin that detects carbohydrate patterns and activates the lectin pathway of the complement system. The cell surrounding is scanned by membrane-bound receptors – such as C-type lectin receptors (CLRs) – that are mainly responsible for detecting fungal PAMPs like mannose, fucose and glucans (McGreal et al. 2005), and the scavenger receptor that is activated by modified low-density lipoprotein (LDL) particles as well as polyanionic ligands from the bacterial surface (Peiser et al. 2002, Peiser et al. 2002). Toll-like receptors (TLRs) that detect a wide range of PAMPs (lipid-based bacterial cell wall components, microbial

proteins and nucleic acid structures) are either present at the plasma membrane surface or are expressed within the endosomal compartment (endolysosome and endoplasmic reticulum) to monitor bacterial and viral entry routes.

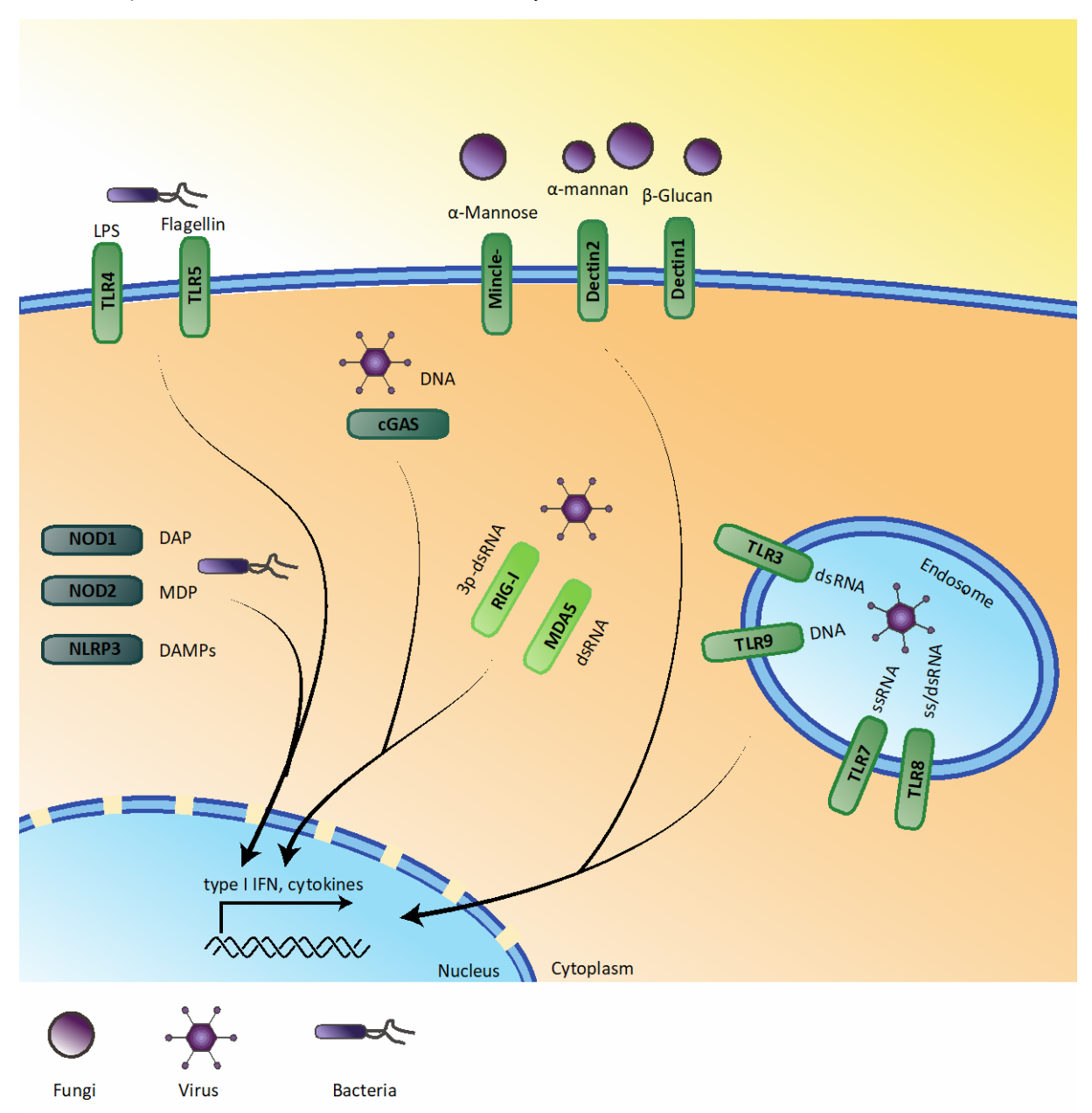


Figure 3.1: PRRs and their ligands

CLRs such as Mincle, Dectin-1 and Dectin-2, are located on the plasma membrane and mainly detect modified sugars from fungi. TLR4 and TLR5 are also expressed on the plasma membrane and are activated by LPS and flagellin respectively. Endolysosomal expressed TLRs detect viral nucleic acids. While TLR3 detects long dsRNA, TLR7 and TLR8 detect ssRNA. TLR7 can also be activated by dsRNA. DNA with unmethylated CpG motifs is the ligand for TLR9. Viral RNA structures in the cytoplasm are recognized by RIG-I and MDA5. cGAS detects DNA in the cytoplasm. NLRs such as NOD1, NOD2 and NLRP3, are activated by a wide range of structures such as DAP, MDP and ROS. Activation of the receptors leads to the induction of type I IFN and cytokines. MDP: muramyl dipeptide, DAP: diaminopimelic acid, ROS: reactive oxygen species.

So far ten members of the TLR group have been identified in humans. TLR4 and TLR5 are localized on the plasma membrane and recognize lipopolysaccharides (LPS), an important

component of the outer cell membrane of gram-negative bacteria (Muzio et al. 1998, Chow et al. 1999) and flagellin (Hayashi et al. 2001) respectively. TLR7, TLR8 and TLR9 belong to the group of endosomal expressed TLRs and screen for foreign nucleic acids (Kawai et al. 2008, Kumar et al. 2009). TLR7 and TLR8 detect single-stranded RNA (ssRNA), and in the case of TLR7 also dsRNA (Diebold et al. 2004, Heil et al. 2004, Hornung et al. 2005). TLR9 meanwhile recognizes DNA with unmethylated CpG motifs (Hemmi et al. 2000). TLR3, which can be present in the cell membrane and in the endosomal compartment, is activated by long dsRNA (Alexopoulou et al. 2001, Matsumoto et al. 2003).

Pathogen detection in the cytosol is performed by several groups of receptors. DNA is sensed by the cyclic GMP-AMP synthase (cGAS) (Sun et al. 2013, Wu et al. 2013), while nucleotide-binding domain (NOD)-like receptors (NLR) are activated by a wide range of PAMPs and damage-associated molecular patterns (DAMPs) such as nucleic acids, bacterial peptidoglycan, asbestos and silica. They are therefore not only sensors for infections, but also for stress (Chen et al. 2009, Kanneganti 2010). 22 NLRs have been identified in humans. Depending on the stimulus, upon activation NLRs orchestrate an inflammatory response, autophagy or cell death.

While TLRs in the endosome scan viral entry routes, retinoic acid-inducible gene I (RIG-I)-like receptors (RLR) — RIG-I, Melanoma Differentiation-Associated protein 5 (MDA5) and Laboratory of Genetics and Physiology 2 (LGP2) — detect viral RNA in the cytoplasm, the place of viral replication (Yoneyama et al. 2005, Hornung et al. 2006, Kato et al. 2006, Loo et al. 2008, Schlee et al. 2009). These receptors will be discussed in more detail in the next section.

3.3. The RIG-I like receptors

The detection of viruses is an especially challenging task, as viruses use the host's translation machinery for replication. This means that only little foreign or pathogenic structures enable the immune system to identify a viral infection. Additionally, there is plenty of endogenous RNA in the cytoplasm, such as ribosomal RNA (rRNA), messenger RNA (mRNA) and transfer RNA (tRNA). It is therefore important for these receptors to differentiate between self and non-self to prevent an unwanted autoinflammatory response. As the basic molecular structure of RNA (as well as DNA) is shared for all organisms, differentiating between self and non-self is obviously a challenging task and minor differences in RNA modifications are essential to detect viral RNA. RLRs belong to the family of DExD/H (Asp-Glu-X-Asp/His) box

RNA helicases and share a distinct domain structure consisting of an RNA-binding C-terminal domain (CTD) (Cui et al. 2008), an ATP-binding and hydrolyzing helicase domain, and, in the case of MDA5 and RIG-I, an N-terminal tandem caspase activation and recruitment domain (CARD) (Yoneyama et al. 2004, Saito et al. 2007). Upon binding of a ligand, MDA5 and RIG-I translocate to the mitochondria and via their CARDs interact with mitochondrial antiviral-signaling protein (MAVS) (also known as IPS-1, Cardif or VISA) (Kawai et al. 2005, Meylan et al. 2005, Seth et al. 2005, Xu et al. 2005) to initiate downstream signaling cascades (Kawai et al. 2005, Seth et al. 2005, Xu et al. 2005). Since LGP2 lacks this domain, it is unable to directly initiate antiviral pathways via MAVS (Bruns et al. 2012).

MDA5 and RIG-I seem to detect different viruses and thereby complement each other to cover a wide range of virus infections (Kato et al. 2005, Sumpter et al. 2005, Schlee 2013). While RIG-I is able to recognize amongst others VSV (Kato et al. 2005, Furr et al. 2010) and IAV (Siren et al. 2006, Rehwinkel et al. 2010), MDA5 detects Picornaviruses such as encephalomyocarditis virus (EMCV) (Kato et al. 2006). Which receptor recognizes what virus seems to depend on the length of the viral ligand (Kato et al. 2008) as RIG-I is able to detect short RNAs while longer RNAs are needed for MDA5 activation (Kato et al. 2008). High molecular weight (HMW) polyinosinic:polycytidylic acid (polyI:C) (7kb) was mainly recognized by MDA5, while shorter polyI:C fractions (< 300 bp), partially digested with RNase III, solely activated RIG-I (Kato et al. 2008).

Although polyI:C is a useful tool to investigate MDA5 activation (Gitlin et al. 2006), the exact motif requirements for the MDA5 ligand have not yet been resolved (Peisley et al. 2011, Peisley et al. 2012, Wu et al. 2013). The role of LGP2 in antiviral immunity is more controversial and it seems that LGP2 has regulatory effects on RIG-I and MDA5 (Rothenfusser et al. 2005, Satoh et al. 2010, Ahmad et al. 2015). RIG-I is the main focus of this thesis and the signaling pathways initiated upon RIG-I activation will be discussed in the next section.

3.4. RIG-I signaling pathways

In 1957, Isaacs and Lindemann described a substance they called IFN (Isaacs et al. 1957). They found that when heat-killed viruses were added to cells, that these cells resisted subsequent infections with live viruses. The addition of dead viruses prompted the cells to secrete IFN, named so because it interfered with viral infections. After the discovery of IFNs, certain nucleic acids – mimicking viral infection – were found to induce this key antiviral

cytokines (Isaacs et al. 1963). The signaling cascade leading to the secretion of IFN and also other cytokines and chemokines is initiated by PRRs.

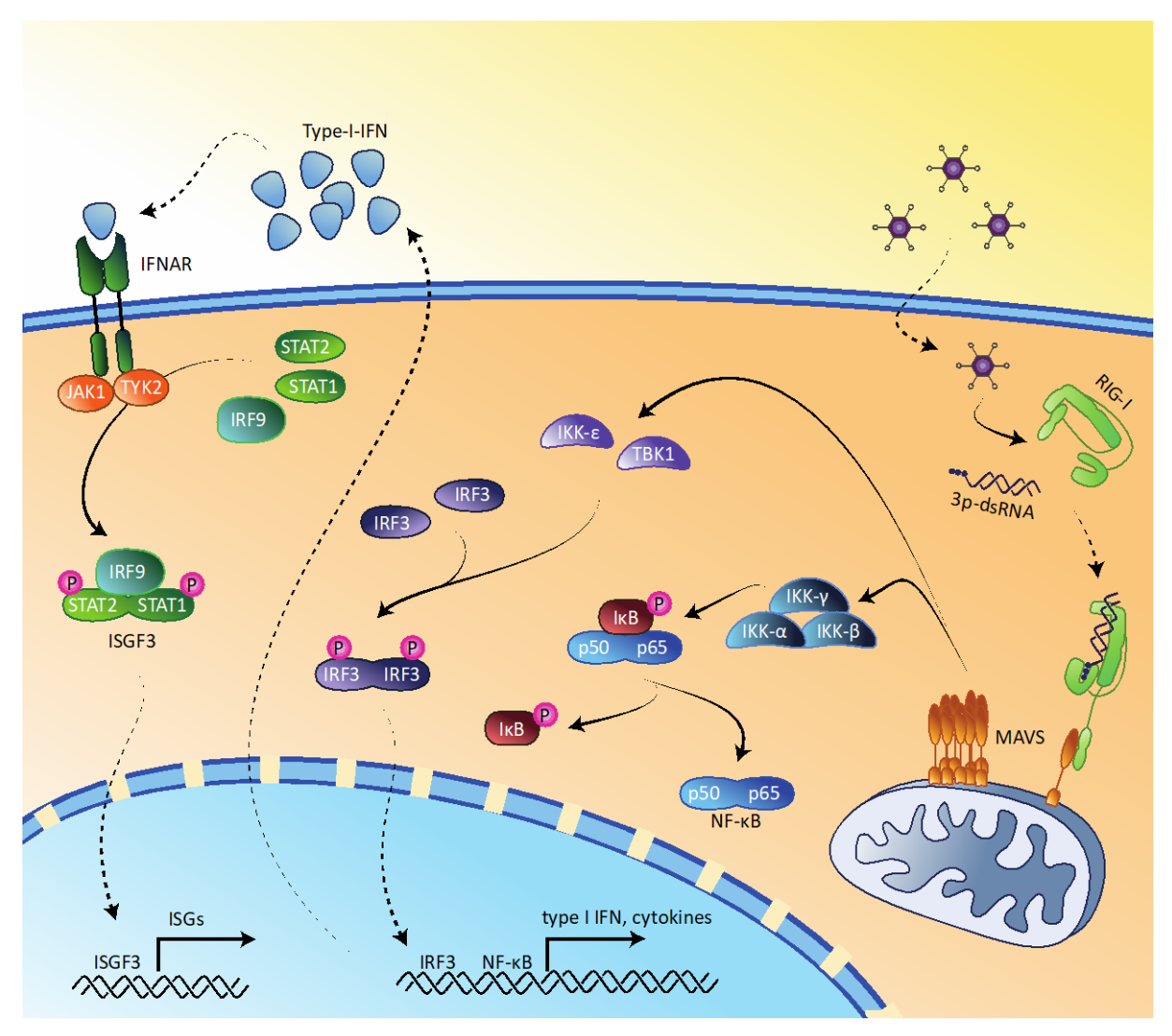


Figure 3.2: RIG-I signaling pathway

Detection and binding of viral RNA to RIG-I causes conformational changes and ultimately leads to the exposure of CARDs and their interaction with MAVS, localized on mitochondria. MAVS filament formation is a platform for the induction of downstream pathways. IKK- α , - β and - γ cause the phosphorylation, ubiquitination and degradation of IkB. NF-kB is subsequently released and translocates to the nucleus. Moreover, MAVS activation triggers the phosphorylation and dimerization of IRF3 by TBK1 and IKK- ϵ , which then also translocates to the nucleus. There IRF3 and NF-kB induce the transcription of type I IFN and cytokines. Secreted type I IFN binds to IFNAR on the infected and neighboring cells, which induces the JAK/STAT-pathway. STAT1 and STAT2 are phosphorylated by JAK1 and TYK2 and then build, together with IRF9, the ISGF3 complex. Active ISGF3 translocates to the nucleus and induces ISG expression.

In contrast to other PRRs, RIG-I is expressed almost ubiquitously (Barchet et al. 2008) and therefore plays an indispensable role in viral detection and subsequent elimination. Upon activation by viral RNA, RIG-I initiates signaling via MAVS (Figure 3.2). MAVS is located in the outer mitochondrial membrane and its oligomerization provides a scaffold for the recruitment of downstream signaling molecules, leading to the activation of transcription factors interferon regulatory factor 3 (IRF3), IRF7 and nuclear factor kappa-light-chain-

enhancer of activated B cells (NF- κ B) (Lee et al. 2007, Sin et al. 2012). Inactivated NF- κ B is bound to inhibitor of nuclear factor kappa-B (I κ B), which masks the nuclear localization sequence (NLS) motif. Upon immune activation, I κ B is phosphorylated by the canonical I κ B kinase (IKK) complex – IKK- α , - β and - γ (also known as NEMO) – and is subsequently ubiquitinated and degraded by the proteasome. NF- κ B is released and translocates to the nucleus to induce the transcription of pro-inflammatory cytokines (Lee et al. 2007, Takeuchi et al. 2010). The non-canonical IKK complex, consisting of TANK- binding kinase 1 (TBK-1) and inhibitor of I-kappa-B kinase subunit epsilon (IKK- ϵ), causes the phosphorylation and dimerization of IRF3 and IRF7. Upon phosphorylation, IRF3 and IRF7 form homo- or heterodimers and translocate to the nucleus to induce type I IFNs (Doyle et al. 2002, Sharma et al. 2003, Yoneyama et al. 2004).

Secreted type I IFNs bind to the IFN- α/β receptor (IFNAR) leading to the subsequent activation of Janus kinases (JAK1/TYK2). This in turn causes the phosphorylation of the transcription factors signal transducer and activator of transcription 1 (STAT1) and STAT2. Together with IRF9, STAT1 and STAT2 then form the transcription factor complex ISGF3 which enters the nucleus and, by binding to IFN-stimulated response elements (ISRE), induces the expression of IFN-stimulated genes (ISGs). Examples of ISGs include cytokines, chemokines, RIG-I and PRRs with direct antiviral activity such as PKR, IFN-induced protein with tetratricopeptide repeats 1 (IFIT1) and oligoadenylate synthetase (OAS) (Yoneyama et al. 2009). In addition to causing NF- κ B and IRF activation, MAVS activation leads to an increased apoptosis probability through several pathways (Besch et al. 2009, Kumar et al. 2015).

To summarize this section, RIG-I activation initiates the production of cytokines such as type I IFNs and chemokines, leading to the recruitment of immune cells to the site of infection. Furthermore, an antiviral state in the infected and neighboring cells is induced, causing direct inhibition of viral replication and leads to an increased apoptosis rate. The ligands that activate RIG-I and cause the induction of these pathways will be discussed extensively in the next section.

3.5. RIG-I ligands

The protein RIG-I was first described in 1997 when it was found to be upregulated by retinoic acid treatment (Sun 1997). The important antiviral function of RIG-I however remained elusive until 2004, when RIG-I was first described as an antiviral sensor by

Yoneyama et al. (Yoneyama et al. 2004). It was shown that RIG-I can bind to and is activated by polyI:C, and that RIG-I expression reduces viral yield after VSV and EMCV infection. However, the precise ligand requirements were not further explored (Yoneyama et al. 2004).

3.5.1. Optimal RIG-I ligand

Two independent groups established 5'triphosphate (3p)-RNA as an important motif for RIG-I activation (Hornung et al. 2006, Pichlmair et al. 2006). Hornung et al. showed that RIG-I is the crucial receptor for the detection of 3p-RNA and the induction of type I IFN in monocytes

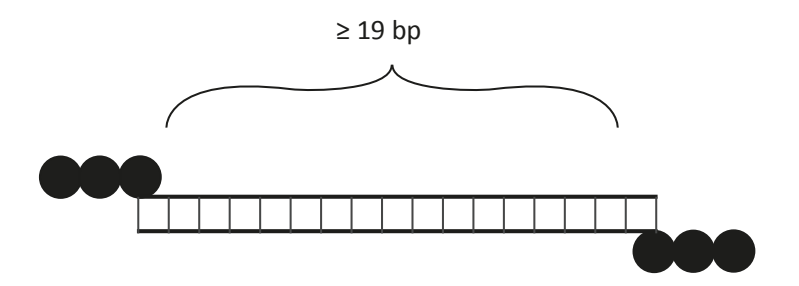


Figure 3.3: The optimal RIG-I ligand

The optimal RIG-I ligand possesses a 5'triphosphate or 5'diphosphate modification and is blunt-ended. Furthermore, the RNA is double-stranded with a minimal length of ≥ 19 bp.

(Hornung et al. 2006), while the removal of the 5'3p abolished IFN- α induction (Hornung et al. 2006). The incorporation of nucleotides (nt) with modified bases (pseudouridine, 2-thiouridine) or backbone modifications (2'O-methyl at uridines) also abolished IFN- α induction (Hornung et al. 2006). By using a method to generate well defined synthetic 3p-RNA (modified after the standard cyclotriphosphate protocol of triphosphate synthesis (Ludwig et al. 1989)), dsRNA was identified as another recognition motif for RIG-I (Schlee et al. 2009, Schmidt et al. 2009). The minimal dsRNA length for RIG-I activation was defined as 19 base pairs (bp) (Schlee et al. 2009, Schmidt et al. 2009). It was later shown that stimulation with 2p-dsRNA also induces RIG-I activation, albeit slightly lower than 3p-dsRNA (Goubau et al. 2014).

3.5.2. Suboptimal RIG-I ligands

The results defining 5'3p/2p-dsRNA as a minimal recognition motif for RIG-I-dependent signaling are in contrast to the observations that RIG-I was activated by polyI:C (Yoneyama et al. 2004, Kato et al. 2008), a long dsRNA homopolymer synthesized from inosine diphosphate and cytidine diphosphate supposedly possessing monophosphates at the 5'end (Grunberg-Manago 1967). Moreover, in studies that were published before the 5'3p motif

Introduction

was established for RIG-I, it was shown that synthetic OH-dsRNA oligonucleotides can stimulate RIG-I (Marques et al. 2006). This was found by comparing blunt-ended siRNAs with siRNAs possessing an overhang. While blunt-ended siRNAs lead to a RIG-I-dependent ISG upregulation, siRNAs with a 5'overhang or a 3'overhang reduced or abolished this effect (Marques et al. 2006). Takahasi et al. tested RIG-I activation with synthetic OH-, 5'p- and 3'p-dsRNAs and found that while non-modified OH-dsRNA did not cause RIG-I activation, 5'p- and 3'p-RNA triggered a type I IFN response (Takahasi et al. 2008). In accordance with the study by Marques et al., 3'overhangs at the 5'p side were not tolerated. Interestingly, they showed that the increased stimulative activity of p-dsRNA was not due to an increased binding of RIG-I, but due to the fact that 5'p increased the stability of the RNA in the cytosol and therefore increased the availability to RIG-I (Takahasi et al. 2008).

In the studies establishing dsRNA as a requirement for RIG-I binding and activation, different RNA modifications and RNAs with overhangs were also tested (Schlee et al. 2009, Schmidt et al. 2009). A 1 nt overhang at the 5'3p side abolished RIG-I activation completely, while a 2 nt 3'overhang reduced RIG-I activity substantially. The optimal RIG-I stimuli seemed to be blunt-ended. 5'p or 5'OH dsRNA led to no IFN induction (Schlee et al. 2009). Furthermore, Schmidt et al. tested the same RNA sequences as Takahasi et al. and could not observe any IFN induction (Schmidt et al. 2009). However, OH-dsRNA and p-dsRNA induced RIG-I ATPase activity at higher concentrations in both studies (Schlee et al. 2009, Schmidt et al. 2009). Another study using in-vitro transcription (IVT) transcribed 3p-dsRNA also concluded that the 5'end of the RNA has to be base-paired for efficient RIG-I activation (Marq et al. 2010). In all these studies short RNAs (10-45 bp) were tested. However, different ligand specificities might be applicable for longer RNAs. In the aforementioned study by Kato et al., polyI:C fragments were used to differentiate between RIG-I and MDA5 activation. PolyI:C was digested with RNase III for different periods of time resulting in RNAs of different length with 5'p and 2 nt 3'overhangs (Kato et al. 2008). While very long RNA (7 kb) was mainly detected by MDA5, partially digested RNA (<300 bp) was solely detected by RIG-I. Having said this, complete digestion to 10-20 nt RNA also abolished RIG-I activation (Kato et al. 2008). This suggests that only longer RNA might be recognized end-independently. In accordance with this, another study found that longer RNAs (more than 100 bp) activate RIG-I endindependently. The study showed that removing the 3p with phosphatase treatment resulting in an OH-end, had no effect on RIG-I pathway activation (Binder et al. 2011). Both studies therefore showed a 3p-end-independent activation of RIG-I by longer RNAs (>100 bp), while dephosphorylation of short dsRNA (40 bp) had a detrimental effect on immune activation. This led to speculation about two different binding modes for RIG-I: 1) 5'end-dependent for short RNAs, and 2) 5'end-independent for longer RNAs. Binder et al. speculated that the availability of huge amounts of nonspecific internal initiation sites might compensate for the lack of highly efficient initiation motifs like 5'3p (Binder et al. 2011). Summarizing this and the previous section, 3p/2p-dsRNA seems to be the optimal RIG-I ligand. Having said this, RIG-I can also be activated by short and longer RNAs with differing 5'ends at higher concentrations. It is therefore interesting to look at viral infections and determine which viral ligands activate RIG-I during an infection.

3.5.3. Viral ligands

RIG-I was shown to be involved in the recognition of a wide range of viruses such as VSV, SeV, Newcastle disease virus (NDV), IAV, Hepatitis C virus (HCV) and Dengue virus (DENV) (Kato et al. 2005, Yoneyama et al. 2005, Kato et al. 2006, Loo et al. 2008, Saito et al. 2008). However, from these studies the question arose if the defined 3p-dsRNA ligand occurs during viral infections, and if it is decisive for RIG-I-dependent viral recognition and initiation of the immune response. This next section will discuss different classes of viruses and their possible RIG-I ligands.

3.5.3.1. dsRNA viruses/(+)ssRNA viruses

Considering that the optimal ligand for RIG-I is 3p-dsRNA, it is not surprising that dsRNA viruses are recognized by RIG-I. Reoviruses are non-enveloped viruses whose genome is divided into 10 segments that form blunt-ended hairpin structures. Initially it was thought that they evade RIG-I recognition by trimming their 5´3p ends to 5´2p ends. However, as mentioned above, it was later shown that 5´2p can also serve as a recognition motif for RIG-I, and that to control reovirus infection in cultured cells and mice, a RIG-I-dependent response is indispensable (Goubau et al. 2014). Furthermore, the same study showed that genomes from reoviruses with 5´2p-termini bind and activate RIG-I (Goubau et al. 2014).

The genome of (+)ssRNA viruses is directly used as mRNA, which is then translated into proteins by using the host ribosomal machinery. An RNA-dependent RNA polymerase copies the RNA and forms a double-stranded intermediate. Several studies proved that (+)ssRNA viruses produce a substantial amount of dsRNA intermediates during replication (Weber et

al. 2006, Targett-Adams et al. 2008, Feng et al. 2012, Triantafilou et al. 2012). Moreover, MDA5 as well as RIG-I initiate an immune response after murine hepatitis virus (MHV) infection (Li et al. 2010), and are both involved in detecting West Nile virus (WNV) (Errett et al. 2013) and DENV infection (Loo et al. 2008, Nasirudeen et al. 2011).

3.5.3.2. (-)ssRNA viruses

Viruses with a (-)ssRNA genome (NSV) cause multiple diseases such as measles, mumps, neuronal infections, hemorrhagic fever and respiratory problems. While numerous studies have shown that RIG-I is responsible for limiting the viral growth of many NSVs even before the optimal RIG-I ligand was defined (Kato et al. 2005, Yoneyama et al. 2005, Cardenas et al. 2006, Hornung et al. 2006, Kato et al. 2006, Plumet et al. 2007, Habjan et al. 2008, Loo et al. 2008), the question remained if RIG-I recognizes the genome of the virus or replicative intermediates. Their genomic RNA is copied by an RNA replicase to form a (+) sense RNA that can then act as the mRNA. NSVs are divided into two subgroups, the first group having a linear non-segmented genome (ns-NSV) and the second group having a genome divided into up to eight segments (s-NSV).

The genome of s-NSV contains highly complementary 5' and 3'sequences (Desselberger et al. 1980). It was shown for Bunyavirales such as La Crosse encephalitis virus (LACV), that the 5' and 3' ends of the viral genome can hybridize to form short double-stranded blunt-ended structures called panhandles in vitro (Hewlett et al. 1977, Hsu et al. 1987, Raju et al. 1989). The panhandle contains a 24-27 bp double-stranded stretch, hence building a perfect RIG-I ligand (Raju et al. 1989). Furthermore, it was shown that LACV viral capsids containing panhandles can act as RIG-I agonists during infection in the absence of replication (Weber et al. 2013). IAV has a genome containing eight segments which, similar to LACV, form panhandles although with shorter double-strand stretches (about 15 bp) including mismatches and bulge loop structures (Desselberger et al. 1980, Hsu et al. 1987). Indeed, during IAV infection RIG-I associates with all genomic sequences, but preferentially with shorter segments such as the NS and M segments (Baum et al. 2010) as predicted by Schlee et al. (Schlee et al. 2009). Another study confirmed that RIG-I response to IAV infection is mediated by genomic RNA rather than mRNA (Rehwinkel et al. 2010). Moreover, it was recently shown that, together with cytoplasmic RIG-I, a pool of nuclear-resident RIG-I is involved in sensing IAV replication in the nucleus and can induce a MAVS-dependent signaling cascade (Liu et al. 2018).

ns-NSVs have all genes on one ssRNA strand that are separated by intergenic regions that act as transcriptional promoters and possess a regulatory leader as well as a trailer sequence at the 5' and 3' end. Viral particles of SeV and Measles morbillivirus (MeV) contain mainly linear nucleocapsids, as structural proteins on the RNA prevent the formation of doublestranded regions or panhandle structures (Bhella et al. 2004, Loney et al. 2009, Gerlier et al. 2011). Having said this, ns-NSVs such as SeV and VSV produce defective interfering (DI) viral genomes during their life cycle (Kolakofsky 1976, Perrault et al. 1978, Lazzarini et al. 1981). These are named so because they compete with the full-length genome for replication resources and it seems that a certain percentage of DI genomes are incompletely encapsidated (Strahle et al. 2006). Three different types of DI genomes were defined: 1) DI genomes with internal deletions, 2) 5'promoter duplications leading to completely complementary 5'-3'end (panhandle), and 3) hairpin DI genomes (snapback). At least the last two fulfill the RIG-I ligand requirements. Indeed, Baum et al. reported that RIG-I binds genomic RNA of defective interfering particles and not full-length RNA genomes or mRNA during SeV infection (Baum et al. 2010). Furthermore, Strahle et al. compared infection and IFN induction with different SeV stocks containing snapback or internal deletion DI genomes or only non-defective (ND) genomes for their ability to induce IFN. They could show that IFNβ induction was due to the presence of copyback DI genomes and that IFN production positively correlated with that of DI genome replication and the ratio of DI to ND genomes during infection (Strahle et al. 2006). These snapback DI genomes do not show encapsidation and are therefore able to form panhandle structures during replication in the infected cells (Strahle et al. 2007). It therefore seems that for ns-NSV, RNA products that occur during replication or unwanted replication byproducts are more likely to be RIG-I stimulating species than the RNA genome itself (Plumet et al. 2007, Bitko et al. 2008, Baum et al. 2010, Gerlier et al. 2011, Runge et al. 2014).

Summarizing this section, for s-NSV incoming nucleocapsids can be directly detected by RIG-I. This is in contrast to ns-NSV, where RIG-I must wait for regular and irregular products of viral RNA synthesis.

3.6. Viral escape strategies

The activation of RIG-I causes the induction of a signaling cascade leading to the upregulation of cytokines, IFNs and ISGs in infected and neighboring cells. For a successful viral replication, it is therefore essential for the virus to minimize the immune response.

Introduction

Looking at viruses' counter mechanisms might be interesting as it can hint at the structures RIG-I detects and how it differentiates between self and non-self RNA. As shown in the previous sections, the optimal RIG-I ligand is blunt-ended, double-stranded and has a 5'3p. Moreover, RIG-I ligands are present during viral replication. However, viruses have evolved diverse mechanisms to turn their RNA into less optimal RIG-I ligands. Since the 5'end of the RNA is detrimental for RIG-I recognition, it is not surprising that there are several viral strategies to modify it. Some viruses encode for their own capping enzyme to conceal the 5'end of the RNA from RIG-I. s-NSV use a mechanism called cap-snatching: they cut the 5'terminal ends of host mRNA and use it as a primer for their own mRNA generation (Fechter et al. 2005, Hyde et al. 2015). This removes their own 5'3p end and at the same time inhibits efficient host mRNA translation.

The (+)ssRNA picornaviruses and caliciviruses avoid RIG-I activation (Gitlin et al. 2006, Kato et al. 2006) by substituting 5'3p with a peptide called viral protein genome-linked (VpG) that is linked via a tyrosine residue to 5'p (Lee et al. 1977, Hruby et al. 1978, Rohayem et al. 2006). The peptide is also important for an efficient initiation of viral RNA translation. Correspondingly, purified RNA from picornaviruses does not induce RIG-I activation (Feng et al. 2012).

Some arenaviruses use the so-called prime-and-realign mechanism which generates 1 nt 5'overhangs in their genomes (Marq et al. 2010) to prevent RIG-I recognition (Schlee et al. 2009). Bunyavirales and Bornaviridae use a combination of prime-and-realign mechanisms to generate a 5'overhang in their panhandle and the cleavage of the 5'terminal base of their genomic RNA which generates a 5'p end (Habjan et al. 2008). It was shown that the RNA of these viruses does not bind to RIG-I and was not able to stimulate RIG-I in HEK cells (Habjan et al. 2008). Furthermore, (-)ssRNA viruses prevent the formation of double-stranded stretches in their RNA by using nucleocapsid proteins or by introducing mismatches in their genomic panhandles (Weber et al. 2006, Anchisi et al. 2016). Some heavily segmented viruses – such as Thogoto virus (THOV) and IAV – replicate in the nucleus instead of in the cytoplasm, possibly to avoid RIG-I as much as possible (Osterlund et al. 2012, Killip et al. 2014).

In case the virus cannot prevent RIG-I recognition, it has to use a broader approach to prevent an immune response. Some examples are the non-structural protein 2 (NS2) of respiratory syncytial virus (RSV) and the Z protein of New World Arenaviruses that, by

directly interacting with RIG-I, prevent its association with MAVS (Ling et al. 2009, Fan et al. 2010).

The previous sections have extensively discussed RIG-I ligands. The following section will analyze how the specific RIG-I structure provides for the specific ligand requirements.

3.7. RIG-I structure

Because of several RIG-I crystal structures with and without a ligand, the necessity for the previously discussed RIG-I ligand requirements are well understood (Cui et al. 2008, Takahasi et al. 2008, Lu et al. 2010, Wang et al. 2010, Civril et al. 2011, Jiang et al. 2011, Kowalinski et al. 2011, Lu et al. 2011, Luo et al. 2011). RIG-I is a multi-domain protein consisting of 925 amino acids. It is composed of a N-terminal tandem CARD (Yoneyama et al. 2004, Saito et al. 2007, Luo et al. 2013), a central DexD/H-box helicase domain (Hel-1 and Hel-2, with a specified Hel-2i insertion) and a CTD. While the CARDs are essential for signal transduction via MAVS, the helicase domains create an active site for ATP binding and hydrolysis as well as an extended RNA-binding surface (Figure 3.4A). The CTD binds the RNA ends and is connected to Hel-1 via a unique elbow shaped helical extension named pincer domain (or bridging helices) (Kowalinski et al. 2011, Luo et al. 2011). In its unbound state, RIG-I is present as a monomer. CARD2 interacts with Hel2i and is therefore not available for downstream signaling. Moreover, Hel2i is prevented from binding to the RNA backbone. The CTD is free to monitor the cytosol for viral RNA (Kowalinski et al. 2011). Binding of the CTD to the 5'3p end of the RNA causes conformational changes, leading to the disruption of the CARD2-Hel2i interaction which is facilitated by ATP binding in the helicase domain (Zheng et al. 2015). Upon binding of the CTD to the 5'end of the RNA, RIG-I is put in an active state where the RNA is completely surrounded by the protein and the helicase domains make several connections with the RNA backbone (Kolakofsky et al. 2012). Four tandem CARDs are proposed to build a helical core for CARD-CARD interactions with MAVS and its subsequent filament formation (Jiang et al. 2012, Peisley et al. 2013, Peisley et al. 2014). TRIM25dependent K63-polyubiquitination (Gack et al. 2007) or binding of unanchored K63-linked polyubiquitin chains (Zeng et al. 2010, Jiang et al. 2012) to the exposed CARDs stabilizes RIG-I multimerization. However, recent studies also hint towards an ubiquitination-independent activation and downstream signaling (Peisley et al. 2013). The first RIG-I-CTD crystal structures (Lu et al. 2010, Wang et al. 2010) explained the before mentioned optimal ligand requirements: 3p, ds and blunt-ended (Schlee et al. 2009). While the helicase domain binds

to the RNA backbone, a positively charged binding pocket within the CTD (amino acids 802-925) was described as the site were the 5′ RNA ends are bound (Cui et al. 2008, Takahasi et al. 2008, Kolakofsky et al. 2012).

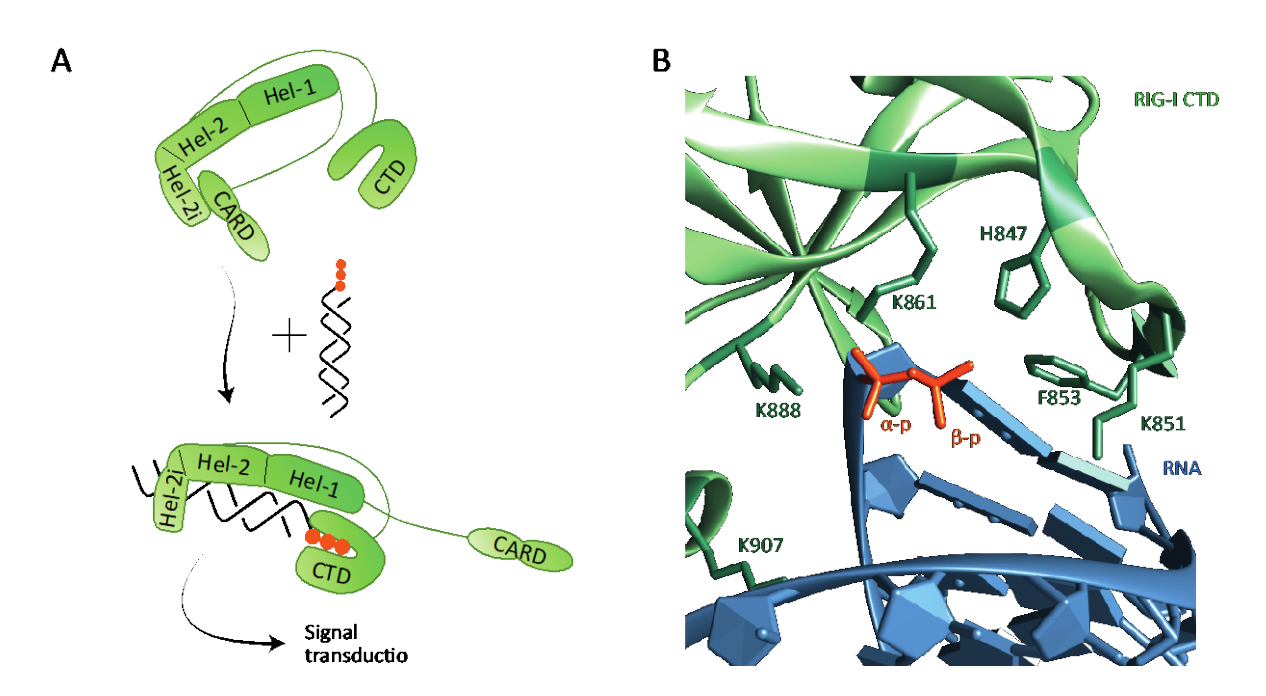


Figure 3.4: RIG-I structure

A) RIG-I has several domains: a CTD, a tandem CARD and a helicase domain, conisting of Hel-1, Hel-2 and Hel-2i. Without a ligand, RIG-I is present in an autoinhibited state where CARD2 is bound to Hel-2i and the CTD is free to scan the cytoplasm. Binding of 3p-dsRNA causes conformational changes and the CARDs are released and available for downstream signaling via MAVS. RIG-I is depicted in green, the RNA backbone in black and the 3p in orange. B) Crystal structure of RIG-I CTD with 2p-dsRNA. RIG-I CTD is depicted in light green. Amino acids important for 3p-dsRNA binding are depicted in dark green. RNA is depicted in blue and the α - and β -phosphate in orange.

In this binding cleft, amino acids involved in binding the triphosphate, the 5´terminal base-pair and the backbone phosphate were identified (Wang et al. 2010) (Figure 3.4B). While mutations of amino acids that are in proximity of the γ -phosphate (K849 and K851) impaired RIG-I activation only slightly, the mutation of amino acids that are in contact with the β - and α -phosphate (K858, H847, K861, K888) abrogated RIG-I activation completely (Wang et al. 2010). This is line with the finding that a 2p-dsRNA is sufficient to activate RIG-I (Goubau et al. 2014). Moreover, a lysine (K907) located in proximity of the backbone phosphate between nucleosides 2 and 3 was identified. Since its mutation to alanine completely abrogated RIG-I activation, this amino acid appears critical for the detection and binding of the ribose backbone of a dsRNA structure, and thereby excludes ssRNA binding (Wang et al. 2010).

Another CTD amino acid – F853 – is involved in a stacking interaction with the 5' terminal base-pair and only makes a stable interaction when the dsRNA is blunt-ended. This amino acid prevents the free rotation of the RNA strand and might thereby help correct RNA assembly in the CTD and facilitates RNA backbone binding to the helicase domain (Wang et al. 2010, Kolakofsky et al. 2012).

Crystallization of OH-dsRNA bound to the RIG-I CTD showed that binding of non-triphosphorylated RNA to the binding cleft is possible (Lu et al. 2011), even if 3p-dsRNA binds to full-length RIG-I 126 times stronger than OH-dsRNA (Vela et al. 2012). Although RIG-I belongs to the DEXD/H family of RNA helicases, there is no indication that RIG-I actually unwinds the dsRNA. Having said this, it was shown that RIG-I translocates in an ATP-dependent way from the 5´end of the RNA to the inner RNA and forms filaments (Myong et al. 2009, Kolakofsky et al. 2012, Peisley et al. 2013, Devarkar et al. 2018).

The autoinhibited mode and the CTD binding cleft seem to be the key mechanisms to prevent nonspecific RNA binding (Wang et al. 2010, Jiang et al. 2011, Kowalinski et al. 2011, Lu et al. 2011, Luo et al. 2011). Discrimination between self and non-self is supported by ATP hydrolysis through dissociating RIG-I from nonspecific RNAs. Recently, a group proposed a translocation-throttling mechanism whereby RIG-I selectively translocates and oligomerizes on potent RIG-I ligands to support discrimination between self and non-self (Devarkar et al. 2018). ATP hydrolysis leads to a three to sevenfold faster release of non-3pRNA compared to 3p-RNA, and the dissociation of RIG-I from the RNA occurred by translocation from the RNA 5' end into the stem region. Interestingly, translocation on 3p-RNA is throttled compared to non-PAMPs, thereby possibly facilitating binding of a second RIG-I, supporting oligomerization, and increasing the time bound to the RNA and for downstream signaling because of exposed CARDs.

This and the previous sections discussed the RIG-I structure and the perfect and suboptimal RIG-I ligands. The following section will put the spotlight on endogenous RNA and modifications that exclude them from RIG-I recognition.

3.8. Endogenous RNA

The task to differentiate between endogenous RNAs that are necessary for cell survival and metabolism, and viral RNA that could harm the cell, is even more difficult if one takes into consideration the abundance of endogenous RNA in the cytoplasm. There are different types of RNA in the eukaryotic cell that are structurally adapted to their specific task. Because of

its importance for RIG-I activation, it is interesting to look at the 5'ends of endogenous RNA to identify possible markers of self or non-self.

RNA synthesis is based on the linkage between 3´OH and 5´3p of nucleotide triphosphates (NTPs) and leaves a free 5´3p. As previously discussed, 5´3p is a recognition motif for RIG-I. However, eukaryotic RNA synthesis takes place in the nucleus, while RIG-I is mostly present in the cytosol. Before their transportation to the cytoplasm, RNAs are further processed and modified according to their specific function. In eukaryotic cells, tRNAs and 5S rRNA are transcribed by RNA polymerase (Pol) III and make up about 15% of eukaryotic RNA, while the majority of RNAs are RNA Pol I transcribed rRNAs (about 75%). All mRNAs as well as most regulatory and untranslated RNAs are synthesized by RNA Pol II. As they usually have a high turn-over rate, mRNAs only make up about 5-10% of the eukaryotic RNA pool (Warner 1999).

3.8.1. mRNAs

The 5'end of mRNAs are capped via a 5'-5'-linked guanosine methylated at N7 (^{m7}G cap). mRNAs with a ^{m7}G cap are called cap0 RNAs (Figure 3.5). The cap structure was first described in 1974 and blocks the 5'end of the RNA from degradation through exonucleases (Reddy et al. 1974, Fechter et al. 2005). Furthermore, cap0 is important for exporting to the cytoplasm and for efficient translation initiation by recruiting ribosomes to the mRNA via eukaryotic initiation factor 4 (eIF4) (Gingras et al. 1999). mRNA capping is fulfilled by several enzymes that are associated with RNA Pol II. First, the capping enzyme removes one phosphate from the 3p and transfers the so far unmethylated guanosine to the 5'terminal base. A second enzyme, the N7G-methyltransferase, is then responsible for methylation of the guanine (Furuichi et al. 2000, Shatkin et al. 2000, Proudfoot et al. 2002). While CMTR1 confers cap0 to cap1 by methylation of the penultimate nucleotide (N1), CMTR2 catalyzes methylation of some, but not all, antepenultimate nucleotides (N2), creating cap2 (Banerjee 1980, Belanger et al. 2010, Werner et al. 2011). The cap1 and the cap2 structures are a signature of higher eukaryotes (Banerjee 1980, Reddy et al. 1992, Abbas et al. 2013) and have been implicated in the differentiation between self and non-self RNA (Abbas et al. 2013, Habjan et al. 2013, Kimura et al. 2013, Abbas et al. 2017). Since not all mRNAs are permanently needed, a timely degradation is indispensable. Cytoplasmic eukaryotic mRNA decay can occur by three pathways: 1) endonucleolytic cleavage-dependent, 2) deadenylation-independent, and 3) deadenylation-dependent (Braun et al. 2012). The latter

Figure 3.5: mRNA cap structure

Eukaryotic mRNAs possess a 5'cap structure. A guanosine methylated at N7 is 5'-5'- linked to the triphosphate (cap0). 2'O-methylation of the penultimate nucleotide (N1) confers cap0 to cap1. Additional methylation of the antepenultimate nucleotide (N2) confers cap1 to cap2.

is the most common pathway. The first step is the removal of the polyA-tail by deadenylases (Chen et al. 2011). Afterwards, RNAs are either degraded in a 3′--> 5′way or a 5′--> 3′way. The first is performed by the exosome (Houseley et al. 2006). In the 5′--> 3′ pathway, mRNAs are de-capped by the decapping enzyme DCP2 after deadenylation, and then degraded by 5′-3′-exoribonuclease 1 (XRN1) (Ling et al. 2011, Nagarajan et al. 2013).

3.8.2. rRNAs

As components of the ribosomes, rRNAs are an essential part of translation. The 5S rDNA and the 45S rDNA array encode for the 5S rRNA and the 5.8S, 18S and 28S rRNA respectively (Warner 1999, Grummt 2003, Moss et al. 2007, Pederson 2011, Woolford et al. 2013). While RNA Pol III is responsible for the transcription of 5s rRNA and tRNA, RNA Pol I co-transcribes the other three rRNAs to a single precursor rRNA (Woolford et al. 2013, Henras et al. 2015). Further processing in the nucleolus, nucleoplasm and cytoplasm leads to the formation of the mature ribosomes containing rRNAs and riboproteins (Eichler et al. 1994, Fatica et al. 2002, Granneman et al. 2005, Raska et al. 2006, Henras et al. 2008). In this process, the 5'3p end is maturated to a 5'p end and modifications such as methylations, dihydrouridine and pseudouridine are introduced (Helm et al. 2014, Sloan et al. 2017). The large ribosomal

subunit (LSU) is composed of the 28S, 5S, 5.8S rRNAs and 47 proteins, while the small ribosomal subunit (SSU) consists of a single 18S rRNA and 33 proteins (Ben-Shem et al. 2011, Khatter et al. 2015).

3.8.3. tRNAs

tRNAs, like 5s rRNA, are transcribed by RNA Pol I. They are the decisive link that helps translate the mRNA sequence into the protein amino acid sequence. The most common tRNAs consist of about 76 nucleotides (Rich et al. 1976). They are highly conserved in all three kingdoms of life and have a characteristic cloverleaf-like structure that terminates with a CCA trinucleotide at the 3´end. tRNAs are the most highly and complex modified of all RNAs (Helm et al. 2014, Li et al. 2014). About 300 different cytoplasmic tRNA molecular sequences are encoded by the genome. Like rRNAs, the 5´3p of tRNAs is maturated to a 5´monophosphate.

3.8.4. mtRNAs

The current theory is that mitochondria originated from proteobacteria that entered an archaebacterium. This endosymbiosis provided the requirements to form multicellular organisms with specialized cell types. In eukaryotes, mitochondria have an essential function in providing cellular energy through the generation of ATP, while also playing important roles in intracellular calcium signaling, reactive oxygen species production and apoptosis. They are also the platform for MAVS and RIG-I interaction. During evolution, most of the ancestral bacterial genome was lost or transferred to the nucleus and only a compact circular double-stranded mitochondrial DNA (mtDNA) of 16.6 kb remained in the mitochondria. The DNA encodes 2 rRNAs, 22 tRNAs and 11 mRNAs, which are translated into 13 proteins. The mitochondrial rRNAs and tRNAs form, together with nuclear encoded and imported proteins, a separate translational apparatus in the mitochondria. This is necessary to transcribe and translate the mitochondrial mRNA as there is a different genetic code used in the mitochondria compared to the rest of the cell (Barrell et al. 1979). Mt-mRNA is polyadenylated by the addition of adenosines to the 3'ends of mRNAs, which has a stabilizing effect on the RNA (Ojala et al. 1981, Fernandez-Silva et al. 2003). Although human mitochondrial genes do not contain introns, transcripts contain large noncoding regions that have to be degraded to prevent the formation of long dsRNAs. One protein that was shown to be important for the degradation of mtRNA is the helicase SUV3 (Dmochowska et al.

1999), which is predominantly localized in the mitochondria. Expression of a dominant-negative variant increases mt-mRNA steady-state levels and results in the accumulation of mt-mRNA decay intermediates (Khidr et al. 2008, Szczesny et al. 2010). Polynucleotide phosphorylase (PNPase), which has a 3′-5′exoribonuclease activity, forms a functional degradosome with SUV3 in vitro (Piwowarski et al. 2003, Wang et al. 2009) and copurifies with SUV3 (Szczesny et al. 2010). The knockdown (KD) of SUV3 or PNPase leads to an accumulation of mt-dsRNA and, in a PNPase-dependent manner, its release into the cytoplasm. There the RNA is able to activate MDA5 leading to IFN induction (Dhir et al. 2018).

3.9. RNA-sensing receptors with direct antiviral activity

The main effect of RLRs is the secretion of type I IFNs, which subsequently causes an antiviral state in the infected and neighboring cells mediated by the upregulation of ISGs. However, there are also RNA-sensing receptors with a direct antiviral activity such as PKR, IFIT1 and OAS, which are often ISGs themselves. They do not induce activation of transcription factors, but directly inhibit viral replication. Since viruses do not possess their own ribosomes and tRNAs, viral replication is dependent on using the host's translation machinery. Many direct antiviral mechanisms therefore target the viral (IFIT1) or both viral and endogenous (PKR, OAS) translation process.

Although the outcome of their activation is different, the recognition motifs of PKR, OAS and IFIT1 are partly overlapping with the ones of RLRs. IFIT1 (also known as p56 and ISG56), one of the most potently induced ISGs, IFIT5 (also known as p58 and ISG58) (Daffis et al. 2010, Pichlmair et al. 2011, Abbas et al. 2013, Kumar et al. 2014) and PKR (Nallagatla et al. 2007) recognize 5′ 3p-RNA. Although IFIT5 and IFIT1 recognize dsRNA with a 5 nt or 3 nt ssoverhang respectively (Abbas et al. 2013), their main recognition motif seems to be, contrary to RIG-I, ssRNA. Since a cap0 structure (^{m7}G cap) enhances IFIT1 affinity for the RNA compared to uncapped RNA, it is thought that IFIT1 targets the mRNA instead of directly binding the viral genomic RNA (Habjan et al. 2013, Kumar et al. 2014). The main effect of IFIT1 RNA binding is sequestering viral cap0 RNA from translation. IFIT1 plays a decisive role in containing infections with different (-)ssRNA viruses (VSV and IAV) and (+)ssRNA viruses (WNV and MHV). Having said this, picornaviruses – by concealing their 5′end with a VpG peptide – can evade IFIT1 recognition (Daffis et al. 2010, Pichlmair et al. 2011, Habjan et al. 2013).

Introduction

The PKR ligands seem to be more diverse compared to IFIT1 ligands. On the one hand, PKR was described to be activated by 5'3p-ssRNA with secondary structures with a minimal length of 47 nt, while a ^{m7}G cap and 3p removal abolished PKR activation (Nallagatla et al. 2007). On the other hand in another study PKR activation was dependent on a 5' and 3' ssRNA tail on a base-paired stem and 5'3p-independent (Mayo et al. 2016). PKR activation causes autophosphorylation and the dimerization of PKR, which subsequently leads to the phosphorylation and inactivation of eukaryotic translation initiation factor 2α (eIF2 α). This not only inhibits the host's cap-dependent protein synthesis, but also the translation of viral RNA and hence viral replication (Levin et al. 1978, Balachandran et al. 2000). PKR, as well as OAS, are also activated by polyI:C. There are four OAS genes in humans, all upregulated by IFN. Three of these genes – OAS1, OAS2 and OAS3 – encode catalytically active proteins and upon RNA binding and activation, lead to the synthesis of 2'-5'-oligomers of adenosine (2'-5´A) from ATP, which function as a second messenger (Hovanessian et al. 1977, Zilberstein et al. 1978) and activate ribonuclease L (RNase L) (Zhou et al. 1993). While the knockout (KO) of OAS1 and OAS2 caused a higher viral load after infection with WNV, Sindbis virus (SINV), IAV, and Vaccinia virus (VACV) in A549 cells, the effect in OAS3 deficient cells was substantially more pronounced (Li et al. 2016). Compared to OAS1 and OAS2, OAS3 also displays a higher affinity for dsRNA. RNase L activation by 2'-5'A subsequently leads to endonucleolytic cleavage and the degradation of long endogenous and viral RNA (Player et al. 1998), thereby blocking viral replication (Hovanessian et al. 1978). Main RNase L targets are 28S rRNA (lordanov et al. 2000) and mRNA (Toots et al. 1988, Brennan-Laun et al. 2014) and, at early time-points of its activation, tRNA (Donovan et al. 2017). One group showed that activation of RNase L with 2'-5'A led to the production of small RNA cleavage products (<200 nt) derived from endogenous cellular RNA (Malathi et al. 2007). These small RNAs induced RIG-I- and MDA5-dependent IFN release. In a follow-up paper they showed that RIG-I binds to HCV genome sequence-derived RNase L cleavage products (Malathi et al. 2010).

Concluding this section, target structures of direct and indirect antiviral receptors are overlapping, and the receptors might work hand in hand to increase antiviral efficiency.

3.10. Aim of the study

RIG-I plays an indispensable role in the detection of many RNA viruses. To prevent the development of harmful diseases, RIG-I has to sensitively and specifically detect viral RNA. This task is especially challenging if one takes into account the excess of endogenous RNA in the cytoplasm where RIG-I is located. RIG-I overactivation can have severe consequences. Indeed, RIG-I activation by endogenous RNA is implicated in autoinflammatory diseases such as Singleton Merten Syndrome (SMS).

This study therefore aimed to investigate how RIG-I is able to differentiate between self and non-self. First, it intended to identify modifications that mark RNAs as self. Second, it planned to investigate which structural features in the RIG-I CTD help to exclude these self RNAs from binding and activating RIG-I.

On the one hand, understanding which viral RNAs activate RIG-I and the immune system, and what escape-strategies viruses use, might help to develop new antiviral therapies. On the other hand, because of its ubiquitous expression, RIG-I is a promising target for immunotherapy. As was made clear in the introduction, the optimal RIG-I ligand is 5′triphosphorylated, blunt-ended and double stranded RNA. However, it was proposed that RIG-I is able to detect long RNAs in a 5′end-independent mechanism. This thesis aimed to characterize RIG-I CTD mutants that are important to detect features of the optimal RIG-I ligand, such as the blunt end and the triphosphate. It intended to generate a panel of HEK Trex Flp-In™ cells expressing either RIG-I WT or RIG-I CTD mutants. This panel could then be used to investigate if there is indeed a 5′end-independent RIG-I activation mechanism and to identify what ligands are detected by RIG-I during a viral infection. Additionally, this thesis aimed to investigate the hypothesis that long RNA has a higher immunostimulatory potential compared to short RNA. Characterizing RIG-I activation mechanisms and its interplay with other PRRs can give helpful insights for the development of new ligands for immunotherapy.

4. Material and methods

4.1. Material

Table 4.1: Equipment

Table 4.1: Equipment				
Equipment	Manufacturer	Headquarter		
384 Well Plate full, Skirted Thin-	BIOplastics	Landgraaf, The Netherlands		
wall	υιομιαστιτο	Lanugraar, The Netherlands		
8-tube strip 0.2 ml	BIOplastics	Landgraaf, The Netherlands		
Amersham nitrocellulose				
western blotting membranes	GE Healthcare	Chalfont St Giles, UK		
(0.45 μm, 0.2 μm)				
Autoclave dx-200	Systec	Linden		
Autoclave vx-150	Systec	Linden		
Automated cell counter TC20™	Bio-Rad	Hercules, USA		
Balance, electronic	Sartorius	Göttingen		
Biometra compact casting system	Analytik Jena	Jena		
Block heater, HX-1	VWR	Radnor, USA		
Blotting equipment	Bio-Rad	Hercules, USA		
Blotting Paper	GE Healthcare	Chalfont St Giles, UK		
C1000 Touch™ Thermal Cycler	Bio-Rad	Hercules, USA		
CanoScan 4400F	Cannon	Hanau		
Cell Counting Slides	Bio-Rad	Hercules, USA		
Cell culture flask (T25, T75, T175)	Sarstedt	Nümbrecht		
Cell strainer (70 µm, nylon)	Corning	Amsterdam, The		
Cell strainer (70 μm, mylon)	Corning	Netherlands		
Centrifuge 5424	Eppendorf	Hamburg		
Centrifuge 5430R	Eppendorf	Hamburg		
Centrifuge 5810R	Eppendorf	Hamburg		
Centrifuge tubes (15 ml, 50 ml)	Greiner Bio-One	Frickenhausen		
Cluster tubes	Corning	Amsterdam, The		
	_	Netherlands		
CO ₂ incubator MCO-20AIC	Sanyo	Osaka, Japan		
Corning® Costar® Stripette®	_			
Serological pipettes (5 ml, 10 ml,	Merck	Darmstadt		
25 ml)				
Cryo tubes	Greiner Bio-One	Frickenhausen		
Digital Gram Scale TE1502S	Sartorius	Göttingen		
Disposable Pipetting Reservoirs	VWR	Radnor, USA		
Disposable standard scalpel	Pfm medical	Cologne		
ED124S analytical balance	Sartorius	Göttingen		
ELISA plates	Thermo Fisher Scientific	Waltham, USA		
EnVision 2104 Multilabel reader	PerkinElmer	Waltham, USA		
Epoch™ Microplate	BioTek	Winooski, USA		
Spectrophotometer		·		
FACS Canto	BD Biosciences	Franklin Lakes, USA		
FiveEasy Plus pH meter	Mettler Toledo	Greifensee, Switzerland		

Material and methods

Flat 8-Cap Strip	BIOplastics	Landgraaf, The Netherlands
Flex Thermocycler	Analytik Jena	Jena
Fluorescence Microscope Ax10	Zeiss	Oberkochen
Freezer (-20°C)	AEG	Frankfurt am Main
Immunofluorescence microscope	Leica Biosystems	Wetzlar
Incubator Shaker Innova™ 42	Thermo Fisher Scientific	Waltham, USA
KIMTECH precision cloths	Kimberly Clark	Irving, USA
Latex gloves	Ansell	Tamworth, UK
LUMITRAC™ 200 microplate, white	Greiner Bio-One	Frickenhausen
MACS Multistand	Miltenyi Biotec	Bergisch Gladbach
Magnetic hotplate stirrer, VMS-A	VWR	Radnor, USA
Magnetic stirrer	Velp Scientific	Usmate, Italy
Microcentrifuge 5415R	Eppendorf	Hamburg
Microcentrifuge, MiniStar silverline	VWR	Radnor, USA
Microlances (30 G, 0.3 x 13 mm)	BD Biosciences	Franklin Lakes, USA
Micropipette tips	Greiner Bio-One	Frickenhausen
Micropipette tips	Mettler-Toledo	Greifensee, Switzerland
Micropipette tips, RNase free	Corning	Amsterdam, The Netherlands
Micropipette tips, with filter	Corning	Amsterdam, The Netherlands
Micropipettes	Eppendorf	Hamburg
Micropipettes Microplates 96-well (flat/ round bottom)	Eppendorf Greiner Bio-One	Hamburg Frickenhausen
Microplates 96-well (flat/ round		
Microplates 96-well (flat/ round bottom)	Greiner Bio-One	Frickenhausen
Microplates 96-well (flat/ round bottom) Microscope Eclipse TS100	Greiner Bio-One Nikon	Frickenhausen Minato, Japan
Microplates 96-well (flat/ round bottom) Microscope Eclipse TS100 Mr. Frosty™ Freezing container MSC-Advantage™ Biological	Greiner Bio-One Nikon Thermo Fisher Scientific	Frickenhausen Minato, Japan Waltham, USA
Microplates 96-well (flat/ round bottom) Microscope Eclipse TS100 Mr. Frosty™ Freezing container MSC-Advantage™ Biological Safety Cabinets	Greiner Bio-One Nikon Thermo Fisher Scientific Thermo Fisher Scientific	Frickenhausen Minato, Japan Waltham, USA Waltham, USA
Microplates 96-well (flat/ round bottom) Microscope Eclipse TS100 Mr. Frosty™ Freezing container MSC-Advantage™ Biological Safety Cabinets Multichannel pipette	Greiner Bio-One Nikon Thermo Fisher Scientific Thermo Fisher Scientific VWR International	Frickenhausen Minato, Japan Waltham, USA Waltham, USA Darmstadt
Microplates 96-well (flat/ round bottom) Microscope Eclipse TS100 Mr. Frosty™ Freezing container MSC-Advantage™ Biological Safety Cabinets Multichannel pipette NanoDrop™ One	Greiner Bio-One Nikon Thermo Fisher Scientific Thermo Fisher Scientific VWR International Thermo Fisher Scientific	Frickenhausen Minato, Japan Waltham, USA Waltham, USA Darmstadt Waltham, USA
Microplates 96-well (flat/ round bottom) Microscope Eclipse TS100 Mr. Frosty™ Freezing container MSC-Advantage™ Biological Safety Cabinets Multichannel pipette NanoDrop™ One Nitril® BestGen®	Greiner Bio-One Nikon Thermo Fisher Scientific Thermo Fisher Scientific VWR International Thermo Fisher Scientific Meditrade	Frickenhausen Minato, Japan Waltham, USA Waltham, USA Darmstadt Waltham, USA Kiefersfelden
Microplates 96-well (flat/ round bottom) Microscope Eclipse TS100 Mr. Frosty™ Freezing container MSC-Advantage™ Biological Safety Cabinets Multichannel pipette NanoDrop™ One Nitril® BestGen® Odyssey® Fc Imaging System	Greiner Bio-One Nikon Thermo Fisher Scientific Thermo Fisher Scientific VWR International Thermo Fisher Scientific Meditrade LI-COR Biotechnology	Frickenhausen Minato, Japan Waltham, USA Waltham, USA Darmstadt Waltham, USA Kiefersfelden Lincoln, USA
Microplates 96-well (flat/ round bottom) Microscope Eclipse TS100 Mr. Frosty™ Freezing container MSC-Advantage™ Biological Safety Cabinets Multichannel pipette NanoDrop™ One Nitril® BestGen® Odyssey® Fc Imaging System Orbital Shaker	Greiner Bio-One Nikon Thermo Fisher Scientific Thermo Fisher Scientific VWR International Thermo Fisher Scientific Meditrade LI-COR Biotechnology NeoLab	Frickenhausen Minato, Japan Waltham, USA Waltham, USA Darmstadt Waltham, USA Kiefersfelden Lincoln, USA Heidelberg
Microplates 96-well (flat/ round bottom) Microscope Eclipse TS100 Mr. Frosty™ Freezing container MSC-Advantage™ Biological Safety Cabinets Multichannel pipette NanoDrop™ One Nitril® BestGen® Odyssey® Fc Imaging System Orbital Shaker Parafilm® M	Greiner Bio-One Nikon Thermo Fisher Scientific Thermo Fisher Scientific VWR International Thermo Fisher Scientific Meditrade LI-COR Biotechnology NeoLab Merck	Frickenhausen Minato, Japan Waltham, USA Waltham, USA Darmstadt Waltham, USA Kiefersfelden Lincoln, USA Heidelberg Darmstadt
Microplates 96-well (flat/ round bottom) Microscope Eclipse TS100 Mr. Frosty™ Freezing container MSC-Advantage™ Biological Safety Cabinets Multichannel pipette NanoDrop™ One Nitril® BestGen® Odyssey® Fc Imaging System Orbital Shaker Parafilm® M PCR SingleCap 8er-SoftStrips	Greiner Bio-One Nikon Thermo Fisher Scientific Thermo Fisher Scientific VWR International Thermo Fisher Scientific Meditrade LI-COR Biotechnology NeoLab Merck Biozym Scientific	Frickenhausen Minato, Japan Waltham, USA Waltham, USA Darmstadt Waltham, USA Kiefersfelden Lincoln, USA Heidelberg Darmstadt Hessisch Oldendorf
Microplates 96-well (flat/ round bottom) Microscope Eclipse TS100 Mr. Frosty™ Freezing container MSC-Advantage™ Biological Safety Cabinets Multichannel pipette NanoDrop™ One Nitril® BestGen® Odyssey® Fc Imaging System Orbital Shaker Parafilm® M PCR SingleCap 8er-SoftStrips PCR tubes (0.2 ml) Peha-soft® nitrile white	Greiner Bio-One Nikon Thermo Fisher Scientific Thermo Fisher Scientific VWR International Thermo Fisher Scientific Meditrade LI-COR Biotechnology NeoLab Merck Biozym Scientific Biozym Scientific	Frickenhausen Minato, Japan Waltham, USA Waltham, USA Darmstadt Waltham, USA Kiefersfelden Lincoln, USA Heidelberg Darmstadt Hessisch Oldendorf Hessisch Oldendorf
Microplates 96-well (flat/ round bottom) Microscope Eclipse TS100 Mr. Frosty™ Freezing container MSC-Advantage™ Biological Safety Cabinets Multichannel pipette NanoDrop™ One Nitril® BestGen® Odyssey® Fc Imaging System Orbital Shaker Parafilm® M PCR SingleCap 8er-SoftStrips PCR tubes (0.2 ml) Peha-soft® nitrile white powderfree	Greiner Bio-One Nikon Thermo Fisher Scientific Thermo Fisher Scientific VWR International Thermo Fisher Scientific Meditrade LI-COR Biotechnology NeoLab Merck Biozym Scientific Biozym Scientific Hartmann	Frickenhausen Minato, Japan Waltham, USA Waltham, USA Darmstadt Waltham, USA Kiefersfelden Lincoln, USA Heidelberg Darmstadt Hessisch Oldendorf Hessisch Oldendorf Heidenheim an der Brenz
Microplates 96-well (flat/ round bottom) Microscope Eclipse TS100 Mr. Frosty™ Freezing container MSC-Advantage™ Biological Safety Cabinets Multichannel pipette NanoDrop™ One Nitril® BestGen® Odyssey® Fc Imaging System Orbital Shaker Parafilm® M PCR SingleCap 8er-SoftStrips PCR tubes (0.2 ml) Peha-soft® nitrile white powderfree Petri dishes (10 cm)	Greiner Bio-One Nikon Thermo Fisher Scientific Thermo Fisher Scientific VWR International Thermo Fisher Scientific Meditrade LI-COR Biotechnology NeoLab Merck Biozym Scientific Biozym Scientific Hartmann Sarstedt	Frickenhausen Minato, Japan Waltham, USA Waltham, USA Darmstadt Waltham, USA Kiefersfelden Lincoln, USA Heidelberg Darmstadt Hessisch Oldendorf Hessisch Oldendorf Heidenheim an der Brenz Nümbrecht
Microplates 96-well (flat/ round bottom) Microscope Eclipse TS100 Mr. Frosty™ Freezing container MSC-Advantage™ Biological Safety Cabinets Multichannel pipette NanoDrop™ One Nitril® BestGen® Odyssey® Fc Imaging System Orbital Shaker Parafilm® M PCR SingleCap 8er-SoftStrips PCR tubes (0.2 ml) Peha-soft® nitrile white powderfree Petri dishes (10 cm) pH meter	Greiner Bio-One Nikon Thermo Fisher Scientific Thermo Fisher Scientific VWR International Thermo Fisher Scientific Meditrade LI-COR Biotechnology NeoLab Merck Biozym Scientific Biozym Scientific Hartmann Sarstedt Hanna instruments	Frickenhausen Minato, Japan Waltham, USA Waltham, USA Darmstadt Waltham, USA Kiefersfelden Lincoln, USA Heidelberg Darmstadt Hessisch Oldendorf Hessisch Oldendorf Heidenheim an der Brenz Nümbrecht Woonsocket, USA
Microplates 96-well (flat/ round bottom) Microscope Eclipse TS100 Mr. Frosty™ Freezing container MSC-Advantage™ Biological Safety Cabinets Multichannel pipette NanoDrop™ One Nitril® BestGen® Odyssey® Fc Imaging System Orbital Shaker Parafilm® M PCR SingleCap 8er-SoftStrips PCR tubes (0.2 ml) Peha-soft® nitrile white powderfree Petri dishes (10 cm) pH meter Pipetboy acu 2	Greiner Bio-One Nikon Thermo Fisher Scientific Thermo Fisher Scientific VWR International Thermo Fisher Scientific Meditrade LI-COR Biotechnology NeoLab Merck Biozym Scientific Biozym Scientific Hartmann Sarstedt Hanna instruments Integra Biosciences	Frickenhausen Minato, Japan Waltham, USA Waltham, USA Darmstadt Waltham, USA Kiefersfelden Lincoln, USA Heidelberg Darmstadt Hessisch Oldendorf Hessisch Oldendorf Heidenheim an der Brenz Nümbrecht Woonsocket, USA Biebertal

Material and methods

qPCR plates	Sarstedt	Nümbrecht
QuantStudio™ 5 Real-Time PCR System	Thermo Fisher Scientific	Waltham, USA
Quick spin oligo columns (mini)	Roche	Basel, Switzerland
Reagent reservoirs	Brand	Wertheim
Roller 10 basic	IKA	Staufen im Breisgau
SDS-gel electrophoresis equipment	Bio-Rad	Hercules, USA
Spin columns	Centic Biotec	Heidelberg
Sterile bench	Thermo Fisher Scientific	Waltham, USA
Syringes (5ml)	BD Biosciences	Franklin Lakes, USA
T100™ Thermal Cycler	Bio-Rad	Hercules, USA
Test tubes (0.5 ml, 1.5 ml, 2ml)	Sarstedt	Nümbrecht
ThermoClean DC	Bioanalytic	Umkirch
Thermocycler	Analytik Jena	Jena
Thermomixer	Eppendorf	Hamburg
Thermomixer comfort	Eppendorf	Hamburg
Tissue culture dish 100	Sarstedt	Nümbrecht
Tissue culture flask T25, T75, T175	Sarstedt	Nümbrecht
Tissue culture test plates	TPP	Trasadingen, Switzerland
TLC glass plates	Merck	Darmstadt
Tube rotator	VWR	Radnor, USA
Ultrasonic Homogenizer	Hielscher	Mount Holly, USA
UV Transilluminator UVT-22 BE LED	Herolab	Wiesloch
UVP UVG-11 compact UV lamp	Thermo Fisher Scientific	Waltham, USA
Vacuum pump	Gardner Denver	Ilmenau
Water bath	Julabo	Seelbach
Waterbath	Memmert	Schwabach
Zirconia beads (1 mm diameter)	Biospec Products	Bartlesville, USA
ZX3 Advanced Vortex Mixer	Velp Scientifica	Usmate, Italy
Zymo-Spin IIICG Columns	Zymo Research	Irvine, USA

Table 4.2: Chemicals

Chemicals	Manufacturer	Headquarter
2-Propanol (≥ 99.5%)	Carl Roth	Karlsruhe
Acetic acid	Carl Roth	Karlsruhe
Aqua	B. Braun	Melsungen
Bacillol® AF	Hartmann	Heidenheim an der Brenz
Chloroform	Carl Roth	Karlsruhe
Coelenterazine native	Synchem UG & Co. KG	Elk Grove Village, USA
cOmplete [™] , Mini, EDTA-free Protease Inhibitor Cocktail	Roche	Basel, Switzerland
D-Luciferin	Synchem UG & Co. KG	Elk Grove Village, USA

Material and methods

Ethanol (≥ 96%, denatured)	Carl Roth	Karlsruhe
Ethanol (≥ 99.5%)	Carl Roth	Karlsruhe
Ethanol (70% (v/v))	Otto Fischar GmbH	Saarbrücken
Glycerol (≥ 99.5%)	Carl Roth	Karlsruhe
Glycogen	Thermo Fisher Scientific	Waltham, USA
NaCl (0.9% [w/v])	Fresenius	Bad Homburg vor der Höhe
PageRuler Plus Prestained Protein Ladder	Thermo Fisher Scientific	Waltham, USA
RNaseZap	Thermo Fisher Scientific	Waltham, USA
Roti-C/I	Carl Roth	Karlsruhe
Roti-Quant 5x Konzentrat	Carl Roth	Karlsruhe
Rotiphorese Gel 30, 37.5:1	Carl Roth	Karlsruhe
Rotiphorese NF-Acrylamid/Bis- Lösung 30% (29:1)	Carl Roth	Karlsruhe
Sodium Pyruvate	Thermo Fisher Scientific	Waltham, USA
TEMED	Carl Roth	Karlsruhe
Tris (1M), pH 7.0	Thermo Fisher Scientific	Waltham, USA
Tris (1M), pH 8.0	Thermo Fisher Scientific	Waltham, USA
Triton X-100	Carl Roth	Karlsruhe
Tween-20	Carl Roth	Karlsruhe
Universal Agarose	VWR	Radnor, USA

Table 4.3: Enzymes and Biological reagents

Enzymes and Biological reagents	Manufacturer	Headquarter
Biocoll cell separation solution	Merck Millipore	Burlington, USA
DreamTaq DNA Polymerase	Thermo Fisher Scientific	Waltham, USA
EvaGreen® QPCR-Mix II (ROX)	Bio-Budget	Krefeld
FastAP Alkaline Phosphatase	Thermo Fisher Scientific	Waltham, USA
FastDigest Restriction Enzymes	Thermo Fisher Scientific	Waltham, USA
GeneRuler 1kb DNA ladder	Thermo Fisher Scientific	Waltham, USA
Gibson Assembly Master Mix	New England Biolabs	Ipswich, USA
Human IFN-1α (IFNβ, recombinant)	Miltenyi Biotec	Bergisch Gladbach
Human IFN-α Module Set	eBioscience	San Diego, USA
IP10 ELISA	BD Biosciences	Franklin Lakes, USA
Lipofectamine™ 2000	Thermo Fisher Scientific	Waltham, USA
Lipofectamine™ RNAiMAX	Thermo Fisher Scientific	Waltham, USA
Page Ruler Prestained Plus	Thermo Fisher Scientific	Waltham, USA
Phusion DNA Polymerase	Thermo Fisher Scientific	Waltham, USA
RevertAid Reverse Transcriptase	Thermo Fisher Scientific	Waltham, USA
RiboLock RNase-Inhibitor	Thermo Fisher Scientific	Waltham, USA
RNA 5´Polyphosphatase	Lucigen	Middleton, USA
ScriptCap 2´O-Methyltransferase	New England Biolabs	Ipswich, USA
ScriptCap m7G Capping System	New England Biolabs	Ipswich, USA
SYBR gold nucleic acid gel stain	Thermo Fisher Scientific	Waltham, USA

T4 DNA Ligase	Thermo Fisher Scientific	Waltham, USA
Terminator Exonuclease	Lucigen	Middleton, USA
TransIT®-LT1	Mirus Bio	Madison, USA
Trypan blue solution 0.4%	Sigma-Aldrich	St. Louis, USA
Ultra Low Range Ladder	Thermo Fisher Scientific	Waltham, USA

Table 4.4: Commercial buffer

Commercial buffers	Manufacturer	Headquarter
ELISA substrate solutions	BD Biosciences	Franklin Lakes, USA
Odyssey Blocking Buffer (PBS)	Li-cor Biosciences	Lincoln, USA
RLT Lysis Buffer	Qiagen	Hilden
RNA Wash Buffer	Zymo Research	Irvine, USA
RWI Wash Buffer	Qiagen	Hilden
TBE buffer (10X)	AppliChem	Darmstadt

Table 4.5: Antibodies

Antibodies	Manufacturer	Headquarter
DYKDDDDK Tag (9A3) Mouse mAb	Cell signaling Technology	Danvers, USA
eIF2alpha (L57A5) Mouse mAb	Cell signaling Technology	Danvers, USA
IRDye 680RD Goat anti-Mouse	Li-cor Biosciences	Lincoln, USA
IRDye 680RD Goat anti-Rabbit	Li-cor Biosciences	Lincoln, USA
IRDye 800CW Goat anti-Mouse	Li-cor Biosciences	Lincoln, USA
IRDye 800CW Goat anti-Rabbit	Li-cor Biosciences	Lincoln, USA
IRF3 (D6I4C) XP (R) Rabbit mAb	Cell signaling Technology	Danvers, USA
MAVS Rabbit Ab	Cell signaling Technology	Danvers, USA
P-eIF2alpha (S51) (D9G8) XP (R) Rabbit mAb	Cell signaling Technology	Danvers, USA
p-IRF-3 (S396) (4D4G) Rabbit mAb	Cell signaling Technology	Danvers, USA
p-TBK1/NAK (S172) (D52C2) XP (R) Rabbit mAb	Cell signaling Technology	Danvers, USA
PKR Rb mAb (Y117)	Abcam	Cambridge, UK
pPKR Rb mAb (E120)	Abcam	Cambridge, UK
RIG-I (D14G6) Rabbit mAb	Cell signaling Technology	Danvers, USA
TBK1/NAK (D1B4) Rabbit mAb	Cell signaling Technology	Danvers, USA
β-actin Mouse mAb	Li-cor Biosciences	Lincoln, USA
β-actin Rabbit mAb	Li-cor Biosciences	Lincoln, USA

Table 4.6: Kits

Kit	Manufacturer	Headquarter
innuPREP Gel Extraction Kit	Analytik Jena	Jena
innuPREP PCRpure Kit	Analytik Jena	Jena
NucleoSpin Plasmid - Miniprep	Macherey-Nagel	Düren

Kit		
NucleoSpin® Gel and PCR Clean- Up	Macherey-Nagel	Düren
NucleoTrap mRNA Kit	Macherey-Nagel	Düren
Pierce BCA Protein Assay Kit	Thermo Fisher Scientific	Waltham, USA
PureLink HiPure Plasmid Filter Maxiprep Kit	Thermo Fisher Scientific	Waltham, USA
PureLink HiPure Plasmid Filter Midiprep Kit	Thermo Fisher Scientific	Waltham, USA
Ribominus™ Human/Mouse Transcriptome Isolation Kit	Thermo Fisher Scientific	Waltham, USA
TranscriptAid™ T7 High Yield Transcription Kit	Thermo Fisher Scientific	Waltham, USA

Table 4.7: Bacteria

Strain	Genotype
DH10β	F– mcrA Δ(mrr-hsdRMS-mcrBC) φ80lacZ Δ M15 ΔlacX74 recA1 endA1 araD139 Δ(ara leu)7697 galU galK λ-rpsL nupG λ-, Invitrogen
Stbl3	F— mcrB mrr hsdS20 (rB—, mB—) recA13 supE44 ara-14 galK2 lacY1 proA2 rpsL20 (StrR) xyl-5 λ— leu mtl-1, Invitrogen

Table 4.8: Cell culture substances

Cell culture substances	Manufacturer	Headquarter
Blasticidin solution	InvivoGen	San Diego, USA
Dimethylsulfoxide (DMSO)	Carl Roth	Karlsruhe
Gibco® DMEM	Thermo Fisher Scientific	Waltham, USA
Gibco® DPBS	Thermo Fisher Scientific	Waltham, USA
Gibco® EDTA (0.5M, pH 8.0)	Thermo Fisher Scientific	Waltham, USA
Gibco® Fetal calf serum	Thermo Fisher Scientific	Waltham, USA
Gibco® Non-essential Amino Acids solution (100X)	Thermo Fisher Scientific	Waltham, USA
Gibco® Opti-MEM™ Reduced Serum Medium	Thermo Fisher Scientific	Waltham, USA
Gibco® Penicillin-Streptomycin	Thermo Fisher Scientific	Waltham, USA
Gibco® RPMI-1640	Thermo Fisher Scientific	Waltham, USA
Gibco® Sodium Pyruvate (100x)	Thermo Fisher Scientific	Waltham, USA
Gibco® Trypsin-EDTA (0.25%)	Thermo Fisher Scientific	Waltham, USA
Hygromycin B Gold solution	InvivoGen	San Diego, USA
Puromycin solution	InvivoGen	San Diego, USA
Zeocin solution	InvivoGen	San Diego, USA

Table 4.9: Cell lines

Cell lines	Manufacturer	Headquarter
HEK Flp-In™ Trex 293	Thermo Fisher Scientific	Waltham, USA
HEK293FT	Thermo Fisher Scientific	Waltham, USA
HEK-Blue™ IFN-α/β	InvivoGen	San Diego, USA
Thp1-Dual™	InvivoGen	San Diego, USA

4.1.1. Oligonucleotides

All DNA oligonucleotides and random hexamer primers were ordered from IDT (Coralville, USA). RNA oligonucleotides were ordered from Biomers (Ulm). CMTR1 siRNAs were ordered from Thermo Fisher Scientific (Waltham, USA). All other siRNAs were ordered from Biomers (Ulm). siRNA sequences are listed in Table 4.10 and qPCR primer sequences are listed in Table 4.11. Yeast tRNA was ordered from Thermo Fisher Scientific (Waltham, USA).

Table 4.10: siRNA sequences

siRNA	Sense	Antisense
SUV3 A	UGGCUAAGCUACCGAUUUA	UAAAUCGGUAGCUUAGCCA
SUV3 B	GUAAGGAUGAUCUACGUAA	UUACGUAGAUCAUCCUUAC
PNPT1 A	GACAGAAGUAGUAUUGUAA	UUACAAUACUACUUCUGUC
PNPT1 B	GAAUGUAAGUUGUGAGGUA	UACCUCACAACUUACAUUC
Ctrl Luc	GAUUAUGUCCGGUUAUGUAUU	AAUACAUAACCGGACAUAAUC
XRN-1 A	AGAUGAACUUACCGUAGAA	UCUUAGUAUAUCCAGGUAC
XRN-1 B	GUACCUGGAUAUACUAAGA	GGCUACGUCCAGGAGCGCA
Ctrl GFP	UGCGCUCCUGGACGUAGCC	UUCUACGGUAAGUUCAUCU
CMTR1 A	UUUAAGGGAUUGUGCUAUA	UAUAGCACAAUCCCUUAAA
CMTR1 B	GCACACUGCUUUCACUAAU	AUUAGUGAAAGCAGUGUGC

Table 4.11: qPCR primer sequences

Table 4.11. qr CK primer sequences			
Gene	Fwd primer	Rev primer	
GAPDH	AAGGTGAAGGTCGGAGTCAA	AATGAAGGGTCATTGATGG	
DDx58	GAAAGACTTCTTCAGCAATGTCC	GTTCCTGCAGCTTTTCTTCAA	
IFIT1	TCCACAAGACAGAATAGCCAGAT	GCTCCAGACTATCCTTGACCTG	
XRN1	TCCAACTGTATCACACCAGGA	GCTTTGCTTTCTCGGATCTGA	
CXCL10	GAATGCTCTTTACTTCATGGACTTC	GGTAGCCACTGAAAGAATTTGG	
ND1	CCCTACTTCTAACCTCCCTGTTCTTAT	CATAGGAGGTGTATGAGTTGGTCGTA	
ND5	ATTTTATTTCTCCAACATACTCGGATT	GGGCAGGTTTTGGCTCGTA	
ND6	CCAATAGGATCCTCCCGAAT	AGGTAGGATTGGTGCTGTGG	
COX	ACGTTGTAGCCCACTTCCAC	TGGCGTAGGTTTGGTCTAGG	
MYC	AAAGGCCCCCAAGGTAGTTA	GCACAAGAGTTCCGTAGCTG	
SUV3	TGCTGATTATGGACTTGATGCTC	CCACATCCAGGGAATGAGACT	
PNPase	GCGAGCACTATGGAGTAGCG	GCAGTGTCACCTGACTGTACTA	
18S rRNA	AGTCGGAGGTTCGAAGACGAT	GCGGGTCATGGGAATAACG	

CMTR1	CGAAGTTCTTTGAGCTAATCCAG	CAGCGGTAGTCAAACACAGG
IFN-β	CATTACCTGAAGGCCAAGGA	CAGCATCTGCTGGTTGAAGA
DHX58	CAGTTTTGGATTCTCTGGGC	AAAACCCAGATCCTGTGTGC
DDX60	CCTCAGGGAGATCATCAAGG	TGGCACATCTCTTTGGAAGAA

4.1.2. Plasmids

Table 4.12: Plasmid

Plasmid	Туре	Plasmid Origin
pEF-BOS RIG-I WT	RIG-I expression plasmid with C-terminal FLAG- and His-tag	Prof. Veit Hornung
pEF-BOS RIG-I F853A pEF-BOS RIG-I K861A pEF-BOS RIG-I H830A	RIG-I expression plasmid with C-terminal FLAG- and His-tag and indicated point-mutation	Dr. Christine Schuberth- Wagner
pEF-BOS RIG-I 1875A	RIG-I expression plasmid with C-terminal FLAG- and His-tag and indicated point-mutation	This thesis
pIFN-β –Gluc	Reporter plasmid, Gaussia luciferase expression under the control of the IFN-β promoter	Prof. Veit Hornung
pEF1α –Fluc	Reporter plasmid, Firefly luciferase expression under the control of the EF1 α promoter	Dr. Thomas Zillinger
pcDNA™5/FRT	Expression vector, used for generation of stable Flp-In™ expression cell lines	Thermo Fisher Scientific, modified by Steven Wolter
pcDNA™5/FRT RIG-I WT	RIG-I expression vector, used for generation of stable Flp-In™ expression cell lines	This thesis
pcDNA™5/FRT RIG-I F853A pcDNA™5/FRT RIG-I K861A pcDNA™5/FRT RIG-I H830A pcDNA™5/FRT RIG-I I875A	RIG-I expression vector, used for generation of stable Flp-In [™] expression cell lines with indicated point-mutations	This thesis
pcDNA™5/FRT RIG-I WT Are pcDNA™5/FRT RIG-I F853A Are pcDNA™5/FRT RIG-I K861A Are pcDNA™5/FRT RIG-I H830A Are pcDNA™5/FRT RIG-I I875A Are	RIG-I expression vector, used for generation of stable Flp-In™ expression cell lines, WT or with indicated pointmutations, with Are site	This thesis
pOG44	Expression plasmid for Flp recombinase, used for generation of stable Flp-In™ expression cell lines	Thermo Fisher Scientific

4.1.3. Buffers and solutions

4.1.3.1. General buffers

10x TBS	
Tris, pH 7.6	0.1 M
NaCl	1.5 M

10x PBS		
NaCl	1.5 M	
Na ₂ HPO ₄	100 mM	
KH ₂ PO ₄	O ₄ 180 mM	
KCl	25 mM	

50x TAE buffer	
Tris	2 M
EDTA	50 mM
Acetic acid	5.71% (w/v)

RIG-I binding buffer	
Hepes pH 7.4 100 mM	
MgCl ₂	30 mM
Glycerin 50%	
DTT	10 mM

Luria bertani (LB)-Medium	
Bacto-Trypton 1%	
Yeast extract	0.5%
NaCl	10 g/l

pH 7.0, Storage 4°C

TB-buffer	
KCI	18.65 g
CaCl ₂	2.2 g
PIPES 0.5 M 20 ml	
H ₂ O	Ad 800 ml

pH 6.7

Gradually add: MnCl_{2:} 10.88g

 H_2O ad 1 l

1x TBS-T	
TBS	1x
Tween-20	0.1% (w/v)

1x PBS-T	
PBS	1x
Tween-20	0.05% (w/v)

Gel extraction buffer	
Ammonium acetate	0.5 M
EDTA-NaOH pH8	1 mM

Protein buffer	
Tris-HCl, pH 7.5	20 mM
NaCl	50 mM
DTT	1 mM

LB-Agar-Plates	
Bacto-Trypton	1%
Yeast extract	0.5%
NaCl	10 g/l
Agar	1.5%

Storage 4°C

DNA lysis buffer	
Tris-HCl pH 7.5	50 mM
EDTA	1 mM
NaCl	150 mM
Glycerol	10% (w/v)
Triton-X-100	0.3% (w/v)
Natriumorthovanadat	0.5 mM

Storage 4°C

Phosphatase-Inhibitor-Cocktail 1x cOmplete Protease inhibitor 1x

Storage -20°C

10x Annealing buffer	
Tris pH 7.4	250 mM
NaCl	250 mM

10x Tris-Glycin	
Tris	2.9% (w/v)
Glycin	14.4% (w/v)

Storage 4°C

4.1.3.2. Western Blot buffers

Blocking buffer A		
BSA		0.5% (w/v) in TBST

RIPA buffer	
Tris pH 8.0	50 mM
NaCl	150 mM
Triton-X-100	1% (v/v)
Sodium deoxycholate	0.5% (w/v)
SDS	0.1% (w/v)
Protease inhibitor mix	1x

Storage 4°C

Ponceau staining solution	
Ponceau	0.1% (w/v)
Acetic acid	3% (v/v)

10x Electrophoresis buffer	
Tris	24 mM
Glycin	192 mM
SDS	0.1% (w/v)

4.1.3.3. ELISA buffers

ELISA coating buffer (IP10)	
NaHCO ₃	100 mM
Na ₂ CO ₃	33.6 mM
in DRS nH Q 5	

in PBS, pH 9.5 Storage 4°C

Blocking buffer B	
1\/111K 1\(1\\\\/111\)	5% (w/v) in TBST or PBST

2x Lämmli buffer		
Tris pH 6.8	120 mM	
SDS	4% (w/v)	
Glycerol	20% (v/v)	
DTT	20 mM	
Orange G		

Storage -20°C

1x Transfer buffer	
Tris	24 mM
Glycin	192 mM
Ethanol denatured	20% (w/v)
CI 40C	

Storage 4°C

ELISA assay buffer (IP10)	
FCS	10%
PenStrep	1%

in PBS Storage 4°C

ELISA wash buffer	
Tween-20	0.05% (v/v)
in PBS	
Storage 4°C	

ELISA assay buffer (IFN-α)		
BSA	0.5%	
Tween-20	0.05% (v/v)	
in PBS		
Storage 4°C		

4.1.3.4. Acrylamide gels

Native PAGE (15%)		
Acrylamide	7.5 ml	
1x TBE buffer	1.5 ml	
H ₂ O	5.85 ml	
10% APS	150 μΙ	
TEMED	15 μΙ	

Denaturing PAGE (12%)		
Acrylamide	6 ml	
10x TBE buffer	1.5 ml	
Urea	7.2 g	
H ₂ O	1.57 ml	
10% APS	150 μΙ	
TEMED	15 μl	

SDS acrylamide running gel (10%)		
H ₂ O 2.71 ml		
1 M Tris, pH8.8	3.75 ml	
Acrylamide	3.33 ml	
10% SDS	100 μΙ	
10% APS	100 μΙ	
TEMED	8 μΙ	

SDS-acrylamide stacking gel (3%)		
H ₂ O 2.64 ml		
1 M Tris, pH6.8	440 μΙ	
Acrylamide	350 μΙ	
10% SDS	35 μΙ	
10% APS	35 μΙ	
TEMED	3.5 μΙ	

4.2. Methods

4.2.1. Molecular biology

4.2.1.1. Production of chemocompetent bacteria

Chemocompetent E.coli bacteria of the strain Stbl3 or DH10 β were grown on a LB-agar plate overnight at 37°C. The following day 200 ml LB medium was inoculated with several colonies from this LB-agar plate and then incubated at 200 rpm at RT until an OD₆₀₀ of 0.6 was determined via photometric measurement with the Nanodrop. The subsequent procedure was performed with ice cold buffers, consumables and bacteria. The bacterial solution was divided into four 50 ml falcons. After centrifugation of the bacterial solution at 4°C and 3000 rpm, the supernatant was discarded and the bacterial pellets were resuspended with 5 ml TB-buffer. Two falcons were pooled and 40 ml TB-buffer were added. After 10 min of incubation on ice, samples were centrifuged at 4°C and 3000 rpm for 10 min. The supernatant was discarded and the pellet was resuspended in TB-freezing buffer (10 ml TB-supernatant was discarded and the pellet was resuspended in TB-freezing buffer (10 ml TB-supernatant was discarded and the pellet was resuspended in TB-freezing buffer (10 ml TB-supernatant was discarded and the pellet was resuspended in TB-freezing buffer (10 ml TB-supernatant was discarded and the pellet was resuspended in TB-freezing buffer (10 ml TB-supernatant was discarded and the pellet was resuspended in TB-freezing buffer (10 ml TB-supernatant was discarded and the pellet was resuspended in TB-freezing buffer (10 ml TB-supernatant was discarded and the pellet was resuspended in TB-freezing buffer (10 ml TB-supernatant was discarded and the pellet was resuspended in TB-freezing buffer (10 ml TB-supernatant was discarded and the pellet was resuspended in TB-freezing buffer (10 ml TB-supernatant was discarded and the pellet was resuspended in TB-freezing buffer (10 ml TB-supernatant was discarded and the pellet was resuspended in TB-freezing buffer (10 ml TB-supernatant was discarded and the pellet was resuspended in TB-supernatant was discarded and the pellet was resuspended in TB-supernatant was discarded and the pellet was resuspended in

Puffer + 0.8 ml DMSO) and incubated on ice for 10 min. The solution was aliquoted in 0.5 ml eppendorf-tubes and immediately shock frozen in liquid nitrogen. The chemocompetent bacteria were stored at -80°C. To test for efficient chemocompetency, 50 μ l of the bacteria were transformed with 10 pg of the plasmid pUC19. 10 μ l of transformed bacteria solution were streaked on an ampicillin-containing agar-plate and incubated overnight at 37°C. The following day visible colonies were counted. Each colony accounts for 10 7 cfu/ μ g DNA.

4.2.1.2. Plasmid DNA purification

Mini preparation

For amplification and purification of plasmid DNA, 1.5 ml of LB medium containing the appropriate antibiotic was inoculated with one bacterial colony and cultivated overnight at 37°C and 1000 rpm on a thermocycler. The purification was performed with the NucleoSpin[®] Plasmid Kit according to the manufacturer's instructions. Shortly afterwards, cultivated bacteria were harvested by centrifugation at 11000 rcf for 30 sec. To lyse cells supernatant was discarded and the pellet was thoroughly resuspended in $250~\mu$ l buffer A1 containing RNase. $250~\mu$ l of buffer A2 were added and the solution was mixed gently by inverting the tube. After 5 min incubation at RT, cell lysis was stopped by adding $300~\mu$ l buffer A3. Clarification of the lysate was performed by centrifugation at 11000~rcf for 10~min at RT. The supernatant was loaded onto at column. Flow-through was discarded after centrifugation at 11000~rcf for 1~min. The column was washed with $500~\mu$ l buffer AW and $600~\mu$ l buffer A4, and dried by centrifugation at full speed for 2~min. Elution of the DNA was performed by adding $50~\mu$ l H₂O and centrifugation for 1~min at 11000~rcf. Concentration and purity were determined using the NanoDrop One.

Midi and Maxi preparation

If a higher amount of plasmid DNA was needed, Midi or Maxi preparations were performed. For this the PureLinkTM HiPure Plasmid Midiprep or Maxiprep kit was used. All steps were performed according to the manufacturer's protocol. LB medium containing the appropriate antibiotic was inoculated with one bacterial colony overnight. The next day cells were sedimented by centrifugation at 4000 rcf for 10 min. The supernatant was discarded and cells were resuspended in buffer R3 and lysed by addition of buffer L7. After gentle mixing and incubation at RT for 1 min, precipitation buffer N3 was added. Subsequently, the lysate was loaded onto an equilibrated column and allowed to drain by gravity flow. After two washing steps, the DNA was eluted with buffer E4. The flow-through was collected in a new

tube. DNA was precipitated with isopropanol and centrifugation at 12000 rcf at 4°C for 30 min. The DNA pellet was washed with 70% ethanol and air-dried at RT for 10 min. The pellet was resuspended in H_2O and DNA quality and concentration was measured using the NanoDrop One.

4.2.1.3. Polymerase chain reaction (PCR)

PCR was used to produce DNA-fragments for cloning, for analytical purposes such as colony PCR, or to obtain template DNA for IVT. While Phusion polymerase was used for cloning and the production of template DNA for IVT, DreamTaq polymerase was used to check for correct sequence and cloning. The general PCR conditions for Phusion PCR and DreamTaq PCR are depicted in Table 4.13 and Table 4.14.

Table 4.13: Phusion PCR program

Phusion	Temperature	Time
Initial denaturation	98°C	30 sec
A manalification	98°C	10 sec
Amplification	Primer dependent	30 sec
(35x)	72°C	30 sec/kb
Final extension	72°C	5 min
Hold	4°C	∞

Table 4.14: DreamTaq PCR program

DreamTaq	Temperature	Time
Initial denaturation	95°C	1 min
A : f: + :	95°C	30 sec
Amplification	Primer dependent	30 sec
(35x)	72°C	60 sec/kb
Final extension	72°C	5 min
Hold	4°C	∞

Colony PCR

Colony PCR was performed to check if a bacterial colony contains the desired plasmid without the need to perform mini preparations and sequencing. 15 μ l of a PCR reaction mix (DreamTaq) were inoculated with bacteria of one E.coli colony. PCR was carried out with appropriate primers and positive clones were visualized on an agarose gel.

Mutagenesis PCR

To introduce point mutations into a plasmid mutagenesis PCR was performed. The new desired sequence is introduced via specifically designed primers. Subsequently, the mutated PCR products were cloned into the appropriate backbone via gibson assembly and transformed into bacteria. Correct sequence was controlled via mini preparation and subsequent Sanger sequencing.

IVT template PCR

Linearized plasmid, a PCR product or synthetic DNA oligonucleotides were used as a template for IVT. For IVT with T7 polymerase all template DNAs have to contain a double-stranded T7 promoter region. For PCR templates the T7 promoter sequence was introduced via the primers.

4.2.2. Cloning

4.2.2.1. Preparation of the vector backbone

The vector was opened by digestion with FastDigest restriction enzymes in 1x FastDigest buffer at 37°C for 30 min. The backbone was purified via agarose gel electrophoresis and subsequent gel extraction with the innuPREP Gel Extraction Kit according to the manufacturer's instructions.

4.2.2.2. Preparation of the insert

The insert was produced with Phusion PCR. The correct size of the PCR product was verified via agarose gel electrophoresis and the PCR product was isolated from the gel using the innuPREP Gel Extraction Kit according to the manufacturer's instructions. In other cases, the insert was obtained by cutting it from a plasmid with restriction enzymes compatible with the prepared backbone.

4.2.2.3. Assembly of the backbone and the insert

Classic ligation

For classic ligation of an insert into a backbone, the purified PCR product was digested with the according restriction enzymes and purified via agarose gel electrophoresis and subsequent gel extraction. Ligation of the backbone and the insert were performed with T4 ligase at RT for 1 h in 1x T4 ligase buffer. Subsequently, 5 μ l of the ligation mix were transformed into chemocompetent bacteria.

Gibson assembly

Gibson assembly was used to join a backbone with one or several inserts containing homologous ends. Homologous ends on the inserts were introduced via PCR. Inserts and backbone were mixed in a ratio of 3:1, 5 μ l gibson assembly master mix was added and the reaction mix was incubated at 50°C for 1 h. 2.5 μ l of the mix was used for transformation into chemocompetent bacteria.

4.2.2.4. Transformation of chemocompetent bacteria

Chemocompetent bacteria of the strain Stbl3 or DH10 β were transformed with ligation mix (5 µl), gibson assembly mix (2.5 µl) or 100 ng plasmid DNA for retransformation. DNA was added to ice cold bacteria and incubated on ice for 20 min. After heat shock at 42°C for 45 sec and another 5-10 min incubation on ice, 1 ml of LB medium was added and the bacteria were incubated at 800 rpm at 37°C on a thermocycler for 1 h. The bacteria-LB solution was centrifuged for 2 min at 1000 rpm and 1 ml of supernatant was discarded. The bacterial pellet was resuspended in the remaining LB medium and plated on LB-agar plates containing the appropriate antibiotic. The LB-agar plate was incubated at 37°C overnight. To check for correct assembly of insert and backbone, either a colony PCR or a mini preparation with subsequent Sanger sequencing was performed.

4.2.3. Nucleic acid preparation

4.2.3.1. RNA extraction using spin columns

Cells were directly lysed in culture test plates by resuspension in 150 μ l RLT buffer per 24-well and freezing at -80°C for at least 10 min. Following the addition of 150 μ l 70% ethanol, the solution was loaded onto spin columns placed in 2 ml test tubes. Flow-through was discarded after centrifugation at 10000 rpm for 1 min. Columns were washed with 350 μ l RW1 buffer and Zymo RNA wash buffer and dried by centrifugation for 2 min at full speed. Elution was performed by addition of 30-50 μ l H₂O, incubation for 2 min and subsequent centrifugation at 10000 rpm for 1 min. RNA concentration and purity was determined by photometric measurement using the NanoDrop One.

In case a DNase I digestion was needed for subsequent applications, this was performed on the column after the Zymo RNA wash buffer step. 5 μ l DNase I, 8 μ l DNase I buffer, 3 μ l H₂O and 64 μ l Zymo RNA wash buffer were mixed and added to the column. Following incubation at RT for 30 min, a washing step with 400 μ l Zymo RNA wash buffer was performed. Subsequently, the column was dried and RNA was eluted as described above.

4.2.3.2. RNA extraction using TRIzol reagent

Not more than $1x\ 10^7$ cells were directly lysed in culture test plates by resuspension in 1 ml TRIzol. After incubation at RT for 5 min, 200 μ l chloroform:isoamylalcohol 24:1 per 1 ml TRIzol were added. The sample was mixed vigorously for 20 sec and incubated at RT for 5 min. Following 15 min centrifugation at 4°C and full speed, the upper aqueous phase

containing the RNA was transferred to a new tube. The aqueous phase was mixed with 0.1 volume 3 M NaAc pH 5.2, 1 μ l glycogen (20 mg/ml) and 1 ml 99% EtOH or 500 μ l isopropanol. Prior to RNA precipitation via centrifugation at 4°C for 30 min at full speed, samples were incubated at -80°C for 15 min. The supernatant was removed and the RNA pellet was washed twice with 75% EtOH (centrifugation, full speed, 5 min, 4°C). Removal of residual ethanol was performed by air-drying for 5-10 min. The RNA was resuspended in H₂O. RNA concentration and purity was determined by photometric measurement using the NanoDrop One.

4.2.3.3. RNA extraction from polyacrylamide gels

To purify RNA after IVT, RNA was run on a denaturing polyacrylamide gel. To visualize the RNA, UV shattering was used and RNA of the correct size was excised and placed into a 0.5 ml eppendorf tube. To shatter the gel piece containing the RNA, it was centrifuged from a 0.5 ml eppendorf tube containing a hole (introduced using a syringe) into a 2 ml eppendorf tube. Afterwards, 0.7 ml gel extraction buffer was added and the gel was incubated overnight at 4°C while rotating. The next day 1 ml TRIzol reagent was added and the RNA was extracted according to the protocol (4.2.3.2).

4.2.3.4. polyA RNA extraction

Purification of polyA RNA from whole cell RNA (extracted using TRIzol) was performed with the NucleoTrap® mRNA Kit according to the manufacturer's instructions. RNA was incubated with oligo(dT) latex beads at 68°C for 5 min. After 10 min incubation at RT, the beads were pelleted by centrifugation for 15 sec at 2000 rcf and 2 min at 11000 rcf. The polyA⁻ RNA fraction was extracted from the supernatant using TRIzol. The pellet containing the beads were resuspended in buffer RM2 and transferred into the NucleoTrap Microfilter. Following two washing steps with buffer RM3, beads were dried via centrifugation for 1 min at 11000 rcf. polyA⁺ RNA was eluted by resuspension of the beads in pre-warmed H₂O (68°C), incubation at 68°C for 7 min and subsequent centrifugation for 1 min at 11000 rcf. RNA concentration and purity was determined by photometric measurement using the NanoDrop One.

4.2.3.5. rRNA extraction

rRNA was extracted from whole cell RNA extracts using the RiboMinus™ Kit or by excision and extraction of the 18S and 28S RNA bands from an agarose gel.

Extraction with the RiboMinus[™] Kit was performed according to the manufacturer's instructions. Afterwards, total RNA was mixed with hybridization buffer and RiboMinus[™] probe and incubated for 5 min at 50°C. Samples were slowly cooled to 37°C. RiboMinus[™] Magnetic Beads were prepared by washing with H₂O and hybridization buffer. The cooled RNA sample was mixed with the prepared magnetic beads and incubated at 37°C for 15 min. The tube containing the mix was placed on a magnetic stand for 1 min to pellet the rRNA-probe complex. The supernatant contained the rRNA-fraction. The rRNA-fraction was isolated using columns while the rRNA+fraction was isolated from the beads using TRIzol extraction. The RNA concentration of both fractions was determined using the NanoDrop One.

To extract rRNA using gel electrophoresis, whole cell RNA extracts were run on a 1% agarose gel in RNase free conditions. RNA bands according to the size of the 18S and 28S rRNA were cut from the agarose gel and extraction was performed using the NucleoSpin® Gel and PCR Clean-Up Kit. The extraction was performed according to the manufacturer's protocol for RNA extractions from agarose gels using the buffer NTC. Shortly afterwards, the gel slice containing the RNA was solubilized by incubation in buffer NTC at 50°C for 5 min. The solubilized sample was loaded onto a column. After several centrifugation and washing steps, RNA was eluted in NE buffer by centrifugation for 1 min at 11000 rcf. RNA concentration and purity was determined by photometric measurement using the NanoDrop One.

4.2.3.6. cDNA synthesis

cDNA synthesis was performed using Revert Aid reverse transcriptase. Within one experiment the same RNA amount (maximal 1 μ g) was used for cDNA synthesis for all samples. If necessary, the RNA was prediluted in H₂0 to a final volume of 5.75 μ l. Per sample 2 μ l 5x reaction buffer, 1 μ l dNTPs (each 10 mM), 0.5 μ l random hexamer primer (100 μ M), 0.5 μ l RevertAid reverse transcriptase (200 U/ μ l) and 0.25 μ l RiboLock RNase inhibitor (40 U/ μ l) were added and mixed. cDNA synthesis was performed in a thermocycler with the following program: 25°C for 10 min, 42°C for 60 min, 85°C for 5 min and cooling to 4°C. 30 μ l H2O were added to each sample, and the samples were either directly used for qPCR or stored at -20°C.

4.2.3.7. Quantitative polymerase chain reaction (qPCR)

qPCR was performed using my-Budget 5x EvaGreen® QPCR-Mix II (ROX). EvaGreen intercalates in dsDNA and the resulting DNA-EvaGreen complex emits light. The fluorescent

signal of EvaGreen is recorded after each amplification step and is proportional to the DNA concentration in the sample. For correct quantification, it is essential that the PCR results only in one product and that there are no side products. To exclude this, a dissociation curve analysis was performed after the amplification reaction. Only primers that resulted in a single peak (for a single specific PCR product) in the melting curve analysis were used for qPCR, therefore excluding target-unspecific amplification or primer dimerization. Furthermore, primer efficiency was tested beforehand and only primer pairs with an efficiency between 1.9 and 2.1 were used. Per sample 2 μ l 5x EvaGreen® QPCR-Mix were mixed with 5.4 μ l H₂O and 0.6 μ l primer mix (containing forward and reverse primer, each 5 μ M). This mix was pipetted in a qPCR 384-well plate and 2 μ l cDNA was added. The plate was sealed with an adhesive and optically clear foil. The PCR reaction was performed with a QuantStuido 5. The thermal profile was as follows:

Table 4.15: qPCR program

qPCR	Temperature	Time
Initial denaturation	95°C	15 min
Amplification	95°C	15 sec
	60°C	20 sec
(40x)	72°C	20 sec
Final extension	54°C	30 sec
Dissociation curve	95°C	15 sec

Unless stated otherwise, target mRNA expression was normalized to a housekeeping gene according to $2^{CtR}/2^{CtT}$ (Ct = cycle threshold, R = reference gene, T = target gene).

4.2.3.8. IVT

Either a PCR product, a synthetic DNA or a restriction-digested plasmid was used as a template for in vitro transcription. It is important to note that the primers used for amplification of the DNA introduced a T7 promoter sequence at the 5′end. The PCR product was checked via agarose gel electrophoresis for correct size and was purified using the innuPREP Gel extraction kit. Since a double-stranded template is needed for efficient in vitro transcription, the ordered synthetic ssDNA was annealed beforehand with a complementary antisense DNA. The RNA synthesis was performed using the TranscriptAid™ T7 High Yield Transcription Kit according to the manufacturer's instructions. A DNase I (37°C, 15 min) digestion was included to remove the template DNA from the mix. Afterwards the RNA was

purified via TRIzol extraction and the correct size of the product was checked on a denaturing polyacrylamide gel.

4.2.3.9. Enzyme treatment

Alkaline Phosphatase (AP)

AP removes phosphate groups from DNA, RNA and nucleotides and leaves a hydroxyl group. FastAP (Thermo Scientific) was used to remove 5′ phosphates from RNA samples to generate 5′OH-RNA. 0.25 μ g RNA was incubated with 0.1 volume 10x FastAP reaction buffer and 1 μ l (1 U) FastAP for 30 min at 37°C.

Polyphosphatase (PP)

RNA 5´Polyphosphatse sequentially removes the γ - and β - phosphates from 5´3p- and 5´2p-RNA and leaves a 5´p on the RNA. 5 μ g RNA was incubated with 0.1 volume RNA 5´Polyphosphatase 10X reaction buffer and 1 μ l (20U) RNA 5´Polyphosphatase for 30 min at 37°C.

Terminator Exonuclease (TE)

Terminator[™] 5′- Phosphate-Dependent Exonuclease treatment was performed to remove 5′p-RNA from an RNA pool. The enzyme is a processive 5′-> 3′ exonuclease that specifically digests RNA having a 5′p. 5 μ g RNA was incubated with 0.1 volume Terminator 10x reaction buffer A and 1 μ l (1 U) Terminator Exonuclease for 30 min at 30°C.

Capping and N1-2'O-methylation

All IVT transcribed RNA possess a 3´p. A cap0 structure can be introduced using the vaccinia capping system. To generate cap1-RNA, N1-methylation was introduced simultaneously with the m7 G-cap in a one-step capping and 2´O-methylation reaction. For both methods 10 µg RNA were mixed with H_2O to a final volume of 15 µl. The mix was incubated at 65°C for 5 min and subsequently placed 5 min on ice.

Cap0

RNA was mixed with 2 μ l capping buffer (10x), 1 μ l GTP (10 mM), 1 μ l SAM (2 mM) and 1 μ l vaccinia capping enzyme (10 U/ μ l). The mix was incubated at 37°C for 30 min.

Cap1

RNA was mixed with 2 μ l capping buffer (10x), 1 μ l GTP (10 mM), 1 μ l SAM (4 mM), 1 μ l vaccinia capping enzyme (10 U/ μ l) and 1 μ l mRNA cap 2´O-methyltransferase (50 U/ μ l). The mix was incubated at 37°C for 60 min for RNAs longer than 200 nt, and 120 min for RNAs shorter than 200 nt.

4.2.3.10. Annealing of two single-stranded nucleic acids

Hybridization of two nucleic acids was performed by mixing the same molar amounts of each nucleic strand and adding 0.1 volume of 10x annealing buffer. The single stranded-nucleic acids were first denatured for 5 min at 72°C and then slowly cooled down (1°C/min) to 18°C and subsequent cooled at 4°C until the RNA was used. siRNAs were annealed without annealing buffer.

4.2.4. Polyacrylamide gel electrophoresis (PAGE) of nucleic acids

Analysis of RNA oligonucleotides was performed either with native or denaturing PAGE. The percentage of gel was chosen according to RNA size. The gel was put into a running chamber filled with 1x TBE-buffer after polymerization. 10x loading buffer for native gels was as follows: 30% (v/v) Glycerol, 0.05% (w/v) Orange G. Denaturing gels were pre run without samples for 20 min at 120 V. Denaturing loading buffer was added to samples for denaturing PAGE. Samples were incubated for 10 min at 90°C and then loaded on the gel. Gels were run with 120 V for 60-90 min. Either fluorescently labelled RNA was used and visualized using the Odyssey Fc reader (700 nm) or RNA was visualized using SYBR Gold. For this the gel was incubated in a 1x SYBR Gold solution (TBE buffer) for 10 min on a shaker and subsequently recorded using the Odyssey FC reader (600 nm).

4.2.5. Protein based assays

4.2.5.1. Enzyme-linked immunosorbent assay (ELISA)

To measure released cytokines and chemokines, supernatant was collected 20 h after transfection if not stated otherwise. Human IP10 in the supernatant was measured using the BD ELISA Set and IFN- α was measured using the human IFN- α Module Set. The assays were performed according to the manual but with half the volumes and half the antibody concentration. Briefly, ELISA plates were coated with the respective capture antibody in coating buffer (IP10) or PBS (IFN- α) and incubated at 4°C overnight. After washing the plates three times with ELISA wash buffer, unspecific binding sites were blocked by 1 h incubation with the respective assay buffer. Samples were diluted in assay buffer to not exceed the highest standard and added to the plate after three washing steps. For IP10 ELISA, after incubation at RT on a shaker for 2 h, the plate was washed five times and biotinylated antibody and streptavidin-HRP were added simultaneously. Subsequently, the plate was incubated at RT on a shaker for 1 h. For IFN- α ELISA, HRP was added immediately after the

samples and the plate was incubated at RT on a shaker for 2 h. After seven and three washing steps for IP10 and IFN- α ELISA respectively, TMB substrate reagent set was used as HRP substrate. The reaction was stopped using 1 M H_2SO_4 and absorbance at OD450 against OD570 was measured using an Epoch microplate spectrophotometer. Protein concentration was calculated using excel and the protein standard curve.

4.2.5.2. Cell based measurement of cytokines

HEK-Blue™ IFN-α/β cells or Thp1-Dual™ cells were used according to the manufacturer's instructions for cell-based measurement of cytokines. To measure IFN induction with HEK-Blue™ cells, cells were seeded in a 96-well culture plate (50.000 cells/well in 180 μl medium). 20 μl harvested supernatant was added and as a reference recombinant IFN-α was used (highest standard 3000 U/ml). Samples were diluted to not exceed the highest standard. 20 h later 40 μl HEK-Blue™ supernatant was mixed with 40 μl PNPP-buffer in a flat 96-well plate and incubated for 15-45 min. Absorbance at OD405 was measured using an Epoch microplate spectrophotometer. Thp1-Dual™ cells were either transfected directly or supernatant was added to the cells as described for HEK-Blue™ cells. 20 h later IRF3 induction was measured via luciferase measurement and NFκB induction was measured using SEAP according to the protocol for HEK-Blue™ cells.

4.2.5.3. Sodium dodecyl sulfate (SDS)-PAGE and Western Blot

Sample preparation

To measure intracellular protein levels, cells were either harvested by direct addition of Lämmli buffer or by protein extraction with RIPA buffer. For harvesting with Lämmli buffer, 1x Lämmli buffer was directly added to the cells in the culture plate after one washing step with PBS to remove residual FCS. Cells were then transferred to a 1.5 ml eppendorf tube containing two zirconia beads. Samples were treated with ultrasound for 90 sec. For protein extraction with RIPA, cells were trypsinized, centrifuged and washed with PBS prior to resuspension in RIPA buffer. Following incubation for 30 min on ice, lysates were cleared by centrifugation at full speed for 15 min at 4°C. All protein samples were denatured at 95°C for 5 min before loading onto the gel.

SDS-PAGE

SDS-PAGE was performed to separate charged proteins according to their molecular mass. Based on the mass of the protein of interest, proteins were separated on gels with different polyacrylamide concentration (6-15%). Gel electrophoresis was performed at 30 mA/gel for 60-90 min in electrophoresis running buffer.

Western Blot

After gel electrophoresis, proteins were transferred to nitrocellulose membranes (0.2 μ M or 0.45 μ M) in transfer buffer at 450 mA for 90 min (60 min for proteins < 20 kDa). Afterwards nitrocellulose membrane was incubated for 5 min in PonceauS-solution to confirm successful transfer. Subsequent to decolouring with washing buffer (TBS-T), unspecific binding was blocked by incubation with Odyssey-, BSA- or milk powder-based blocking buffer for 1 h at RT on a roller. Membranes were incubated with 4 ml antibody solution overnight at 4°C on a roller. The following day the membrane was washed twice with TBS-T and once with TBS prior to incubation with the respective IRDye secondary antibody in 5 ml antibody solution for at least 1 h at RT on a roller. The membrane was subsequently washed four times with TBS-T and two times with TBS. An Odyssey Fc reader was used for protein detection.

4.2.5.4. Electrophoretic mobility shift assay (EMSA)

EMSA was performed to measure RIG-I CTD binding to RNA with different end structures. Protein was diluted in protein buffer to the intended concentration. RNA – RIG-I complex formation can be visualized by a slower movement through the gel compared to unbound RNA. RNA was diluted in protein buffer or H_2O . 0.1 V RIG-I binding buffer was added. Protein and RNA were mixed and incubated for 10 min at RT. Subsequently, protein-RNA mix was loaded on a native acrylamide gel (7.5%) and run at 100 V for 60-90 min.

To visualize the shift, either RNA was stained with SYBR gold or Cy5 fluorescently labelled RNAs were used. Absorption was measured using an Odyssey Fc reader.

4.2.6. Cell culture

4.2.6.1. Splitting of cells

Cells were grown either in Petri dishes or tissue flasks and were kept in a humidified incubator at 37°C and 5% CO₂. To split adherent cells, the media was removed and the cells were carefully washed with PBS. After incubation with trypsin/EDTA and thereby detaching the cells from the surface, cells were resuspended with the according cultivation medium and the required proportion was kept while the rest was discarded. New culture media was added to the cells. To split suspension cells, cells were resuspended in cultivation media and

the appropriate amount of media was subsequently removed and the culture flask was filled up with new media. The used cell culture media for each cell line are depicted in Table 4.16.

Table 4.16: Cell culture media

Cells	Medium
PBMCs	RPMI + 10% FCS + 1% Pen/strep
Thp1-Dual™	RPMI + 10% FCS + 1% Pen/strep
A549	DMEM + 10% FCS + 1% Pen/strep
HEK 293FT	
Flp-In™ Trex 293	DMEM + 10% FCS + 1% Pen/strep
HEK-Blue™ IFN-α/β	

4.2.6.2. Freezing of cells

In order to cryo conserve cells, suspension cells or with trypsin detached adherent cells were precipitated via centrifugation for 5 min at 400 rcf. Supernatant was discarded and the cell pellet was resuspended in freezing medium (FCS, 10% DMSO). The cells were then slowly frozen using a Mr Frosty freezing container at -80°C in cryo vials. Cells were transferred to a -150°C freezer for long-term storage 3 days later. To thaw cells, the cells were resuspended with 10 ml medium. After precipitation of the cells, supernatant was removed and the cells were seeded in a 10 cm cultivation dish in new medium.

4.2.6.3. Cell seeding

To seed cells, adherent cells were washed and trypsinized as described in 4.2.6.1. Cells were centrifuged (400 g, 5 min) and the pellet was resuspended in new culture medium. Cell number was determined using an automatic cell counter. Suspension cells were either centrifuged or directly counted. Adherent cells were seeded at least 6 h before the experiment, but usually the day before. Cell numbers per well and cell line are indicated in Table 4.17.

Table 4.17: Cell seeding

Cell line	96-well	24-well	6-well
A549	3x 10 ⁴	1.5x 10 ⁵	-
Thp1-Dual™	6x 10 ⁴	2x 10 ⁵	-
HEK 293FT			
Flp-In™ Trex 293	3.5x 10 ⁴	2x 10 ⁵	1x 10 ⁶
HEK-Blue™			

4.2.6.4. Isolation of peripheral blood mononuclear cells (PBMCs)

To isolate human PBMCs, 20 ml blood concentrate of buffy coats was mixed with an equal volume of NaCl solution (0.9%) and carefully layered on 15 ml Biocoll in a 50 ml falcon tube. Centrifugation at 800 rcf for 20 min without brake established the gradient. The mononuclear cell layer above the Biocoll-cushion was transferred to a new 50 ml falcon tube and filled up with 0.9% NaCl-solution. After precipitation of cells (centrifugation, 5 min, 400 rcf, 4°C), cells were washed with 0.9% NaCl solution and centrifuged again. Supernatant was aspirated and cells were resuspended in 5 ml erythrocyte-lyse buffer and incubated for 5 min at RT. Afterwards, the tube was filled up with 0.9% NaCl solution and centrifugation was performed at 400 rcf, 4°C for 5 min. Cells were plated in 96-well plates (4x 10^5 /well, 200 μ l/well) in RPMI-1640 (10% FCS, 1x Pen/Strep) and chloroquine was added (5 μ g/ml) to inhibit TLR stimulation. Cells were transfected with the according stimuli 30 min later.

4.2.6.5. Transfection and stimulation of cells

To perform stimulation experiments, cells were harvested as described above and cell number was determined either using a Neubauer chamber and trypan blue staining or an automatic cell counter. Cells were seeded in culture test plates. Transfection of siRNAs was performed using Lipofectamine RNAiMAX and polyI:C was transfected using TransIT LT1. All other transfections were performed with Lipofectamine 2000. The transfection reagent was mixed with OptiMEM and was incubated for 5 min at RT. RNA or DNA was mixed with the equal amount of OptiMEM and combined with the OptiMEM-transfection reagent mix. The transfection mix was added to the cells after 20 min of incubation at RT. Subsequently, cells were immediately placed back in the incubator until harvesting.

4.2.6.6. siRNA knockdown

siRNAs were used to transiently knockdown the expression of specific genes. All siRNAs were ordered with a 3'dTdT modification. Cells were seeded in 24-well or 48-well plates. The transfection of siRNAs was performed using Lipofectamine RNAiMAX with the general transfection protocol. siRNA KD was performed for 72 h unless stated otherwise. KD was verified either via gene expression analysis using qPCR or protein expression analysis using immunoblot.

4.2.6.7. KO generation using CRISPR-Cas9

KO cells were either generated using a plasmid-based method or using recombinant Cas9.

Plasmid-based method

pLenti-Cas9 plasmid was digested with Swal and purified using the gel extraction kit. The DNA oligo with the gene specific target sequence was annealed with the universal antisense DNA and cloned into the linearized pLenti-Cas9 using gibson assembly. The plasmid was then transformed into chemocompetent Stbl3 and correct insertion of target sequence into the plasmid was analyzed via Sanger sequencing. 200 ng pLenti-Cas9 with the target sequence was transfected into cells using Lipofectamin 2000.

Recombinant Cas9 method

Recombinant Cas9, crRNA and tracrRNA were purchased from IDT. Target sequences are listed in Table 4.18. The 67 mer tracrRNA and the crRNA, containing the gene specific target sequence, were annealed at equimolar concentrations to form the functional guide RNA (gRNA). Annealed gRNA (1 μ M) was then incubated with recombinant Cas9 enzyme (1 μ M) in OptiMem at RT for 5 min to assemble the ribonucleoprotein (RNP) complex. The RNP complex was then transfected using Lipofectamin 2000.

Cells were cultivated in limited dilution to obtain single-cell clones for both methods one day after transfection. KO was confirmed by immunoblot, deep-sequencing, Sanger sequencing and functional testing.

Table 4.18: CRISPR target sequences

	•
Target gene	Target sequence
DDX58	GGGTCTTCCGGATATAATCCTGG
STAT1	CAGGAGGTCATGAAAACGGATGG
PKR	TGGTACAGGTTCTACTAAACAGG

4.2.6.8. MTT Assay

The metabolic activity of cells as a measure for cell-viability was determined with thiazolyl blue (MTT). 20 μ l MTT-solution (5 mg/ml in PBS) per 96-well was added to the cell medium. Metabolically active cells turn thiazolyl blue into a violet dye in form of crystals. 60-90 min later the reaction was stopped by adding 100 μ l 10% SDS. To allow the dissolving of the crystals, the 96-well plate was incubated overnight at 37°C and absorption at 570 nm was measured the following day with an Epoch reader. The more MTT was converted, the higher the metabolic activity of the cells.

4.2.6.9. Luciferase Dual Assay

Cells were seeded in 96-well plates and were allowed to adhere overnight. Cells were cotransfected with 10 ng pIFN- β -G-Luc and 5 ng pLenti-Ef1 α -F-Luc (ctrl plasmid) per 96-well. The transfection of stimuli was performed at least 6 h later. Luciferase assay was performed 20 h after stimulation. To measure Gaussia luciferase production, as a surrogate for IFN- β promoter activation, 25 μ l Coelenterazine-solution (1 μ g/ml in H $_2$ O) was added to 25 μ l supernatant in a white microplate. Chemiluminescence was immediately measured with the EnVision 2104 Multilabel reader. To measure Firefly luciferase as a control, supernatant was aspirated and 40 μ l 1x SAP-solution was added and cells were lysed for 20 min at RT on a shaker. Afterwards, 25 μ l of lysed cells in SAP were added to 25 μ l Firefly luciferase substrate (Luciferin) and chemiluminescence was measured with the EnVision 2104 Multilabel reader. To control for transfection, efficiency and translation efficiency, Luc $_G$ was divided by Luc $_F$.

4.2.6.10. Transient protein overexpression

The pEF-BOS vector was used for transient overexpression of proteins. Plasmid containing the gene of interest was transfected into cells using Lipofectamin 2000 one day after cell seeding. 25 ng plasmid/96-well were used unless stated otherwise. Protein expression was controlled using immunoblot.

4.2.6.11. Generation of stable Flp-In[™] Expression Cell Lines

Stable HEK Flp-In[™] Host Cell Lines were obtained from Invivogen. These cells contain a FRT site in their genome that serves as a binding site for Flp recombinase (Gronostajski et al. 1985, Sauer 1994). First the gene of interest was cloned into the pcDNA5/FRT[™] expression vector and a Midi plasmid preparation was performed. HEK Flp-In[™] cells were seeded in 6-well culture plates (1×10^6 cells in 3 ml/well) and allowed to adhere overnight. The following day 700 ng pOG44, expressing the Flp recombinase, was transfected simultaneously with 70 ng of pcDNA5/FRT plasmid containing the gene of interest. For this purpose, 2 μ l Lipofectamine 2000 were incubated for 5 min in 100 μ l OptiMEM. Subsequently, this was mixed with 100 μ l OptiMEM containing the plasmid DNA and incubated for 20 min before the transfection mix was added to the cells. After 48 h of incubation, cells were trypsinized and resuspended in selection media containing 150 μ g/ml hygromycin and 10 μ g/ml blasticidin and seeded in new 6-well plates. The correct integration of the expression construct confers cells resistant to hygromycin and the gene of interest is expressed in a

doxycycline-dependent manner. After the selection process, the expression of the gene of interest was confirmed by functional assays and western blot.

4.2.6.12. Generation of mtDNA depleted cells

A549 cells were cultivated in a medium containing ethidium bromide (EtBr) (50 ng/ml), sodium pyruvate (1 mM) and NEAA (1x) for at least 7 days. Cells with depleted mtDNA do not produce new mtRNA. Therefore, successful mtDNA depletion can be measured via gene expression analysis of mt-mRNA using qPCR. Control cells were incubated in medium containing sodium pyruvate (1 mM) and NEAA (1x), but without EtBr.

4.2.7. Virological methods

4.2.7.1. Viral infection

5x 10⁵ A549 cells were seeded in 24-well plates. The next day cells were infected with the indicated multiplicity of infection (MOI) in PBS containing 1% FCS. The inoculum was withdrawn 1 h after infection and the culture medium was added. Either RNA was extracted from infected cells or supernatant was harvested to determine virus released in the supernatant via plaque assay.

4.2.7.2. Plaque assay

BHK-J cells were seeded in 35 mm culture dishes. The next day tenfold serial dilutions of supernatant from viral infection were made in PBS containing 1% FCS and BHK-J cells were inoculated with the dilutions at 37°C for 1 h. The inoculum was removed and the cell monolayer was overlaid with 3 ml 1.2% agarose and 2x MEM in a ratio of 1:2. Cells were incubated for 2 days and subsequently fixed in 7% formaldehyde for at least 30 min. Agarose was removed and cells were stained with 1% crystal violet in 50% ethanol for 15 min. Plaque formation was counted after removing the crystal violet, washing with water and drying the dishes. Plaques are visible as unstained spots. Plaque forming units (PFU) per ml were calculated as follows: counted plaques x 10³ x dilution.

4.2.8. Software

Statistical analysis was performed using GraphPad Prism 6. All figures were made using GraphPad Prism 6 and Adobe Illustrator CS6. Image studio Lite was used to quantify western blots. Sequence comparison was performed using Geneious prime. Protein crystal structures were analyzed using Chimera 1.12.0.

4.2.9. Statistical Analysis

Experiments were performed as technical duplicates and biological triplicates unless indicated otherwise. Statistical differences were determined using two-tailed student's t-tests, one-way analysis of variance (ANOVA) or two-way ANOVA with a confidence interval of 95% depending on the data set to be analyzed using GraphPad Prism6. Significances are indicated as follows: * (p < 0.05), ** (p < 0.01), *** (p < 0.001), **** (p < 0.0001), ns: not significant.

5. Results

Initially, all polymerase transcribed RNAs possess a 5´3p, and although most RNAs are single-stranded, they form complex secondary structures with base-paired regions. These two features, combined with a base-paired or even blunt-ended 5´end, would make a good RIG-I ligand. However, the 5´ends of RNAs are further processed in the nucleus before they reach the cytosol where RIG-I is located in uninfected cells.

In this thesis, RNA modifications that prevent the recognition of endogenous ligands by RIG-I were investigated. Furthermore, it examined amino acids in the CTD of RIG-I that mediate tolerance to self-RNAs. Moreover, ligand specifications of RIG-I CTD mutants were characterized. These CTD mutants were then on the one hand used to identify viral RIG-I ligands, and on the other hand RIG-I activation mechanisms by long and non-triphosphorylated RNAs. The outcome of PKR activation on RIG-I-dependent immune stimulation was studied and the information gained was used to develop new potent RIG-I ligands which avoid stimulation of PKR.

5.1. N1-2´O-methylation mediates immunotolerance towards endogenous RNA

mRNAs of higher eukaryotes possess a cap structure consisting of a ^{m7}G cap and 2′O-methyl-modification at N1 and in about 50% of the RNAs 2′O-methylation of N2. While the ^{m7}G cap is necessary for an efficient translation, the role of N1 and N2 methylations remained elusive. The first indications came from a study by Wang et al., where a crystal structure of the RIG-I CTD bound to 3p-dsRNA was described (Wang et al. 2010). Amino acids in the basic binding cleft that make contacts to the 3p of the RNA were identified. These are indispensable for RIG-I activation by 3p-dsRNA. Interestingly, the crystal structure exhibited a highly conserved histidine (H830) building hydrogen bonds to the sugar 2′-OH of N1. Type I IFN induction was completely abrogated after stimulation with N1-2′O-methylated 3p-dsRNA. It was hypothesized that this was due to a steric conflict between the methyl group and the side chain of H830. So far it had been assumed that the ^{m7}G cap prevents RIG-I binding and activation by endogenous mRNA.

To examine this further, the contribution of different cap structures on RIG-I binding and activation was evaluated in the PhD thesis of Christine Schuberth-Wagner (Schuberth 2011). Surprisingly, it was found that the ^{m7}G cap on RNAs only partially reduced RIG-I-dependent type I IFN induction, while N1-2′O-methylation of 3p-dsRNA (3p-N1-dsRNA) completely abrogated RIG-I activation. Type I IFN induction was fully restored after stimulation with 3p-

N1-dsRNA in cells expressing RIG-I H830A. Additionally, the K_d values of full-length RIG-I WT and RIG-I H830A were assessed by Alphascreen. Mirroring the activation data, the binding affinity of RIG-I WT to 3p-N1-dsRNA was 4.5 times lower compared to unmethylated 3p-dsRNA. In contrast, binding affinities for RIG-I H830A were comparable with 3p-N1-dsRNA and 3p-dsRNA. Long-term expression of RIG-I H830A in cells led to an increased IP10 induction compared to RIG-I WT expressing cells, which pointed towards the presence of endogenous N1-methylated ligands.

5.1.1. CMTR1 knockdown induces RIG-I-dependent immune stimulation

Hypothesizing that endogenous mRNAs are excluded from RIG-I WT binding through their N1-2′O-methylation, removal of this methylation should restore RIG-I WT binding and activation. In this thesis RNAi of CMTR1 that catalyzes the N1-2′O-methylation of mRNAs in the nucleus was performed to test this hypothesis. KD of CMTR1 leads to the presence of

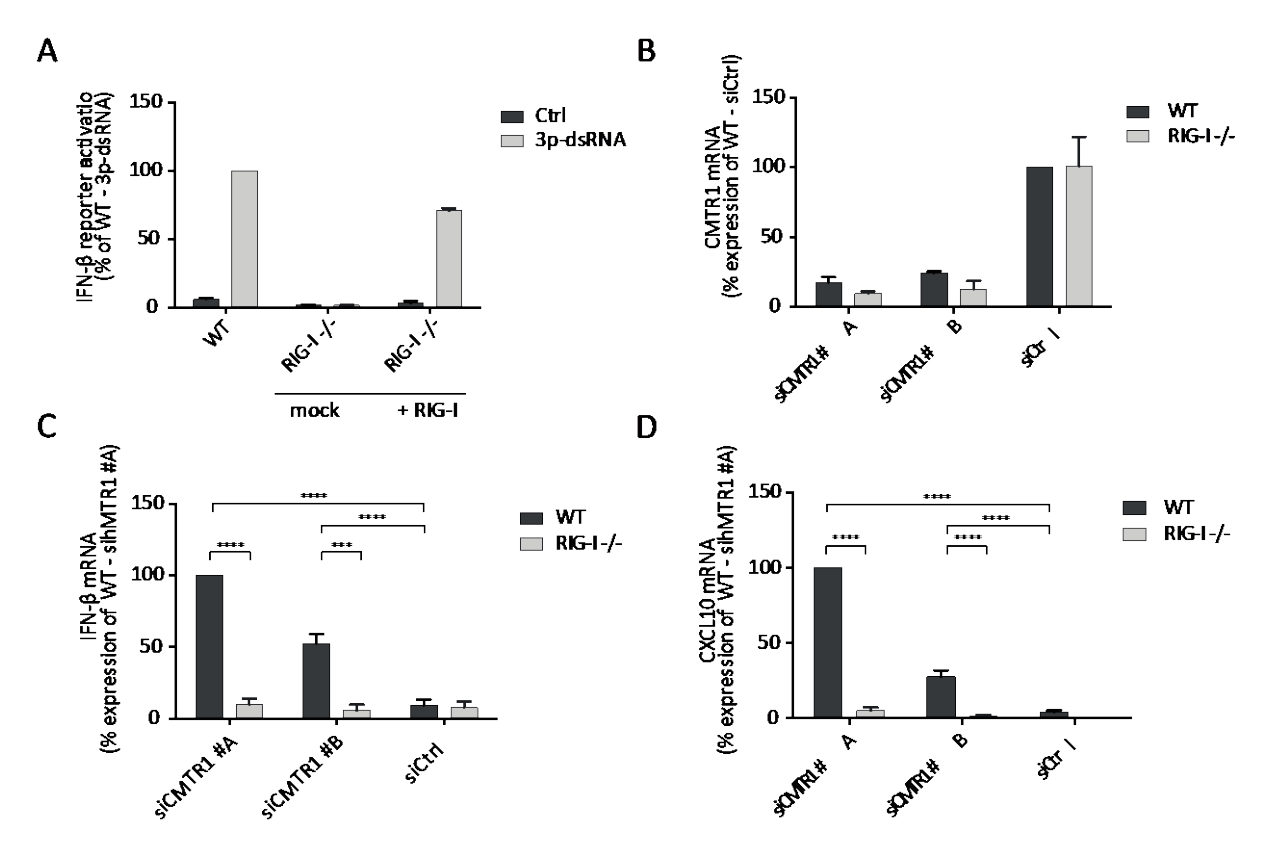


Figure 5.1: Knockdown of CMTR1 induces RIG-I-dependent immune activation

A) A549 WT, A549 RIG -/- (mock) and A549 RIG-I -/- with reconstituted RIG-I (+RIG-I) cells were stimulated with 3p-dsRNA (20 ng). 24 h after RNA transfection IFN- β induction was measured by dual-luciferase assay (n=2, mean + SEM). B-D) A549 WT and RIG-I -/- cells were transfected with the indicated siRNAs and primed with 1000 U/ml IFN- α . RNA was isolated 72 h after siRNA treatment. B) CMTR1 mRNA expression was analyzed by qPCR. C) IFN- β mRNA induction was measured by qPCR. D) CXCL10 mRNA expression was determined by qPCR B-D) n=3, mean + SEM, two-way ANOVA, Tukey's post-test. Significances are indicated as follows: *** (p < 0.001), **** (p < 0.0001).

mRNAs that lack the N1-2′O-methylation and solely possess a cap0 structure. siRNA KD was performed in A549 WT cells and A549 cells deficient for RIG-I (RIG-I -/-). RIG-I KO was introduced via CRISPR-Cas9 and verified by western blot and sequencing. Furthermore, functional testing revealed complete abrogation of type I IFN induction in RIG-I -/- cells upon 3p-dsRNA stimulation (Figure 5.1A). Clonal variations or unspecific cutting effects by Cas9 were excluded since transient reconstitution of RIG-I -/- cells with RIG-I WT restored immune activation by 3p-dsRNA to a similar level as seen in WT cells (Figure 5.1A). CMTR1 KD was performed with two siRNAs targeting different sequences (siCMTR1 #A and siCMTR1 #B) and was compared to a Ctrl siRNA (siCtrl) against Gaussia luciferase. Gene expression of CMTR1, IFN-β and CxCL10 was analyzed via qPCR 72 h after siRNA transfection in A549 WT and RIG-I -/- cells. Compared to cells treated with siCtrl, CMTR1 expression was more than 75% reduced in cells treated with siRNA against CMTR1 (siCMTR1) (Figure 5.1B). Interestingly, KD of CMTR1 in A549 WT cells caused a significant induction of IFN-β and CxCL10 mRNA expression (Figure 5.1C+D). These results reveal that CMTR1 is indispensable to prevent RIG-I-dependent activation by endogenous RNA.

5.1.2. YFV escapes RIG-I recognition by N1-methylation of viral RNA

Viral polymerases, like eukaryotic polymerases, produce 5'3p-RNAs during the transcription process. However, viruses have evolved several mechanisms to escape immune recognition including capping and the methylation of their RNA. Flaviviruses ((+)ssRNA) replicate in the cytosol and express a protein, NS5, that on the one hand functions as an RNA-dependent RNA polymerase, and on the other hand performs N1-2'O-methylation (Dong et al. 2008). Mutation of NS5-E218 to alanine (E218A) abrogates 2'O-methylation activity of NS5 and renders viral RNA N1-2'O-unmethylated (Zhou et al. 2007). The outcome of this mutation on immune activation caused by the virus and viral replication was assessed in A549 WT, RIG-I -/- and STAT1 -/- cells. Cells were infected with wild type YFV (YFV wt) or YFV with the E218A mutation (YFV E218A) and virus production was quantified 72 h after infection via plaque assay. KO of STAT1 and RIG-I led to a general higher viral titer compared to A549 WT cells, but no difference in the viral load was detected between YFV wt and mutant viruses in the KO cells (Figure 5.2A). YFV E218A replication in A549 WT cells was impaired compared to YFV wt by 15-fold. This effect was reflected in the results on immune activation. Here again A549 WT and KO cells were infected with YFV wt and E218A. 8 h after infection RNA was extracted and IFIT1 mRNA expression was analyzed via qPCR. No IFIT1 mRNA induction was detected in RIG-I and STAT1 deficient A549 cells. While YFV wt infection led to a moderate IFIT1 mRNA expression in A549 WT cells, this effect was increased four times after infection with YFV E218A (Figure 5.2B).

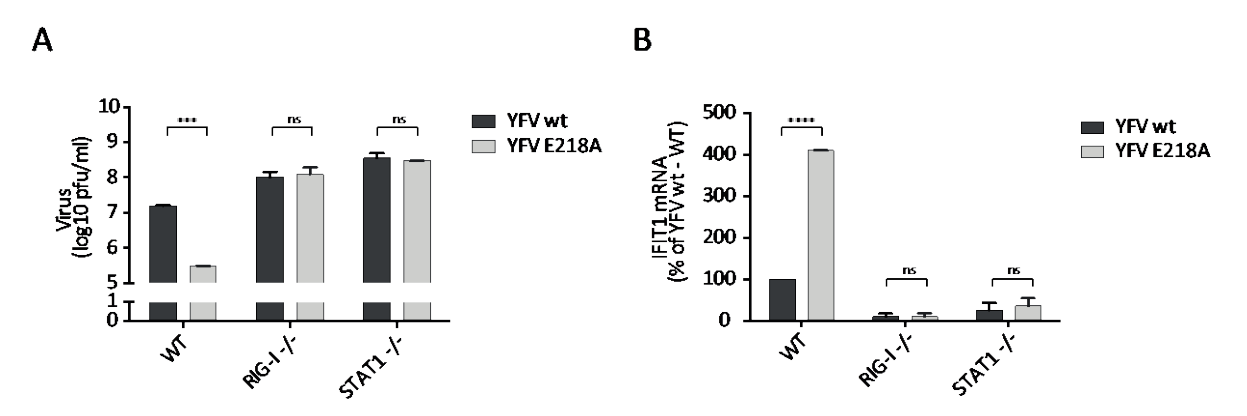


Figure 5.2: YFV 2'O-methyltransferase prevents immune recognition by RIG-I

A) A549 WT, RIG-I -/- or STAT1 -/- cells were infected with YFV wt or YFV E218A (MOI 0.01). Virus production was quantified by plaque assay in BHK cells 72 h after infection (n=2, mean + SEM, two-way ANOVA, Tukey's post-test). B) A549 WT, RIG-I -/- or STAT1 -/- cells were infected with YFV wt or YFV 218 (MOI 1). RNA was extracted 8 h after infection and IFiT1 mRNA expression was analyzed by qPCR (n=2, mean + SEM, two-way ANOVA, Tukey's post-test). Significances are indicated as follows: *** (p < 0.001), **** (p < 0.0001), ns: not significant. Virus production, infections and titer quantification were performed by the lab of Beate Kümmerer.

In summary, viruses without 2'O-methylation activity have a lower viral production and induce an increased RIG-I-dependent immune response. This shows that YFV uses methylation of the first nucleotide to escape RIG-I recognition (Schuberth-Wagner et al. 2015).

5.2. Impact of RNA modifications on RIG-I activation

As discussed in the introduction, RIG-I has specific ligand requirements such as a 5´3p and a base-paired 5´end. However, RIG-I activation by suboptimal ligands such as OH-dsRNA and RNAs with overhangs has been reported previously (Marques et al. 2006, Takahasi et al. 2008, Yoneyama et al. 2008, Schlee et al. 2009). In this thesis, different modifications on the optimal RIG-I ligand were introduced and their effect on RIG-I WT activation were assessed. Furthermore, ligand recognition was investigated using cells expressing RIG-I with CTD mutations (RIG-I F853A and RIG-I K861A). The side chain of F853 makes stacking interactions with the terminal 5´base pair of the RNA (Figure 5.3A). Base pairing stabilizes a planar assembly of the bases that is important for a strong stacking interaction. K861 forms hydrogen bonds with the α - and β -phosphate (Figure 5.3A) and it was previously shown that mutation to alanine abrogates RIG-I activation by 3p-dsRNA (Wang et al. 2010). The outcome of this mutation on immune activation by RNAs with other 5´end modifications was not

examined. In this thesis, RIG-I WT, RIG-I F853A or RIG-I K861A were reintroduced into HEK Trex Flp-In™ cells deficient for RIG-I and MDA5 (RM -/-) to investigate the impact of RIG-I CTD mutations on the recognition of ligands with different 5′end modifications. This information was then used to study which ligands are recognized during a viral infection by RIG-I. Moreover, the CTD mutant panel was used to examine if RIG-I is able to detect long RNA in an end-independent manner. Equal expression of RIG-I in cells expressing WT or RIG-I mutants was controlled for by Western Blot (data not shown).

5.2.1. Characterization of RIG-I activation by 3p-dsRNA and OH-dsRNA

Synthetic RNAs (Table 8.1) were transfected using lipofection and immune activation was assessed by dual-luciferase assay 20 h after stimulation. As expected, 3p-dsRNA (3p-asOH)

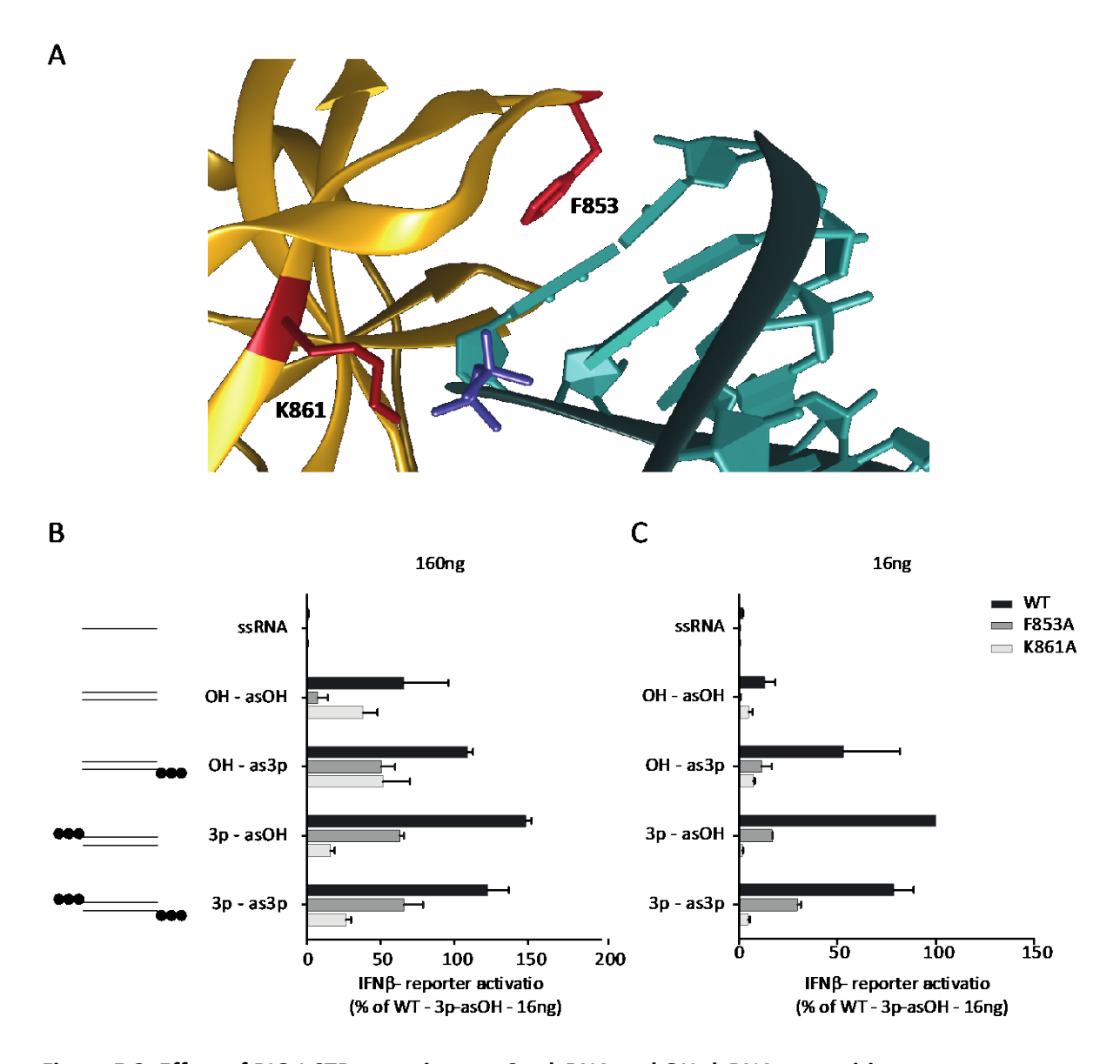


Figure 5.3: Effect of RIG-I CTD mutations on 3p-dsRNA and OH-dsRNA recognition

A) Excerpt of the RIG-I CTD crystal structure with 2p-dsRNA (PDB: 3NCU). RNA backbone is depicted in gren, diphosphate in blue and RIG-I CTD in yellow. Amino acids F853 and K861 are highlighted in red. Illustration was made using Chimera. B-C) HEK Trex RM -/- cells expressing either RIG-I WT, RIG-I F853A or RIG-I K861A were stimulated with indicated synthetic RNAs. IFN- β induction was assessed 20 h after RNA transfection by dual-luciferase assay (n=2, mean + SD) B) 160 ng RNA/96-well were transfected C) 16 ng RNA/96-well were transfected.

led to a high immune activation in RIG-I WT expressing cells (Figure 5.3). The addition of 3p at the 5'end of the as-RNA (3p-as3p) did not further increase IFN-β induction. While cells expressing K861A only caused a minor immune stimulation even at high 3p-dsRNA concentrations, cells expressing F853A showed a substantial IFN-β induction, albeit lower than WT expressing cells. While K861A activation by 3p-asOH was comparable to stimulation with 3p-as3p, OH-as3p RNA led to a considerable immune activation in K861A expressing cells (Figure 5.3). Since 3p-asOH and OH-as3p both have one OH-end that can activate K861A, the difference in activation potential by these RNAs hints to other ligand specifications such as the sequence. Stimulation with OH-dsRNA caused comparable immune activation in cells expressing RIG-I WT or RIG-I K861A. However, no immune activation was detected in cells expressing F853A. Introducing a 3p at either 5'end (3p-asOH or OH-as3p) restored immune activation (Figure 5.3).

5.2.2. RIG-I activation by 3p- and OH-dsRNA with overhangs

Next, the effect of introducing overhangs in the 3p-dsRNA on RIG-I activation was studied. Synthetic RNAs used for this experiment are listed in Table 8.2. While the addition of nucleotides at the 5'end of the antisense strand (3p-as5'+2AA) had no impact on RIG-I activation, introducing a 5'overhang at the triphosphorylated RNA site by removing nucleotides from the 3'end of the antisense strand (3p-as5'+2AA_3'-1nt, 3p-as5'+2AA_3'-2nt, 3p-as5'+2AA_3'-3nt) were not tolerated in all tested cells (Figure 5.4A+B). While a 2nt 3'overhang caused a moderate immune activation in RIG-I WT expressing cells, RIG-I F853A cells showed no IFN-β induction. As expected, cells expressing K861A were not activated by any of the 3p-dsRNAs tested (Figure 5.3A+B). As shown in the previous experiment, OH-dsRNA also causes a substantial immune activation in RIG-I WT and RIG-I K861A cells. With this in mind, the tolerance of overhangs on OH-dsRNA was assessed. As expected, OH-dsRNA with overhangs were not immunostimulatory in RIG-I F853A cells (Figure 5.3C). 5'overhangs on OH-dsRNA completely abrogated immune activation in RIG-I WT and RIG-I K861A cells, but

compared to 3p-dsRNA with 3'overhangs, the immune response reduction was more pronounced Figure 5.4C.

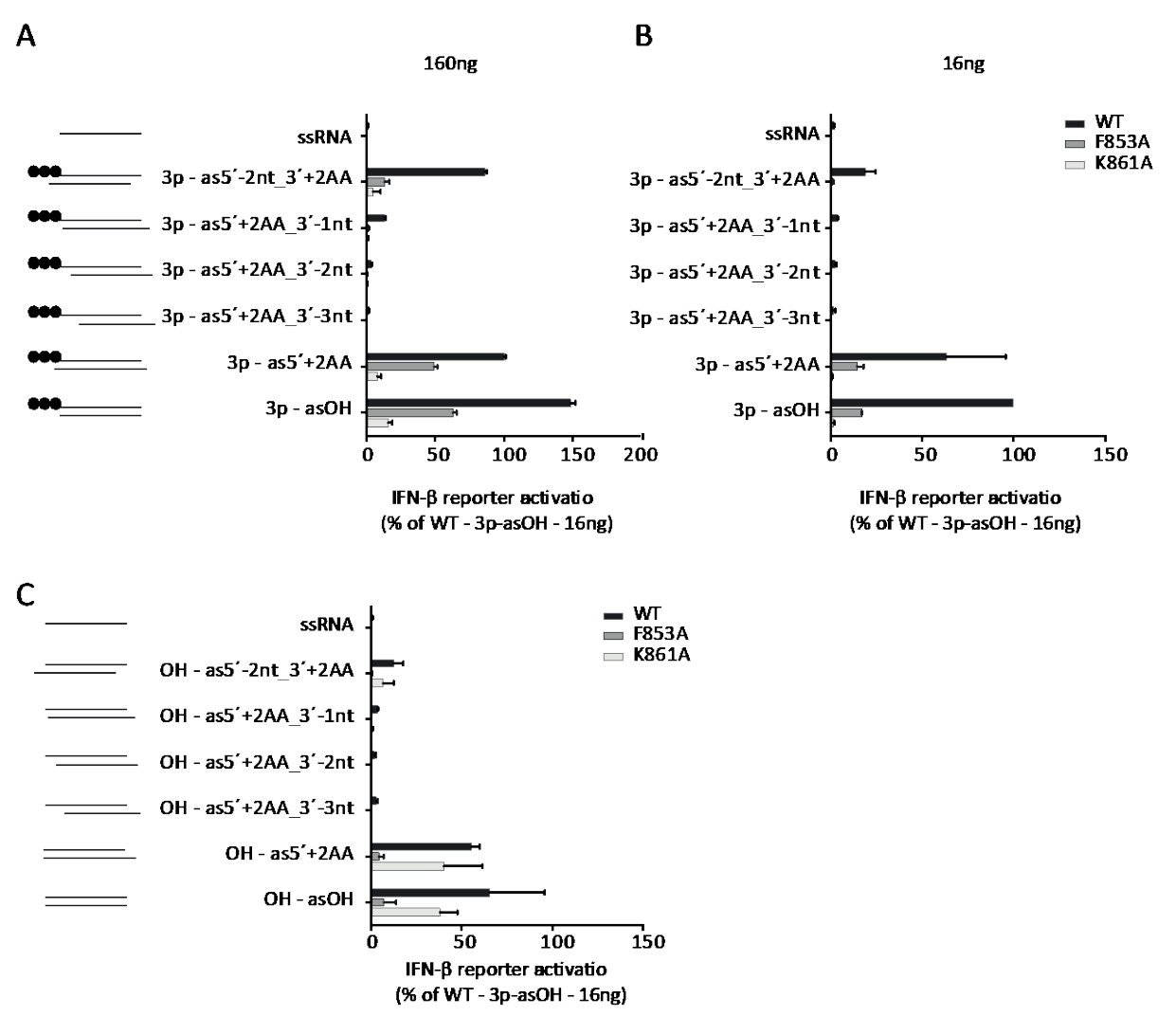


Figure 5.4: Activation potential of 3p- and OH-dsRNA with overhangs

A-C) HEK Trex RM -/- cells expressing either RIG-I WT, RIG-I F853A or RIG-I K861A were stimulated with indicated synthetic RNAs. IFN- β induction was assessed 20 h after RNA transfection by dual-luciferase assay (n=2, mean + SD) A+C) 160 ng RNA/96-well were transfected. B) 16 ng RNA/96-well were transfected.

5.2.3. Minimal RNA length for RIG-I activation

Since there are conflicting reports on the length requirements of the double-stranded stem for RIG-I activation (Schlee et al. 2009, Schmidt et al. 2009), synthetic RNAs with differing stem lengths were studied (10 bp up to 24 bp) (Table 8.3). The shortest 3p-dsRNA tested (3p-as5´10nt) — with a 10 bp stem — still caused immune activation in RIG-I WT expressing cells (Figure 5.5A), albeit 10 times lower than 3p-dsRNA with a 24 bp stem (3p-asOH). In general, immune activation positively correlated with the length of the bp stem.

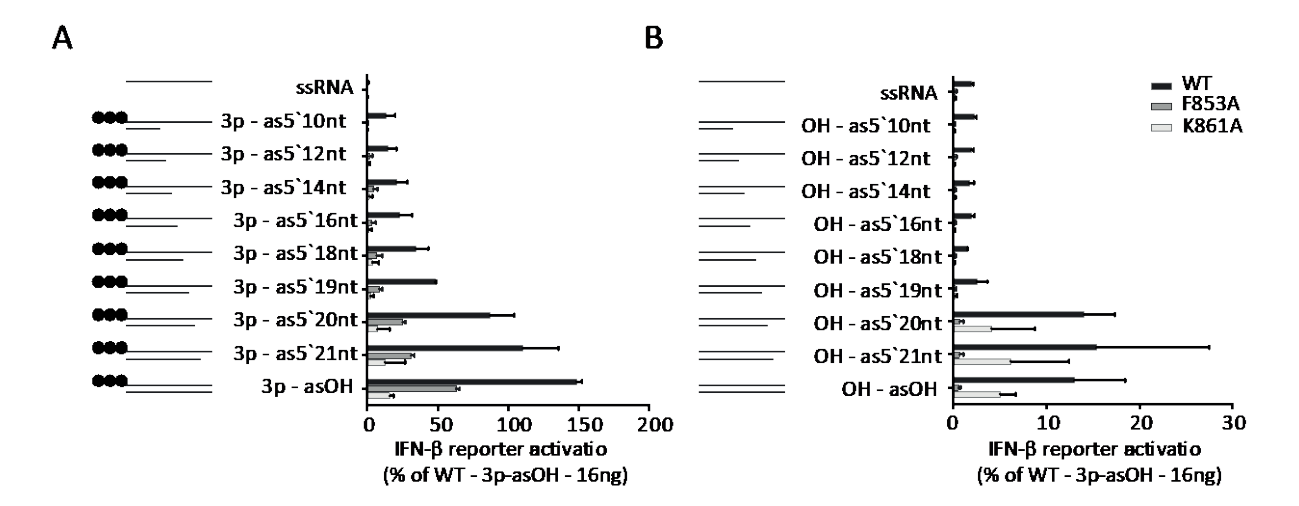


Figure 5.5: Characterization of minimal double-strand stem length of 3p- and OH-ligands A+B) HEK Trex RM -/- cells expressing either RIG-I WT, RIG-I F853A or RIG-I K861A were stimulated with indicated synthetic RNAs (160 ng/96-well). IFN- β induction was assessed 20 h after RNA transfection by dual-luciferase assay (n=2, mean + SD).

OH-dsRNA with a 19 bp or shorter stem only showed background activation. The cut off for RIG-I K861A cells was also at 19 bp stem for OH-dsRNA, while F853A expressing cells showed, as expected, no activation by any of the OH-dsRNAs (Figure 5.5B). For 3p-dsRNA F853A was only activated by 19 bp stems or longer (Figure 5.5A).

5.2.4. Viral recognition by RIG-I CTD mutants

After defining what RNA modifications are important for RIG-I recognition and what modifications are tolerated by which RIG-I CTD mutants, this information was used to study RIG-I activation during viral infection. In the RIG-I K861A mutant 5'3p binding is disturbed, therefore 3p-dsRNA and OH-dsRNA should induce an equal response. F853 strengthens binding of 3p-dsRNA and plays an important role for activation by 3p-dsRNA with 3'overhangs. For OH-dsRNA F853 is the only 5'contact. RIG-I F853A is not activated by OH-dsRNA or 3p-dsRNA with 3'overhangs. Viruses that on the one hand activate RIG-I WT, but on the other hand do not activate K861A produce 3p-ligands during infection, while no immune activation in F853A points to OH-viral ligands or ligands with a 3'overhang. It is often the case that in order to study viral ligands, viral RNA has to be extracted from cells. However, during the extraction, purification and analysis, secondary structures of the RNA might be destroyed and viral proteins that possibly mask the viral RNA or prevent the formation of base pairing are removed. In the present system by using the RIG-I CTD mutants whose expression is induced by the addition of doxycycline, viral ligand structures can be studied without extraction artefacts. Moreover, transfection of RIG-I expression

plasmids that might falsify the results is avoided. RIG-I expression was induced 4 h before virus infection. Cells were infected with a MOI of 0.05 and 0.5 and RNA was extracted 6 h

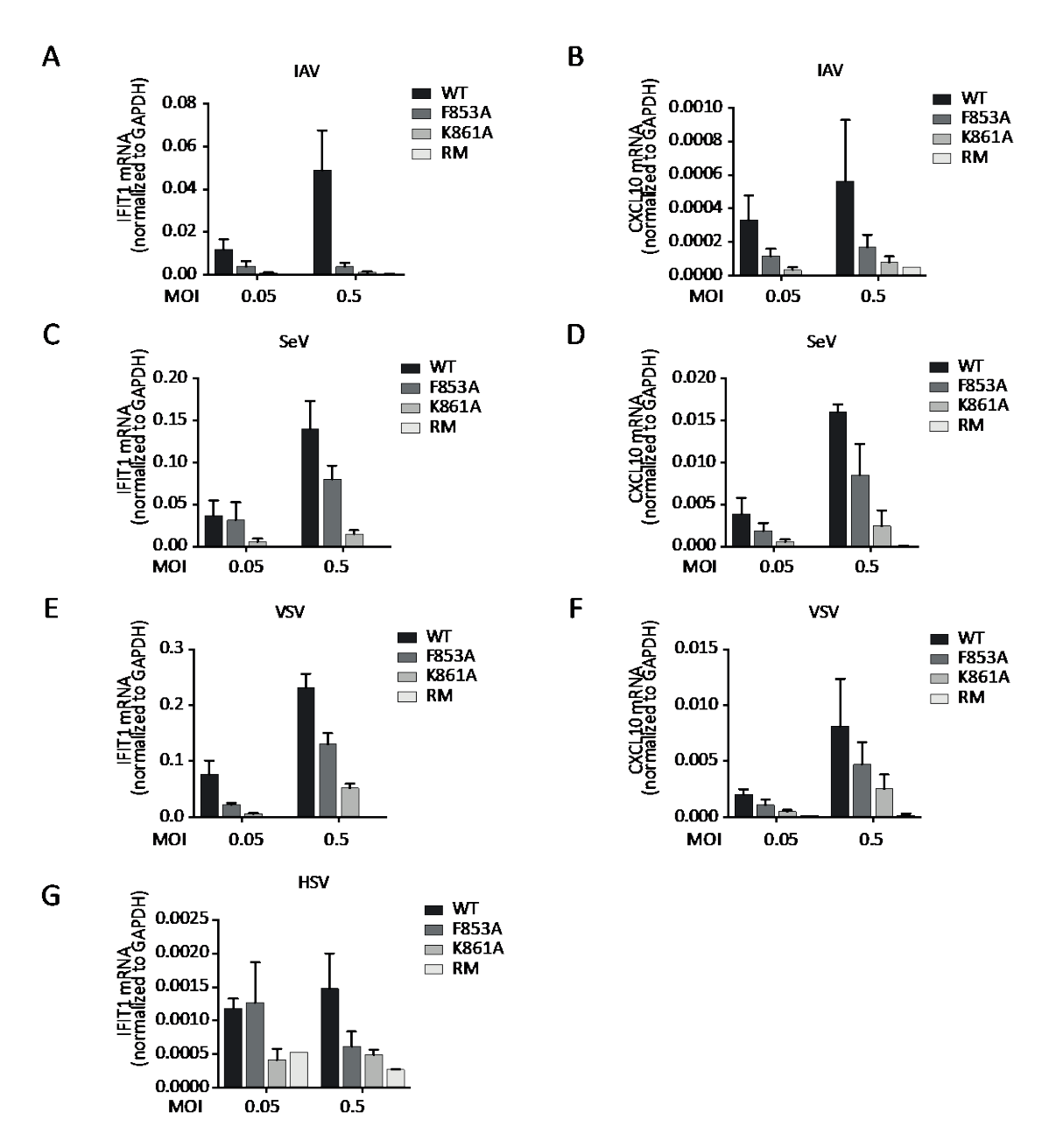


Figure 5.6: Viral recognition by RIG-I CTD mutants

A-G) HEK Trex RM -/- cells expressing either RIG-I WT, RIG-I F853A, RIG-I K861A or no RIG-I (RM) were infected with viruses IAV (A+B), SeV (C+D), VSV (E+F) and HSV (G). RNA was extracted 6 h after infection and analyzed for IFIT1 mRNA (A, C, E, G) or CXCL10 mRNA (B, D, F) expression via qPCR (n=2, mean + SEM), MOI: Multiplicity of infection as determined by plaque assay.

after infection to analyze ISG induction. While infection with the s-NSV IAV caused a substantial ISG induction in cells expressing RIG-I WT, cells expressing RIG-I F853A and RIG-I K861A only showed a slight increase in IFIT1 and CXCL10 expression compared to cells lacking RIG-I (Figure 5.6A+B). SeV and VSV infection induced a high immune activation in RIG-I WT cells. This effect was partially reduced in RIG-I F853A cells, while cells expressing

RIG-I K861A showed only a minor IFIT1 and CXCL10 expression (Figure 5.6B-E). Both SeV and VSV are ns-NSV. HSV, a DNA virus, showed only a low immune activation in RIG-I WT cells that was hardly above the background level (Figure 5.6G). Since infection with the s-NSV IAV caused no immune activation in K861A or F853A cells, viral ligands detected by WT RIG-I are probably triphosphorylated and might possess a 3′overhang or a 5′OH-end. In contrast to IAV, SeV and VSV caused substantial immune activation in F853A cells, while only a minor immune activation was detected in K861A expressing cells. This effect hints at triphosphorylated viral ligands that are recognized by RIG-I WT probably with a base-paired 5′end. Since HSV infection caused only a very minor immune activation, this shows that no dsRNA that is detectable by RIG-I originates during HSV infection.

5.2.5. RNA RIG-I recognition does not occur end-independently

Synthetic RNAs that were not longer than 24 bp were used in the preceding experiments. The outcome of 3p removal, introducing overhangs or a shorter double-stranded stem structure were investigated. Evidently the 24 bp RNA was detected in a 5'dependent manner. However, Binder et al. reported an end-independent RIG-I activation mechanism for longer RNAs (Binder et al. 2011). They showed that phosphatase treatment of short 3p-dsRNA (40 bp) had detrimental effects on RIG-I-dependent immune activation, while phosphatase treatment of longer 3p-dsRNAs (100 - 400 bp) did not change the immunostimulatory potential. Binder et al. speculated that an increased amount of internal initiation sites might compensate for the lack of highly efficient 5' motifs like 3p. In this thesis, this finding was investigated using RIG-I CTD mutants and IVT-RNAs of 40, 60, 100 and 200 bp length. After polyacrylamide gel purification, RNAs were either left untreated (3p-RNA) or were enzymatically digested with AP, which produces OH-dsRNA, like in the Binder et al. study. Additionally, 5'polyphosphatase treatment, which produces p-dsRNA, was included in the present experiment. AP is able to remove the α -, β - and γ -phosphates from DNA and RNA, creating 5'OH-ends. PP only digests β- and γ-phosphates, leaving a 5'p end. RNAs were transfected at different concentrations in HEK Trex RM -/- RIG-I WT, RIG-I F853A and RIG-I K861A cells and immune activation was assessed via dual-luciferase assay 20 h after stimulation. If RIG-I is able to detect long RNAs end-independently, AP and PP treatment would not change the immune stimulatory potential of long RNAs. Additionally, RIG-I WT, F853A and K861A expressing cells should show the same immune activation for long RNAs. 3p-RNA of all tested lengths showed no immune activation in cells expressing RIG-I K861A.

Compared to RIG-I WT IFN- β reporter activation was partially reduced in cells expressing RIG-I F853A after 3p-RNA stimulation (Figure 5.7, 3p-RNA).

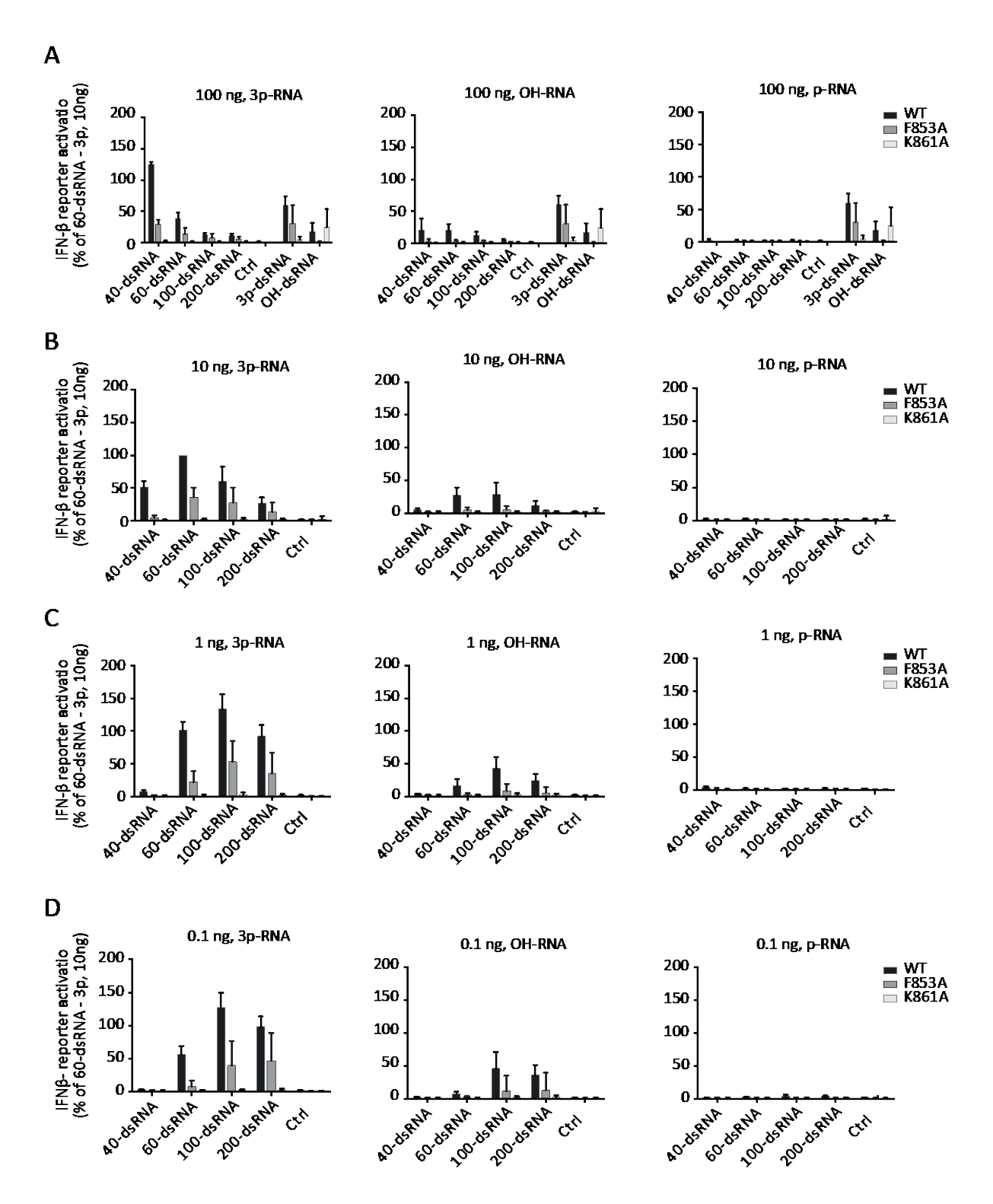


Figure 5.7: RIG-I activation by RNAs with differing lengths and 5'modifications

A-D) HEK Trex RM -/- cells expressing RIG-I WT, F853A or K861A were stimulated with 3p-, OH- or p-IVT RNAs with differing lengths and at different concentrations. IFN- β induction was assessed 20 h after RNA transfection by dual-luciferase assay. A) 100 ng/96-well (n=5 mean + SD), B) 10 ng/96-well (n=6, mean + SD), C) 1 ng/96-well (n=6, mean + SD), D) 0.1 ng/96-well (n=6, mean + SD).

Furthermore, AP treated RNA (OH-RNA) had a decreased immunostimulatory potential for RIG-I WT compared to 3p-RNA for all concentrations tested. OH-RNA did not cause immune activation in cells expressing RIG-I F853A and, unexpectedly, neither in RIG-I K861A cells (Figure 5.7, OH-RNA). Surprisingly, PP treatment of the RNA (p-RNA) caused complete abrogation of the immune response at all concentrations, for all RNA lengths and in all cells tested (Figure 5.7, p-RNA). Thus, in contrast to previous publications, no end-independent RIG-I activation mechanism was observed in these experiments. Notably at high RNA concentrations (10 ng and 100 ng) long 3p-RNAs (100 bp and 200 bp) displayed lower immune activation potential compared to shorter RNAs (40 bp and 60 bp), while at low RNA concentrations (1 ng and 10 ng) long 3p-RNAs caused a higher RIG-I activation compared to short RNAs (Figure 5.7).

5.3. 5'p mediates immunotolerance towards endogenous RNA

Reports whether RIG-I is activated by 5'p-RNA are not consistent. While there are studies on RIG-I-dependent recognition of p-RNA (Takahasi et al. 2008), others report that p-RNA is not detected by RIG-I (Schmidt et al. 2009, Ren et al. 2019).

5.3.1. 5'p inhibits RIG-I-dependent immune stimulation

In the previous experiment, it was shown that RIG-I-dependent immune activation was completely abrogated by 5'p (Figure 5.7). To study this further and investigate if this is a general effect, HEK Trex RM -/- RIG-I WT cells were transfected with 24 bp or 40 bp OHdsRNA, p-dsRNA or ssRNA (Table 8.4). Immune activation was measured 20 h after RNA stimulation via dual-luciferase assay. While 24 bp OH-dsRNA led to a considerable RIG-I activation, p-dsRNA induced like ssRNA no RIG-I activation (Figure 5.8A). A similar effect was observed for 40 bp RNA where immune activation after p-dsRNA transfection was clearly reduced compared to OH-dsRNA. Having said this, it was slightly higher than after ssRNA stimulation (Figure 5.8B). To test if this effect is also true for other cells, PBMCs were isolated and transfected with the same RNAs. RNA delivery to the cytoplasm via lipofection uses a passive transfection process that does not include an endosomal passage. To additionally exclude a TLR-dependent immune activation, PBMCs were treated with chloroquine (5 µg/ml) 30 min before RNA transfection. Chloroquine inhibits endosomal acidification, a prerequisite for TLR activation. RIG-I activation was analyzed 20 h after stimulation by measuring IFN- α in the supernatant via ELISA. Corresponding effects, as in HEK cells, were observed in PBMCs. 24 bp OH-dsRNA caused substantial RIG-I activation, while 24 bp p-RNA was completely unstimulatory. 40 bp p-RNA led to a minor IFN- α induction, albeit 6-fold lower compared to 40 bp OH-dsRNA. This shows that while OH-dsRNA causes substantial RIG-I activation, RIG-I does not tolerate 5′p.

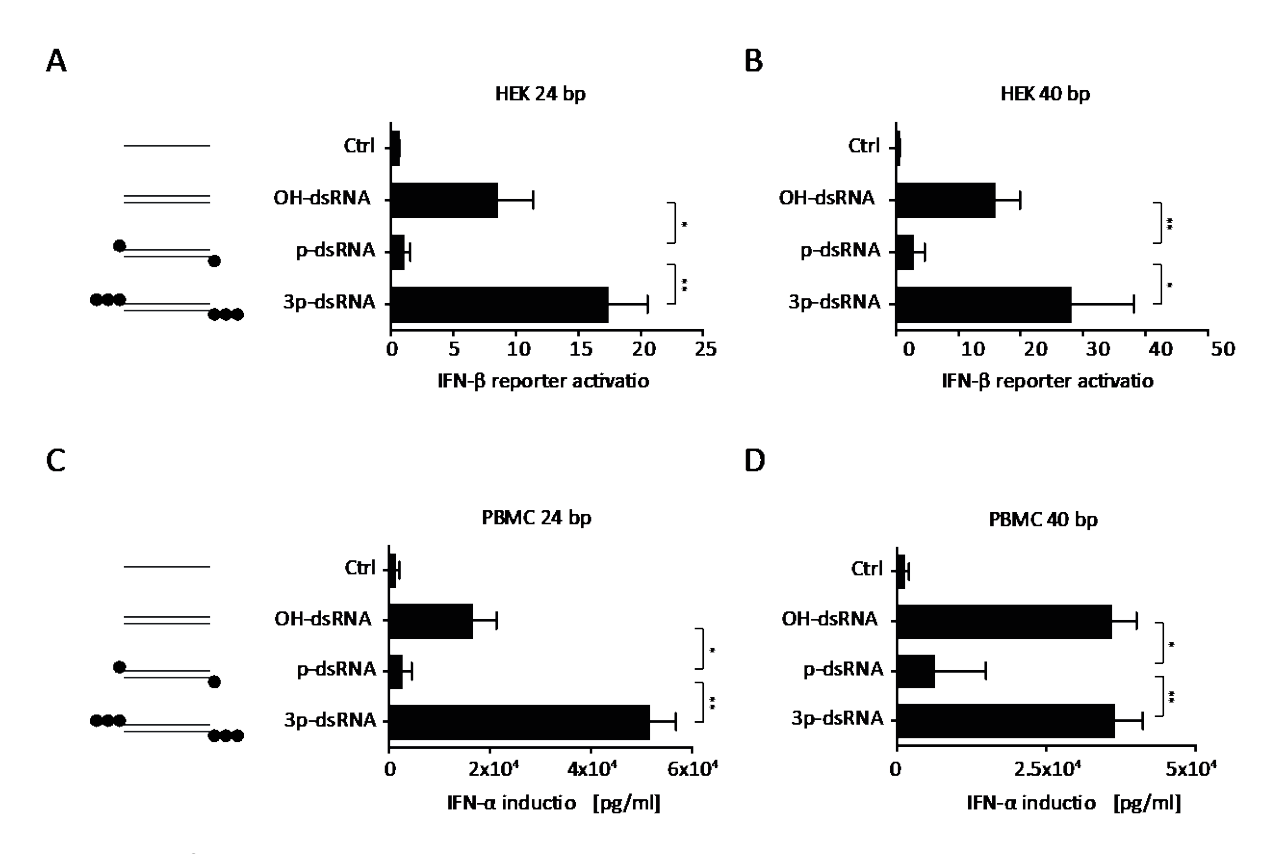


Figure 5.8: 5'p prevents RIG-I activation in HEK Trex cells and PBMCs

A+B) HEK Trex RM -/- cells expressing RIG-I WT were stimulated with indicated synthetic RNA ligands (0.1 μ g/ml). IFN- β induction was determined by dual-luciferase assay 20 h after RNA transfection. A) 24 bp RNA (n=4 + SD, one-way ANOVA, Dunnett 's post-test). C+D) Chloroquine treated PBMCs were stimulated with indicated synthetic RNA ligands (0.1 μ g/ml). IFN- α in the supernatant was determined by ELISA 20 h after transfection. C) 24 bp RNA (n=4 + SD, one-way ANOVA, Dunnett 's post-test) * (p < 0.05), ** (p < 0.01)

As discussed, RIG-I activation by 5′p-RNA was previously described (Takahasi et al. 2008). This is contradictory to the present results. However, the authors concluded that 5′ or 3′p enhances RNA stability not binding to RIG-I. In the next step, stimulation with RNAs from the publication (same sequence and same length) and additional control RNAs were tested for RIG-I activation in our cell system (Table 8.5). HEK Trex RM -/- RIG-I WT, RIG-I F853A and RIG-I K861A cells were transfected with the same RNAs and immune activation was measured via dual-luciferase assay 20 h after stimulation. Blunt-ended dsRNA with OH-groups on both 5′ends (1+4) caused substantial IFN-β induction in RIG-I WT and RIG-I K861A expressing cells (Figure 5.9B+C). In line with previous experiments, modification of the 3′end by addition of a phosphate (2+4) had no negative effect on RIG-I WT and RIG-I K861A activation. All dsRNAs tested that possess an overhang (1+3; 2+3;6+3,1+5,2+5,6+5) induced

RIG-I WT or mutant activation, albeit substantially lower compared to blunt-ended OH-dsRNA (1+4). While RNA with a phosphate on the 5'end of the antisense strand (2+4) had no immunostimulatory potential, RNA with a phosphate on the 5'end of the sense strand (6+4)

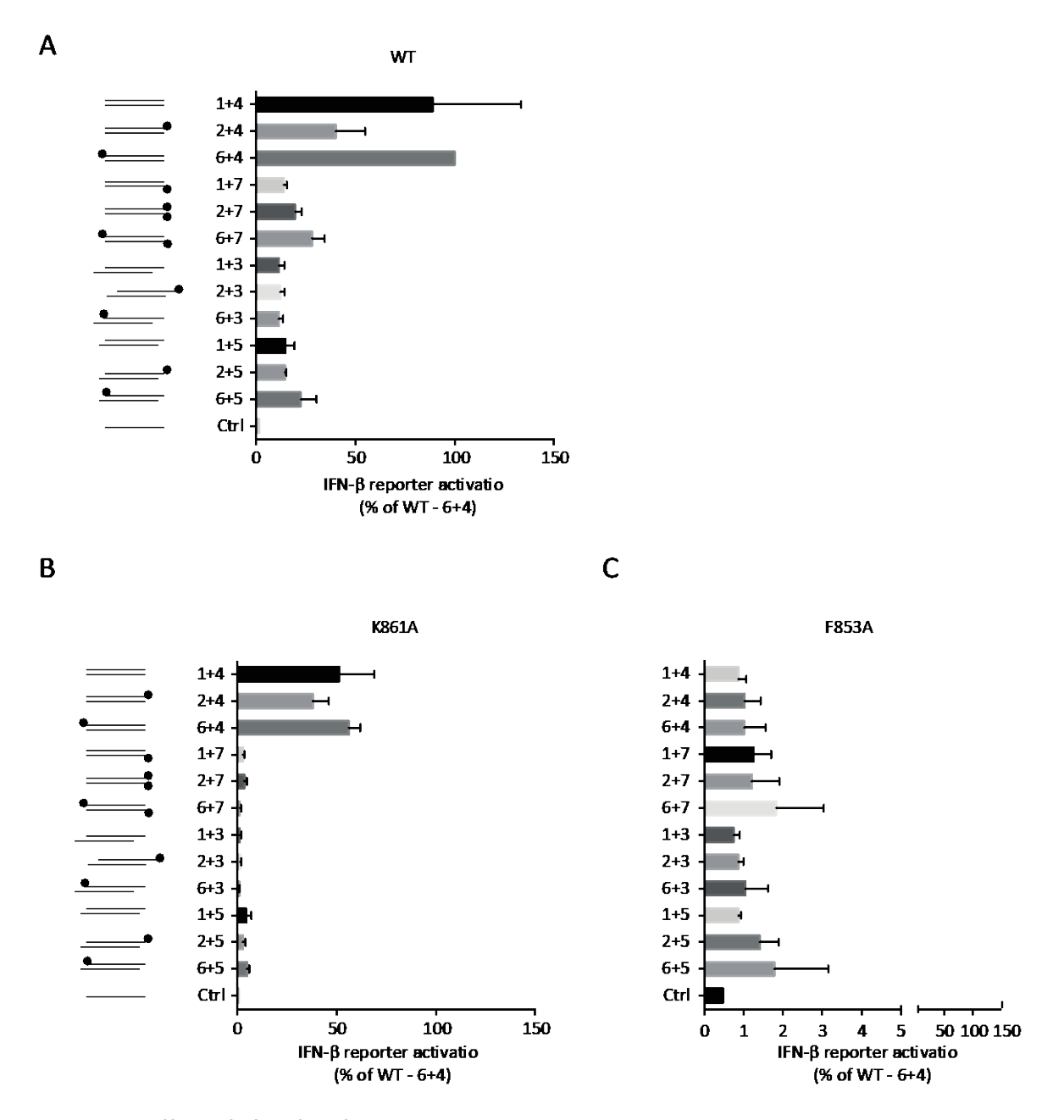


Figure 5.9: Effect of 5′p, 3′p, 5′OH and overhangs on RIG-I activation A-C) HEK Trex RM -/- cells expressing either RIG-I WT (A), RIG-I F853A (B) or RIG-I K861A (C) were stimulated with indicated synthetic RNAs (0.05 μ g/ml). IFN- β induction was assessed 20 h after RNA transfection by dual-luciferase assay (n=2, mean + SD).

caused RIG-I activation. Having said this, both RNAs possess a blunt-ended OH-end, which can be detected and bound by RIG-I, thereby explaining the immunostimulatory potential of the RNAs. Of note, recognition of monophosphorylated dsRNA was not sensitive to K861A mutation, indicating a mechanism not related to 5'p recognition (Figure 5.9B). RIG-I

activation in these experiments indeed seems to occur via binding of the 5'OH-dsRNA ends, since cells expressing the RIG-I F853A that does not detect OH-dsRNA did not respond to any of the tested ligands (Figure 5.9C).

5.3.2. 5'p prevents RIG-I CTD binding

Marq et al. proposed a non-stimulatory RIG-I binding mode. They showed binding of 3p-dsRNA with a 1 nt 5'overhang bound to RIG-I. However, it did not cause downstream RIG-I signaling, demonstrating that some ligands might be able to bind RIG-I and thereby block the RIG-I RNA binding cleft without causing immune activation (Marq et al. 2011). EMSAs were performed to test if a lack of RIG-I-dependent immune activation after stimulation with p-dsRNA is due to non-stimulatory binding or no binding. OH-dsRNA or p-dsRNA with a 5'Cy5 labelled antisense strand were mixed with RIG-I CTD protein and incubated for 10 min at RT. The Cy5 label is attached via a 5'p to the antisense strand and prevents RIG-I binding. Therefore, only the unlabelled RNA end can contribute to RIG-I binding. Subsequently, loading dye buffer was added and samples were applied to a native acrylamide gel.

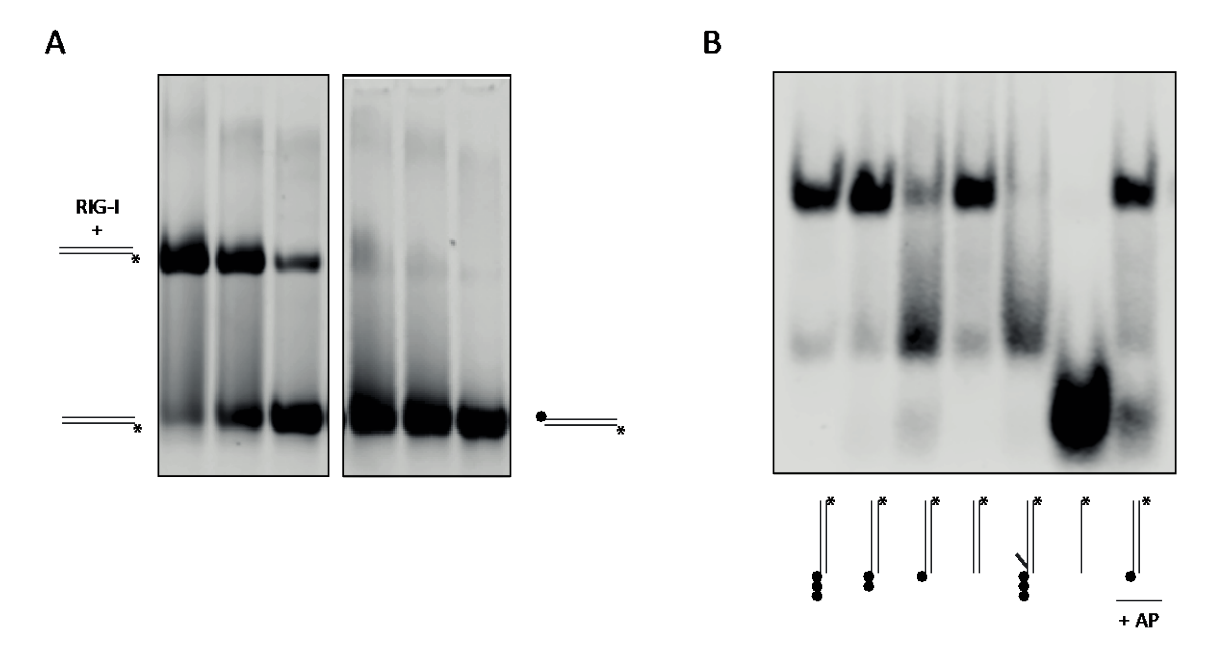


Figure 5.10: 5'p prevents RIG-I CTD binding

A) EMSA of RIG- WT CTD with OH-dsRNA and p-dsRNA. c[RNA]= 1 μ M, c[CTD]= 20, 10, 5 μ M. RNAs were labeled with Cy5 for visualization. B) EMSA of RIG- WT CTD with 3p-dsRNA, 2p-dsRNA, p-dsRNA, OH-dsRNA, 3p-N1 methylated, ssRNA and p-dsRNA treated with alkaline phosphatase (+ AP). c[RNA]= 1 μ M, c[CTD]= 20 μ M. RNAs were labeled with Cy5 for visualization. A+B) Gels were recorded using the Odyssey Fc reader. * indicates Cy5 modification.

While strong binding of RIG-I CTD to OH-dsRNA was observed even at lower protein concentrations, no binding was detectable for p-dsRNA to RIG-I CTD even at high CTD

concentration (Figure 5.10A). While binding affinity of OH-dsRNA resembled that of 3p-dsRNA and 2p-dsRNA (Figure 5.10B), hardly any RIG-I binding was detected for p-dsRNA. In accordance with the observations in Figure 5.1, 3p-N1-dsRNA like the control ssRNA displayed no RIG-I binding either (Figure 5.10B, lanes 5+6). Treatment of p-dsRNA with AP for 30 min at 37°C restored binding to the RIG-I CTD (Figure 5.10B, lane 7). AP dephosphorylates 5′and 3′ends of RNA and DNA and leaves a 5′OH. With this experiment, degradation or incorrect hybridization of the p-dsRNA that could account for the non-binding of the p-dsRNA to the CTD was excluded.

5.3.3. Identification of a conserved amino acid in the RIG-I CTD that mediates tolerances to p-dsRNA

As shown in the previous experiments, 5'p abolishes not only RIG-I activation but also RIG-I binding. To identify the structural reasons for this effect, amino acids in the RIG-I CTD that

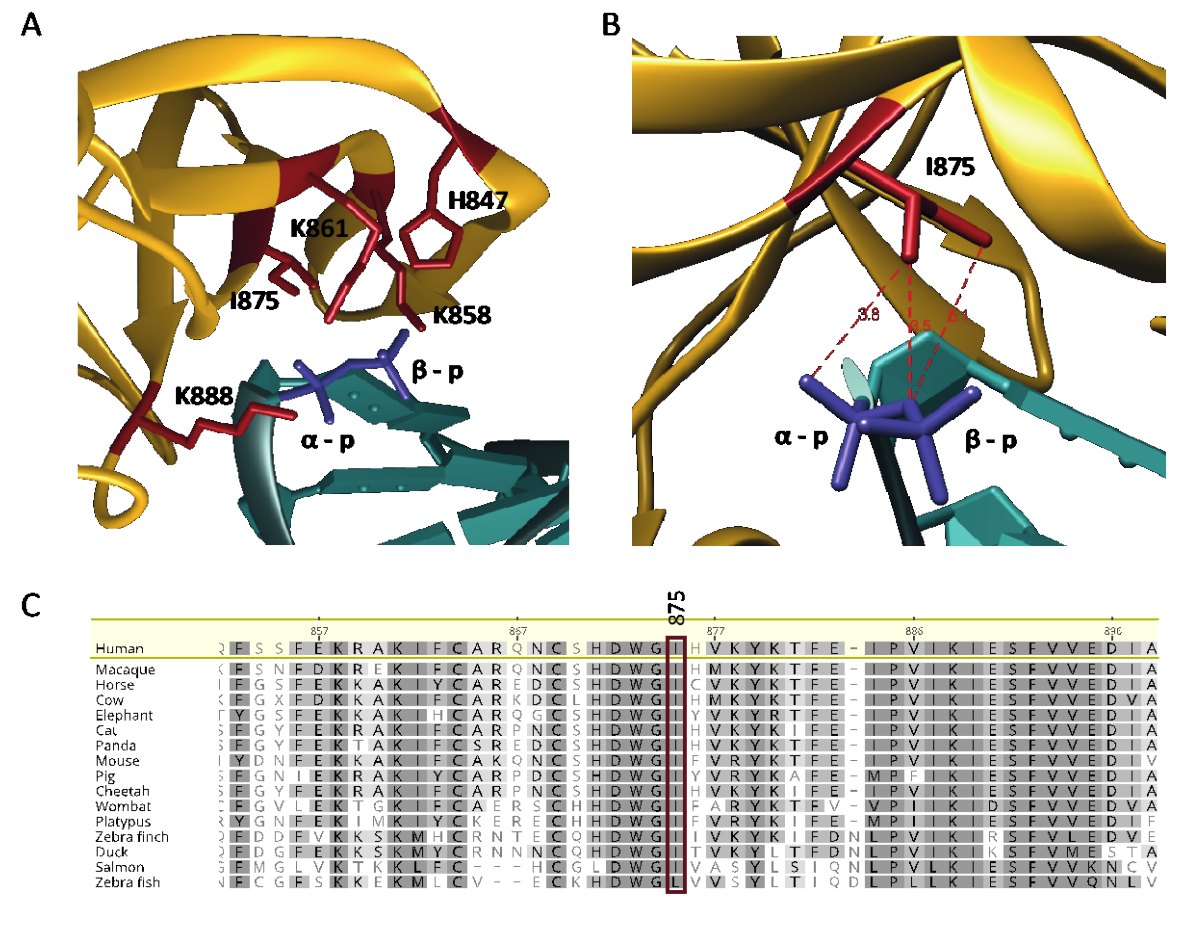


Figure 5.11: Amino acids in the RIG-I CTD in proximity to the α -phosphate

A+B) Excerpts of the RIG-I CTD crystal structure with 2p-dsRNA (PDB: 3NCU). RNA backbone is depicted in green, 2p in blue and RIG-I CTD in yellow. Graphs were made using Chimera. A) Amino acids which have a distance < 5 Å to the α -p are depicted in red: K888, K861, I875, H847, K858. B) Amino acid I875 is depicted in red. The distances between I875 and the α -p are indicated in Å. C) Amino acid alignment of RIG-I of 16 species. I875 is highlighted with a red box. Alignment was performed using Geneious Prime.

are closer than 5 Å to the α -p of the RNA were determined with distance analysis in the RIG-I CTD WT - 3p-dsRNA co-crystal structure (Wang et al. 2010) using UCSF Chimera (Pettersen et al. 2004) (Figure 5.11A). All identified amino acids (K858, K861, K888 and H847) except for I875 are involved in binding to the triphosphate. Mutation of these amino acids decreases or completely abrogates immune stimulation with 3p-dsRNA (Wang et al. 2010, Schuberth 2011) (this thesis Figure 5.3). However, the involvement of the amino acid closest to the α -p, I875 (Figure 5.11B), in binding the triphosphate has not been described so far. Of note, isoleucine has a hydrophobic side chain that exerts rather repulsive forces to OH or p. The fact that I875 is highly conserved in many species (Figure 5.11C) hints to the fact that it has an important function.

5.3.3.1. Mutation of I875 restores RIG-I activation by p-dsRNA

To test if I875 indeed plays a role in discrimination against p-RNA, HEK Trex RM -/- cells either expressing RIG-I WT, RIG-I 1875A or no RIG-I in a doxycycline-dependent manner were stimulated with 24 bp 3p-dsRNA, p-dsRNA, OH-dsRNA and ssRNA (Table 8.6). Immune activation was analyzed 20 h after stimulation and doxycycline addition via dual-luciferase assay. As expected, no immune activation in control cells (RM) was detected with any of the tested RNAs. IFN-β induction was comparable in RIG-I WT and RIG-I 1875A expressing cells after OH-dsRNA (OH-asOH) stimulation. As expected, stimulation with p-dsRNA (P-asP) caused no activation of RIG-I WT. Having said this, immune activation after p-dsRNA stimulation was comparable to OH-dsRNA stimulation in cells expressing RIG-I 1875A (Figure 5.12A). While RNA with a 5'p on the sense strand and a 5'OH on the antisense (P-asOH) could not restore RIG-I WT activation, RNA with a 5'p on the antisense strand and a 5'OH on the sense strand (OH-asP) led to immune activation comparable to OH-dsRNA (OH-asOH), indicating a sequence dependent RIG-I activation. This is in line with the results seen in Figure 5.3. A second RNA sequence with 40 bp was tested for its immunostimulatory potential in HEK Trex RM -/- cells expressing RIG-I 1875A and RIG-I WT. Similar effects compared to the 24 bp RNA were observed. OH-dsRNA (OH-asOH) caused equal RIG-I activation for WT and I875A, while p-dsRNA (P-asP) was only tolerated in cells expressing RIG-I 1875A (Figure 5.12B). For this sequence, RNA with OH on either 5'end partially restored IFN-β induction in RIG-I WT expressing cells. If the lack of RIG-I WT activation by p-dsRNA is

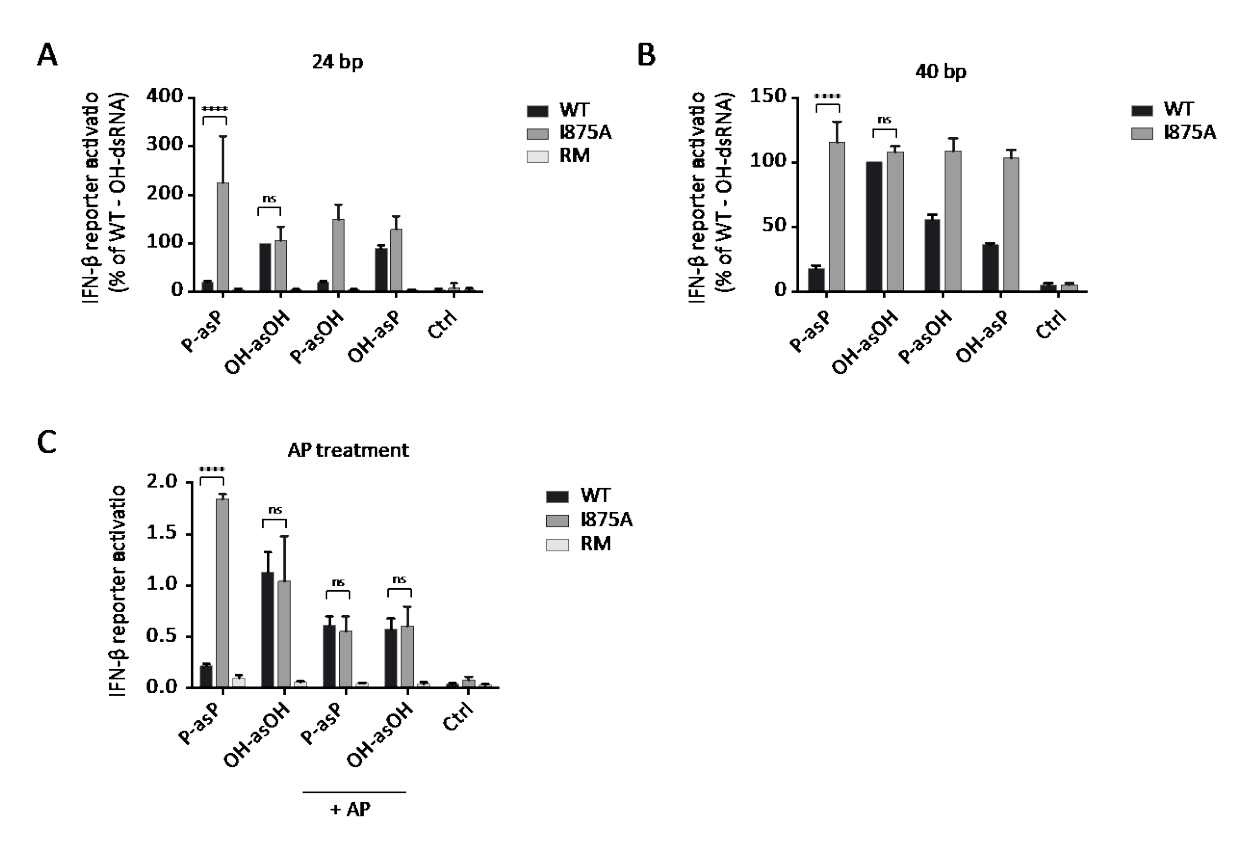


Figure 5.12: RIG-I I875A is activated by 5'p-RNA

A) HEK Trex RM -/- cells expressing RIG-I WT, RIG-I I875A or no RIG-I (RM) were stimulated with 24 bp RNAs $(0.05\mu g/ml)$ with differing 5'ends. IFN- β induction was assessed 20 h after RNA transfection by dual-luciferase assay (n=3, mean + SD, two-way ANOVA, Tukey's post-test). B) HEK Trex RM -/- cells expressing RIG-I WT or RIG-I I875A were stimulated with 40 bp RNAs $(0.05\mu g/ml)$ with differing 5'ends. IFN- β induction was assessed 20 h after RNA transfection by dual-luciferase assay (n=3, mean + SD, two-way ANOVA, Sidak's post-test). C) HEK Trex RM -/- cells expressing RIG-I WT, RIG-I I875A or no RIG-I (RM) were stimulated with 24 bp RNAs with differing 5'ends $(0.05\mu g/ml)$. + AP indicates alkaline phosphatase treatment of the RNA prior to transfection. IFN- β induction was assessed 20 h after RNA transfection by dual-luciferase assay (n=4, mean + SD, two-way ANOVA, Tukey's post-test). Significances are indicated as follows: **** (p < 0.0001), ns: not significant.

indeed due to the 5′p and not due to degradation or defective synthesis of the pRNA, this effect should be reversible by removing the 5′p. RNA was enzymatically digested with AP for 30 min at 37°C. Subsequently, HEK cells were transfected with the digested and control RNAs, and 20 h afterwards RIG-I activation was determined by IFN- β reporter assay. As expected, removal of the 5′p by AP treatment led to a comparable type I IFN induction as observed for OH-dsRNA in RIG-I WT expressing cells, while AP treatment had no effect on RIG-I 1875A (Figure 5.12C). This demonstrates that 5′p is indeed the modification that renders the p-dsRNA immune inactive.

To test if this effect is specific for p-dsRNA, RNAs with overhangs were tested on their stimulatory potential in I875A expressing cells and were compared to activation in RIG-I WT cells. RIG-I expression was induced by doxycycline before the cells were stimulated with the indicated RNAs (Table 8.7). Immune activation was assessed 20 h later by an IFN- β reporter.

No difference in the immunostimulatory potential of 3p-dsRNA with a 2nt 3'overhang was detected between cells expressing RIG-I WT or RIG-I I875A (Figure 5.13A). As already shown in Figure 5.4, 3p-dsRNA with a 2nt 5'overhang (ligand 2) caused no activation in cells expressing RIG-I WT. The same RNA led to a minor immune activation in I875A expressing cells, albeit lower compared to p-dsRNA (P-asP) and not significantly different compared to RIG-I WT cells. Stimulation with 3p-dsRNA (ligand 5) also showed no differences in immune activation between WT and I875A (Figure 5.13A). A similar pattern was observed for OH-dsRNA with overhangs. Although transfection of OH-dsRNA with a 2nt 5'overhang (ligand 6)

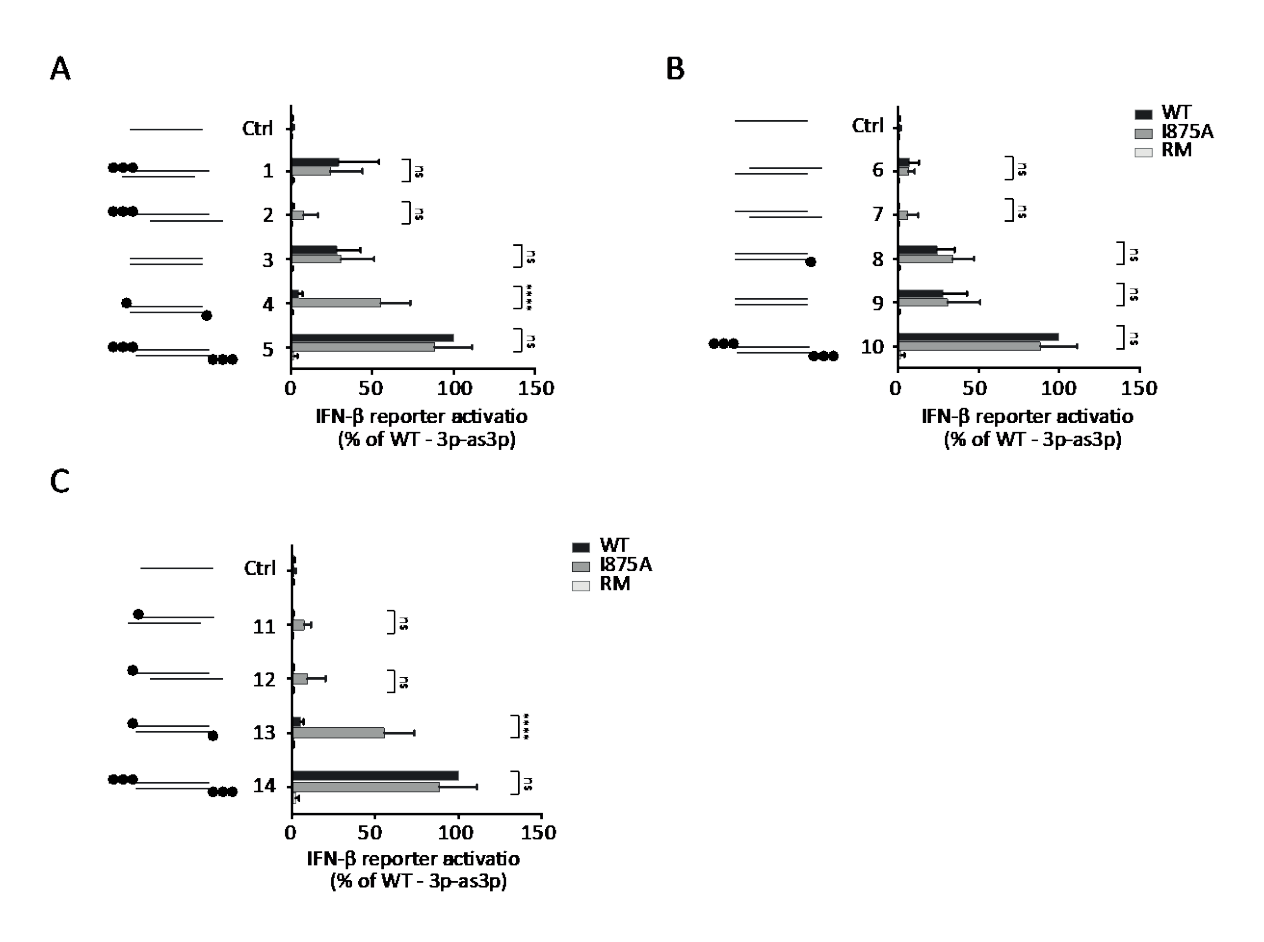


Figure 5.13: Effect of overhangs on RIG-I I875A activation

A-C) HEK Trex RM -/- cells expressing RIG-I WT, RIG-I I875A or no RIG-I (RM) were stimulated with indicated 24 bp RNAs (0.05 μ g/ml) with differing 5´ends and overhangs. IFN- β induction was assessed 20 h after RNA transfection by dual-luciferase assay (n=3, mean + SD) Significances are indicated as follows: **** (p < 0.0001), ns: not significant.

also led to a minor immune response in RIG-I I875A expressing cells, this effect was not significantly different to RIG-I WT cells. OH-dsRNA with a 2nt 3´overhang (ligand 7) caused low IFN- β induction in WT and I875A expressing (Figure 5.13B). P-dsRNA with overhangs expectedly did not lead to immune activation in WT cells, while both the 5´ and 3´overhang

RNA (ligand 11 and 12) caused a low immune activation in I875A cells, albeit again not significantly different to WT cells (Figure 5.13C).

These results demonstrate that the increased activation of RIG-I I875A is highly specific for 5'monophosphorylated RNAs, while no differences in the immune response for other RNA modifications are observed in cells expressing RIG-I WT or RIG-I I875A.

In order to compare RIG-I activation at low and high doses, titration curves of 3p-dsRNA, OH-dsRNA, p-dsRNA, 3p-N1-dsRNA or ssRNA were performed in HEK Trex RM -/- cells expressing RIG-I WT, RIG-I I875A or RIG-I H830A. While the binding curves for 3p-dsRNA and OH-dsRNA were comparable between RIG-I WT and RIG-I I875A expressing cells, the activation curve for p-dsRNA was significantly different.

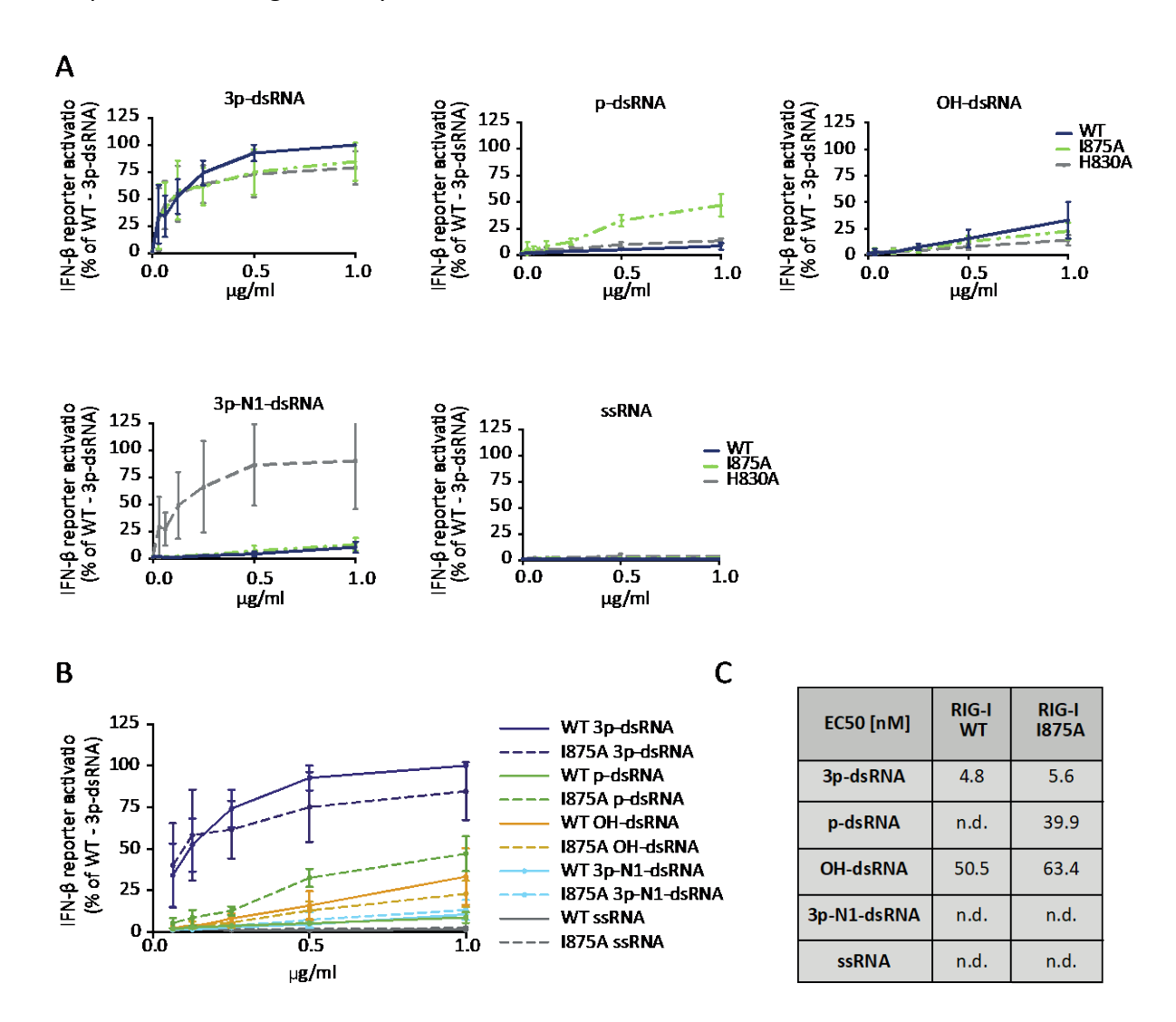


Figure 5.14: Titration curves of RIG-I WT and RIG-I 1875A with different ligands

A) Titration curves of HEK Trex RM -/- cells expressing RIG-I WT, RIG-I I875A or no RIG-I H830A with indicated RNAs. IFN- β induction was assessed 20 h after RNA transfection by dual-luciferase assay (n=4, mean \pm SD). B) Titration curves of HEK Trex RM -/- cells expressing RIG-I WT or RIG-I I875A with indicated RNAs. IFN- β induction was assessed 20 h after RNA transfection by dual-luciferase assay (n=4, mean \pm SD). C) EC50 values were determined by nonlinear regression on data from B) using Prism6. n.d. = not determined.

No activation at any concentration by ssRNA and 3p-N1-dsRNA was detected in WT and I875A cells, while the RIG-I H830A cells showed — in line with previous experiments (Schuberth 2011, Schuberth-Wagner et al. 2015) — a strong response to 3p-N1-dsRNA. The EC50 values for RIG-I WT and RIG-I I875A are in the same range for OH-dsRNA (50.5 nM vs 63.4 nM) and 3p-dsRNA (4.8 nM vs 5.6 nM). While EC50 of RIG-I I875A with p-dsRNA was 39.9 nM, and therefore comparable to the EC50 for OH-dsRNA, the EC50 for RIG-I WT and p-dsRNA could not be calculated because no RIG-I activation was detectable. EC50 of ssRNA and 3p-N1-dsRNA with RIG-I WT and RIG-I I875A could not be determined.

5.3.3.2. Mutation of I875 restores binding to p-dsRNA

EMSAs were performed as previously described to test if the identified amino acid (I875) also prevents p-dsRNA binding. RNA at constant concentration (0.6 μ M) was mixed with CTD protein ranging from 13 μ M to 2.5 nM. RNA-protein shifts were visualized on a native polyacrylamide gel with the Odyssey Fc Reader using Cy5 labelled RNAs. The binding of 3p-dsRNA, OH-dsRNA, p-dsRNA or ssRNA to RIG-I CTD WT or RIG-I CTD I875A protein was investigated.

Binding of 3p-dsRNA and OH-dsRNA to 1875A CTD was slightly lower compared to WT CTD. No binding of ssRNA to WT CTD or I875A CTD was detected. As already shown in Figure 5.10, no binding of p-dsRNA to WT CTD was observed. However, binding of p-dsRNA to I875A CTD was comparable to the binding of OH-dsRNA to I875A CTD and WT CTD (Figure 5.15A). Quantification of the bound RNA fractions of three independent experiments using the ImageStudioLite software showed comparable binding curves for I875A with p-dsRNA and OH-dsRNA. Slightly stronger binding for WT CTD to OH-dsRNA was detected compared to 1875A CTD, while no binding for p-dsRNA even at high CTD concentration was detected (Figure 5.15B). Similar results were obtained with Surface Plasmon Resonance: while WT CTD and I875A CTD showed K_d values in the nanomolar range for 3p-dsRNA (0.19 nM and 0.35 nM respectively), no binding was detected for ssRNA. WT CTD binding to OH-dsRNA was 20 times stronger compared to p-dsRNA, while binding of OH-dsRNA to I875A CTD was 2.5 weaker compared to p-dsRNA. Binding of p-dsRNA to I875A CTD was 10 times stronger compared to WT CTD (Figure 5.15C). In summary, mutation of 1875 to alanine rescues pdsRNA binding and activation by p-dsRNA to a similar level as observed for OH-dsRNA, while activation and binding by 3p-dsRNA and OH-dsRNA is not increased compared to WT RIG-I.

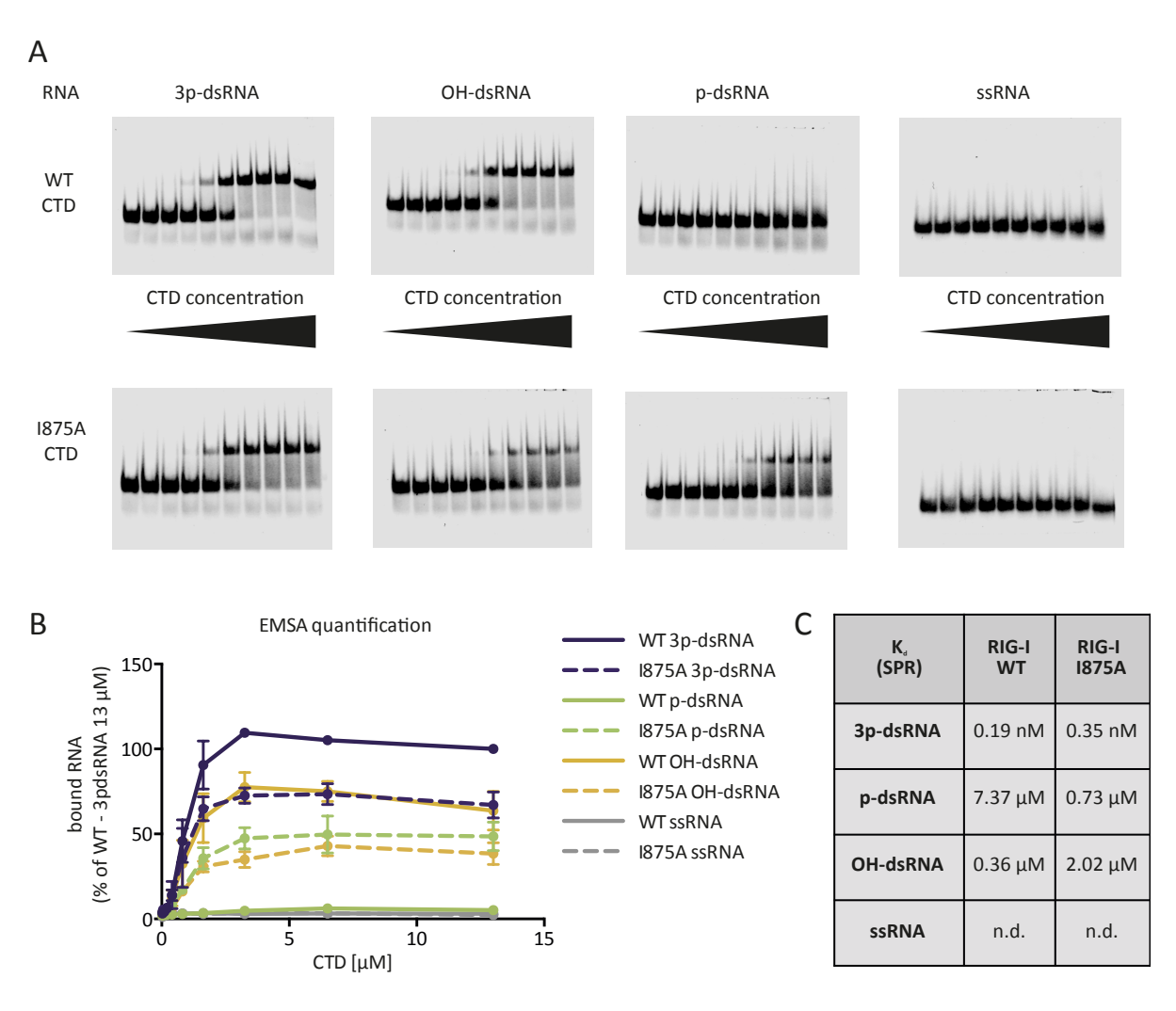


Figure 5.15: Binding studies of RIG-I I875A with different RNA ligands

A) EMSA of RIG- WT CTD or RIG-I 1875A CTD with 3p-dsRNA, OH-dsRNA, p-dsRNA or ssRNA. c[RNA]= $0.6~\mu$ M, c[CTD]= 13 - $0.025~\mu$ M. RNAs were labeled with Cy5 for visualization. One representative of three independent experiments is shown. B) Bound RNA fractions from EMSAs like in A) were quantified using ImageStudioLite (n=3). Dotted line: I875A CTD, Solid line: WT CTD, blue: 3p-dsRNA, green: p-dsRNA, orange: OH-dsRNA, grey: ssRNA C) K_d values of RIG-I WT CTD and RIG-I 1875A CTD with indicated RNAs were determined using Surface plasmon Resonance (SPR) (experiment was performed by Karl Gatterdam). n.d. = not determined.

5.3.4. Long-term expression of RIG-I I875A leads to immune stimulation

Constitutively active RIG-I can have serious implications and has been associated with the establishment of interferonopathies (Jang et al. 2015, Lassig et al. 2018). The previous experiments established that 5'p prevents RIG-I activation and that this effect is mediated by a single amino acid - I875 - in the RIG-I CTD. The question arose why RIG-I needs to differentiate between p-dsRNA and OH-dsRNA. It is interesting to note that many abundant endogenous RNA species possess a 5'p, such as rRNAs and tRNAs. Would endogenous ligands in the cytosol activate RIG-I if it was not able to discriminate between OH-dsRNA and p-dsRNA, as it is the case in cells expressing RIG-I I875A? If this is indeed true, expression of

RIG-I 1875A without addition of exogenous ligands should cause immune activation, as was seen for RIG-I H830A (Schuberth-Wagner et al. 2015).

RIG-I WT, I875A or H830A expression was induced with doxycycline in HEK Trex RM -/- cells. RNA was extracted 72 h after doxycycline addition and mRNA expression of RIG-I and the ISGs IFIT1 and Lgp2 was assessed via qPCR. RIG-I mRNA expression was equal in all cell lines treated with doxycycline, thus excluding effects caused by differential expression of the RIG mutants (Figure 5.16A). Long-term expression of RIG-I H830A led to an increased ISG expression compared to RIG-I WT, which is in line with previous data (Schuberth 2011, Schuberth-Wagner et al. 2015). However, ISG upregulation was highest after long-term expression of RIG-I I875A and significantly increased compared to cells expressing RIG-I WT or RIG-I H830A (Figure 5.16B+C).

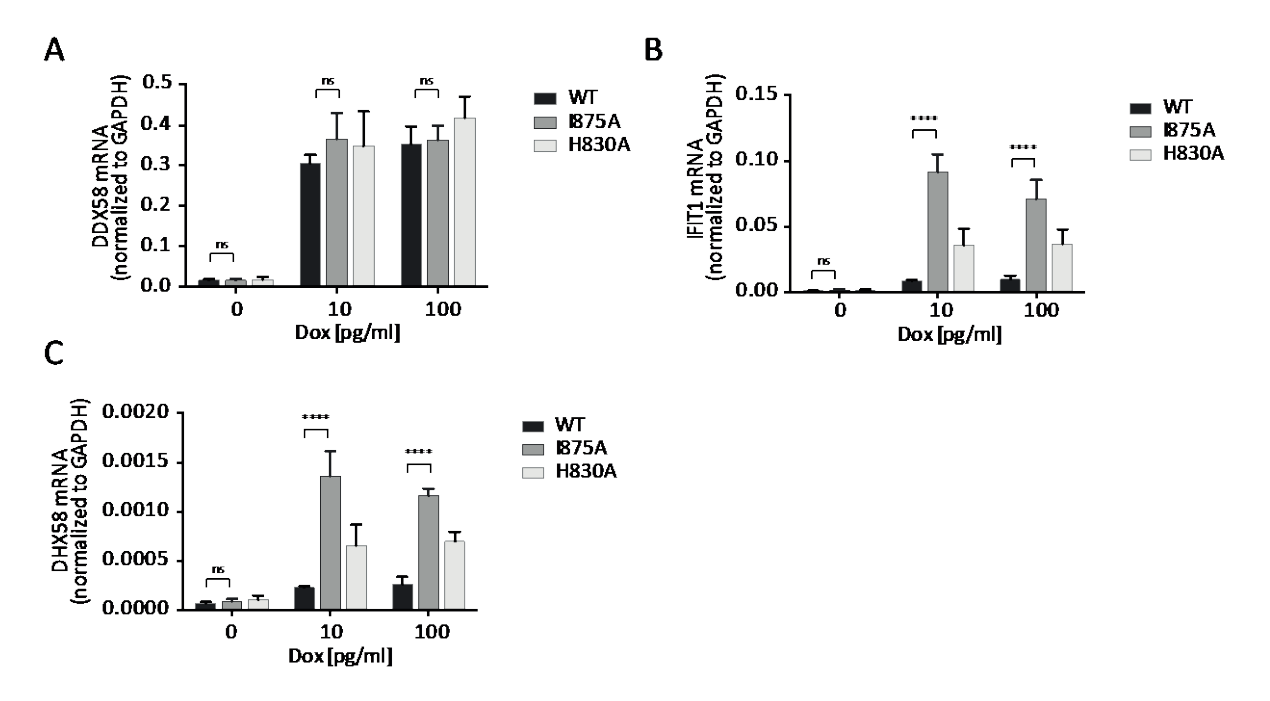


Figure 5.16: Long-term expression of RIG-I 1875A causes ISG upregulation without addition of exogenous stimuli

A-C) RIG-I WT, RIG-I 1875A or RIG-I H830A expression was induced in HEK Trex RM -/- cells in the absence of exogenous RIG-I stimuli. RNA was extracted 72 h later and mRNA expression of DDX58 (A, n=4), IFIT1 (B, n=4) and DHX58 (C, n=3) were analyzed by qPCR and normalized to GAPDH (mean + SD, two- way ANOVA, Tukey's post test). Significances are indicated as follows: * (p < 0.05), (p < 0.001), **** (p < 0.0001), ns: not significant. Dox: Doxycycline

Next, whether immune activation was only observed on the RNA level or also on the protein level was assessed. Here again RIG-I WT or mutant expression was induced with doxycycline and 72 h later protein expression of RIG-I and phosphorylation of IRF3 was assessed via immunoblot and normalized to β -actin expression. The RIG-I protein levels in doxycycline treated cells were comparable in all cell lines (Figure 5.17A+C). Resembling the RNA data,

IRF3 phosphorylation was increased in H830A cells compared to WT cells. However, pIRF3 was strongest in RIG-I I875A expressing cells (Figure 5.17B+C). This data shows that RIG-I I875A is activated by endogenous RNA and to an even higher extent than RIG-I H830A. Long-term expression of RIG-I I875A in the absence of exogenous stimuli causes immune activation on the RNA and protein levels, underscoring the need for RIG-I to discriminate against p-dsRNA.

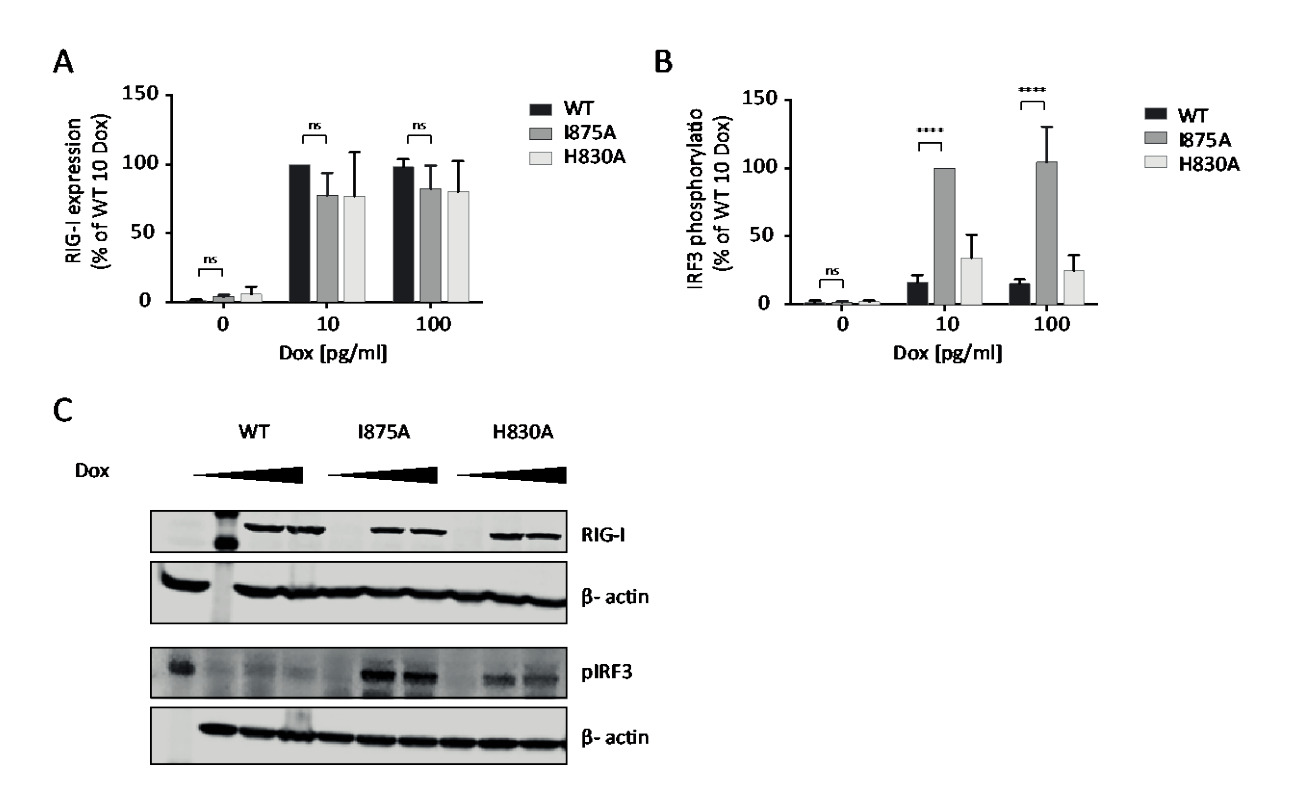


Figure 5.17: Long-term expression of RIG-I I875A induces phosphorylation of IRF3 without addition of exogenous stimuli

A-B) RIG-I WT, RIG-I 1875A or RIG-I H830A expression was induced in HEK Trex RM -/- cells in the absence of exogenous RIG-I stimuli. Protein was extracted 72 h later and RIG-I expression (A) and phosphorylation of IRF3 (B) were analyzed by western blot and normalized to β -actin (n=4, mean + SD, two-way ANOVA, Tukey's post test). C) One representative experiment of B) is shown. Significances are indicated as follows: **** (p < 0.0001), ns: not significant. Dox: Doxycycline

5.3.5. Identification of endogenous ligands activating RIG-I I875A

Long-term expression of RIG-I I875A showed that there are indeed endogenous ligands that would activate RIG-I without I875 mediated immune tolerance. To identify the actual stimulating ligand, different RNA species were tested for their potential to activate RIG-I I875A.

5.3.5.1. Immune stimulation with whole cell RNA extracts

First, whole cell RNA was isolated from A549 cells using TRIzol extraction, and HEK Trex RM – /- cells expressing RIG-I WT or RIG-I 1875A were tested for immune activation after short-term stimulation with this RNA. While the RNA also induced an immune response in RIG-I WT expressing cells, IFN-β induction was significantly increased in cells expressing RIG-I 1875A for both RNA concentrations tested (Figure 5.18). RNA was treated with Terminator Exonuclease (TE) to test if this immune activation is 5p-dependent. TE specifically digests ssRNA possessing a 5′p in a 5′ to 3′ direction. It does not digest RNA that has a 5′3p, 5′cap or 5′OH. Additionally, RNA was treated with AP to remove 5′phosphates and PP as a control. If the 1875A stimulating ligand in the whole cell RNA pool is 5′monophosphorylated, RNA should on the one hand lose its activating potential in cells expressing RIG-I 1875A after TE digestion. On the other hand, AP treatment should render the RNA as stimulatory in cells expressing RIG-I WT as in cells expressing RIG-I 1875A, because it leaves an OH at the 5′end which has the same stimulatory potential in WT an 1875A cells.

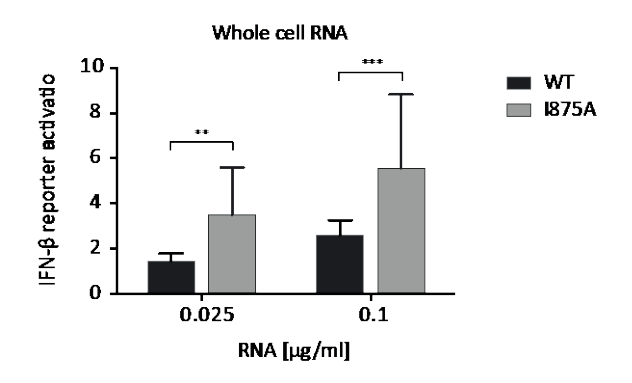


Figure 5.18: Whole cell RNA is highly stimulatory for RIG-I 1875A

Whole cell RNA was extracted with TRIzol from A549 cells. HEK Trex RM -/- cells expressing RIG-I WT or RIG-I l875A were stimulated with whole cell RNA extracts. IFN- β induction was assessed 20 h after RNA transfection by dual-luciferase assay (n=8 (0.025 μ g/ml), n=9 (0.1 μ g/ml), mean + SD, paired t-test) Significances are indicated as follows: ** (p < 0.01), *** (p < 0.001).

PP removes the γ- and β- phosphates of 3p-dsRNA and leaves a 5′p. In case the RNA species activating RIG-I I875A in the whole cell RNA pool is 5′monophosphorylated, PP treatment should not change the activation pattern compared to untreated whole cell RNA. RNAs were enzymatically treated and subsequently transfected into HEK Trex RM -/- cells expressing RIG-I WT or RIG-I I875A. Immune activation was assessed 20 h later by dual-luciferase assay. TE treatment reduced the activation potential of whole cell RNA, but unexpectedly did not lead to a complete loss of RIG-I I875A activation (Figure 5.19A). Furthermore, AP treatment

had no effect on the stimulating potential of the RNA in cells expressing WT or I875A RIG-I, while as expected, PP treatment showed no effect on the activation potential of the RNA in WT and I875A expressing cells (Figure 5.19A). Terminator exonuclease is mainly active on ssRNA. Since a dsRNA structure is indispensable for RIG-I activation, it is possible that TE is not able to degrade all I875A stimulating RNA because they are double-stranded. To test this hypothesis RNA was digested with RNase A in low and high salt buffers. RNase A cleaves

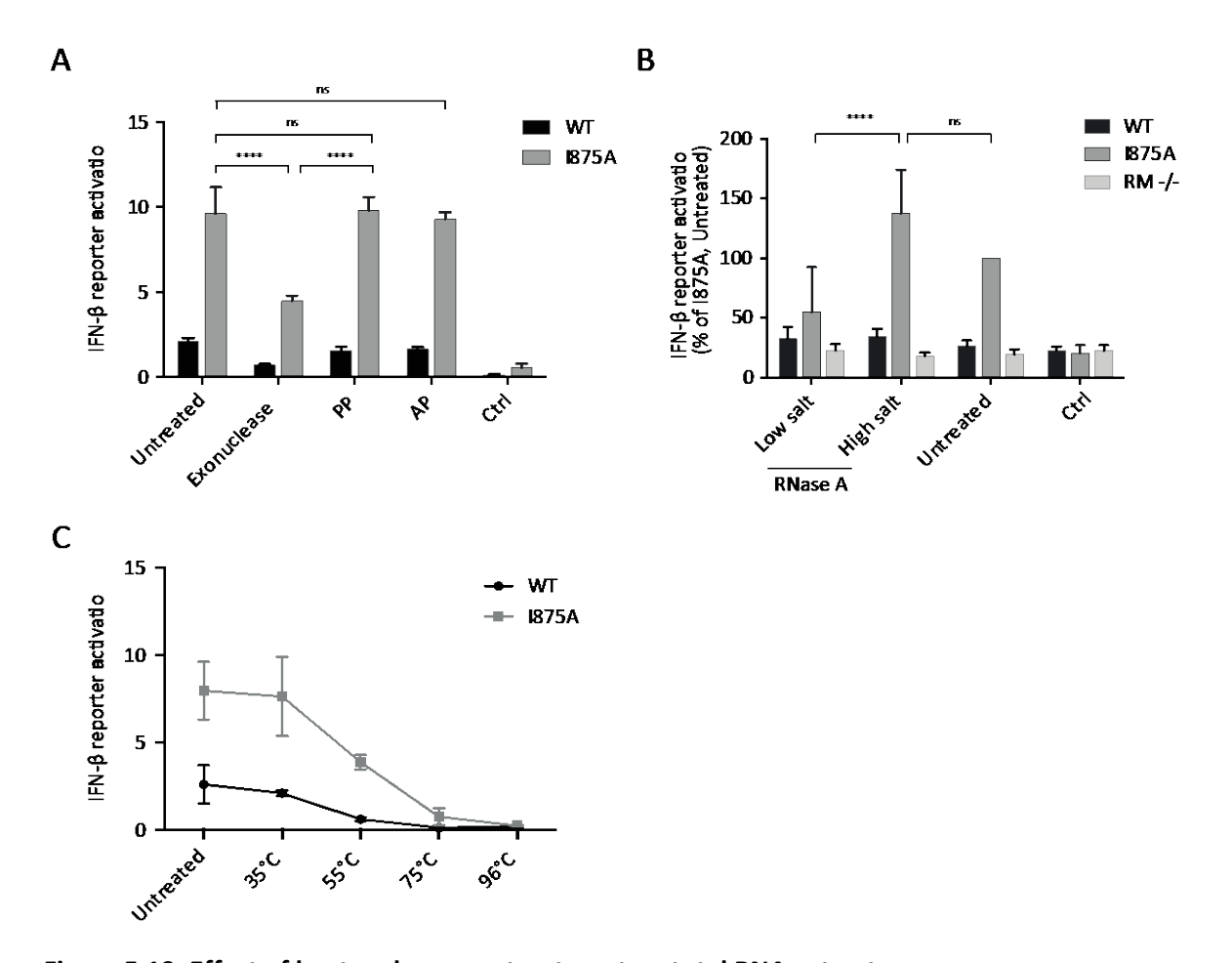


Figure 5.19: Effect of heat and enzyme treatment on total RNA extracts

A) Whole cell RNA was extracted using TRIzol from A549 cells. RNA was treated with terminator exonuclease (TE), polyphosphatase (PP), alkaline phosphatase (AP) or left untreated. RNA was transfected into HEK Trex RM -/- cells expressing RIG-I WT or RIG-I I875A. IFN- β induction was assessed 20 h after RNA transfection by dual-luciferase assay (n=3, mean + SD, two- way ANOVA, Tukey's post test). Significances are indicated as follows: ***** (p < 0.0001), ns: not significant. B) Whole cell RNA was extracted using TRIzol from A549 cells. RNA was treated with RNase in low salt (50 mM NaCl) or high salt (200 mM NaCl) conditions or left untreated. RNA was transfected into HEK Trex RM -/- cells expressing RIG-I WT or RIG-I I875A. IFN- β induction was assessed 20 h after RNA transfection by dual-luciferase assay (n=5, mean + SD, two- way ANOVA, Tukey's post test). Significances are indicated as follows: **** (p < 0.0001), ns: not significant. C) Whole cell RNA was extracted using TRIzol from A549 cells. RNA was incubated at the indicated temperatures for 30 min. RNA was transfected into HEK Trex RM -/- cells expressing RIG-I WT or RIG-I I875A. IFN- β induction was assessed 20 h after RNA transfection by dual-luciferase assay (n=4, mean \pm SD).

ssRNA as well as dsRNA at low salt concentrations (up to 100 mM NaCl). At high salt concentrations (> 300 mM NaCl) RNase A specifically digests ssRNA. Indeed, RNase A

digestion at low salt concentrations reduced the immune stimulatory potential of the RNA significantly compared to untreated RNA (Figure 5.19B). RNA treated with RNase A in a high salt buffer triggered the same IFN- β promoter reporter activation as untreated RNA, which demonstrates that the stimulatory RNA is indeed double-stranded. Next, RNA was incubated at different temperatures for 30 min. Increasing the incubation temperature negatively correlated with the immunostimulatory potential of the RNA (Figure 5.19C). Higher temperatures might either cause degradation of the RNA or destroy secondary structures such as double-strand stretches that are essential for the activating potential of the RNA.

5.3.5.2. Investigation of tRNA and rRNA as possible I875A activators

Compared to RIG-I WT cells, whole cell RNA extracts showed increased activation in cells expressing RIG-I 1875A and this RNA was partially sensitive to TE treatment. There are different RNA species in the cell that were described in the introduction of this thesis. Looking at their 5'end, tRNAs and rRNAs stand out as RNA species that possess a 5'p and are present in the cytoplasm. Usually rRNAs and tRNAs are single-stranded RNAs and should accordingly be excluded from RIG-I activation. However, RNAs - especially rRNAs - form secondary structures with double-strand stretches that might cause RIG-I activation. Lässig et al. showed that long base-paired expansion segments of rRNAs can stimulate RIG-I E373Q (Lassig et al. 2015). This constitutive active RIG-I mutant is not able to hydrolyze ATP and is therefore locked on suboptimal RNA ligands. This shows that RIG-I has access to certain rRNA segments. These two RNA species were therefore the most promising candidates to be the stimulating species in the whole cell RNA pool for RIG-I 1875A. tRNAs possess a 5'p and have a cloverleaf like structure with base-paired stretches. Since it is difficult to isolate pure tRNA, commercial yeast tRNA was used and immune activation in HEK Trex RM -/- cells expressing RIG-I WT or RIG-I 1875A with several yeast tRNA concentrations was tested. No immune activation was detected 20 h after RNA transfection (Figure 5.20A), and hence tRNAs were excluded to be the stimulating species in the RNA pool.

rRNAs were subsequently investigated. There are several mature rRNAs in the cytosol. While 18S, 28S and 5.8S rRNAs are transcribed from one precursor RNA by RNA Pol I, 5.8 rRNA is transcribed by RNA Pol III that is also responsible for tRNA transcription. Since rRNA contributes up to 75% of the RNA in cells, separation on an agarose gel of whole cell RNA shows two characteristic RNA bands that stand out from the whole RNA pool: the 18S and 28S band (Figure 5.20B). To test for the stimulating potential of 18S and 28S rRNA, these two

bands were excised from the gel and RNA was extracted using a gel extraction kit. HEK Trex RM -/- cells were transfected with the gel-extracted RNA and untreated whole cell RNA (total RNA). In contrast to total RNA, 18S rRNA led to no substantial immune activation in

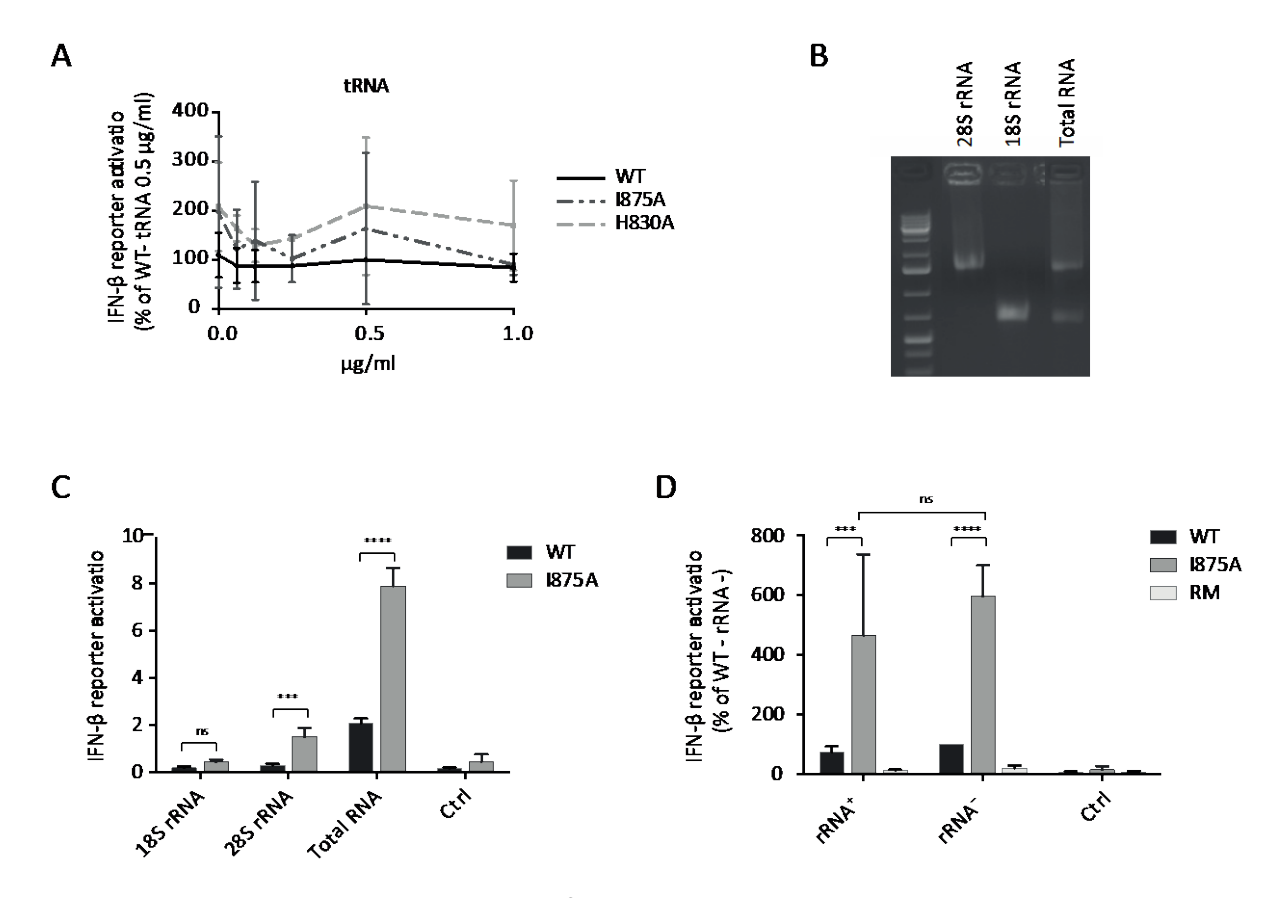


Figure 5.20: Immune activation potential of tRNA and rRNA

A) HEK Trex RM -/- cells expressing RIG-I WT or RIG-I 1875A were stimulated with yeast tRNA. IFN- β induction was determined 20 h after RNA transfection by dual-luciferase assay (n=2, mean \pm SD, one- way ANOVA, Tukey's post test). B) Exemplary agarose gel of extracted 18S rRNA, 29S rRNA and whole cell RNA (total RNA). C) Whole cell RNA was extracted from A549 cells using TRIzol and seperated on an agarose gel. 18S rRNA and 28S rRNA were extracted from the gel. HEK Trex RM -/- cells expressing RIG-I WT or RIG-I 1875A were transfected with untreated whole cell RNA (total RNA), 18S rRNA and 28S rRNA (0.1 µg/ml). IFN- β induction was assessed 20 h after RNA transfection by dual-luciferase assay (n=4, mean \pm SD, two-way ANOVA, Sidak's post test). D) Whole cell RNA was extracted using TRIzol from A549 cells. RNA was fractionated into a rRNA and rRNA fraction using the ribominus kit. Fractionated RNA was transfected into HEK Trex RM -/- cells expressing RIG-I WT or RIG-I 1875A (0.1 µg/ml). IFN- β induction was assessed 20 h after RNA transfection by dual-luciferase assay (n=4, mean + SD, two- way ANOVA, Tukey's post test). Significances are indicated as follows: **** (p < 0.001), ***** (p < 0.0001), ns: not significant.

WT or I875A cells. RNA extracted from the band corresponding to 28S rRNA caused immune activation in RIG-I I875A cells that was significantly increased compared to RIG-I WT cells (Figure 5.20C). However, the IFN- β induction was 5 times lower compared to the stimulation with total RNA in RIG-I I875A cells. On the one hand, gel electrophoresis might destroy secondary rRNA structures important for the RIG-I activation potential of the RNA. On the other hand, gel extraction occurs at 65°C, which decreases the immunostimulatory potential

of the RNA (Figure 5.19C). To exclude that the extraction method is responsible for the low activation potential of the rRNA, a second rRNA extraction method was applied. Specific locked-nucleic acid (LNA) probes against 18S and 28S rRNA were used to purify these RNAs (rRNA⁺) from the whole cell RNA pool, and the remaining RNA (rRNA⁻) was extracted using ethanol precipitation. HEK Trex RM -/- cells expressing RIG-I WT or RIG-I 1875A were stimulated with rRNA⁺ and rRNA⁻ and their activation potential was analyzed 20 h after transfection by dual-luciferase assay. In contrast to the gel extracted rRNA, rRNA⁺ caused immune activation to a similar level as rRNA⁻ in RIG-I 1875A cells and was increased 6-fold compared to RIG-I WT cells (Figure 5.20D). Of note, gel extracted rRNA was compared to whole cell RNA extracts while LNA extracted rRNA (rRNA⁺) was studied in comparison to rRNA⁻.

In conclusion, these results show that rRNA might be contributing to the stimulatory potential of whole cell RNA extracts in RIG-I I875A cell, but that it is not the sole and main activator.

5.3.5.3. polyA RNA is the activating RNA species in the whole cell RNA extracts Other prominent RNAs in the cytosol are polyadenylated RNAs. mRNAs are the main polyadenylated RNA species, but also rRNAs were found to contain polyA tails. Like tRNAs and rRNAs, mRNAs are single-stranded but form secondary structures leading to base-paired stretches. Additionally, mRNAs usually possess a cap1 or cap2 structures that exclude mRNA from RIG-I activation as discussed in section 5.1. Having said this, many mRNAs have a high turnover rate to quickly adjust to the momentary needs of the cell. Degradation of the RNA involves de-capping and in this process mRNA is shortly present in a 5′p state. Thus, mRNA might also be a candidate RNA species involved in activation of RIG-I 1875A.

Whole cell RNA extracts (total RNA) were incubated with polyA beads to separate polyA⁺ RNA from RNA without a polyA tail (polyA⁻ RNA). qPCR on the RNA fractions was performed to test if the separation had worked. Nuclear expressed mRNAs such as GAPDH and Myc were significantly enriched in the polyA⁺ fraction compared to total RNA and the polyA⁻ fraction. Equally, mitochondrial expressed mRNAs (NADH-ubiquinone oxidoreductase chain 1 (ND1) and ND5) were also enriched in the polyA⁺ fraction. Contrarily, 18S rRNA was enriched in the polyA⁻ fraction compared to total RNA and the polyA⁺ fraction (Figure 5.21B). The fractionated RNA and total RNA were transfected into cells expressing RIG-I WT or RIG-I 1875A. Analysis of IFN-β induction 20 h after RNA transfection displayed, as expected and

shown in previous experiments, an increased immune activation in RIG-I I875A compared to WT cells by total RNA. Surprisingly, I875A activation was completely abrogated in cells treated with the polyA⁻ RNA, while polyA⁺ RNA caused a significantly increased immune activation in RIG-I I875A expressing cells even compared to total RNA (Figure 5.21A).

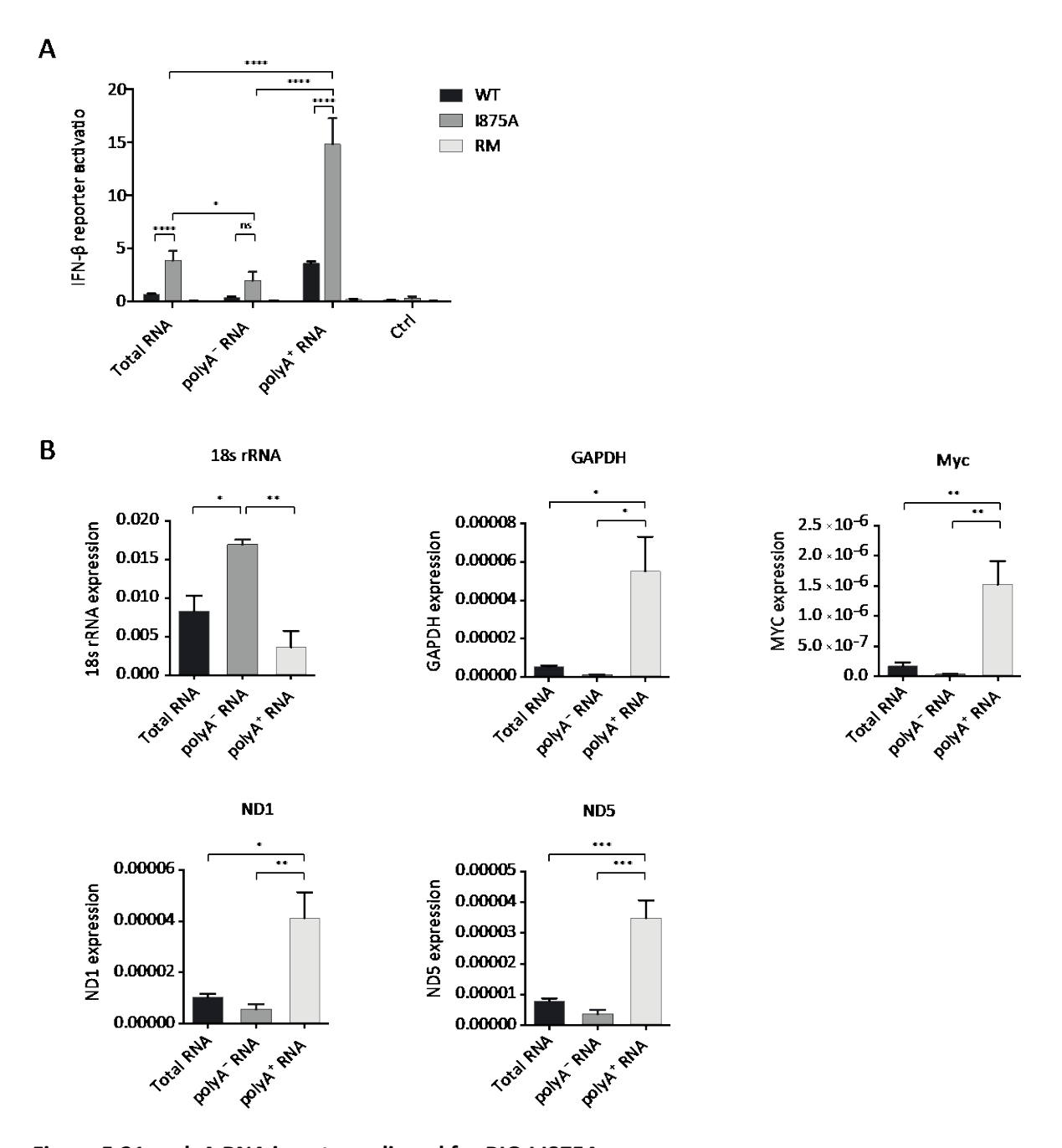


Figure 5.21: polyA RNA is a strong ligand for RIG-I 1875A

A) Whole cell RNA was extracted from A549 cells using TRIzol. RNA was fractionated into a polyA and polyA fraction using polyA Beads. Fractionated RNA and whole cell RNA (total RNA) (0.1 μ g/ml) was transfected into HEK Trex RM -/- cells expressing RIG-I WT, RIG-I I875A or no RIG-I (RM). IFN- β induction was assessed 20 h after RNA transfection by dual-luciferase assay (n=5, mean + SD, two- way ANOVA, Tukey´s post test). B) Total RNA, polyA and polyA RNA were analyzed via qPCR for content of indicated RNAs (n=5, mean + SD, two- way ANOVA, Tukey´s post test). Significances are indicated as follows: * (p < 0.05), *** (p < 0.01), **** (p < 0.001), ns: not significant.

As mentioned, mRNA is degraded and this degradation is performed in multiple pathways by different enzymes, depending on the target RNA and the state of the cell. The main pathway for polyA RNA degradation is performed by Dcp2 and XRN1. Dcp2 decaps the mRNA and leaves a 5′p. The exonuclease XRN1 subsequently degrades the RNA 5′p-dependent in the 5′-3′direction. Hypothesizing that inhibition of this RNA degradation might increase the immune stimulation by endogenous RNA, RNAi of XRN1 was performed. Two siRNAs targeting different XRN1 sequences were transfected in HEK Trex RM -/- cells expressing either RIG-I WT or RIG-I I875A. Immune activation in these cells was compared to untreated

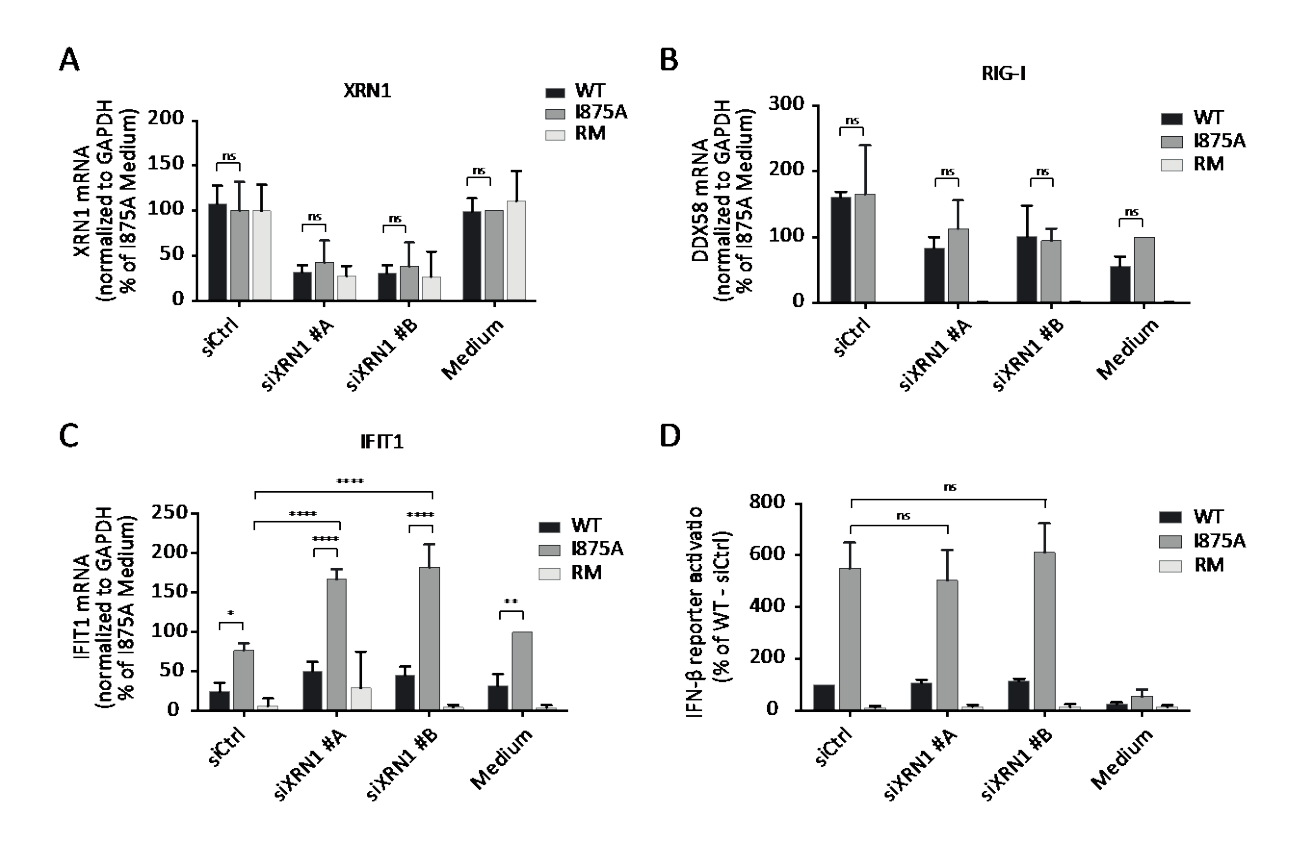


Figure 5.22: XRN1 KD increases immune activation in cells expressing RIG-I I875A

A-C) HEK Trex RM -/- cells were treated with indicated siRNAs. Expression of RIG-I WT or RIG-I I875A was induced or left untreated 24 h after siRNA transfection. RNA was extracted 4 days after siRNA treatment. mRNA expression of XRN1 (A), DDX58 (B) and IFIT1 (C) were analyzed by qPCR and normalized to GAPDH (n=3, mean + SD, two- way ANOVA, Tukey's post test). D) HEK Trex RM -/- cells were treated with siCtrl, siXRN1 #A. siXRN1 #B or no siRNA (medium). RNA was extracted 72 h later and HEK Trex RM -/- cells expressing RIG-I WT, RIG-I I875A or no RIG-I were transfected with the RNA (0.05 μ g/ml). IFN- β induction was determined 20 h after RNA transfection by dual-luciferase assay (n=5, mean + SD, two- way ANOVA, Tukey's post test). Significances are indicated as follows: * (p < 0.05), ** (p < 0.01), **** (p < 0.001), ns: not significant.

cells (medium) and cells treated with a control siRNA against gaußia luciferase (siCtrl). RIG-I expression was induced 24 h after siRNA transfection by addition of doxycycline. RNA was extracted 72 h later and qPCR was performed. XRN1 expression levels were decreased for all cells treated with either siRNA targeting XRN1 compared to untreated cells and cells treated

with the control siRNA (Figure 5.22A). As expected, there was no difference in RIG-I expression between WT and I875A cells (Figure 5.22B).

Long-term expression of RIG-I I875A caused increased immune activation in untreated cells or cells treated with control siRNA when compared to WT cells as described earlier. KD of XRN1 caused an increase of this immune activation in I875A cells, while no difference in WT cells between control siRNA and XRN1 siRNA treated cells was observed (Figure 5.22C). This shows that XRN1 KD and the inhibition of exonuclease degradation of polyA RNA causes an accumulation of I875A activating RNA species. However, in contrast to this finding, RNA extracted from cells that were treated with XRN1 siRNAs had no increased immunostimulatory potential compared to RNA from untreated or control siRNA treated cells when transfected into HEK Trex RM -/- cells expressing RIG-I WT or RIG-I I875A (Figure 5.22D).

5.3.5.4. mtRNA is the stimulating species for I875A

Another polyadenylated RNA species of eukaryotic cells is often overlooked: mitochondrial (mt)-mRNAs. There are 13 mt-mRNAs in humans that mainly encode for proteins of the electron transport chain. It has been shown that indeed most of the mt-mRNAs possess a polyA tail. mt-tRNAs are excised from a long polycistronic precursor RNA by RNase P and Z, causing the release of mt-mRNAs which are localized between the tRNAs on the genomic DNA strands. RNase Z cuts the 3'end of the tRNA and thus also the 5'end of the mRNA. This leaves a monophosphate at the 5'end of mRNAs.

The occurrence of mt-dsRNA was previously reported and it was demonstrated that mtRNAs are able to activate MDA5 if secreted into the cytoplasm (Dhir et al. 2018). Furthermore, another study showed mtRNA-dependent PKR phosphorylation (Kim et al. 2018). Similar to MDA5 and PKR RIG-I also detects dsRNA structures and since mtRNA was shown to occur in a polyA-tailed and 5′monophosphorylated state, mt-mRNAs were an interesting candidate for activation of RIG-I I875A. Furthermore, as shown in this thesis, the polyA⁺ RNA fraction indeed contains mt-mRNAs (Figure 5.21B).

To study the immunostimulatory potential of mtRNAs on I875A, mtDNA – and thus subsequently mtRNA – was depleted in A549 cells. Long-term incubation with low doses of ethidium bromide (EtBr) causes loss of mtDNA due to a reduced mtDNA replication rate (King et al. 1996). A549 cells were incubated for at least 7 days in EtBr containing medium. Subsequently, whole cell RNA was extracted from these cells (RNA +EtBr) and from cells that

were cultivated in control medium (RNA -EtBr) using TRIzol (Figure 5.23A). To control for efficient mtRNA depletion, RNA expression of the extracted RNAs was analyzed via qPCR.

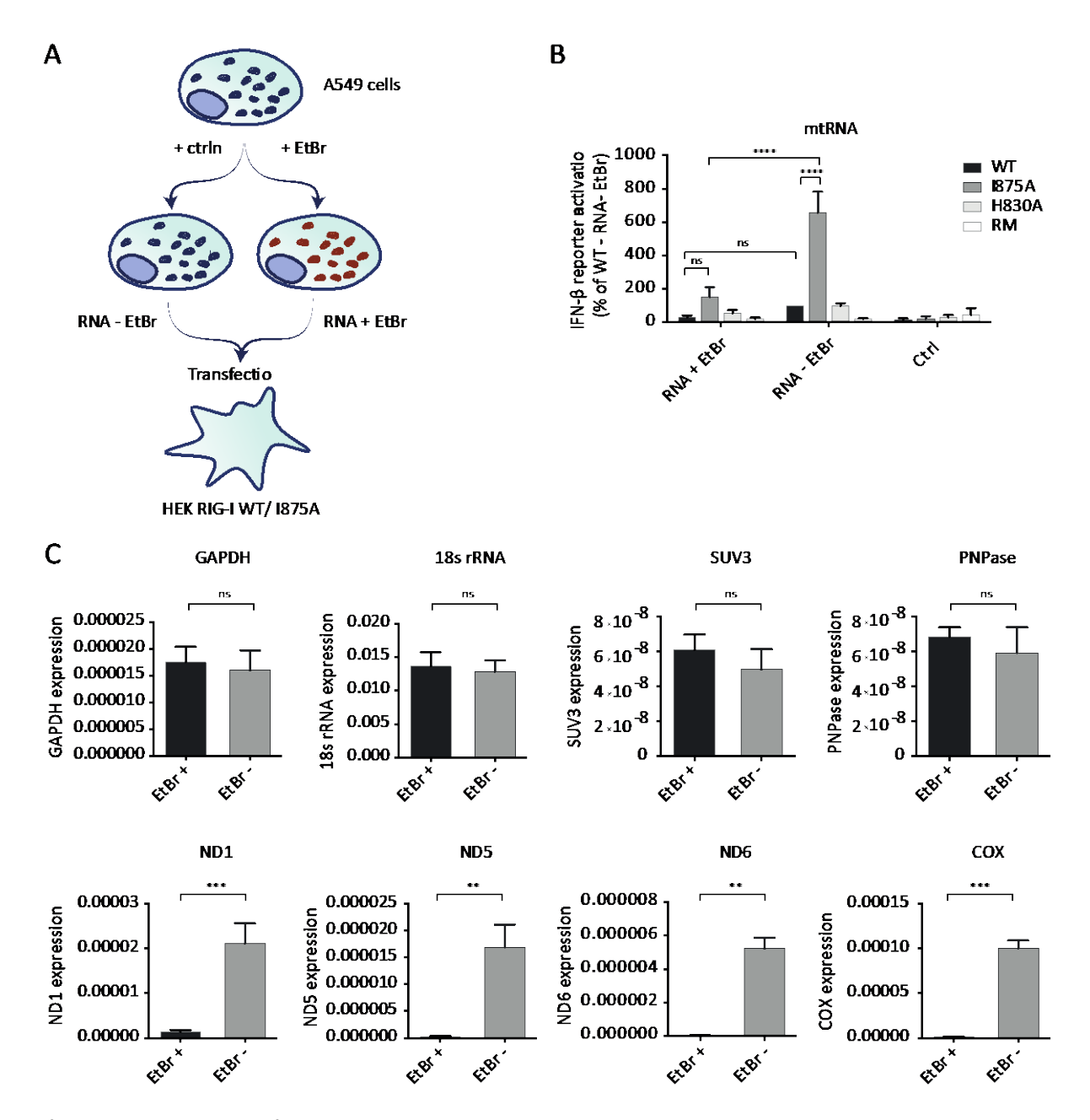


Figure 5.23: mtRNA activates RIG-I I875A

A) Experimental setup. A549 cells were incubated in ctrl medium or medium containing EtBr. EtBr treatment depletes mtDNA and subsequently mtRNA. After at least 7 days RNA was extracted and transfected into HEK cells. B) Whole cell RNA was extracted using TRIzol from A549 that were cultivated in ctrl medium (RNA - EtBr) or ethdium bromide containing medium (RNA + EtBr) for at least 7 days. HEK Trex RM -/- cells expressing RIG-I WT, RIG-I 1875A, RIG-I H830A or no RIG-I were transfected with the RNA (0.1 μ g/ml). IFN- β induction was determined 20 h after RNA transfection by dual-luciferase assay (n=3, mean + SD, two- way ANOVA, Tukey's post test). C) RNA EtBr + and RNA - EtBr was analyzed via qPCR for content of indicated RNAs. (n=5, mean + SD, paired t test). Significances are indicated as follows: ** (p < 0.01), **** (p < 0.001), **** (p < 0.0001), ns: not significant.

While mt-mRNAs like ND1, ND5, ND6 and COX were highly expressed in control cells (EtBr -), expression was significantly reduced in EtBr treated cells (EtBr +) (Figure 5.23C). Nuclear

encoded mRNAs like GAPDH and 18S rRNA were unchanged between RNA -EtBr and RNA +EtBr. Furthermore, mRNAs like SUV3 and PNPase that are encoded in the nucleus but play a role in mt-mRNA degradation, were also unchanged between control and EtBr treated cells. This highlights that the EtBr effect is specific for mtRNA. Next, the immunostimulatory potential of the extracted RNAs was compared in HEK Trex RM -/- cells expressing RIG-I WT, RIG-I 1875A, RIG-I H830A or no RIG-I. In line with previous experiments, RNA -EtBr transfection in cells expressing RIG-I 1875A showed increased IFN-β promoter reporter activity compared to RIG-I WT cells. Interestingly, this effect was nearly completely abrogated with RNA that was extracted from cells lacking mtRNA (Figure 5.23B). These experiments demonstrate that mtRNA is the main activator of 1875A in the RNA pool extracted from cells.

5.4. PKR activation by long RNAs inhibits the RIG-I mediated antiviral response

Some PRRs with direct antiviral activity have similar ligand recognition motifs as RIG-I but display different effector functions. PKR activation inhibits viral and cap-dependent translation via the phosphorylation of eIF2 α . OAS activation triggers RNase L activation,

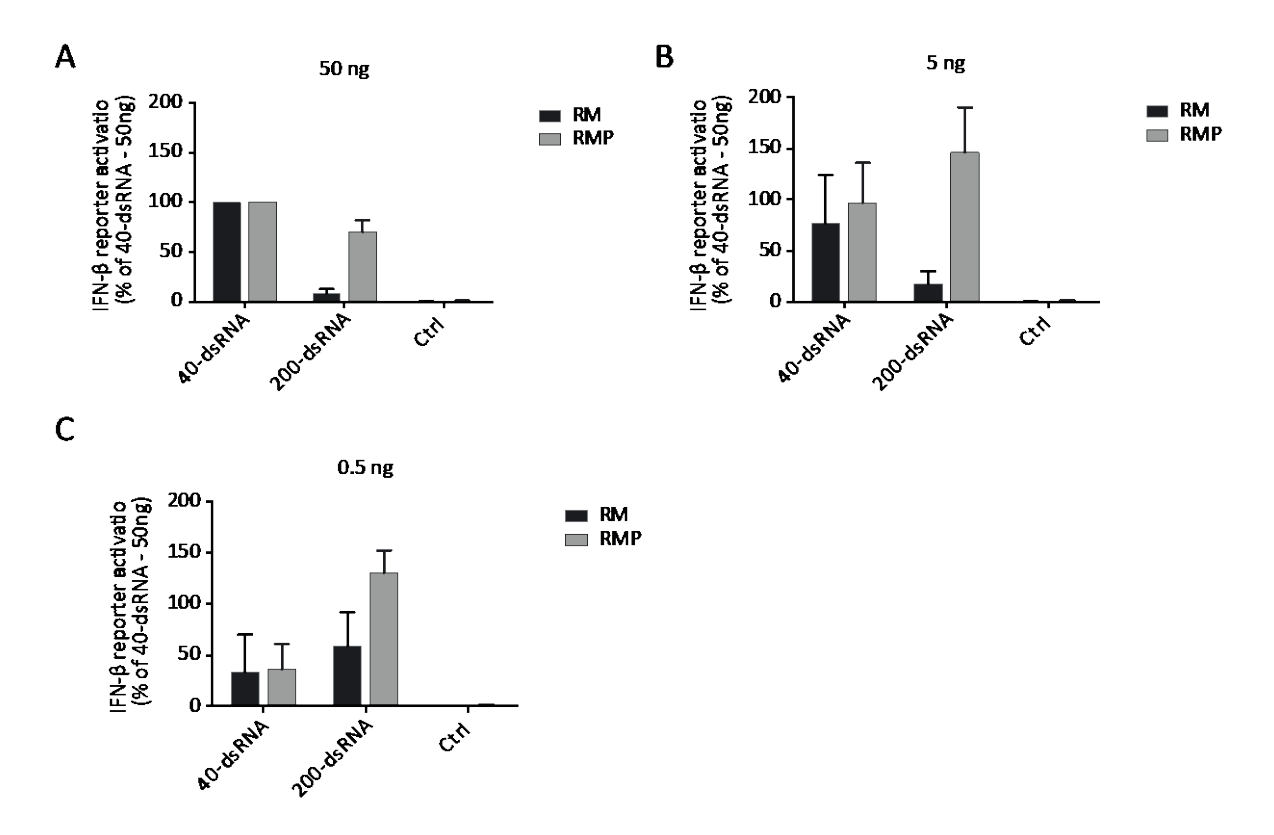


Figure 5.24: PKR KO rescues immune activation by long RNAs

A-C) HEK Trex RM -/- and HEK Trex RMP -/- cells expressing RIG-I WT were transfected with short (40 bp) and long (200 bp) IVT RNA. RIG-I activation was assessed 20 h after RNA transfection by dual-luciferase assay. A) 50 ng/96-well (n=3, mean + SD), B) 5 ng/96-well (n=3, mean+ SD).

which degrades long RNA such as rRNA and thereby causes translational arrest. To test the hypothesis that activation of these PRRs is responsible for the decreased immune stimulatory potential of long RNAs at high concentrations observed Figure 5.7, RIG-I WT was expressed in cells with a RIG-I and MDA5 KO (RM -/-) and cells with a RIG-I, MDA5 and PKR KO (RMP -/-). Cells were stimulated with short (40 bp) and long (200 bp) RNA and IFN-β reporter activation was measured 20 h later. Short RNA led to comparable immune activation in cells with a RM -/- and RMP -/- background at all concentrations tested (Figure 5.24). Long RNA only showed RIG-I activation at the lowest concentration (0.5 ng) in RM -/- cells, while no immune activation was detected with higher concentrations (5 ng and 50 ng). In cells with a RMP -/- background long RNAs caused IFN-β reporter activation even at the highest concentration (50 ng) (Figure 5.24). This demonstrates that long RNAs indeed cause PKR activation, which inhibits RIG-I induced cytokine production. Interestingly the highest concentration (50 ng) caused a lower immune activation compared to stimulation with 5 ng even in PKR KO cells (Figure 5.24A+B).

A549 and Thp1-Dual™ (IFN reporter) cells were used to test if long dsRNA only causes PKR activation and translational arrest in HEK cells, or in other cell types as well. First, Thp1-Dual™ cells were transfected with synthetic 3p-RNA (24 bp) and IVT dsRNA of differing lengths (40 bp - 200 bp) and PKR phosphorylation was assessed 6 h and 9 h after transfection via western blot. In line with the previous experiment, PKR phosphorylation was only detected for RNAs longer than 40 bp (60, 80, 100 and 200 bp) at 6 and 9 h (Figure 5.25A+B). Furthermore, Thp1-Dual™, A549 WT and PKR KO cells were transfected with the same RNAs and IP10 in the supernatant was determined 20 h later via ELISA. IP10 levels for short RNA (24 bp and 40 bp) was comparable in WT and PKR -/- cells for both concentrations tested (Figure 5.25C-F). Compared to WT cells, long RNA (60 -200 bp) caused strongly increased IP10 induction in PKR -/- cells. Interestingly, stimulation with the longest tested RNA (200 bp) showed decreased IP10 levels at the higher concentration tested (100 ng) compared to shorter RNA and the lower concentration tested (10 ng) (Figure 5.24C-F). This effect was even more pronounced in A549 cells where the longest RNA (200 bp) caused no IP10 induction at the higher concentration (100 ng) (Figure 5.24E). Together this data demonstrates that PKR activation by long dsRNAs at high concentrations causes translational arrest in HEK, Thp1 and A549 cells. Since this effect is not completely rescued at high

concentrations and for very long RNAs by PKR KO, additional factors such as the OAS-RNase L system might contribute to the decreased immune response.

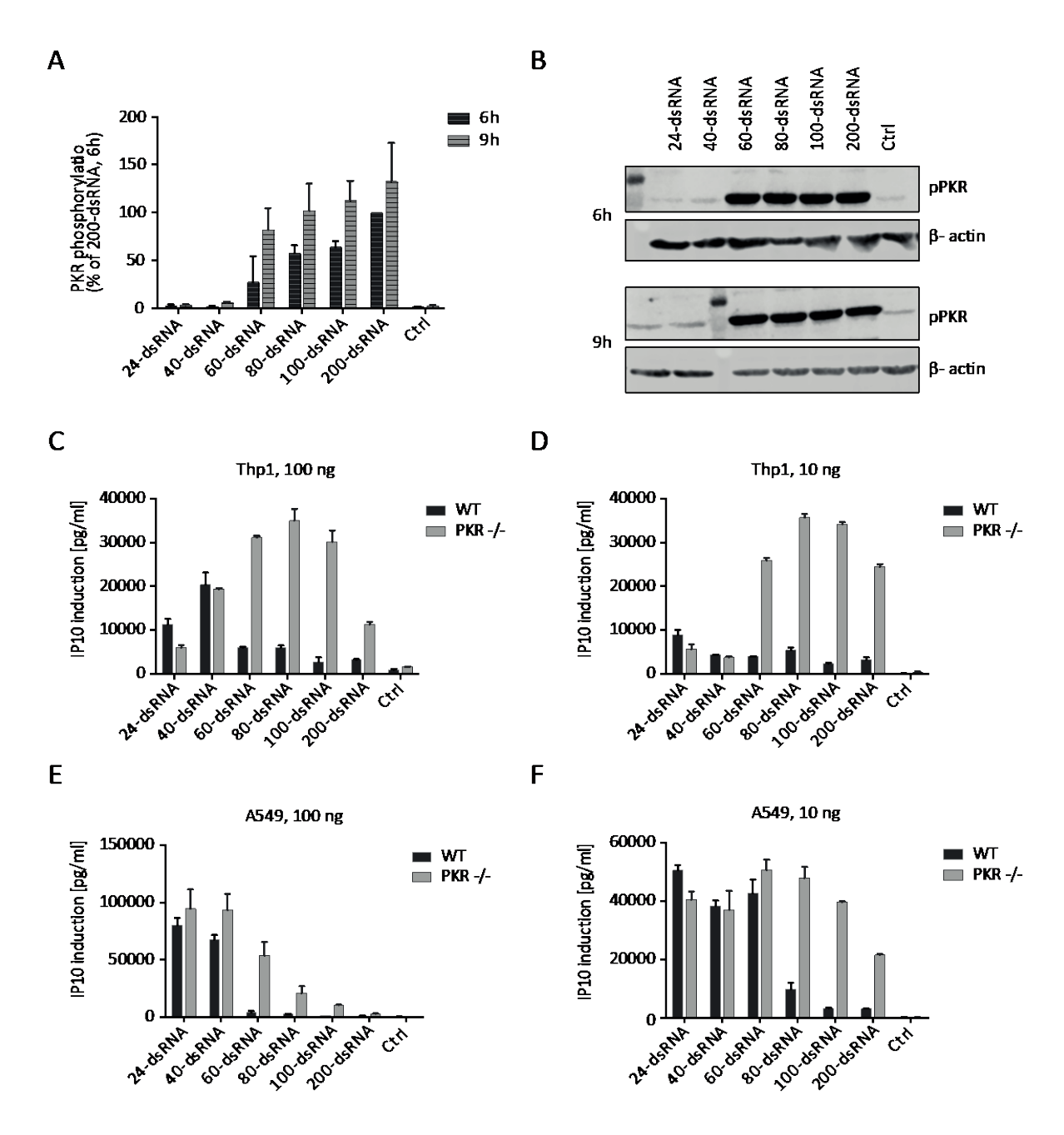


Figure 5.25: Long RNAs activate PKR in A549 and Thp1-Dual™ cells

A) Thp1-Dual[™] cells were transfected with 600 ng IVT 3p-RNA or synthetic 3p-RNA (24 bp)/24-well. Protein was harvested and PKR phosphorylation was determined via western blot and normalized to β-actin 6 h and 9 h after transfection (n=2, mean + SD). B) One exemplary blot of A) is shown. C+D) Thp1-Dual[™] WT and PKR -/cells were transfected with 100 ng (C) or 10 ng (D) of the indicated RNAs. IP10 in the supernatant was determined 20 h after stimulation via ELISA (n=1, technical duplicates, mean + SD). E+F) A549 WT and PKR -/cells were transfected with 100 ng (C) or 10 ng (D) of the indicated RNAs. IP10 in the supernatant was determined 20 h after stimulation via ELISA (n=1, technical duplicates, mean + SD).

5.5. Characterization of a highly potent RIG-I ligand

As shown in the previous experiments longer 3p-RNAs are more potent RIG-I stimuli than shorter 3p-RNAs. However, long RNA also led to the activation and phosphorylation of PKR and possibly RNase L, which causes translational arrest and abrogates cytokine release (Figure 5.7). The high immunostimulatory potential of long RNAs is most probably due to the fact that they can harbor several RIG-I molecules. It was proposed that four RIG-I tandem CARDs build a helical core for CARD-CARD interactions with MAVS (Jiang et al. 2012, Peisley et al. 2013, Peisley et al. 2014). A RIG-I ligand that is able to accommodate at least 4 RIG-Is might be highly effective in initiating downstream signaling since RIG-I CARDs are brought into close proximity. Additionally, it is speculated that an already RNA bound RIG-I molecule might facilitate subsequent binding of a second RIG-I. In this thesis a RIG-I ligand that can harbor four RIG-Is was characterized and tested for its immunostimulatory potential. The tested ligand consists of four 3p-dsRNAs (11 bp) that are connected via linkers resembling a cloverleaf (CL) structure. Since the double-stranded stems are only 11 bp long which is below the activation limit of PKR, it was speculated that this new ligand does not cause a PKR dependent translational inhibition of cytokine release. Developing and characterizing a RIG-I ligand that can harbor four RIG-I molecules without activating PKR might be highly interesting for immunotherapy.

First, RNA with a single hexaethylenglycol (HEG) linker (CL 1) was compared to a double HEG-HEG linker (CL 2), a U linker (CL 3) and a UUU linker (CL 4) (Figure 5.26A). HEK cells and PBMCs were transfected with the indicated RNAs and IFN- β reporter activation or IFN- α in the supernatant was determined 20 h later. As seen in Figure 5.26A CL 1 and CL 2 have a comparable immune stimulatory potential. CL 3 and CL 4 also induce a similar immune activation albeit clearly reduced compared to CL 1 and CL 2. Interestingly, CL 3 and CL 4 induce a similar RIG-I activation as an RNA ligand with two 3p-dsRNAs (11 bp) that are connected via a HEG linker (RNA 1). The U and UUU linker are shorter than HEG linkers and are less flexible. Therefore, one could speculate that while CL 1 and CL 2 are able to accommodate four RIG-Is, CL 3 and CL 4, although they possess four 3p-ends, only allow the binding of two RIG-Is (Figure 5.26A). The EC50 of CL 1 in HEK cells is 0.026 nM and in PBMCs 0.366 nM. The EC50 of the standard RIG-I ligand with two 3p-dsRNA ends in HEK cells is 0.825 nM and in PBMCs 6.153 nM. The activation potential of CL1 is thus 16-30 times higher than a classic RIG-I ligand with two 3p-ends.

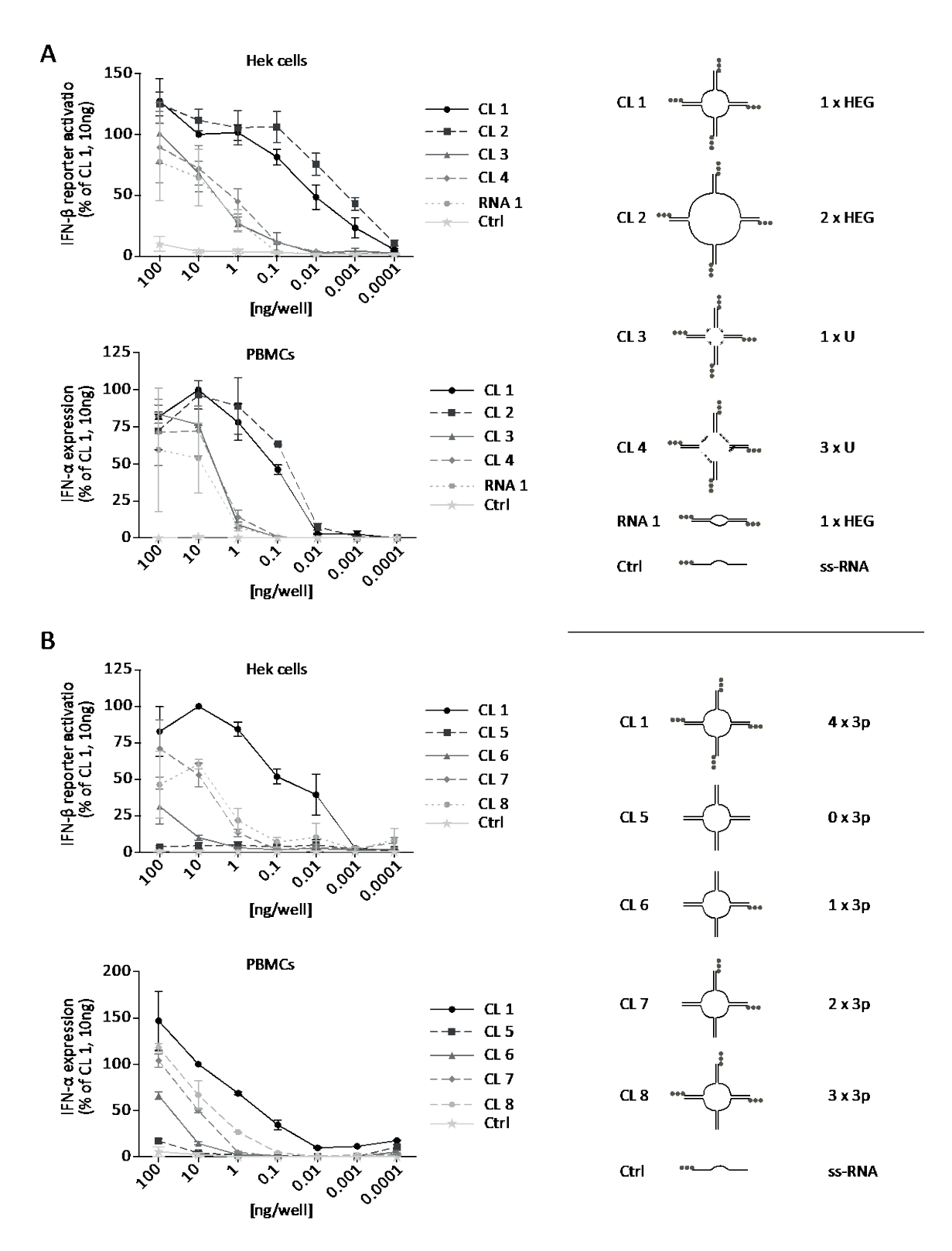


Figure 5.26: Characterization of a new RIG-I ligand

A) HEK Trex RM -/- cells expressing RIG-I WT and PBMCs were transfected with the indicated RNAs. PBMCs were treated with chloroquine (5 μ g/ml) 30 min before RNA transfection. IFN- β reporter activation in HEK cells was assessed 20 h after transfection. For PBMCs IFN- α in the supernatant was determined via ELISA 20 h after RNA transfection. HEK cells: n = 4, mean \pm SEM; PBMCs: n=2, mean \pm SEM. B) HEK Trex RM -/- cells expressing RIG-I WT and PBMCs were transfected with the indicated RNAs. PBMCs were treated with chloroquine (5 μ g/ml) 30 min before RNA transfection. IFN- β reporter activation in HEK cells was assessed 20 h after transfection. For PBMCs IFN- α in the supernatant was determined via ELISA 20 h after RNA transfection. HEK cells: n = 4, mean \pm SEM; PBMCs: n=2, mean \pm SEM.

Next, CL 1 with four 3p ends was compared to the same RNA ligand but with 1, 2, 3 or 4 OH-ends (Figure 5.26B). Unexpectedly, the ligand with 4 OH-ends (CL 5) caused no RIG-I activation. Increasing the number of 3p-ends gradually increased the immunostimulatory potential of the RNA (CL6 < CL 7 < CL 8 < CL 1) (Figure 5.26B).

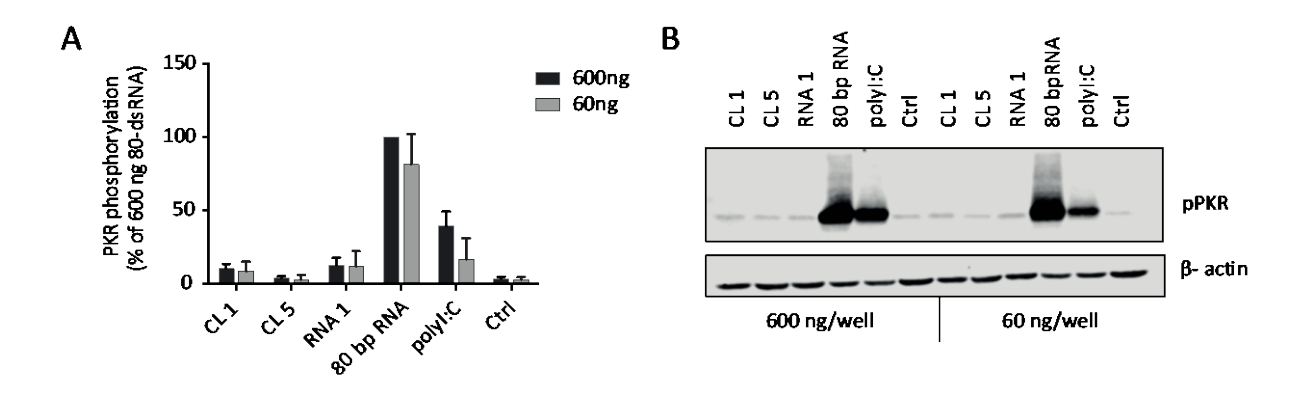


Figure 5.27: CL 1 does not activate PKR

A) Thp1-DualTM cells were transfected with 60 ng and 600 ng of the indicated RNAs. Protein was extracted and PKR phosphorylation was determined via western blot and normalized to β -actin 9 h after stimulation (n=3, mean + SEM). B) One exemplary blot of A) is shown.

To test if this ligand is indeed highly stimulatory for RIG-I without showing PKR activation, Thp1 cells were transfected with CL 1, CL 5, RNA 1, an IVT 3p-RNA (80 bp) and polyI:C, and as a control with ssRNA (Ctrl, 22 bp). PKR phosphorylation was assessed via western blot 9 h after transfection. While the 80-dsRNA and polyI:C caused PKR phosphorylation, CL 1, CL 5, RNA 1 and the control ssRNA displayed no PKR activation even at high RNA concentrations (Figure 5.27). Thus, the new RIG-I ligand CL 1 is highly RIG-I stimulatory without activating PKR.

6. Discussion

RIG-I is a ubiquitously expressed PRR that is crucial for the detection of a wide range of RNA viruses. Located in the cytoplasm where most viruses replicate, it is faced with the challenge of efficiently and selectively differentiating between viral RNA and an excess of endogenous RNA. This thesis has shown that two crucial mechanisms to differentiate between self and non-self RNA are embedded in the 5'RNA binding cleft of the RIG-I CTD. Modifications that render endogenous RNA non-immunogenic were identified and the structural prerequisites for this differentiation in the RIG-I CTD were determined. Moreover, ligand detection by several RIG-I CTD mutants were characterized and used to identify RIG-I activating viral and endogenous RNA species. Additionally, these CTD mutants were employed to investigate whether RIG-I was able to detect RNA in a 5'end-independent manner. Furthermore, PKR activation was found to impair the RIG-I induced immune response and a RIG-I ligand avoiding PKR stimulation was characterized and tested.

6.1. CMTR1 is indispensable to prevent RIG-I-dependent activation by endogenous RNA RIG-I has several ligand requirements to be fully activated. The optimal RIG-I ligand is 5'triphosphorylated, blunt-ended and double-stranded RNA. All RNA polymerase transcribed RNAs possess a 5'3p. However, these ends are further modified in posttranscriptional steps taking place in the nucleus and cytoplasm. While the 5'3p-ends of tRNAs and rRNAs are enzymatically digested to a 5'p, mRNAs are polyadenylated at the 3'end and a complex cap structure is added at the 5'end of the RNAs in higher eukaryotes. The mRNA capping is a five step co-transcriptional process in the nucleus. First, RNA 5'triphosphatase hydrolyzes the triphosphate to a diphosphate. Second, RNA guanylyl transferase caps the 5'end with GMP in a two-step mechanism. A methyl group on the guanin is subsequently introduced by the guanin-N7-methyltransferase. The resulting structure is called a cap0 (m7G-pppRNA) and is conserved in all eukaryotes. Its importance for several cellular processes such as the nuclear export of the mRNA and cap-dependent mRNA translation has been shown (Shatkin et al. 2000, Ghosh et al. 2010). It was also assumed that the ^{m7}G-cap prevents immune activation by endogenous mRNA. The last steps of mRNA capping only occur in higher eukaryotes (Banerjee 1980). The nuclear CMTR1 methylates the first nucleotide of the RNA at the 2'O position of the ribose to generate cap1 (Belanger et al. 2010). A cap2 structure is formed on about 50% of all mRNAs by methylation of the second nucleotide by cytoplasmic CMTR2. The function and importance of these methylations have been unknown. Christine

Schuberth-Wagner could show for the first time in her PhD thesis – by using synthetic RNAs – that the N1-methylation is actually the decisive modification that renders 3p-dsRNA non-stimulatory to RIG-I, while the ^{m7}G cap alone only partially reduced RIG-I activation (Schuberth 2011). Furthermore, a single highly conserved amino acid – H830 – in the CTD of RIG-I was identified that mediates this self-tolerance mechanism towards N1-methylated RNA. Long-term expression of RIG-I H830A in RIG-I deficient cells caused an immune activation in the absence of exogenous ligands (Schuberth-Wagner et al. 2015).

If N1-methylation is decisive to prevent RIG-I activation, removal of the methylation on endogenous mRNAs should lead to immune activation. Indeed, in the present study RNAi of CMTR1, which leaves mRNAs in a cap0 state, was shown to cause a RIG-I-dependent immune activation in IFN- α primed cells. This, together with the long-term expression experiments with RIG-I H830A, show that endogenous ligands would continuously activate RIG-I if it was not able to differentiate between cap0 and cap1 structures.

In the study where the enzymatic function of CMTR1 was first described, a siRNA KD was performed as well and no effect under stress and normal conditions on protein synthesis was reported (Belanger et al. 2010). However, the data is not shown in the publication and it is not described in detail how the siRNA KD was performed and for how long (Belanger et al. 2010). The immune activation by CMTR1 KD was rather low and was only seen when cells were primed with IFN- α in the present experiments. Therefore, the time point of analysis and the RIG-I expression in the cells might be decisive to see the reported effect. Nevertheless, although the immune response is low compared to RIG-I activation by its optimal ligand 3p-dsRNA, continuous long-term activation might have serious implications and could cause autoinflammatory diseases.

The specific endogenous ligand that is able to activate RIG-I in the absence of N1-methylation has not yet been identified. As previously discussed, the optimal RIG-I ligand is not only triphosphorylated but also base-paired and blunt-ended. While there are conflicting results if and which overhangs might be tolerated by RIG-I, it was shown that ssRNA, even if triphosphorylated, does not activate RIG-I (Schlee et al. 2009). mRNAs are single-stranded and should therefore be excluded from RIG-I recognition without the need for an additional mechanism like N1-methylation. However, longer mRNAs form complex secondary structures with base-paired stretches which might lead to the occurrence of RIG-I ligands in the absence of N1-methylation. Furthermore, long non-coding RNAs which have similar

structural features as mRNAs such as a 5′cap, a polyA tail and strong secondary structures, could be a candidate for the activating species (Washietl et al. 2005, Zampetaki et al. 2018). Shortly after our data was published (Schuberth-Wagner et al. 2015), another group verified our results, and by using crystallography, could shed further light on the structural mechanism used by RIG-I to discriminate between cap0 and cap1 structures (Devarkar et al. 2016). Co-crystal structures of RIG-I Δ (CARD) with uncapped 3p-dsRNA and cap0 3p-dsRNA showed no differences in binding affinities. However, additional N1-methylation on uncapped or cap0 RNA decreased binding affinities by 20- and 200-fold respectively. Furthermore, analyzing crystal structures of RIG-I WT with uncapped and cap0 revealed no specific interactions of RIG-I with the m7 G moiety, therefore explaining the tolerance of cap0 RNA as RIG-I ligands.

6.2. YFV uses RNA N1-2'O-methylation to avoid RIG-I recognition

It was previously shown that dsRNA structures occur during viruses' life cycle as panhandles in the genome, replicative intermediates, or as DI genomes. If present in the cytosol, these dsRNAs structures can activate RIG-I and cause the initiation of a signaling cascade, leading to the upregulation of ISGs including multiple antiviral proteins such as PKR and OAS. From the point of view of a virus, it is therefore detrimental to avoid RIG-I recognition or inhibit the downstream signaling cascade.

Intriguingly, many viruses possess 2´O-methylated cap structures either obtained by cap-snatching or encoding for their own methyltransferase (Plotch et al. 1981, Sampath et al. 2009). This thesis investigated if these cap structures are used to evade RIG-I recognition by exploiting the self-tolerance mechanism of RIG-I towards cap1 RNA. A549 WT, RIG-I KO and STAT KO cells were infected with the flavivirus YFV. The NS5 protein of YFV possesses a 2´O-methylation activity which can be disrupted by point mutation of E218 to alanine. E218 is part of the highly conserved KDKE motif, which is distinctive for methyltransferases. This motif is not only conserved in flaviviruses (Zhou et al. 2007), but was also described for other viruses such as SARS-CoV (Zust et al. 2011).

The viral titers of YFV E218A in A549 WT cells were strongly decreased compared to the titers of YFV WT while no difference of the viral titers were observed in A549 RIG-I and STAT1 KO cells. On the one hand this shows that E218 mutation does not generally impair viral replication. On the other hand, it also demonstrates that the decreased viral load is RIG-I-dependent. Compared to WT cells, the general slightly higher viral titers in A549 RIG-I KO

and STAT1 KO cells point to other non N1-dependent structures that are recognized by RIG-I. Possibly not all viral RNAs are N1-methylated. By qPCR analysis it was shown that the lower viral replication of YFV-E218A in WT cells is accompanied and probably caused by an elevated RIG-I-dependent immune activation. IFIT1 mRNA induction was increased in cells infected with YFV E218A when compared to YFV WT infected cells, while no immune activation was observed in RIG-I KO and STAT1 KO cells. The data clearly shows that YFV actually exploits RIG-I's self-tolerance mechanism to escape immune recognition.

Another group previously investigated another flavivirus – WNV – comparing it to its mutant WNV-E218A with regards to IFIT1 activation (Daffis et al. 2010). Their experiments showed that the IFIT family inhibits WNV-E218A replication and concluded that WNV, by capping it's RNA, circumvents IFIT-mediated replication suppression. IFIT1 is an ISG that binds cap0 but not cap1 RNA and sequesters the RNA from the translation machinery, thereby inhibiting viral replication. Data presented in this thesis show a clear RIG-I-dependent mechanism in recognition of YFV-E218A viruses, contradicting data found in the other study. However, RIG-I activation and subsequent immune induction leads to the upregulation of ISGs like IFIT1, which might then act downstream of RIG-I to sequester the viral unmethylated RNA from efficient translation. RIG-I is accordingly indispensable for alarming the immune system to take action, while IFIT1 then executes the actual inhibition of the viral replication.

6.3. Interaction of the RIG-I CTD with non-optimal ligands

Several RIG-I crystal structures have been published and helped to understand the specific RIG-I ligand requirements. A positively charged binding cleft in the CTD has been identified that binds the 5'end of the RNA. Amino acids that interact with the triphosphate were described, as well as an amino acid that explains the requirement for base-paired RNA. Mutation of amino acids (e.g. K861, K888) making contacts with the triphosphate left RIG-I unresponsive to 3p-dsRNA, while mutation of the amino acid important for 5' base pair stacking (F853) reduced RIG-I response to 3p-dsRNA partially (Wang et al. 2010). However, no other RIG-I structures like 5' and 3'overhangs were investigated. In this thesis, HEK Trex cells were used to study the activation potential of a wide range of synthetic well-defined RNA ligands in RIG-I WT, RIG-I K861A and RIG-I F853A expressing cells. First, RIG-I and MDA5 were knocked out and subsequently RIG-I WT and RIG-I mutants were reintroduced in a stable, doxycycline inducible manner. This allowed the investigation of ligand requirements in a well-defined system where it was easy to control for comparable RIG-I expression and

where all cells had the same genetic background. Additionally, doxycycline inducible RIG-I expression circumvented plasmid transfection which could stress the cells and interfere with RNA stimulation.

Surprisingly, dsRNA with a 3p on one 5'end (3p-asOH) was as stimulatory as dsRNA where both 5'ends were triphosphorylated (3p-as3p). It was shown previously that a 24 bp dsRNA can accommodate two RIG-I molecules (Peisley et al. 2013). Therefore, one would expect an increased stimulatory potential of 3p-as3p compared to 3p-asOH because RIG-I can bind with high affinity on both ends. However, it was shown that RIG-I translocates from one RNA end to the other along the dsRNA in an ATP-dependent manner (Devarkar et al. 2018). Furthermore, that group showed that the 3p-end throttles RIG-I translocation, which increases the time that RIG-I is bound to the RNA. They proposed that this facilitates binding of a second RIG-I. It might therefore be optimal to have a 3p on one RNA end so that RIG-I can bind in a highly efficient manner and facilitate the binding of a second RIG-I in an as efficient manner as binding to a second 3p on the other RNA end. By modeling, they calculated that the binding affinity of RIG-I to the RNA is 28-fold higher when another RIG-I molecule is bound to the 5'end of the RNA, and postulated a threading mechanism of RIG-I binding (Devarkar et al. 2018). Furthermore, as was previously shown, 3p-dsRNA stimulation of K861A expressing cells only showed residual RIG-I activation even at high RNA concentrations, while mutation of F853 led to a partially reduced IFN response. Comparable immune activation was detected in WT and K861A after OH-dsRNA (OH-asOH) stimulation, while immune activation was completely abrogated in F853A cells. Introducing a 3p at either 5'end restored immune activation in F853A cells. Since OH-dsRNA makes no contact with K861, the fact that there is no effect of this mutation on OH-dsRNA stimulation is not surprising. The binding affinity of OH-dsRNA is decreased 126 times compared to 3p-dsRNA on full-length RIG-I (Vela et al. 2012), probably because it lacks the contacts between the 3p of the RNA and the positively charged CTD cavity. F853 stacks over both bases of the terminal 5'base pair of the RNA and thereby stabilizes RNA-protein orientation and binding. Mutation of this amino acid further decreases the binding affinity of OH-dsRNA to RIG-I, probably preventing OH-dsRNA binding or diminishing the response below the detection limit. Interestingly, the stimulation of K861A with 3p-asOH caused a differing IFN response when compared to OH-as3p. Both RNAs possess one 5'3p end and one 5'OH end, and one could assume that both RNAs are equally stimulatory. While this is actually true for the detection of the 3p end as 3p-asOH and OH-as3p are as stimulatory in WT and F853A (which are not activated by OH-dsRNA) cells, obviously another mechanism is important in OH-dsRNA end recognition. This might be caused by a sequence-specific recognition mode for OH-dsRNA. Intensive research in this area was not conclusive (data not shown) because different commercial OH-RNA synthesis batches showed variability in their immunostimulatory potential even when the same sequence was ordered. Therefore, no specific sequence preferences for RIG-I and OH-dsRNA could be manifested. Furthermore, these results show that the 5´3p end in K861A cells behaves like 5´p in RIG-I WT expressing cells and not like 5´OH.

As described earlier (Gondai et al. 2008, Schlee et al. 2009), 3'overhangs were partially tolerated by RIG-I WT, while 5'overhangs completely abrogated immune activation. As expected, K861A expressing cells showed no immune activation by 3p-dsRNA with overhangs, while F853A was less tolerant towards 3'overhangs compared to WT cells. As was made clear earlier, mutation of F853 probably decreases binding affinity to dsRNA and makes it more susceptible to deviations from the optimal RNA recognition motif that might still be tolerated by RIG-I WT. Similar effects were observed for stimulation with OH-dsRNA with overhangs. While 5'overhangs were not tolerated at 3p-dsRNA, 3'overhangs still caused a certain immune activation. Since OH-dsRNA is a weaker ligand compared to 3p-dsRNA, further modifications of the ligand might have more detrimental effects compared to 3p-dsRNA.

Definition of minimal base pair length requirements for RIG-I were described. Even though our group determined a minimal length of 19 bp (Schlee et al. 2009), another group defined RIG-I activation with ligands as short as 10 bp (Schmidt et al. 2009). While 3p-dsRNA with a stem of 10 bp still caused IFN-β induction in RIG-I WT cells, albeit 10 times lower compared to 24 bp RNA, OH-dsRNA was only active with a stem of at least 19 bp in the present experiments. In a study investigating RIG-I filamentation on long dsRNAs, it was shown that one RIG-I occupies about 14 bp of the RNA while the end-capping RIG-I only occupies 10 bp (Peisley et al. 2013). However, although RIG-I only occupies short RNA stretches, this does not mean that this is sufficient to initiate a pronounced activation. In the present study a highly sensitive read-out (secreted luciferase assay) and a high RIG-I expression were used in the experiments. This might explain why immune activation with shorter RNA was detected compared to previous studies (Schlee et al. 2009). In contrast to the present data, another

group showed no reduction but a higher RIG-I stimulation with shorter dsRNAs (10 bp and 14 bp) compared to 24 bp RNA (Linehan et al. 2018). However, they also reported a gradual decrease in RIG-I activation from 24 bp over 23 bp to 21 bp RNA and OH-dsRNA had no immunostimulatory activity even when a 24 bp double-strand was used. Interestingly, hairpin RNAs were used for their 10 and 14 bp RNAs instead of annealing two single stranded RNAs as in the present study. Possibly the hairpin RNAs might form other RNA structures as the intended stem-loop with longer double stranded stretches, which might account for the increased immunostimulatory potential. Other explanations might include an increased stability and RNase resistance of hairpin RNAs compared to the RNAs used in the present study.

In this thesis RIG-I ligand specifications were determined for RIG-I WT and RIG-I CTD mutants. As described in previous publications, RIG-I WT detects base-paired 3p-dsRNA. While 3'overhangs were partially tolerated, especially at higher RNA concentrations, RNA with 5'overhangs led to no RIG-I activation. OH-dsRNA also caused a substantial type I IFN induction. While RIG-I CTD K861A showed no immune response to 3p-dsRNA, RIG-I CTD F853A did not tolerate OH-ends and 3'overhangs. ssRNA was completely unstimulatory in RIG-I WT and the CTD mutants even at high RNA concentrations in line with previous publications (Schlee et al. 2009, Schmidt et al. 2009).

6.4. RIG-I ligands during viral infection

The identified activation pattern for RIG-I WT compared to the RIG-I CTD mutants can be used to study which ligands actually activate RIG-I during a viral infection. In order to identify viral RIG-I ligands, cells are often infected with viruses and RNA is subsequently extracted. However, extraction of the RNA might destroy its secondary structures. Additionally, during the RNA extraction process RNA binding proteins, that might prevent the formation of secondary structures or might mask the RNA to block RIG-I binding, are removed, thereby falsifying the results. In the present system with the doxycycline inducible CTD mutants, RIG-I activation can be studied directly during viral infection. Furthermore, no plasmid transfection that might additionally stress the cells is needed.

Interestingly, different activation patterns were observed for the s-NSV IAV and the ns-NSVs SeV and VSV. While IAV mainly caused RIG-I WT activation, cytokine induction was also observed during SeV and VSV infection in cells expressing RIG-I F853A, albeit lower compared to RIG-I WT cells. A minor activation of RIG-I K861A was detectable at high MOIs.

Comparing these results (Table 6.2) with the ligand specifications of the RIG-I CTD mutants (Table 6.1) shows that on the one hand the activation pattern of IAV resembles that of 3p-dsRNA and 3p-dsRNA with 3'overhangs. On the other hand, VSV and SeV represent the activation pattern of 3p-dsRNA with possibly low amounts of OH-dsRNA. No 5'end-independent viral ligand recognition was observed. RIG-I WT and RIG-I mutant expressing cells should show the same immune activation if this would be the case.

Table 6.1: Overview RIG-I ligand detection

RNA	WT	F853A	K861A
3p-dsRNA	++++	+++	-
OH-dsRNA	++	-	++
3p-dsRNA with 5'overhang	-	-	-
3p-dsRNA with 3'overhang	++	-	-
ssRNA	-	-	-

Table 6.2: Overview RIG-I virus detection

Virus	WT	F853A	K861A
IAV	++++	+	-
SeV	++++	+++	+
VSV	++++	+++	+
HSV	+	-	_

In contrast to (+)ssRNA viruses, NSVs have to copy their genomic RNA to form a (+) sense RNA that then serves as the mRNAs. The genome of IAV is separated into 8 single-stranded segments. Each segment has highly conserved complementary 5' and 3'sequences (Desselberger et al. 1980) that form a partial duplex, the so called panhandle structures which function as a promoter for viral transcription and replication. It was previously shown that RIG-I rather associates with genomic IAV RNA instead of mRNA (Baum et al. 2010, Rehwinkel et al. 2010). It is important to note that IAV lacking the NS1 protein was used in this thesis. NS1 prevents immune response during IAV infection via several mechanisms including binding to viral dsRNA and thereby sequestering it from RIG-I (Donelan et al. 2003, Chan et al. 2016) and by inhibiting TRIM25-mediated RIG-I CARD ubiquitination (Gack et al. 2009).

For ns-NSV like SeV it was shown that structural proteins prevent the formation of double-stranded regions in the genome and it is therefore present in a linear state. However, it was shown that DI genomes are produced during the viral life cycle. Strahle et al. compared infection and IFN induction with different SeV stocks containing snapback or internal deletion DI genomes or ND genomes for their ability to induce IFN. They could show that IFN- β induction was due to the presence of copyback DI genomes, and that IFN production correlated with that of DI genome replication and the ratio of DI to ND genomes during

infection (Strahle et al. 2006). These snapback DI genomes did not show encapsidation and are able to form panhandle structures during replication in the infected cells (Strahle et al. 2007). Therefore, while RIG-I is able to directly detect genomic RNA of s-NSVs, RIG-I is activated during ns-NSV infection by regular and irregular products of viral RNA synthesis such as DI genomes. The difference in RNA structures that are detected by RIG-I might also explain the different activation patterns of RIG-I CTD mutants.

Although RIG-I only detects RNA, it was shown that RIG-I is also able to detect DNA via an indirect mechanism. The endogenous RNA Pol III can use AT-rich DNA as a template to generate poly AU-RNA, which then hybridizes to form dsRNA and is a strong RIG-I ligand (Ablasser et al. 2009, Chiu et al. 2009). It was shown that Epstein-Barr virus (EBV) and Adenovirus-encoded small RNA Pol III transcripts are able to activate RIG-I (Samanta et al. 2008, Ablasser et al. 2009, Minamitani et al. 2011). However, these mechanisms do not seem to take place during HSV infection, or only to a small extent, since in the present experiments it only induced a low immune activation in RIG-I WT cells. Having said this, it was previously shown that dsRNA occurs during HSV infection probably generated by overlapping converging transcription (Weber et al. 2006). On the one hand a publication showed MDA5 but not RIG-I-dependent immune activation upon HSV infection (Melchjorsen et al. 2010). On the other hand a HSV protein was shown to inhibit RIG-I and MDA5 activation which hints to a role for RIG-I in HSV infection (Xing et al. 2012).

In general, a system was developed using the RIG-I CTD mutants to investigate viral ligands during infection. In future experiments it would be interesting to test more viruses to investigate if the difference between s-NSV and ns-NSV is manifested. Furthermore, other virus groups such as dsRNA and (+)ssRNA viruses could be tested. Another interesting experiment would be to look if the RIG-I mutant activation pattern is different at the beginning of an infection compared to when it is established. This could be studied by inducing RIG-I expression with doxycycline either before the infection or several hours afterwards. Getting a closer insight into which viral ligands are detected during an infection might help to develop new antiviral therapies.

6.5. RIG-I is not activated by RNA in a 5'end independent mechanism

As there is a debate if RIG-I binding to the 5'end of the dsRNA is a prerequisite for RIG-I activation and translocation or if RIG-I is also able to bind internally on the dsRNA, RNAs with differing lengths and end modifications were investigated. Binder et al. reported that longer

RNAs (≥ 100 bp) activate RIG-I end-independently (Binder et al. 2011). Removing the 3p by AP treatment had no impact on RIG-I activation with longer RNAs, while AP treatment on shorter RNAs had detrimental effects on immune activation compared to 3p-dsRNA. Furthermore, it was shown that RIG-I signaling positively correlates with dsRNA length. Binder et al. proposed that a higher amount of less specific internal binding sites can compensate for the lack of a highly efficient 5′end initiation motif. In the present study, 40, 60, 100 and 200 bp RNAs were transcribed via IVT using DNA oligo or PCR templates. RNAs were either left untreated (3p) or were enzymatically digested with AP (OH-RNA) or PP (p-RNA). If RIG-I was able to detect long RNA 5′end-independently, RIG-I CTD mutant activation should resemble RIG-I WT activation. Furthermore, AP and PP treatment should not affect the immune stimulatory potential of the RNAs.

However, RIG-I K861A which does not detect short 3p-dsRNA was not activated by any of the 3p-IVT RNAs tested, independent of the length. Additionally, AP treatment reduced IFN- β promoter reporter activation at all concentrations tested, while PP digestion surprisingly abrogated immune response completely in all cells tested. Therefore, the present data does not support a fully end-independent RNA binding and activation mechanism of RIG-I.

Unexpectedly, RIG-I activation by AP treated long dsRNA was still highly dependent on the presence of K861. AP is described to dephosphorylate DNA, RNA and nucleotides as well as proteins. However, it is predominantly used for DNA and while AP treatment on short RNAs works well, it might not be optimized for dephosphorylation of long RNAs. The immune activation seen with AP treated RNA in RIG-I WT cells is most probably caused by residual 3p-RNA.

While immune activation by short dsRNA (40 bp) positively correlated with RNA concentrations, a contradictory effect was detected for longer RNAs. A decrease in RIG-I activation for higher RNA concentrations (10 ng and 100 ng) was observed with increasing RNA length. PKR is an example of a PRR that has overlapping ligand requirements with RIG-I (Nallagatla et al. 2007, Nallagatla et al. 2008). PKR activation by auto-phosphorylation and dimerization induces phosphorylation of eIF2 α , which in turn inhibits protein translation. One might speculate that higher RNA concentrations in the present experiment triggers PKR activation, thereby causing a shutdown of translation including that of IFNs. In this thesis, HEK cells were used while Binder et al. used Huh7.5/RIG-I, which might have a lower PKR

expression. Indeed, an RNA length-dependent increase of RIG-I activation was observed with low RNA doses.

6.6. 5'p renders dsRNA non-immunogenic via steric exclusion by the 1875 side chain

When testing RNA with differing lengths and 5'ends, the complete abrogation of RIG-I activation by PP treated and thus monophosphorylated RNA was a surprising finding. A previous study described RIG-I-dependent immune induction with 5'p-RNA, although increased activity was not attributed to increased binding but instead to the higher stability of the RNA (Takahasi et al. 2008). However, in the present study the same effect that was seen for IVT RNAs was also found in HEK Trex cells and PBMCs when stimulated with 24 bp and 40 bp RNA. It is also interesting to note, as was observed in preceding experiments of the present study, that OH-dsRNA caused a robust immune response albeit lower than 3p-dsRNA. 3p-dsRNA and 2p-dsRNA (Goubau et al. 2014) are strong RIG-I activators while p-dsRNA completely abrogates RIG-I activation. Removal of the phosphate, as in OH-dsRNA, causes a moderate immune response. One phosphate has therefore a more detrimental effect on RIG-I activation compared to no phosphate at all.

To compare the results of the aforementioned study with the present system, HEK Trex cells were stimulated with the corresponding RNAs (same length and same sequence) (Takahasi et al. 2008) and additional control RNAs. Immune activation was observed for three of the tested RNAs. While one was the RNA without any phosphorylation, the second stimulating RNA was phosphorylated at the 3'end of the sense strand which was not expected to interfere with RIG-I binding and activation. Although the third activating RNA was 5'monophosphorylated at the sense strand, RIG-I activation can be assigned to the 5'end of the antisense strand which contains an OH-group. Interestingly, as previously observed, not all OH-ends are stimulatory, again pointing to more prerequisites than just the OH-group for RIG-I activation, for example a specific sequence. No stimulatory activity was observed when both 5'ends were phosphorylated. RIG-I activation by the three dsRNAs could be explained by OH-recognition, which was further supported by testing the RNAs in F853A cells (which do not detect OH-dsRNA) where no immune response was observed. In all, 5'p-RNA prevents RIG-I activation in all conditions tested in the present study. Therefore, like N1-2'Omethylation, 5'monophosphorylation of RNA is a modifications that renders RNA non immunogenic to RIG-I. In Figure 6.1 an overview of different RNA ligands and their immunostimulatory potential for RIG-I are depicted.

The question arose why 5'p-RNA is a worse stimulus than OH-dsRNA. Not only 3p-dsRNA but also 2p-dsRNA is a strong ligand for RIG-I (Goubau et al. 2014). Since p-dsRNA should be able to make more contacts to the RIG-I CTD compared to OH-dsRNA, one would expect p-dsRNA to be a better ligand than OH-dsRNA. To find an answer to this question, the crystal structure of RIG-I CTD with 2p-dsRNA (Wang et al. 2010) was analyzed and amino acids that are in close proximity (< 5 Å) to the α -p were identified using the Chimera visualization software. I875 does not only have the shortest distance to the α -p, but also has not been implicated in binding of the 3p contrary to other amino acids that are in close proximity to the α -p (K861, K888, K858, H847). Furthermore, amino acid alignments of multiple species showed that I875 is highly conserved. 15 out of the 16 sequences used in the alignment possess an isoleucine at this position. Only zebra fish has a leucine which is structurally similar to isoleucine.

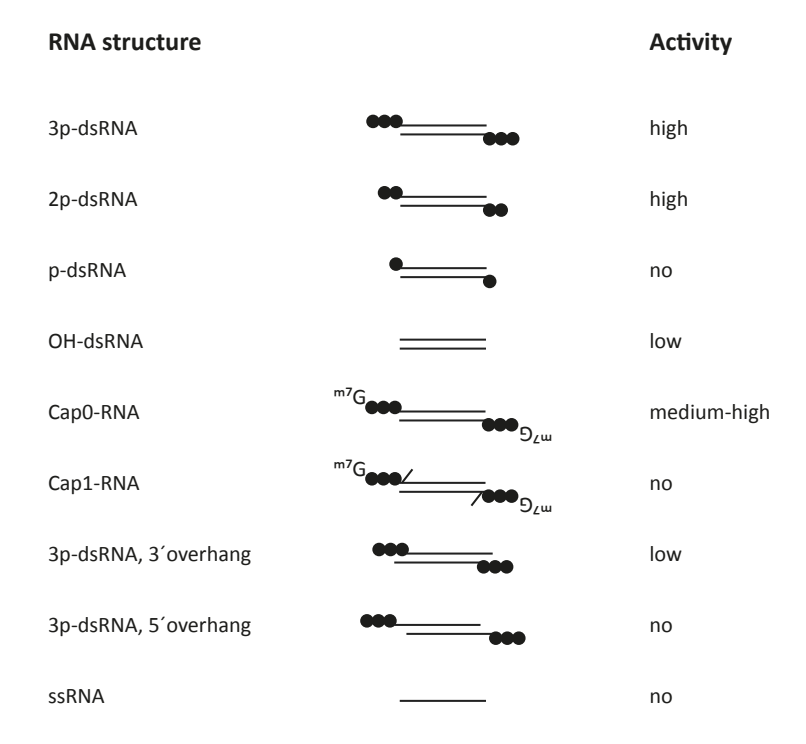


Figure 6.1: Summary: RNA ligands and their RIG-I activation potential RIG-I ligands are shown. Circles depict phosphates. Upper strands are depicte in 5′-3′direction, lower strands are depicted in 3′-5′direction.

A highly conserved structure points to an important function of the amino acid. Indeed, mutation of I875 to alanine restored RIG-I binding to p-dsRNA to a similar level observed for OH-dsRNA. Accordingly, immune activation by p-dsRNA was re-established in cells expressing RIG-I I875A. A certain binding of RIG-I WT CTD to p-dsRNA was observed in SPR, despite the fact that no binding of p-dsRNA in EMSA was detected for WT CTD and the fact

that EC50 for p-dsRNA and RIG-I WT could not be calculated because immune activation was below detection limit. SPR is more sensitive and not as harsh as EMSA and therefore might tolerate lower binding affinities better. Furthermore, the discrepancy between RIG-I binding and RIG-I activation might have several explanations. Previously, non-stimulatory RIG-I binding was described. It was reported that 3p-dsRNA with a 1 nt 5'overhang bound to RIG-I with similar affinity, as 3p-dsRNA with a blunt end, but did not induce immune activation (Marq et al. 2011). On the one hand, p-dsRNA might display a certain amount of this nonstimulatory binding. On the other hand, activation studies were performed with full-length RIG-I while only the CTD of RIG-I was used for the binding studies. When RIG-I is not bound to a ligand, RIG-I is present in an autoinhibited state where the CARDs are bound to the helicase domain and are not available for downstream signaling. Binding of the doublestranded stem of a ligand to the helicase domain displaces the CARDs, which are now able to initiate signaling via MAVS. This mechanism might be facilitated by high and moderate affinity binders such as 3p-dsRNA and OH-dsRNA, rather than low affinity ligands such as pdsRNA. Furthermore, it was reported that ATP hydrolysis by the RIG-I helicase domain has a proofreading function (Lassig et al. 2015) and causes quicker dissociation of RIG-I from nonoptimal ligands (Devarkar et al. 2018). Mutations in the helicase domain that render RIG-I ATPase deficient cause constitutive RIG-I activation and autoimmunity (Jang et al. 2015) because RIG-I is locked on endogenous RNAs (Lassig et al. 2015, Lassig et al. 2018). Therefore, the other RIG-I domains might help discriminate against low affinity ligands and increase the effect seen by CTD alone.

Interestingly, the K_d of CTD I875A with p-dsRNA is 10 times higher compared to WT CTD and is in a similar range as OH-dsRNA with WT CTD and I875A CTD. Accordingly, the EC50 value for I875A and p-dsRNA are comparable to the EC50 values of OH-dsRNA in WT and I875A expressing cells. Mutation of I875 confers p-dsRNA similar binding and activation properties to OH-dsRNA demonstrated for RIG-I WT. How does the RIG-WT structure provide discrimination against p-dsRNA and how can mutation of I875 overcome this exclusion? Unfortunately, albeit best efforts no crystal structure of p-dsRNA bound to WT CTD was obtained, probably due to the low binding affinity of p-dsRNA to RIG-I WT. The only difference between p-dsRNA and OH-dsRNA is obviously the monophosphate which is negatively charged. One might speculate that, in contrast to OH-dsRNA and also 2p-dsRNA, this negative charge is at an unusual location where it might interfere with the side chain of

I875. 2p- and 3p-dsRNA possibly overcome this hindrance by making multiple connections with other amino acids (K861, K888, H847).

A recently published paper also reported a selective RIG-I discrimination against 5'p (Ren et al. 2019). A 3.4 lower K_d for p-dsRNA compared to OH-dsRNA with full-length RIG-I was determined using EMSA. In-vitro and in-vivo studies showed no immune activation by pdsRNA, however OH-dsRNA displayed no (in-vivo) or very low (in-vitro) immune activation either. These results contradict the experiments in the present study. In their experiments, shorter dsRNAs were used (14 bp) than in the experiments in the present study (synthetic 24 bp and 40 bp RNAs or long IVT RNAs). As shown in Figure 5.5, shorter RNAs are less stimulatory and a cut-off at 19 bp for OH-dsRNA was shown. Having said this, RIG-I activation by OH-dsRNA is also supported by other publications (Devarkar et al. 2018). It is difficult to compare the mutational analysis performed in this publication with our data because of this difference in OH-dsRNA immune stimulation already in WT cells. Comparison of crystal structures of 3p-dsRNA and OH-dsRNA bound to RIG-I (Devarkar et al. 2016) revealed that, in the OH-bound state, the Hel2 loop forms interactions with amino acids that usually bind to the 3p. The recently published study proposes that this locks OH-dsRNA on RIG-I in an inactive state until a higher affinity ligand is sensed (Ren et al. 2019). A similar model is proposed for p-dsRNA binding and it is suggested that certain amino acids actively recognize the 5'p, adopting a similar conformation as if bound to OH-dsRNA. In general, they propose that different Hel2 loop conformations are exclusive depending on the ligand. In the case of OH-dsRNA or p-dsRNA binding, this Hel2 conformation might serve as a gate that blocks the CTD recognition pocket until a high affinity ligand is sensed (Ren et al. 2019). Two amino acids, one in the CTD (D872) and one in the Hel2 loop (N668), were identified that caused moderate immune response by p-dsRNA. However, their data also shows an increased immune stimulatory effect of OH-dsRNA with those CTD mutants (Ren et al. 2019), excluding a 5'p specific effect.

In the present study, cells expressing RIG-I I875A showed increased immune stimulation only after p-dsRNA stimulation, while 3p-dsRNA and OH-dsRNA transfection cause similar immune stimulation compared to WT cells. Furthermore, since other RNA modifications like 3′ overhangs only had minor differential effects while others such as 5′overhangs, 3p-N₁-dsRNA and ssRNA showed no difference in I875A activation compared to WT RIG-I, it was shown that this is a highly specific effect. Therefore, in this study a single amino acid in the

CTD of RIG-I was identified that causes the discrimination against p-dsRNA. A crystal structure of the RIG-I I875A CTD with p-dsRNA is in preparation and could shed new light on the mechanism how RIG-I is able to exclude p-dsRNA from binding.

6.7. Endogenous RNA ligands activate RIG-I 1875A

RIG-I is located in the cytoplasm where an abundant amount of endogenous RNA is present. The question arose if RIG-I's ability to discriminate between p-dsRNA and OH-dsRNA has a function in tolerance against these RNAs. Indeed, in the present study long-term expression of RIG-I I875A without the addition of exogenous ligands caused immune activation on the RNA and protein levels, thus proving that endogenous ligands are present in the cytoplasm that would activate RIG-I in case it was not able to reject p-RNA binding and activation. This effect was even stronger in 1875A cells than in H830A expressing cells which are able to detect RNAs with a cap1 structure. The ligand for I875A therefore seems to be stronger ore more abundant and therefore avoidance of pRNA is even more important than avoidance of cap1 recognition. Additionally, whole cell RNA extracts showed more immunostimulatory potential when transfected into I875A compared to WT expressing cells. The activating species in the whole cell RNA pool was double-stranded as shown by RNase A digestion. AP treatment removes phosphates from the RNA ends and leaves an OH-group. Therefore, enzymatic digestion with AP of whole cell RNA extracts should render the RNA as immunogenic in cells expressing RIG-I WT or RIG-I 1875A. Unexpectedly, AP treatment did not change IFN-β reporter activation in WT and I875A compared to untreated cells. While AP treatment of short RNA works very well, AP treatment of longer RNAs seems to be less efficient as seen in previous experiments with longer IVT transcribed RNA: After AP treatment, immune stimulation by long dsRNA was still dependent on K861. This might explain that AP treatment does not lead to RIG-I WT stimulating RNA species in whole cell RNA extracts.

tRNAS and rRNAs are promising candidate RNAs that are located in the cytoplasm and possess a 5′p. tRNAs and rRNAs are transcribed by RNA Pol III and Pol I respectively. The RNAs are further processed and possess a 5′p end in their final functional state. However, yeast tRNA showed no immune activation, neither in I875A cells nor in WT cells. rRNAs were purified with two different methods, first using gel extraction and second using specific LNA probes against 18S and 28S rRNA. rRNAs showed no RIG-I activation in cells transfected with the 18S gel extracted RNA, while only low immune activation for the extracted 28S band was

detectable. Gel extraction is a rather harsh method due to the electrophoresis process and the gel extraction buffer. RNA also has to be incubated at higher temperatures during the extraction, which has a detrimental effect on the immunostimulatory potential of RNAs, as was shown in this thesis. On this account, rRNA purification with LNA probes against 18S and 28S rRNA coupled to magnetic beads was performed and showed differing results. The rRNA⁺ fraction was as immunostimulatory compared to the rRNA⁻ fraction (whole cell RNA extracts minus rRNA). Of note, gel extracted rRNA was compared to whole cell RNA lysates (total RNA), while LNA extracted rRNA was compared to rRNA⁻. Total RNA also contains the stimulating rRNA species while rRNA⁻ does not. Since the rRNA⁻ fraction still stimulated 1875A, rRNA does not seem to be the sole ligand.

Why is tRNA and partly rRNA not recognized by I875A even though they possess a 5′monophosphate? Both RNA species form complex secondary structures. However, the 5′ends of rRNAs are diverse and tRNAs have a 4 nt 3′overhang. As shown in this thesis, while 3′overhangs on 3p-dsRNA are partially tolerated by RIG-I, 3′overhangs on p-dsRNA are not and cause very low immune activation on OH-dsRNA. Furthermore, especially tRNAs but also rRNAs contain highly modified nucleotides that might additionally prevent RIG-I recognition (Limbach et al. 1994, Hornung et al. 2006). rRNA also forms higher order structures with proteins, the small and large ribosomal subunits, which might block RIG-I access to the rRNA. Having said this, interestingly Lässig et al. studied a constitutive active RIG-I mutant – E373A – which is not able to hydrolyze ATP and locks RIG-I on suboptimal RNA ligands. It was found that extension segments of the 28S rRNA bound to this RIG-I mutant, highlighting that RIG-I might have access to at least some structures of the ribosome (Lassig et al. 2015).

Removing the polyadenylated RNA from the whole cell RNA extracts led to surprising results. The polyA⁺ fraction caused RIG-I activation even higher than whole cell RNA extracts when transfected into I875A expressing cells, while the polyA⁻ fraction was not immunostimulatory. As discussed earlier, the main polyadenylated RNA is mRNA. mRNAs usually possess a cap1 or cap2 structure which, as previously shown, completely abrogates RIG-I activation. However, mRNAs also have a high turnover rate which is essential during cell division and is crucial for the cell to adjust to changes in the environment. Indeed, polyA RNAs are temporarily present in a monophosphorylated state during the degradation process. DCP2 de-caps the RNA, leaving a 5′p followed by rapid 5′-3′degradation carried out by the exonuclease XRN1 (Braun et al. 2012). Inhibition of XRN1 might therefore increase immune

activation in I875A expressing cells. Indeed, KD of XRN1 further increased RIG-I activation in cells expressing RIG-I I875A. However, RNA extracted from cells where XRN1 was knocked down showed no elevated immune response compared to RNA from untreated cells. Furthermore, the question remained if the ligands that cause immune activation in untreated I875A expressing cells are also caused by mRNA degradation or if XRN1 KD produces new different I875A ligands. In a normal cell, de-capped RNAs are scarcely detectable suggesting that DCP2 and XRN1 activity is coordinated (Hsu et al. 1993, Braun et al. 2012). However, a constant low dose of p-dsRNA might already be sufficient to activate RIG-I and cause severe effects. Removing the polyA tail usually precedes de-capping and degradation and therefore the stimulating RNA species in the polyA⁺ fraction is supposedly not de-capped RNA.

Mitochondrial mRNA is a polyadenylated RNA in eukaryotic cells that is often overlooked. Three primary polycistronic transcripts are produced by mitochondrial transcription, which are then cut into tRNAs, rRNAs and mRNAs by RNase P and RNase Z (Dubrovsky et al. 2004, Levinger et al. 2004). mt-mRNAs get polyadenylated after cleavage. Interestingly, endonucleolytic cleavage by RNase Z leaves the 5'end of mt-mRNAs monophosphorylated. By depleting mtDNA and thereby also mtRNA through low dose EtBr treatment, it was possible to study the impact of mtRNA on 1875A stimulation. Interestingly, RNA extracted from cells that were incubated in EtBr containing medium had no immunostimulatory potential. Combined with the results from the polyA-RNA fractionation, this shows that the stimulating RNA species in the whole cell RNA extracts can be attributed to mtRNA that is probably polyadenylated.

However, while the results for the extracted RNA are quite clear, the question remains if the identified RNAs (polyA mtRNA) are also the endogenous ligands that cause immune activation by long-term expression of I875A. RNA extraction might cause changes in the RNA secondary structure and RNAs that were previously stimulatory could be lost and vice versa. Additionally, RNA binding proteins that might protect RNAs from RIG-I detection or stabilize a certain RNA conformation are removed during RNA extraction. Furthermore, and probably most puzzling, mtRNA is located in the mitochondria while RIG-I is mainly located in the cytoplasm (although certain nuclear localization has been reported as well) (Liu et al. 2018). To address this question, it is interesting to look at recent publications that show MDA5 activation by mt-dsRNA (Dhir et al. 2018) and mt-dsRNA binding to PKR (Kim et al. 2018).

MDA5 and PKR both have similar ligand requirements as RIG-I, although MDA5 and PKR are supposedly able to detect RNA end-independently. Therefore, while MDA5 and PKR might detect mtRNAs, RIG-I WT activation might be prevented through 5'monophosphate. As RIG-I can detect shorter RNAs than PKR and MDA5, additional mt ligands might be present that are exclusively detected by RIG-I when I875 is mutated.

Dhir et al. showed that dsRNA is present in uninfected cells using a dsRNA specific antibody, and by a pull-down experiment could attribute 99% of the dsRNA to the mitochondrial genome and most of the dsRNA (95%) colocalized with mitochondria. dsRNA was further accumulated when mtRNA degradation was inhibited by KD of SUV3 and PNPase which led to elevated MDA5-dependent immune activation (Dhir et al. 2018). Caused by bidirectional transcription of the H- and L- strand of the mitochondrial circular genome, mtRNAs from the complementary strands might hybridize and form dsRNA when not degraded in time. PKR like RIG-I is localized in the cytoplasm and should thus not be able to access mtRNA either. However, in a study PKR interaction with dsRNA was investigated by formaldehyde crosslinking and subsequent sequencing. It was revealed that the majority of the dsRNA bound to PKR is of mitochondrial origin (Kim et al. 2018). In the paper, it was speculated that PKR might localize with mitochondria.

Both studies attributed most of the dsRNA to the mitochondria. However, in both papers the dsRNA antibody J2 was used. This antibody only detects dsRNA longer than 40 bp (Schonborn et al. 1991). As discussed previously, while PKR and MDA5 only detect longer RNAs, RIG-I is able to detect much shorter RNAs. Presence of shorter dsRNA is not detected with this antibody and might be heavily underestimated. Additionally, mtRNAs have been shown to be present in the intermembrane space of the mitochondria (Liu et al. 2017) where they might be more easily accessible to cytoplasmic localized PRRs such as RIG-I, PKR and MDA5.

In summary, this study identified 5'p RNA as a marker for self-recognition and prevents RIG-I binding and activation. Furthermore, a single amino acid in the CTD of RIG-I (I875) that enables this mechanism was identified. Long-term expression of RIG-I I875A caused robust immune activation by endogenous ligands. Investigation of different RNA species identified mtRNA as an activator of RIG-I I875A. The data shows that RIG-I would be activated by endogenous RNA if it was not able to prevent p-RNA binding and activation. Figure 6.2

summarizes the findings of this thesis regarding RIG-I differentiation between self and non-self.

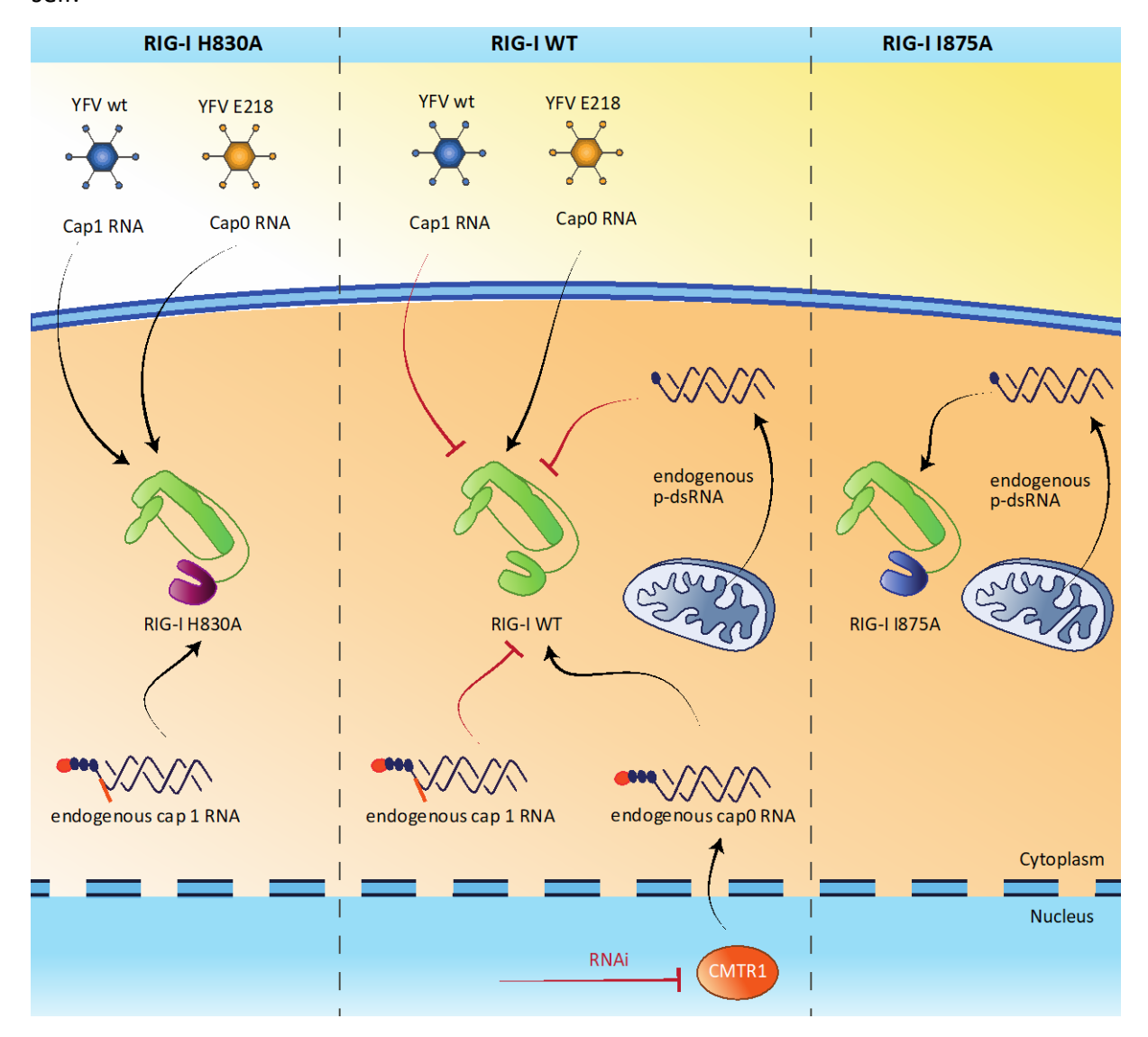


Figure 6.2: Summary: Differentiation between self and non-self by RIG-I

Endogenous Cap1 RNA and 5´p-RNA do not activate RIG-I WT. Mutation of H830 to A restores RIG-I activation by Cap1 RNA. RNAi of CMTR1 which introduces the N1-2´O-methylation renders RNA in a Cap0 state causes RIG-I WT activation. YFV uses N1-2´O-methylation of their RNA to circumvent RIG-I WT activation. YFV with an inactive methyltransferase are recognized by RIG-I WT. Muation of RIG-I I875 to A restores activation by p-dsRNA. Endogenous polyA RNA and mtRNA activate RIG-I I875A.

Although a robust IFN induction was observed by long-term expression of RIG-I I875A and also RIG-I H830A, this was lower compared to stimulation with the RIG-I ligand 3p-dsRNA. Nonetheless a low albeit constitutive immune activation might have serious implications for autoinflammatory diseases or lower specificity towards viral infections. Several single-nucleotide polymorphisms (SNPs) in RIG-I and MDA5 are associated with severe autoinflammatory diseases. Mutations in the IFIH1 gene, encoding for MDA5, also were identified in patients with Aicardi-Goutières syndrome (AGS) (Rice et al. 2014) and MDA5

mutations caused an elevated type I IFN production as well as an increased transcription of ISGs (Oda et al. 2014). Another gain of function mutation of IFIH1 was found in patients with SMS and an elevated level of ISGs was detected in the patients' blood and dental cells, causing early arterial calcification and dental inflammation (Rutsch et al. 2015). Finally other IFIH1 mutations were associated with systemic lupus erythematosus (SLE) (Van Eyck et al. 2015) and type 1 diabetes (Smyth et al. 2006, Liu et al. 2009). SNPs in the DDX58 gene, encoding for RIG-I, causing mutation of E373 to A or C268 to F were also reported to cause atypical SMS (Jang et al. 2015). This was the first report that implicated RIG-I mutations in autoinflammatory diseases. Both mutations are located in the ATP binding motifs of the helicase domain (Hel-1 domain, E373A motif I and C268 in motif II) of RIG-I. The E373A mutant prevents ATP hydrolysis and increases binding of and activation by endogenous dsRNA (Lassig et al. 2015). While RIG-I WT needs RNA and ATP for activation, the C268F mutant is activated solely by RNA and independently of ATP (Lassig et al. 2018). The C268F mutant mimics an already ATP bound state, while the E373A mutant locks RIG-I in an ATP bound state. Expression of these RIG-I mutants induced IRF3 phosphorylation and IRF3 dimerization, suggesting that these RIG-I mutants are constitutively active without external ligands, similar to RIG-I H830A and RIG-I I875A (Jang et al. 2015, Lassig et al. 2015, Lassig et al. 2018). These studies underscore the importance of understanding the RIG-I activation mechanisms and how RIG-I is able to differentiate between self and non-self. While no missense SNP is reported for I875, one missense SNP for H830 is reported in the database of Single Nucleotide Polymorphisms (H [CAT] > Y [TAT], rs1222911556) (Sherry et al. 2001). Here the histidine is replaced by phenylalanine which also harbors a bulgy residue and might fulfill the immunoregulatory function of H830. Furthermore N1-2'O-methylation or 5'monophosphorylation of RNAs can be used to design siRNAs that are non-stimulatory to RIG-I and therefore do not cause unwanted side-effects.

6.8. PKR activation by long RNAs inhibits RIG-I-dependent immune activation

When testing long RNAs it was not only found that 5'p abrogates RIG-I activation but also that long RNA causes no immune activation at higher concentrations as discussed in 6.5. To test if this decreased immune activation of long RNAs is actually caused by PKR activation, HEK cells deficient for PKR were stimulated with long and short RNAs and IFN- β promoter reporter activation was compared to cells expressing PKR. Indeed, while the short RNA (40 bp) had the same immunostimulatory potential in HEK cells with or without PKR, long RNA

(200 bp) only caused immune activation in PKR deficient cells at high concentrations. Interestingly, immune response in PKR KO cells stimulated with the long RNA at the highest RNA concentration (50 ng) was lower compared to immune activation at lower concentrations (5 ng, 0.5 ng). This effect was also observed in Thp1-Dual™ and A549 cells. Immunoblot analysis in Thp1-Dual™ cells showed PKR phosphorylation with RNA of 60 bp or longer. Correspondingly, IP10 in the supernatant after stimulation with long RNA (≥ 60 bp) was only detectable in PKR deficient A549 and Thp1-Dual™ cells and not in WT cells. The RNA binding domain of PKR can bind ligands as short as 15 bp. However, dimerization of PKR is necessary for activation and auto-phosphorylation. 30 bp RNA is the shortest RNA that can accommodate two PKR molecules and bring them in close proximity to enable autophosphorylation (Manche et al. 1992, Lemaire et al. 2008). Manche et al. reported that 23 and 34 bp RNA was only slightly active, 40 bp was partly active and 55-85 bp RNAs were highly active in inducing PKR phosphorylation (Manche et al. 1992). Furthermore, PKR was described to be activated by ssRNA that forms secondary structures with partially doublestranded structures (Nallagatla et al. 2007). If the 5'end of the RNA is unstructured, PKR activation was reported to be 3p-dependent since calf intestinal treatment (CIP) - which removes the 3p and leaves a 5'OH – abrogated PKR phosphorylation. Furthermore, adding a ^{m7}G-cap at the single-stranded 5'end also abolished RIG-I activation. Contrary to these experiments, in this thesis 40 bp RNA did not cause PKR phosphorylation. This might be due to different experimental conditions. Manche et al. tested PKR phosphorylation in a kinase reaction assay and not in a cellular system. Furthermore, IFN treatment prior to RNA stimulation can influence PKR ligand recognition. While RNA with an unstructured 5'end did not induce PKR phosphorylation in a system without functional IFN signaling, dsRNA was still able to induce PKR activation (Nallagatla et al. 2007).

Like in HEK cells, immune activation after stimulation with very long RNAs was increased at the lower concentration compared to the higher RNA concentrations in Thp1-Dual™ and A549 cells. This effect was especially pronounced in A549 cells. This hints to additional factors that influence cytokine expression and secretion after stimulation with long RNA. OAS, which is another PRR with direct antiviral activity, is an interesting candidate that might explain this effect. Three of the four OAS genes in humans – OAS1, OAS2 and OAS3 – are catalytically active. Upon RNA binding and activation of a second messenger, 2′-5′A, is synthesized that activates RNase L (Hovanessian et al. 1977, Zilberstein et al. 1978, Zhou et

al. 1993). RNase L subsequently degrades cellular RNA which causes a general shut down of protein synthesis. KO of all OAS variants increased viral load after infection with multiple viruses. This effect was most pronounced for KO of OAS3 (Li et al. 2016). Indeed, compared to HEK and Thp1 cells OAS3 expression is highest in A549 cells after IFN treatment (data not shown). The present experiments point towards a fine-tuned system of RIG-I, PKR and possibly RNase L activation that is dependent on RNA length and concentration. Low RNA concentrations are sufficient to induce RIG-I activation while PKR activation requires higher RNA concentrations. Short RNAs solely activate RIG-I while PKR phosphorylation is only induced by RNA of 60 bp or longer. The longest RNA tested (200 bp) had the highest PKR activation potential. A third factor, possibly the OAS-RNase L system, might be involved at high RNA concentrations. The longer the RNA, the more pronounced is the effect of the third player on reducing cytokine release. One might speculate that low RNA concentrations are present at the beginning of a viral infection. At this time point the cell is focused on alarming the infected and neighboring cells of the ongoing infection. Higher RNA concentrations might symbolize a more severe and longer ongoing infection, where the cell shuts down global translation due to PKR and RNase L activation. This prevents further virus replication and thus viral spread, however with the side effect of also inhibiting cytokine production and release. In the future, it would be interesting to define the specific ligand requirements of PKR and OAS and compare them to the RIG-I recognition motif. Endogenous RNAs such as rRNA and mRNA that are long enough to activate PKR are present in the cytoplasm. The cap1 structures prevents not only RIG-I activation, but also IFIT1 binding. It would be interesting to study if N1-2'O-methylation has similar effects on PKR and OAS activation and excludes endogenous RNA from PKR binding. Other RNA modifications that might render endogenous ligands non-immunogenic to PKR and OAS could be investigated as well. Furthermore, investigation of PRR activation by different viruses could shed new light on the interplay between RIG-I and other PRRs during infection.

6.9. Characterization of a new potent RIG-I ligand

Type-I IFN is used – often in combination with other drugs – in antiviral, cancer and multiple sclerosis therapy (Sabel et al. 2003, Rijckborst et al. 2010, Verweij et al. 2013). Long-term IFN therapy induces an activation of the immune system, which increases the sensitivity against foreign structures or malignant cells. However, Type-I IFN also causes multiple side effects that often lead to the termination of the therapy. Using specific PRR activating

oligonucleotides has the advantage that a more defined immune response is initiated. Moreover, not only pro-inflammatory pathways are induced but also self-regulatory counter mechanisms that prevent an overshooting immune response. This therapeutic strategy therefore might cause less unwanted side effects. The first PRR ligands tested were CpGoligodesoxyribonucleotides (ODN) that activate TLR9. While repeated CpG-ODN administration caused toxicity in mice, this effect was not observed in humans (Krieg et al. 2004). This is probably due to the fact that, in humans, TLR9 is only expressed in certain immune cells (pDCs and B-cells) (Barchet et al. 2008). RIG-I, because of its ubiquitous expression, including in tumor cells, is a more promising target for immunotherapy. Furthermore, RIG-I activation and subsequent downstream signaling pathways result in tumor cell death. Besch et al. first reported that RIG-I and MDA5 activation triggers a proapoptotic signaling pathway in non-malignant as well as tumor cells. While this pathway causes cell death in melanoma cells, non-malignant cells are less prone to apoptosis because of an intact Bcl-xL counterregulatory pathway (Besch et al. 2009). This effect was not only described for melanoma cells, but also for ovarian and pancreatic cancer cells (Kubler et al. 2010, Duewell et al. 2014). Another group tested bifunctional siRNAs to treat malignant melanoma. Bifunctional siRNAs are targeted to silence key regulators of tumor survival and additionally activate RIG-I. Indeed, these siRNAs caused IFN production as well as an increased apoptosis rate in tumor cells. Furthermore, DCs were activated which subsequently led to the activation of T-cells (Poeck et al. 2008). RIG-I activation also increases the MHC class I and Fas expression on tumor cells, which sensitizes them towards cytotoxic T cell mediated killing. Additionally, cell death initiated by RIG-I activation is described as immunogenic meaning that danger signals like HMGB1 are released (Duewell et al. 2014). All of this together makes RIG-I a promising target for immunotherapy.

As seen at low concentrations and in PKR KO cells, longer RNAs cause an increased immune activation compared to shorter RNAs and are therefore especially interesting as a therapeutic RIG-I ligand. The increased immune activation is probably due to the fact that longer RNAs can accommodate more RIG-I molecules. Each RIG-I monomer occupies 14 bp, with the exception of the end-capping monomer which occupies ~10 bp (Jiang et al. 2011). EMSA studies revealed that 21, 42 and 62 bp RNAs accommodate 2, 3 and 4-5 RIG-I molecules respectively (Peisley et al. 2013). Four tandem CARDs are proposed to build a minimum helical core for CARD-CARD interactions with MAVS and its subsequent filament

formation (Jiang et al. 2012, Peisley et al. 2013, Peisley et al. 2014). Hence, RNA ligands which can accommodate at least four RIG-Is might be highly potent RIG-I activators because they bring RIG-I CARDs into close proximity and might thereby facilitate downstream signaling via MAVS. However, as previously shown, RNAs long enough to harbor four RIG-I molecules activate PKR and cause translational arrest. Additionally, synthesis of long RNAs is more challenging and cost intensive compared to short RNAs.

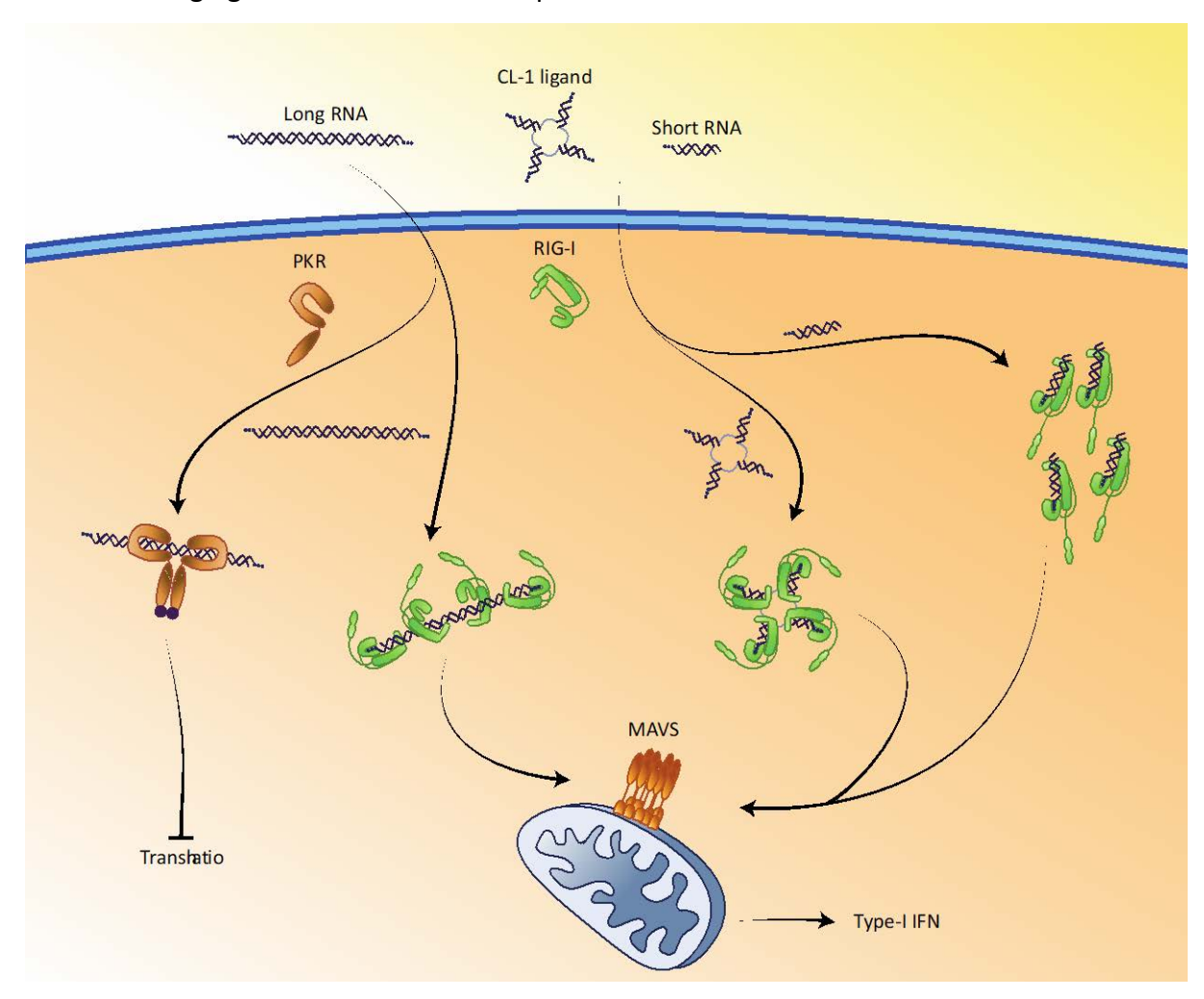


Figure 6.3: Summary: RIG-I and PKR interplay

Short 3p-dsRNA activates RIG-I but not PKR. Long RNA activates PKR and RIG-I. PKR activation and phosphorylation causes translational arrest while RIG-I activation induces Type-I IFN. The CL-1 ligand can accommodate four RIG-Is and is highly active without activating PKR.

Therefore, developing a RIG-I ligand that can harbor four RIG-I molecules without activating PKR might be interesting for immunotherapy. A RIG-I ligand (CL 1) that consists of 4 3p-dsRNAs (each 11 bp) that are connected via a flexible HEG linker were tested in comparison to a classic linear RIG-I ligand. Furthermore, different linkers were tested. While the CL ligand with one HEG linker caused comparable RIG-I activation as the CL ligand with a HEG-

HEG linker, shorter and less flexible linkers (U and UUU) reduced the immune stimulatory potential of the CL ligand substantially. Furthermore, CL 1 and CL 2 were more active than the 24mer linear dsRNA RIG-I ligand with two 3p-ends (RNA 1). The EC50 of CL 1 was 16-30 times lower compared to that of RNA 1. Interestingly, the CL ligands with the U and UUU linker demonstrated a similar activation curve as RNA 1. This might be due to the fact that the non-flexible and shorter linker does not allow the binding of four RIG-Is because of space limitations. Therefore, they might have a comparable RIG-I activation potential as RIG-I ligands with two 3p ends. Furthermore, CL ligands with 5'OH-ends completely abolished RIG-I activation. CL ligands with 1, 2, or 3 3p ends show a gradual increase in RIG-I activation. This highlights that the increased stimulatory potential of the CL ligand is not only due to a more efficient RNA transfection, but that 4 3p-ends are indeed necessary to elicit the highest immune activation in the panel tested.

Moreover, the CL ligand does not show any PKR activation as shown in Thp1 cells. As summarized in Figure 6.3, long RNAs can accommodate several RIG-Is. But they do not only activate RIG-I but also PKR and cause translational arrest. It was shown in this thesis that PKR activation leads to a decreased IP10 secretion and IFN-β induction. Short RNAs that can only harbor one or two RIG-I molecules are less immune active at lower concentrations compared to long RNA. This is probably due to the fact that four RIG-I molecules are needed to initiate MAVS filamentation. In case of long linear RNA or the CL 1 ligand these four RIG-Is are present on one RNA molecule and therefore in close proximity. The newly characterized and tested CL 1 ligand is one the one hand very active and on the other hand does not activate PKR. Therefore, the CL ligand with flexible HEG linkers is indeed a very promising target for RIG-I-dependent immunotherapy. Compared to the classic RIG-I ligand, the new ligands elicit the same immune response with lower RNA concentrations. This is not only more cost efficient but might also facilitate delivery of sufficient amounts of ligand to the target cells. For the future it would be interesting to further optimize this ligand in terms of stability and selectivity. Phosphothioate modifications can enhance the resistance to RNases which prolongs the prevalence of the RNA in the cytosol and its availability to RIG-I. In terms of selectivity it was not examined in this study if the CL ligands also induce TLR activation. It was shown that 2'O-methylation at certain nucleotide positions leads to the abrogation of a TLR dependent immune activation (Tluk et al. 2009). However, 2´O-methylation of N1 also abrogates RIG-I activation (Schuberth-Wagner et al. 2015). It would be therefore interesting

Discussion

to test CL ligands with 2'O-methylations at different positions to identify RNAs that on the one hand are still active for RIG-I but on the other hand do not induce a TLR dependent immune activation.

7. References

- Abbas, Y. M., B. T. Laudenbach, S. Martinez-Montero, R. Cencic, M. Habjan, A. Pichlmair, M. J. Damha, J. Pelletier and B. Nagar (2017). "Structure of human IFIT1 with capped RNA reveals adaptable mRNA binding and mechanisms for sensing N1 and N2 ribose 2'-O methylations." Proc Natl Acad Sci U S A 114(11): E2106-E2115.
- Abbas, Y. M., A. Pichlmair, M. W. Gorna, G. Superti-Furga and B. Nagar (2013). "Structural basis for viral 5'-PPP-RNA recognition by human IFIT proteins." <u>Nature</u> **494**(7435): 60-64.
- Ablasser, A., F. Bauernfeind, G. Hartmann, E. Latz, K. A. Fitzgerald and V. Hornung (2009). "RIG-I-dependent sensing of poly(dA:dT) through the induction of an RNA polymerase III-transcribed RNA intermediate." Nat Immunol **10**(10): 1065-1072.
- Ahmad, S. and S. Hur (2015). "Helicases in Antiviral Immunity: Dual Properties as Sensors and Effectors." <u>Trends Biochem Sci</u> **40**(10): 576-585.
- Alexopoulou, L., A. C. Holt, R. Medzhitov and R. A. Flavell (2001). "Recognition of double-stranded RNA and activation of NF-kappa B by Toll-like receptor 3." <u>Nature</u> **413**(6857): 732-738.
- Anchisi, S., J. Guerra, G. Mottet-Osman and D. Garcin (2016). "Mismatches in the Influenza A Virus RNA Panhandle Prevent Retinoic Acid-Inducible Gene I (RIG-I) Sensing by Impairing RNA/RIG-I Complex Formation." <u>I Virol</u> **90**(1): 586-590.
- Balachandran, S., P. C. Roberts, L. E. Brown, H. Truong, A. K. Pattnaik, D. R. Archer and G. N. Barber (2000). "Essential role for the dsRNA-dependent protein kinase PKR in innate immunity to viral infection." <u>Immunity</u> **13**(1): 129-141.
- Banerjee, A. K. (1980). "5'-terminal cap structure in eucaryotic messenger ribonucleic acids." <u>Microbiol Rev</u> **44**(2): 175-205.
- Barchet, W., V. Wimmenauer, M. Schlee and G. Hartmann (2008). "Accessing the therapeutic potential of immunostimulatory nucleic acids." <u>Curr Opin Immunol</u> **20**(4): 389-395.
- Barrell, B. G., A. T. Bankier and J. Drouin (1979). "A different genetic code in human mitochondria." <u>Nature</u> **282**(5735): 189-194.
- Baum, A., R. Sachidanandam and A. Garcia-Sastre (2010). "Preference of RIG-I for short viral RNA molecules in infected cells revealed by next-generation sequencing." <u>Proc Natl Acad Sci U S A</u> **107**(37): 16303-16308.
- Belanger, F., J. Stepinski, E. Darzynkiewicz and J. Pelletier (2010). "Characterization of hMTr1, a human Cap1 2'-O-ribose methyltransferase." <u>I Biol Chem</u> **285**(43): 33037-33044.
- Ben-Shem, A., N. Garreau de Loubresse, S. Melnikov, L. Jenner, G. Yusupova and M. Yusupov (2011). "The structure of the eukaryotic ribosome at 3.0 A resolution." <u>Science</u> **334**(6062): 1524-1529.
- Besch, R., H. Poeck, T. Hohenauer, D. Senft, G. Hacker, C. Berking, V. Hornung, S. Endres, T. Ruzicka, S. Rothenfusser and G. Hartmann (2009). "Proapoptotic signaling induced by RIG-I and MDA-5 results in type I interferon-independent apoptosis in human melanoma cells." <u>I Clin Invest</u> **119**(8): 2399-2411.
- Bhella, D., A. Ralph and R. P. Yeo (2004). "Conformational flexibility in recombinant measles virus nucleocapsids visualised by cryo-negative stain electron microscopy and real-space helical reconstruction." J Mol Biol 340(2): 319-331.
- Binder, M., F. Eberle, S. Seitz, N. Mucke, C. M. Huber, N. Kiani, L. Kaderali, V. Lohmann, A. Dalpke and R. Bartenschlager (2011). "Molecular mechanism of signal perception and integration by the innate immune sensor retinoic acid-inducible gene-I (RIG-I)." <u>J Biol Chem</u> **286**(31): 27278-27287.
- Bitko, V., A. Musiyenko, M. A. Bayfield, R. J. Maraia and S. Barik (2008). "Cellular La protein shields nonsegmented negative-strand RNA viral leader RNA from RIG-I and enhances virus growth by diverse mechanisms." <u>I Virol</u> **82**(16): 7977-7987.
- Braun, J. E., V. Truffault, A. Boland, E. Huntzinger, C. T. Chang, G. Haas, O. Weichenrieder, M. Coles and E. Izaurralde (2012). "A direct interaction between DCP1 and XRN1 couples mRNA decapping to 5' exonucleolytic degradation." Nat Struct Mol Biol 19(12): 1324-1331.
- Brennan-Laun, S. E., H. J. Ezelle, X. L. Li and B. A. Hassel (2014). "RNase-L control of cellular mRNAs: roles in biologic functions and mechanisms of substrate targeting." <u>J Interferon Cytokine Res</u> **34**(4): 275-288.
- Bruns, A. M. and C. M. Horvath (2012). "Activation of RIG-I-like receptor signal transduction." <u>Crit Rev Biochem Mol Biol</u> **47**(2): 194-206.
- Cardenas, W. B., Y. M. Loo, M. Gale, Jr., A. L. Hartman, C. R. Kimberlin, L. Martinez-Sobrido, E. O. Saphire and C. F. Basler (2006). "Ebola virus VP35 protein binds double-stranded RNA and inhibits alpha/beta interferon production induced by RIG-I signaling." <u>I Virol</u> 80(11): 5168-5178.
- Chan, Y. K. and M. U. Gack (2016). "Viral evasion of intracellular DNA and RNA sensing." <u>Nat Rev Microbiol</u> **14**(6): 360-373.
- Chen, C. Y. and A. B. Shyu (2011). "Mechanisms of deadenylation-dependent decay." <u>Wiley Interdiscip Rev RNA</u> **2**(2): 167-183.

- Chen, G., M. H. Shaw, Y. G. Kim and G. Nunez (2009). "NOD-like receptors: role in innate immunity and inflammatory disease." <u>Annu Rev Pathol</u> 4: 365-398.
- Chiu, Y. H., J. B. Macmillan and Z. J. Chen (2009). "RNA polymerase III detects cytosolic DNA and induces type I interferons through the RIG-I pathway." <u>Cell</u> **138**(3): 576-591.
- Chow, J. C., D. W. Young, D. T. Golenbock, W. J. Christ and F. Gusovsky (1999). "Toll-like receptor-4 mediates lipopolysaccharide-induced signal transduction." <u>J Biol Chem</u> **274**(16): 10689-10692.
- Civril, F., M. Bennett, M. Moldt, T. Deimling, G. Witte, S. Schiesser, T. Carell and K. P. Hopfner (2011). "The RIG-I ATPase domain structure reveals insights into ATP-dependent antiviral signalling." <u>EMBO Rep</u> **12**(11): 1127-1134.
- Cui, S., K. Eisenacher, A. Kirchhofer, K. Brzozka, A. Lammens, K. Lammens, T. Fujita, K. K. Conzelmann, A. Krug and K. P. Hopfner (2008). "The C-terminal regulatory domain is the RNA 5'-triphosphate sensor of RIG-I." Mol Cell 29(2): 169-179.
- Daffis, S., K. J. Szretter, J. Schriewer, J. Li, S. Youn, J. Errett, T. Y. Lin, S. Schneller, R. Zust, H. Dong, V. Thiel, G. C. Sen, V. Fensterl, W. B. Klimstra, T. C. Pierson, R. M. Buller, M. Gale, Jr., P. Y. Shi and M. S. Diamond (2010). "2'-0 methylation of the viral mRNA cap evades host restriction by IFIT family members." Nature 468(7322): 452-456.
- Dempsey, P. W., S. A. Vaidya and G. Cheng (2003). "The art of war: Innate and adaptive immune responses." Cell Mol Life Sci **60**(12): 2604-2621.
- Desselberger, U., V. R. Racaniello, J. J. Zazra and P. Palese (1980). "The 3' and 5'-terminal sequences of influenza A, B and C virus RNA segments are highly conserved and show partial inverted complementarity." Gene 8(3): 315-328.
- Devarkar, S. C., B. Schweibenz, C. Wang, J. Marcotrigiano and S. S. Patel (2018). "RIG-I Uses an ATPase-Powered Translocation-Throttling Mechanism for Kinetic Proofreading of RNAs and Oligomerization." Mol Cell **72**(2): 355-368 e354.
- Devarkar, S. C., C. Wang, M. T. Miller, A. Ramanathan, F. Jiang, A. G. Khan, S. S. Patel and J. Marcotrigiano (2016). "Structural basis for m7G recognition and 2'-0-methyl discrimination in capped RNAs by the innate immune receptor RIG-I." <u>Proc Natl Acad Sci U S A</u> **113**(3): 596-601.
- Dhir, A., S. Dhir, L. S. Borowski, L. Jimenez, M. Teitell, A. Rotig, Y. J. Crow, G. I. Rice, D. Duffy, C. Tamby, T. Nojima, A. Munnich, M. Schiff, C. R. de Almeida, J. Rehwinkel, A. Dziembowski, R. J. Szczesny and N. J. Proudfoot (2018). "Mitochondrial double-stranded RNA triggers antiviral signalling in humans." Nature **560**(7717): 238-242.
- Diebold, S. S., T. Kaisho, H. Hemmi, S. Akira and C. R. E. Sousa (2004). "Innate antiviral responses by means of TLR7-mediated recognition of single-stranded RNA." <u>Science</u> **303**(5663): 1529-1531.
- Dmochowska, A., K. Kalita, M. Krawczyk, P. Golik, K. Mroczek, J. Lazowska, P. P. Stepien and E. Bartnik (1999). "A human putative Suv3-like RNA helicase is conserved between Rhodobacter and all eukaryotes." Acta Biochim Pol 46(1): 155-162.
- Donelan, N. R., C. F. Basler and A. Garcia-Sastre (2003). "A recombinant influenza A virus expressing an RNA-binding-defective NS1 protein induces high levels of beta interferon and is attenuated in mice." <u>I Virol</u> **77**(24): 13257-13266.
- Dong, H., B. Zhang and P. Y. Shi (2008). "Flavivirus methyltransferase: a novel antiviral target." <u>Antiviral Res</u> **80**(1): 1-10.
- Donovan, J., S. Rath, D. Kolet-Mandrikov and A. Korennykh (2017). "Rapid RNase L-driven arrest of protein synthesis in the dsRNA response without degradation of translation machinery." RNA 23(11): 1660-1671.
- Doyle, S., S. Vaidya, R. O'Connell, H. Dadgostar, P. Dempsey, T. Wu, G. Rao, R. Sun, M. Haberland, R. Modlin and G. Cheng (2002). "IRF3 mediates a TLR3/TLR4-specific antiviral gene program." <u>Immunity</u> **17**(3): 251-263.
- Dubrovsky, E. B., V. A. Dubrovskaya, L. Levinger, S. Schiffer and A. Marchfelder (2004). "Drosophila RNase Z processes mitochondrial and nuclear pre-tRNA 3' ends in vivo." <u>Nucleic Acids Res</u> **32**(1): 255-262.
- Duewell, P., A. Steger, H. Lohr, H. Bourhis, H. Hoelz, S. V. Kirchleitner, M. R. Stieg, S. Grassmann, S. Kobold, J. T. Siveke, S. Endres and M. Schnurr (2014). "RIG-I-like helicases induce immunogenic cell death of pancreatic cancer cells and sensitize tumors toward killing by CD8(+) T cells." Cell Death Differ 21(12): 1825-1837.
- Eichler, D. C. and N. Craig (1994). "Processing of eukaryotic ribosomal RNA." <u>Prog Nucleic Acid Res Mol Biol</u> **49**: 197-239.
- Errett, J. S., M. S. Suthar, A. McMillan, M. S. Diamond and M. Gale, Jr. (2013). "The essential, nonredundant roles of RIG-I and MDA5 in detecting and controlling West Nile virus infection." <u>J Virol</u> **87**(21): 11416-11425.
- Fan, L., T. Briese and W. I. Lipkin (2010). "Z proteins of New World arenaviruses bind RIG-I and interfere with type I interferon induction." <u>I Virol</u> **84**(4): 1785-1791.

- Fatica, A. and D. Tollervey (2002). "Making ribosomes." Curr Opin Cell Biol 14(3): 313-318.
- Fechter, P. and G. G. Brownlee (2005). "Recognition of mRNA cap structures by viral and cellular proteins." J Gen Virol 86(Pt 5): 1239-1249.
- Feng, Q., S. V. Hato, M. A. Langereis, J. Zoll, R. Virgen-Slane, A. Peisley, S. Hur, B. L. Semler, R. P. van Rij and F. J. van Kuppeveld (2012). "MDA5 detects the double-stranded RNA replicative form in picornavirus-infected cells." <u>Cell Rep</u> **2**(5): 1187-1196.
- Fernandez-Silva, P., J. A. Enriquez and J. Montoya (2003). "Replication and transcription of mammalian mitochondrial DNA." Exp Physiol 88(1): 41-56.
- Fung-Leung, W. P., M. W. Schilham, A. Rahemtulla, T. M. Kundig, M. Vollenweider, J. Potter, W. van Ewijk and T. W. Mak (1991). "CD8 is needed for development of cytotoxic T cells but not helper T cells." <u>Cell</u> **65**(3): 443-449.
- Furr, S. R., M. Moerdyk-Schauwecker, V. Z. Grdzelishvili and I. Marriott (2010). "RIG-I mediates nonsegmented negative-sense RNA virus-induced inflammatory immune responses of primary human astrocytes." Glia **58**(13): 1620-1629.
- Furuichi, Y. and A. J. Shatkin (2000). "Viral and cellular mRNA capping: past and prospects." <u>Adv Virus Res</u> **55**: 135-184.
- Gack, M. U., R. A. Albrecht, T. Urano, K. S. Inn, I. C. Huang, E. Carnero, M. Farzan, S. Inoue, J. U. Jung and A. Garcia-Sastre (2009). "Influenza A virus NS1 targets the ubiquitin ligase TRIM25 to evade recognition by the host viral RNA sensor RIG-I." <u>Cell Host Microbe</u> **5**(5): 439-449.
- Gack, M. U., Y. C. Shin, C. H. Joo, T. Urano, C. Liang, L. Sun, O. Takeuchi, S. Akira, Z. Chen, S. Inoue and J. U. Jung (2007). "TRIM25 RING-finger E3 ubiquitin ligase is essential for RIG-I-mediated antiviral activity." Nature **446**(7138): 916-920.
- Gerlier, D. and D. S. Lyles (2011). "Interplay between innate immunity and negative-strand RNA viruses: towards a rational model." <u>Microbiol Mol Biol Rev</u> **75**(3): 468-490, second page of table of contents.
- Ghosh, A. and C. D. Lima (2010). "Enzymology of RNA cap synthesis." Wiley Interdiscip Rev RNA 1(1): 152-172.
- Gingras, A. C., B. Raught and N. Sonenberg (1999). "eIF4 initiation factors: effectors of mRNA recruitment to ribosomes and regulators of translation." <u>Annu Rev Biochem</u> **68**: 913-963.
- Gitlin, L., W. Barchet, S. Gilfillan, M. Cella, B. Beutler, R. A. Flavell, M. S. Diamond and M. Colonna (2006). "Essential role of mda-5 in type I IFN responses to polyriboinosinic:polyribocytidylic acid and encephalomyocarditis picornavirus." Proc Natl Acad Sci U S A 103(22): 8459-8464.
- Gondai, T., K. Yamaguchi, N. Miyano-Kurosaki, Y. Habu and H. Takaku (2008). "Short-hairpin RNAs synthesized by T7 phage polymerase do not induce interferon." <u>Nucleic Acids Res</u> **36**(3): e18.
- Goubau, D., M. Schlee, S. Deddouche, A. J. Pruijssers, T. Zillinger, M. Goldeck, C. Schuberth, A. G. Van der Veen, T. Fujimura, J. Rehwinkel, J. A. Iskarpatyoti, W. Barchet, J. Ludwig, T. S. Dermody, G. Hartmann and C. Reis e Sousa (2014). "Antiviral immunity via RIG-I-mediated recognition of RNA bearing 5'-diphosphates." Nature **514**(7522): 372-375.
- Granneman, S. and S. J. Baserga (2005). "Crosstalk in gene expression: coupling and co-regulation of rDNA transcription, pre-ribosome assembly and pre-rRNA processing." <u>Curr Opin Cell Biol</u> **17**(3): 281-286.
- Gronostajski, R. M. and P. D. Sadowski (1985). "Determination of DNA sequences essential for FLP-mediated recombination by a novel method." <u>J Biol Chem</u> **260**(22): 12320-12327.
- Grummt, I. (2003). "Life on a planet of its own: regulation of RNA polymerase I transcription in the nucleolus." Genes Dev **17**(14): 1691-1702.
- Grunberg-Manago, M. (1967). "Polynucleotide phosphorylase: structure and mechanism of action." <u>Biochem</u> **I 103**(3): 62P.
- Habjan, M., I. Andersson, J. Klingstrom, M. Schumann, A. Martin, P. Zimmermann, V. Wagner, A. Pichlmair, U. Schneider, E. Muhlberger, A. Mirazimi and F. Weber (2008). "Processing of genome 5' termini as a strategy of negative-strand RNA viruses to avoid RIG-I-dependent interferon induction." <u>PLoS One</u> 3(4): e2032.
- Habjan, M., P. Hubel, L. Lacerda, C. Benda, C. Holze, C. H. Eberl, A. Mann, E. Kindler, C. Gil-Cruz, J. Ziebuhr, V. Thiel and A. Pichlmair (2013). "Sequestration by IFIT1 impairs translation of 2'O-unmethylated capped RNA." PLoS Pathog **9**(10): e1003663.
- Hayashi, F., K. D. Smith, A. Ozinsky, T. R. Hawn, E. C. Yi, D. R. Goodlett, J. K. Eng, S. Akira, D. M. Underhill and A. Aderem (2001). "The innate immune response to bacterial flagellin is mediated by Toll-like receptor 5." Nature **410**(6832): 1099-1103.
- Heil, F., H. Hemmi, H. Hochrein, F. Ampenberger, C. Kirschning, S. Akira, G. Lipford, H. Wagner and S. Bauer (2004). "Species-specific recognition of single-stranded RNA via toll-like receptor 7 and 8." <u>Science</u> **303**(5663): 1526-1529.
- Helm, M. and J. D. Alfonzo (2014). "Posttranscriptional RNA Modifications: playing metabolic games in a cell's chemical Legoland." Chem Biol **21**(2): 174-185.

References

- Hemmi, H., O. Takeuchi, T. Kawai, T. Kaisho, S. Sato, H. Sanjo, M. Matsumoto, K. Hoshino, H. Wagner, K. Takeda and S. Akira (2000). "A Toll-like receptor recognizes bacterial DNA." <u>Nature</u> **408**(6813): 740-745.
- Henras, A. K., C. Plisson-Chastang, M. F. O'Donohue, A. Chakraborty and P. E. Gleizes (2015). "An overview of pre-ribosomal RNA processing in eukaryotes." <u>Wiley Interdiscip Rev RNA</u> **6**(2): 225-242.
- Henras, A. K., J. Soudet, M. Gerus, S. Lebaron, M. Caizergues-Ferrer, A. Mougin and Y. Henry (2008). "The post-transcriptional steps of eukaryotic ribosome biogenesis." <u>Cell Mol Life Sci</u> **65**(15): 2334-2359.
- Hewlett, M. J., R. F. Pettersson and D. Baltimore (1977). "Circular forms of Uukuniemi virion RNA: an electron microscopic study." <u>I Virol</u> **21**(3): 1085-1093.
- Hornung, V., J. Ellegast, S. Kim, K. Brzozka, A. Jung, H. Kato, H. Poeck, S. Akira, K. K. Conzelmann, M. Schlee, S. Endres and G. Hartmann (2006). "5'-Triphosphate RNA is the ligand for RIG-I." <u>Science</u> **314**(5801): 994-997.
- Hornung, V., M. Guenthner-Biller, C. Bourquin, A. Ablasser, M. Schlee, S. Uematsu, A. Noronha, M. Manoharan, S. Akira, A. de Fougerolles, S. Endres and G. Hartmann (2005). "Sequence-specific potent induction of IFN-alpha by short interfering RNA in plasmacytoid dendritic cells through TLR7." Nat Med 11(3): 263-270.
- Houseley, J., J. LaCava and D. Tollervey (2006). "RNA-quality control by the exosome." <u>Nat Rev Mol Cell Biol</u> **7**(7): 529-539.
- Hovanessian, A. G., R. E. Brown and I. M. Kerr (1977). "Synthesis of low molecular weight inhibitor of protein synthesis with enzyme from interferon-treated cells." <u>Nature</u> **268**(5620): 537-540.
- Hovanessian, A. G. and I. M. Kerr (1978). "Synthesis of an oligonucleotide inhibitor of protein synthesis in rabbit reticulocyte lysates analogous to that formed in extracts from interferon-treated cells." <u>Eur J Biochem 84(1)</u>: 149-159.
- Hruby, D. E. and W. K. Roberts (1978). "Encephalomyocarditis virus RNA. III. Presence of a genome-associated protein." <u>I Virol</u> **25**(1): 413-415.
- Hsu, C. L. and A. Stevens (1993). "Yeast cells lacking 5'-->3' exoribonuclease 1 contain mRNA species that are poly(A) deficient and partially lack the 5' cap structure." Mol Cell Biol 13(8): 4826-4835.
- Hsu, M. T., J. D. Parvin, S. Gupta, M. Krystal and P. Palese (1987). "Genomic RNAs of influenza viruses are held in a circular conformation in virions and in infected cells by a terminal panhandle." <u>Proc Natl Acad Sci U S A</u> **84**(22): 8140-8144.
- Hyde, J. L. and M. S. Diamond (2015). "Innate immune restriction and antagonism of viral RNA lacking 2-0 methylation." <u>Virology</u> **479-480**: 66-74.
- Iordanov, M. S., J. M. Paranjape, A. Zhou, J. Wong, B. R. Williams, E. F. Meurs, R. H. Silverman and B. E. Magun (2000). "Activation of p38 mitogen-activated protein kinase and c-Jun NH(2)-terminal kinase by double-stranded RNA and encephalomyocarditis virus: involvement of RNase L, protein kinase R, and alternative pathways." Mol Cell Biol 20(2): 617-627.
- Isaacs, A., R. A. Cox and Z. Rotem (1963). "Foreign nucleic acids as the stimulus to make interferon." <u>Lancet</u> **2**(7299): 113-116.
- Isaacs, A. and J. Lindenmann (1957). "Virus interference. I. The interferon." <u>Proc R Soc Lond B Biol Sci</u> **147**(927): 258-267.
- Jang, M. A., E. K. Kim, H. Now, N. T. Nguyen, W. J. Kim, J. Y. Yoo, J. Lee, Y. M. Jeong, C. H. Kim, O. H. Kim, S. Sohn, S. H. Nam, Y. Hong, Y. S. Lee, S. A. Chang, S. Y. Jang, J. W. Kim, M. S. Lee, S. Y. Lim, K. S. Sung, K. T. Park, B. J. Kim, J. H. Lee, D. K. Kim, C. Kee and C. S. Ki (2015). "Mutations in DDX58, which encodes RIG-I, cause atypical Singleton-Merten syndrome." Am J Hum Genet 96(2): 266-274.
- Jiang, F., A. Ramanathan, M. T. Miller, G. Q. Tang, M. Gale, Jr., S. S. Patel and J. Marcotrigiano (2011). "Structural basis of RNA recognition and activation by innate immune receptor RIG-I." <u>Nature</u> **479**(7373): 423-427.
- Jiang, X., L. N. Kinch, C. A. Brautigam, X. Chen, F. Du, N. V. Grishin and Z. J. Chen (2012). "Ubiquitin-induced oligomerization of the RNA sensors RIG-I and MDA5 activates antiviral innate immune response." <u>Immunity</u> 36(6): 959-973.
- Kanneganti, T. D. (2010). "Central roles of NLRs and inflammasomes in viral infection." <u>Nat Rev Immunol</u> **10**(10): 688-698.
- Kato, H., S. Sato, M. Yoneyama, M. Yamamoto, S. Uematsu, K. Matsui, T. Tsujimura, K. Takeda, T. Fujita, O. Takeuchi and S. Akira (2005). "Cell type-specific involvement of RIG-I in antiviral response." <u>Immunity</u> **23**(1): 19-28.
- Kato, H., O. Takeuchi, E. Mikamo-Satoh, R. Hirai, T. Kawai, K. Matsushita, A. Hiiragi, T. S. Dermody, T. Fujita and S. Akira (2008). "Length-dependent recognition of double-stranded ribonucleic acids by retinoic acid-inducible gene-I and melanoma differentiation-associated gene 5." <u>I Exp Med</u> **205**(7): 1601-1610.
- Kato, H., O. Takeuchi, S. Sato, M. Yoneyama, M. Yamamoto, K. Matsui, S. Uematsu, A. Jung, T. Kawai, K. J. Ishii, O. Yamaguchi, K. Otsu, T. Tsujimura, C. S. Koh, C. Reis e Sousa, Y. Matsuura, T. Fujita and S. Akira (2006).

References

- "Differential roles of MDA5 and RIG-I helicases in the recognition of RNA viruses." <u>Nature</u> **441**(7089): 101-105.
- Kawai, T. and S. Akira (2008). "Toll-like receptor and RIG-I-like receptor signaling." Ann N Y Acad Sci 1143: 1-20.
- Kawai, T., K. Takahashi, S. Sato, C. Coban, H. Kumar, H. Kato, K. J. Ishii, O. Takeuchi and S. Akira (2005). "IPS-1, an adaptor triggering RIG-I- and Mda5-mediated type I interferon induction." Nat Immunol 6(10): 981-988
- Khatter, H., A. G. Myasnikov, S. K. Natchiar and B. P. Klaholz (2015). "Structure of the human 80S ribosome." Nature **520**(7549): 640-645.
- Khidr, L., G. Wu, A. Davila, V. Procaccio, D. Wallace and W. H. Lee (2008). "Role of SUV3 helicase in maintaining mitochondrial homeostasis in human cells." <u>I Biol Chem</u> **283**(40): 27064-27073.
- Killip, M. J., M. Smith, D. Jackson and R. E. Randall (2014). "Activation of the interferon induction cascade by influenza a viruses requires viral RNA synthesis and nuclear export." <u>I Virol</u> **88**(8): 3942-3952.
- Kim, Y., J. Park, S. Kim, M. Kim, M. G. Kang, C. Kwak, M. Kang, B. Kim, H. W. Rhee and V. N. Kim (2018). "PKR Senses Nuclear and Mitochondrial Signals by Interacting with Endogenous Double-Stranded RNAs." <u>Mol Cell</u> **71**(6): 1051-1063 e1056.
- Kimura, T., H. Katoh, H. Kayama, H. Saiga, M. Okuyama, T. Okamoto, E. Umemoto, Y. Matsuura, M. Yamamoto and K. Takeda (2013). "Ifit1 inhibits Japanese encephalitis virus replication through binding to 5' capped 2'-0 unmethylated RNA." <u>J Virol</u> 87(18): 9997-10003.
- King, M. P. and G. Attardi (1996). "Isolation of human cell lines lacking mitochondrial DNA." <u>Methods Enzymol</u> **264**: 304-313.
- Kolakofsky, D. (1976). "Isolation and characterization of Sendai virus DI-RNAs." Cell 8(4): 547-555.
- Kolakofsky, D., E. Kowalinski and S. Cusack (2012). "A structure-based model of RIG-I activation." <u>RNA</u> **18**(12): 2118-2127.
- Kowalinski, E., T. Lunardi, A. A. McCarthy, J. Louber, J. Brunel, B. Grigorov, D. Gerlier and S. Cusack (2011). "Structural basis for the activation of innate immune pattern-recognition receptor RIG-I by viral RNA." <u>Cell</u> **147**(2): 423-435.
- Krieg, A. M., S. M. Efler, M. Wittpoth, M. J. Al Adhami and H. L. Davis (2004). "Induction of systemic TH1-like innate immunity in normal volunteers following subcutaneous but not intravenous administration of CPG 7909, a synthetic B-class CpG oligodeoxynucleotide TLR9 agonist." <u>Immunother</u> 27(6): 460-471.
- Kubler, K., N. Gehrke, S. Riemann, V. Bohnert, T. Zillinger, E. Hartmann, M. Polcher, C. Rudlowski, W. Kuhn, G. Hartmann and W. Barchet (2010). "Targeted activation of RNA helicase retinoic acid-inducible gene-I induces proimmunogenic apoptosis of human ovarian cancer cells." <u>Cancer Res</u> **70**(13): 5293-5304.
- Kumar, H., T. Kawai and S. Akira (2009). "Toll-like receptors and innate immunity." <u>Biochem Biophys Res Commun</u> **388**(4): 621-625.
- Kumar, P., T. R. Sweeney, M. A. Skabkin, O. V. Skabkina, C. U. Hellen and T. V. Pestova (2014). "Inhibition of translation by IFIT family members is determined by their ability to interact selectively with the 5'-terminal regions of cap0-, cap1- and 5'ppp- mRNAs." <u>Nucleic Acids Res</u> **42**(5): 3228-3245.
- Kumar, S., H. Ingle, S. Mishra, R. S. Mahla, A. Kumar, T. Kawai, S. Akira, A. Takaoka, A. A. Raut and H. Kumar (2015). "IPS-1 differentially induces TRAIL, BCL2, BIRC3 and PRKCE in type I interferons-dependent and -independent anticancer activity." <u>Cell Death Dis</u> **6**: e1758.
- Lassig, C., K. Lammens, J. L. Gorenflos Lopez, S. Michalski, O. Fettscher and K. P. Hopfner (2018). "Unified mechanisms for self-RNA recognition by RIG-I Singleton-Merten syndrome variants." Elife 7.
- Lassig, C., S. Matheisl, K. M. Sparrer, C. C. de Oliveira Mann, M. Moldt, J. R. Patel, M. Goldeck, G. Hartmann, A. Garcia-Sastre, V. Hornung, K. K. Conzelmann, R. Beckmann and K. P. Hopfner (2015). "ATP hydrolysis by the viral RNA sensor RIG-I prevents unintentional recognition of self-RNA." <u>Elife</u> 4.
- Lazzarini, R. A., J. D. Keene and M. Schubert (1981). "The origins of defective interfering particles of the negative-strand RNA viruses." <u>Cell</u> **26**(2 Pt 2): 145-154.
- Lee, M. S. and Y. J. Kim (2007). "Signaling pathways downstream of pattern-recognition receptors and their cross talk." <u>Annu Rev Biochem</u> **76**: 447-480.
- Lee, Y. F., A. Nomoto, B. M. Detjen and E. Wimmer (1977). "A protein covalently linked to poliovirus genome RNA." Proc Natl Acad Sci U S A **74**(1): 59-63.
- Lemaire, P. A., E. Anderson, J. Lary and J. L. Cole (2008). "Mechanism of PKR Activation by dsRNA." <u>J Mol Biol</u> **381**(2): 351-360.
- Levin, D. and I. M. London (1978). "Regulation of protein synthesis: activation by double-stranded RNA of a protein kinase that phosphorylates eukaryotic initiation factor 2." <u>Proc Natl Acad Sci U S A</u> **75**(3): 1121-1125.
- Levinger, L., M. Morl and C. Florentz (2004). "Mitochondrial tRNA 3' end metabolism and human disease." Nucleic Acids Res **32**(18): 5430-5441.
- Li, J., Y. Liu and X. Zhang (2010). "Murine coronavirus induces type I interferon in oligodendrocytes through

- recognition by RIG-I and MDA5." <u>I Virol</u> **84**(13): 6472-6482.
- Li, S. and C. E. Mason (2014). "The pivotal regulatory landscape of RNA modifications." <u>Annu Rev Genomics Hum Genet</u> **15**: 127-150.
- Li, Y., S. Banerjee, Y. Wang, S. A. Goldstein, B. Dong, C. Gaughan, R. H. Silverman and S. R. Weiss (2016). "Activation of RNase L is dependent on OAS3 expression during infection with diverse human viruses." <u>Proc Natl Acad Sci U S A</u> **113**(8): 2241-2246.
- Limbach, P. A., P. F. Crain and J. A. Mccloskey (1994). "The Modified Nucleosides of Rna Summary." <u>Nucleic Acids Research</u> **22**(12): 2183-2196.
- Linehan, M. M., T. H. Dickey, E. S. Molinari, M. E. Fitzgerald, O. Potapova, A. Iwasaki and A. M. Pyle (2018). "A minimal RNA ligand for potent RIG-I activation in living mice." Sci Adv 4(2): e1701854.
- Ling, S. H., R. Qamra and H. Song (2011). "Structural and functional insights into eukaryotic mRNA decapping." Wiley Interdiscip Rev RNA 2(2): 193-208.
- Ling, Z., K. C. Tran and M. N. Teng (2009). "Human respiratory syncytial virus nonstructural protein NS2 antagonizes the activation of beta interferon transcription by interacting with RIG-I." <u>I Virol</u> 83(8): 3734-3742.
- Liu, G., Y. Lu, S. N. Thulasi Raman, F. Xu, Q. Wu, Z. Li, R. Brownlie, Q. Liu and Y. Zhou (2018). "Nuclear-resident RIG-I senses viral replication inducing antiviral immunity." <u>Nat Commun</u> **9**(1): 3199.
- Liu, P., J. Huang, Q. Zheng, L. Xie, X. Lu, J. Jin and G. Wang (2017). "Mammalian mitochondrial RNAs are degraded in the mitochondrial intermembrane space by RNASET2." Protein Cell 8(10): 735-749.
- Liu, S., H. Wang, Y. Jin, R. Podolsky, M. V. P. L. Reddy, J. Pedersen, B. Bode, J. Reed, D. Steed, S. Anderson, P. Yang, A. Muir, L. Steed, D. Hopkins, Y. H. Huang, S. Purohit, C. Y. Wang, A. K. Steck, A. Montemari, G. Eisenbarth, M. Rewers and J. X. She (2009). "IFIH1 polymorphisms are significantly associated with type 1 diabetes and IFIH1 gene expression in peripheral blood mononuclear cells." <u>Human Molecular Genetics</u> **18**(2): 358-365.
- Loney, C., G. Mottet-Osman, L. Roux and D. Bhella (2009). "Paramyxovirus ultrastructure and genome packaging: cryo-electron tomography of sendai virus." <u>I Virol</u> **83**(16): 8191-8197.
- Loo, Y. M., J. Fornek, N. Crochet, G. Bajwa, O. Perwitasari, L. Martinez-Sobrido, S. Akira, M. A. Gill, A. Garcia-Sastre, M. G. Katze and M. Gale, Jr. (2008). "Distinct RIG-I and MDA5 signaling by RNA viruses in innate immunity." <u>I Virol</u> **82**(1): 335-345.
- Lu, C., C. T. Ranjith-Kumar, L. Hao, C. C. Kao and P. Li (2011). "Crystal structure of RIG-I C-terminal domain bound to blunt-ended double-strand RNA without 5' triphosphate." <u>Nucleic Acids Res</u> **39**(4): 1565-1575.
- Lu, C., H. Xu, C. T. Ranjith-Kumar, M. T. Brooks, T. Y. Hou, F. Hu, A. B. Herr, R. K. Strong, C. C. Kao and P. Li (2010). "The structural basis of 5' triphosphate double-stranded RNA recognition by RIG-I C-terminal domain." Structure 18(8): 1032-1043.
- Ludwig, J. and F. Eckstein (1989). "Rapid and Efficient Synthesis of Nucleoside 5'-O-(1-Thiotriphosphates), 5'-Triphosphates and 2',3'-Cyclophosphorothioates Using 2-Chloro-4h-1,3,2-Benzodioxaphosphorin-4-One." <u>Journal of Organic Chemistry</u> **54**(3): 631-635.
- Luo, D., S. C. Ding, A. Vela, A. Kohlway, B. D. Lindenbach and A. M. Pyle (2011). "Structural insights into RNA recognition by RIG-I." <u>Cell</u> **147**(2): 409-422.
- Luo, D., A. Kohlway and A. M. Pyle (2013). "Duplex RNA activated ATPases (DRAs): platforms for RNA sensing, signaling and processing." RNA Biol 10(1): 111-120.
- Malathi, K., B. Dong, M. Gale, Jr. and R. H. Silverman (2007). "Small self-RNA generated by RNase L amplifies antiviral innate immunity." <u>Nature</u> **448**(7155): 816-819.
- Malathi, K., T. Saito, N. Crochet, D. J. Barton, M. Gale, Jr. and R. H. Silverman (2010). "RNase L releases a small RNA from HCV RNA that refolds into a potent PAMP." RNA 16(11): 2108-2119.
- Manche, L., S. R. Green, C. Schmedt and M. B. Mathews (1992). "Interactions between double-stranded RNA regulators and the protein kinase DAI." <u>Mol Cell Biol</u> **12**(11): 5238-5248.
- Marq, J. B., S. Hausmann, N. Veillard, D. Kolakofsky and D. Garcin (2011). "Short double-stranded RNAs with an overhanging 5' ppp-nucleotide, as found in arenavirus genomes, act as RIG-I decoys." <u>J Biol Chem</u> **286**(8): 6108-6116.
- Marq, J. B., D. Kolakofsky and D. Garcin (2010). "Unpaired 5' ppp-nucleotides, as found in arenavirus double-stranded RNA panhandles, are not recognized by RIG-I." J Biol Chem 285(24): 18208-18216.
- Marques, J. T., T. Devosse, D. Wang, M. Zamanian-Daryoush, P. Serbinowski, R. Hartmann, T. Fujita, M. A. Behlke and B. R. Williams (2006). "A structural basis for discriminating between self and nonself double-stranded RNAs in mammalian cells." <u>Nat Biotechnol</u> **24**(5): 559-565.
- Matsumoto, M., K. Funami, M. Tanabe, H. Oshiumi, M. Shingai, Y. Seto, A. Yamamoto and T. Seya (2003). "Subcellular localization of Toll-like receptor 3 in human dendritic cells." <u>J Immunol</u> **171**(6): 3154-3162
- Mayo, C. B., C. J. Wong, P. E. Lopez, J. W. Lary and J. L. Cole (2016). "Activation of PKR by short stem-loop

- RNAs containing single-stranded arms." RNA 22(7): 1065-1075.
- McGreal, E. P., J. L. Miller and S. Gordon (2005). "Ligand recognition by antigen-presenting cell C-type lectin receptors." <u>Curr Opin Immunol</u> **17**(1): 18-24.
- Meffre, E., R. Casellas and M. C. Nussenzweig (2000). "Antibody regulation of B cell development." <u>Nat Immunol</u> **1**(5): 379-385.
- Melchjorsen, J., J. Rintahaka, S. Soby, K. A. Horan, A. Poltajainen, L. Ostergaard, S. R. Paludan and S. Matikainen (2010). "Early innate recognition of herpes simplex virus in human primary macrophages is mediated via the MDA5/MAVS-dependent and MDA5/MAVS/RNA polymerase III-independent pathways." IVITOL 84(21): 11350-11358.
- Meylan, E., J. Curran, K. Hofmann, D. Moradpour, M. Binder, R. Bartenschlager and J. Tschopp (2005). "Cardif is an adaptor protein in the RIG-I antiviral pathway and is targeted by hepatitis C virus." <u>Nature</u> **437**(7062): 1167-1172.
- Minamitani, T., D. Iwakiri and K. Takada (2011). "Adenovirus virus-associated RNAs induce type I interferon expression through a RIG-I-mediated pathway." <u>I Virol</u> **85**(8): 4035-4040.
- Moss, T., F. Langlois, T. Gagnon-Kugler and V. Stefanovsky (2007). "A housekeeper with power of attorney: the rRNA genes in ribosome biogenesis." <u>Cell Mol Life Sci</u> **64**(1): 29-49.
- Muzio, M., G. Natoli, S. Saccani, M. Levrero and A. Mantovani (1998). "The human toll signaling pathway: divergence of nuclear factor kappaB and JNK/SAPK activation upstream of tumor necrosis factor receptor-associated factor 6 (TRAF6)." <u>I Exp Med</u> **187**(12): 2097-2101.
- Myong, S., S. Cui, P. V. Cornish, A. Kirchhofer, M. U. Gack, J. U. Jung, K. P. Hopfner and T. Ha (2009). "Cytosolic viral sensor RIG-I is a 5'-triphosphate-dependent translocase on double-stranded RNA." <u>Science</u> **323**(5917): 1070-1074.
- Nagarajan, V. K., C. I. Jones, S. F. Newbury and P. J. Green (2013). "XRN 5'-->3' exoribonucleases: structure, mechanisms and functions." <u>Biochim Biophys Acta</u> **1829**(6-7): 590-603.
- Nallagatla, S. R. and P. C. Bevilacqua (2008). "Nucleoside modifications modulate activation of the protein kinase PKR in an RNA structure-specific manner." <u>RNA</u> **14**(6): 1201-1213.
- Nallagatla, S. R., J. Hwang, R. Toroney, X. Zheng, C. E. Cameron and P. C. Bevilacqua (2007). "5'-triphosphate-dependent activation of PKR by RNAs with short stem-loops." <u>Science</u> **318**(5855): 1455-1458.
- Nasirudeen, A. M., H. H. Wong, P. Thien, S. Xu, K. P. Lam and D. X. Liu (2011). "RIG-I, MDA5 and TLR3 synergistically play an important role in restriction of dengue virus infection." <u>PLoS Negl Trop Dis</u> **5**(1): e926.
- Oda, H., K. Nakagawa, J. Abe, T. Awaya, M. Funabiki, A. Hijikata, R. Nishikomori, M. Funatsuka, Y. Ohshima, Y. Sugawara, T. Yasumi, H. Kato, T. Shirai, O. Ohara, T. Fujita and T. Heike (2014). "Aicardi-Goutieres Syndrome Is Caused by IFIH1 Mutations." <u>American Journal of Human Genetics</u> **95**(1): 121-125.
- Ojala, D., J. Montoya and G. Attardi (1981). "tRNA punctuation model of RNA processing in human mitochondria." Nature **290**(5806): 470-474.
- Osterlund, P., M. Strengell, L. P. Sarin, M. M. Poranen, R. Fagerlund, K. Melen and I. Julkunen (2012). "Incoming influenza A virus evades early host recognition, while influenza B virus induces interferon expression directly upon entry." LVirol86 (20): 11183-11193.
- Parkin, J. and B. Cohen (2001). "An overview of the immune system." Lancet 357(9270): 1777-1789.
- Pederson, T. (2011). "The nucleolus." Cold Spring Harb Perspect Biol 3(3).
- Peiser, L., M. P. De Winther, K. Makepeace, M. Hollinshead, P. Coull, J. Plested, T. Kodama, E. R. Moxon and S. Gordon (2002). "The class A macrophage scavenger receptor is a major pattern recognition receptor for Neisseria meningitidis which is independent of lipopolysaccharide and not required for secretory responses." Infect Immun 70(10): 5346-5354.
- Peiser, L., S. Mukhopadhyay and S. Gordon (2002). "Scavenger receptors in innate immunity." <u>Curr Opin Immunol</u> **14**(1): 123-128.
- Peisley, A., M. H. Jo, C. Lin, B. Wu, M. Orme-Johnson, T. Walz, S. Hohng and S. Hur (2012). "Kinetic mechanism for viral dsRNA length discrimination by MDA5 filaments." <u>Proc Natl Acad Sci U S A</u> **109**(49): E3340-3349
- Peisley, A., C. Lin, B. Wu, M. Orme-Johnson, M. Liu, T. Walz and S. Hur (2011). "Cooperative assembly and dynamic disassembly of MDA5 filaments for viral dsRNA recognition." Proc Natl Acad Sci U S A 108(52): 21010-21015.
- Peisley, A., B. Wu, H. Xu, Z. J. Chen and S. Hur (2014). "Structural basis for ubiquitin-mediated antiviral signal activation by RIG-I." <u>Nature</u> **509**(7498): 110-114.
- Peisley, A., B. Wu, H. Yao, T. Walz and S. Hur (2013). "RIG-I forms signaling-competent filaments in an ATP-dependent, ubiquitin-independent manner." <u>Mol Cell</u> **51**(5): 573-583.
- Perrault, J. and R. W. Leavitt (1978). "Inverted complementary terminal sequences in single-stranded RNAs and snap-back RNAs from vesicular stomatitis defective interfering particles." <u>I Gen Virol</u> **38**(1): 35-50.
- Pettersen, E. F., T. D. Goddard, C. C. Huang, G. S. Couch, D. M. Greenblatt, E. C. Meng and T. E. Ferrin (2004).

- "UCSF Chimera--a visualization system for exploratory research and analysis." <u>I Comput Chem</u> **25**(13): 1605-1612.
- Pichlmair, A., C. Lassnig, C. A. Eberle, M. W. Gorna, C. L. Baumann, T. R. Burkard, T. Burckstummer, A. Stefanovic, S. Krieger, K. L. Bennett, T. Rulicke, F. Weber, J. Colinge, M. Muller and G. Superti-Furga (2011). "IFIT1 is an antiviral protein that recognizes 5'-triphosphate RNA." <u>Nat Immunol</u> **12**(7): 624-630.
- Pichlmair, A., O. Schulz, C. P. Tan, T. I. Naslund, P. Liljestrom, F. Weber and C. Reis e Sousa (2006). "RIG-I-mediated antiviral responses to single-stranded RNA bearing 5'-phosphates." <u>Science</u> **314**(5801): 997-1001
- Piwowarski, J., P. Grzechnik, A. Dziembowski, A. Dmochowska, M. Minczuk and P. P. Stepien (2003). "Human polynucleotide phosphorylase, hPNPase, is localized in mitochondria." <u>I Mol Biol</u> **329**(5): 853-857.
- Player, M. R. and P. F. Torrence (1998). "The 2-5A system: modulation of viral and cellular processes through acceleration of RNA degradation." <u>Pharmacol Ther</u> **78**(2): 55-113.
- Plotch, S. J., M. Bouloy, I. Ulmanen and R. M. Krug (1981). "A unique cap(m7GpppXm)-dependent influenza virion endonuclease cleaves capped RNAs to generate the primers that initiate viral RNA transcription." *Cell* **23**(3): 847-858.
- Plumet, S., F. Herschke, J. M. Bourhis, H. Valentin, S. Longhi and D. Gerlier (2007). "Cytosolic 5'-triphosphate ended viral leader transcript of measles virus as activator of the RIG I-mediated interferon response." PLoS One 2(3): e279.
- Poeck, H., R. Besch, C. Maihoefer, M. Renn, D. Tormo, S. S. Morskaya, S. Kirschnek, E. Gaffal, J. Landsberg, J. Hellmuth, A. Schmidt, D. Anz, M. Bscheider, T. Schwerd, C. Berking, C. Bourquin, U. Kalinke, E. Kremmer, H. Kato, S. Akira, R. Meyers, G. Hacker, M. Neuenhahn, D. Busch, J. Ruland, S. Rothenfusser, M. Prinz, V. Hornung, S. Endres, T. Tuting and G. Hartmann (2008). "5'-Triphosphate-siRNA: turning gene silencing and Rig-I activation against melanoma." Nat Med 14(11): 1256-1263.
- Proudfoot, N. J., A. Furger and M. J. Dye (2002). "Integrating mRNA processing with transcription." <u>Cell</u> **108**(4): 501-512.
- Rajewsky, K. (1996). "Clonal selection and learning in the antibody system." Nature 381(6585): 751-758.
- Raju, R. and D. Kolakofsky (1989). "The ends of La Crosse virus genome and antigenome RNAs within nucleocapsids are base paired." <u>I Virol</u> **63**(1): 122-128.
- Raska, I., P. J. Shaw and D. Cmarko (2006). "New insights into nucleolar architecture and activity." <u>Int Rev Cytol</u> **255**: 177-235.
- Reddy, R., T. S. Ro-Choi, D. Henning and H. Busch (1974). "Primary sequence of U-1 nuclear ribonucleic acid of Novikoff hepatoma ascites cells." J Biol Chem **249**(20): 6486-6494.
- Reddy, R., R. Singh and S. Shimba (1992). "Methylated cap structures in eukaryotic RNAs: structure, synthesis and functions." <u>Pharmacol Ther</u> **54**(3): 249-267.
- Rehwinkel, J., C. P. Tan, D. Goubau, O. Schulz, A. Pichlmair, K. Bier, N. Robb, F. Vreede, W. Barclay, E. Fodor and C. Reis e Sousa (2010). "RIG-I detects viral genomic RNA during negative-strand RNA virus infection." Cell **140**(3): 397-408.
- Ren, X., M. M. Linehan, A. Iwasaki and A. M. Pyle (2019). "RIG-I Selectively Discriminates against 5'-Monophosphate RNA." Cell Rep 26(8): 2019-2027 e2014.
- Rice, G. I., Y. Del Toro Duany, E. M. Jenkinson, G. M. Forte, B. H. Anderson, G. Ariaudo, B. Bader-Meunier, E. M. Baildam, R. Battini, M. W. Beresford, M. Casarano, M. Chouchane, R. Cimaz, A. E. Collins, N. J. Cordeiro, R. C. Dale, J. E. Davidson, L. De Waele, I. Desguerre, L. Faivre, E. Fazzi, B. Isidor, L. Lagae, A. R. Latchman, P. Lebon, C. Li, J. H. Livingston, C. M. Lourenco, M. M. Mancardi, A. Masurel-Paulet, I. B. McInnes, M. P. Menezes, C. Mignot, J. O'Sullivan, S. Orcesi, P. P. Picco, E. Riva, R. A. Robinson, D. Rodriguez, E. Salvatici, C. Scott, M. Szybowska, J. L. Tolmie, A. Vanderver, C. Vanhulle, J. P. Vieira, K. Webb, R. N. Whitney, S. G. Williams, L. A. Wolfe, S. M. Zuberi, S. Hur and Y. J. Crow (2014). "Gain-of-function mutations in IFIH1 cause a spectrum of human disease phenotypes associated with upregulated type I interferon signaling." Nat Genet 46(5): 503-509.
- Rich, A. and U. L. RajBhandary (1976). "Transfer RNA: molecular structure, sequence, and properties." <u>Annu Rev Biochem</u> **45**: 805-860.
- Rijckborst, V. and H. L. Janssen (2010). "The Role of Interferon in Hepatitis B Therapy." <u>Curr Hepat Rep</u> **9**(4): 231-238.
- Rohayem, J., I. Robel, K. Jager, U. Scheffler and W. Rudolph (2006). "Protein-primed and de novo initiation of RNA synthesis by norovirus 3Dpol." <u>I Virol</u> **80**(14): 7060-7069.
- Rothenfusser, S., N. Goutagny, G. DiPerna, M. Gong, B. G. Monks, A. Schoenemeyer, M. Yamamoto, S. Akira and K. A. Fitzgerald (2005). "The RNA helicase Lgp2 inhibits TLR-independent sensing of viral replication by retinoic acid-inducible gene-I." Immunol 175(8): 5260-5268.
- Runge, S., K. M. Sparrer, C. Lassig, K. Hembach, A. Baum, A. Garcia-Sastre, J. Soding, K. K. Conzelmann and K. P. Hopfner (2014). "In vivo ligands of MDA5 and RIG-I in measles virus-infected cells." PLoS Pathog

- 10(4): e1004081.
- Rutsch, F., M. MacDougall, C. Lu, I. Buers, O. Mamaeva, Y. Nitschke, G. I. Rice, H. Erlandsen, H. G. Kehl, H. Thiele, P. Nurnberg, W. Hohne, Y. J. Crow, A. Feigenbaum and R. C. Hennekam (2015). "A specific IFIH1 gain-of-function mutation causes Singleton-Merten syndrome." Am J Hum Genet 96(2): 275-282.
- Sabel, M. S. and V. K. Sondak (2003). "Pros and cons of adjuvant interferon in the treatment of melanoma." Oncologist 8(5): 451-458.
- Saito, T., R. Hirai, Y. M. Loo, D. Owen, C. L. Johnson, S. C. Sinha, S. Akira, T. Fujita and M. Gale, Jr. (2007). "Regulation of innate antiviral defenses through a shared repressor domain in RIG-I and LGP2." <u>Proc Natl Acad Sci U S A</u> **104**(2): 582-587.
- Saito, T., D. M. Owen, F. Jiang, J. Marcotrigiano and M. Gale, Jr. (2008). "Innate immunity induced by composition-dependent RIG-I recognition of hepatitis C virus RNA." <u>Nature</u> **454**(7203): 523-527.
- Samanta, M., D. Iwakiri and K. Takada (2008). "Epstein-Barr virus-encoded small RNA induces IL-10 through RIG-I-mediated IRF-3 signaling." <u>Oncogene</u> **27**(30): 4150-4160.
- Sampath, A. and R. Padmanabhan (2009). "Molecular targets for flavivirus drug discovery." <u>Antiviral Res</u> **81**(1): 6-15.
- Satoh, T., H. Kato, Y. Kumagai, M. Yoneyama, S. Sato, K. Matsushita, T. Tsujimura, T. Fujita, S. Akira and O. Takeuchi (2010). "LGP2 is a positive regulator of RIG-I- and MDA5-mediated antiviral responses." Proc Natl Acad Sci U S A 107(4): 1512-1517.
- Sauer, B. (1994). "Site-specific recombination: developments and applications." <u>Curr Opin Biotechnol</u> **5**(5): 521-527.
- Schlee, M. (2013). "Master sensors of pathogenic RNA RIG-I like receptors." <u>Immunobiology</u> **218**(11): 1322-1335.
- Schlee, M., A. Roth, V. Hornung, C. A. Hagmann, V. Wimmenauer, W. Barchet, C. Coch, M. Janke, A. Mihailovic, G. Wardle, S. Juranek, H. Kato, T. Kawai, H. Poeck, K. A. Fitzgerald, O. Takeuchi, S. Akira, T. Tuschl, E. Latz, J. Ludwig and G. Hartmann (2009). "Recognition of 5' triphosphate by RIG-I helicase requires short blunt double-stranded RNA as contained in panhandle of negative-strand virus." Immunity 31(1): 25-34.
- Schmidt, A., T. Schwerd, W. Hamm, J. C. Hellmuth, S. Cui, M. Wenzel, F. S. Hoffmann, M. C. Michallet, R. Besch, K. P. Hopfner, S. Endres and S. Rothenfusser (2009). "5'-triphosphate RNA requires base-paired structures to activate antiviral signaling via RIG-I." <u>Proc Natl Acad Sci U S A</u> **106**(29): 12067-12072.
- Schonborn, J., J. Oberstrass, E. Breyel, J. Tittgen, J. Schumacher and N. Lukacs (1991). "Monoclonal antibodies to double-stranded RNA as probes of RNA structure in crude nucleic acid extracts." <u>Nucleic Acids Res</u> **19**(11): 2993-3000.
- Schuberth, C. (2011). "Untersuchung der molekularen Interaktion endogener und synthetischer RNA mit dem zytosolischen Immunrezeptor RIG-I."
- Schuberth-Wagner, C., J. Ludwig, A. K. Bruder, A. M. Herzner, T. Zillinger, M. Goldeck, T. Schmidt, J. L. Schmid-Burgk, R. Kerber, S. Wolter, J. P. Stumpel, A. Roth, E. Bartok, C. Drosten, C. Coch, V. Hornung, W. Barchet, B. M. Kummerer, G. Hartmann and M. Schlee (2015). "A Conserved Histidine in the RNA Sensor RIG-I Controls Immune Tolerance to N1-2'O-Methylated Self RNA." Immunity 43(1): 41-51.
- Seth, R. B., L. Sun, C. K. Ea and Z. J. Chen (2005). "Identification and characterization of MAVS, a mitochondrial antiviral signaling protein that activates NF-kappaB and IRF 3." Cell 122(5): 669-682.
- Sharma, S., B. R. tenOever, N. Grandvaux, G. P. Zhou, R. Lin and J. Hiscott (2003). "Triggering the interferon antiviral response through an IKK-related pathway." <u>Science</u> **300**(5622): 1148-1151.
- Shatkin, A. J. and J. L. Manley (2000). "The ends of the affair: capping and polyadenylation." <u>Nat Struct Biol</u> 7(10): 838-842.
- Sherry, S. T., M. H. Ward, M. Kholodov, J. Baker, L. Phan, E. M. Smigielski and K. Sirotkin (2001). "dbSNP: the NCBI database of genetic variation." <u>Nucleic Acids Res</u> **29**(1): 308-311.
- Sin, W. X., P. Li, J. P. Yeong and K. C. Chin (2012). "Activation and regulation of interferon-beta in immune responses." Immunol Res 53(1-3): 25-40.
- Siren, J., T. Imaizumi, D. Sarkar, T. Pietila, D. L. Noah, R. Lin, J. Hiscott, R. M. Krug, P. B. Fisher, I. Julkunen and S. Matikainen (2006). "Retinoic acid inducible gene-I and mda-5 are involved in influenza A virus-induced expression of antiviral cytokines." <u>Microbes Infect</u> **8**(8): 2013-2020.
- Sloan, K. E., A. S. Warda, S. Sharma, K. D. Entian, D. L. J. Lafontaine and M. T. Bohnsack (2017). "Tuning the ribosome: The influence of rRNA modification on eukaryotic ribosome biogenesis and function." <u>RNA Biol</u> **14**(9): 1138-1152.
- Smyth, D. J., J. D. Cooper, R. Bailey, S. Field, O. Burren, L. J. Smink, C. Guja, C. Ionescu-Tirgoviste, B. Widmer, D. B. Dunger, D. A. Savage, N. M. Walker, D. G. Clayton and J. A. Todd (2006). "A genome-wide association study of nonsynonymous SNPs identifies a type 1 diabetes locus in the interferon-induced helicase (IFIH1) region." Nature Genetics 38(6): 617-619.
- Stevens, T. L., A. Bossie, V. M. Sanders, R. Fernandez-Botran, R. L. Coffman, T. R. Mosmann and E. S. Vitetta

- (1988). "Regulation of antibody isotype secretion by subsets of antigen-specific helper T cells." <u>Nature</u> **334**(6179): 255-258.
- Strahle, L., D. Garcin and D. Kolakofsky (2006). "Sendai virus defective-interfering genomes and the activation of interferon-beta." <u>Virology</u> **351**(1): 101-111.
- Strahle, L., J. B. Marq, A. Brini, S. Hausmann, D. Kolakofsky and D. Garcin (2007). "Activation of the beta interferon promoter by unnatural Sendai virus infection requires RIG-I and is inhibited by viral C proteins." <u>I Virol</u> **81**(22): 12227-12237.
- Sumpter, R., Jr., Y. M. Loo, E. Foy, K. Li, M. Yoneyama, T. Fujita, S. M. Lemon and M. Gale, Jr. (2005). "Regulating intracellular antiviral defense and permissiveness to hepatitis C virus RNA replication through a cellular RNA helicase, RIG-I." <u>I Virol</u> **79**(5): 2689-2699.
- Sun, L., J. Wu, F. Du, X. Chen and Z. J. Chen (2013). "Cyclic GMP-AMP synthase is a cytosolic DNA sensor that activates the type I interferon pathway." <u>Science</u> **339**(6121): 786-791.
- Sun, Y.-W. (1997). <u>RIG-I, a human homolog gene of RNA helicase, is induced by retinoic acid during the differentiation of acute promyelocytic leukemia cell.</u>
- Szczesny, R. J., L. S. Borowski, L. K. Brzezniak, A. Dmochowska, K. Gewartowski, E. Bartnik and P. P. Stepien (2010). "Human mitochondrial RNA turnover caught in flagranti: involvement of hSuv3p helicase in RNA surveillance." Nucleic Acids Res 38(1): 279-298.
- Takahasi, K., M. Yoneyama, T. Nishihori, R. Hirai, H. Kumeta, R. Narita, M. Gale, Jr., F. Inagaki and T. Fujita (2008). "Nonself RNA-sensing mechanism of RIG-I helicase and activation of antiviral immune responses." Mol Cell 29(4): 428-440.
- Takeuchi, O. and S. Akira (2010). "Pattern recognition receptors and inflammation." Cell **140**(6): 805-820.
- Targett-Adams, P., S. Boulant and J. McLauchlan (2008). "Visualization of double-stranded RNA in cells supporting hepatitis C virus RNA replication." <u>I Virol</u> **82**(5): 2182-2195.
- Tluk, S., M. Jurk, A. Forsbach, R. Weeratna, U. Samulowitz, A. M. Krieg, S. Bauer and J. Vollmer (2009). "Sequences derived from self-RNA containing certain natural modifications act as suppressors of RNA-mediated inflammatory immune responses." <u>Int Immunol</u> **21**(5): 607-619.
- Toots, U. E., M. B. Kel've and M. Saarma (1988). "[Degradation of messenger RNA, ribosomal RNA and 2-5A-dependent inhibition of protein biosynthesis]." Mol Biol (Mosk) 22(6): 1473-1481.
- Triantafilou, K., E. Vakakis, S. Kar, E. Richer, G. L. Evans and M. Triantafilou (2012). "Visualisation of direct interaction of MDA5 and the dsRNA replicative intermediate form of positive strand RNA viruses." <u>I Cell Sci</u> **125**(Pt 20): 4761-4769.
- Van Eyck, L., L. De Somer, D. Pombal, S. Bornschein, G. Frans, S. Humblet-Baron, L. Moens, F. de Zegher, X. Bossuyt, C. Wouters and A. Liston (2015). "IFIH1 Mutation Causes Systemic Lupus Erythematosus With Selective IgA Deficiency." <u>Arthritis & Rheumatology</u> **67**(6): 1592-1597.
- Vela, A., O. Fedorova, S. C. Ding and A. M. Pyle (2012). "The thermodynamic basis for viral RNA detection by the RIG-I innate immune sensor." <u>I Biol Chem</u> **287**(51): 42564-42573.
- Verweij, C. L. and S. Vosslamber (2013). "Relevance of the type I interferon signature in multiple sclerosis towards a personalized medicine approach for interferon-beta therapy." <u>Discov Med</u> **15**(80): 51-60.
- Wang, D. D., Z. Shu, S. A. Lieser, P. L. Chen and W. H. Lee (2009). "Human mitochondrial SUV3 and polynucleotide phosphorylase form a 330-kDa heteropentamer to cooperatively degrade double-stranded RNA with a 3'-to-5' directionality." J Biol Chem 284(31): 20812-20821.
- Wang, Y., J. Ludwig, C. Schuberth, M. Goldeck, M. Schlee, H. Li, S. Juranek, G. Sheng, R. Micura, T. Tuschl, G. Hartmann and D. J. Patel (2010). "Structural and functional insights into 5'-ppp RNA pattern recognition by the innate immune receptor RIG-I." Nat Struct Mol Biol 17(7): 781-787.
- Warner, J. R. (1999). "The economics of ribosome biosynthesis in yeast." <u>Trends Biochem Sci</u> **24**(11): 437-440.
- Washietl, S., I. L. Hofacker, M. Lukasser, A. Huttenhofer and P. F. Stadler (2005). "Mapping of conserved RNA secondary structures predicts thousands of functional noncoding RNAs in the human genome." <u>Nat Biotechnol</u> **23**(11): 1383-1390.
- Weber, F., V. Wagner, S. B. Rasmussen, R. Hartmann and S. R. Paludan (2006). "Double-stranded RNA is produced by positive-strand RNA viruses and DNA viruses but not in detectable amounts by negative-strand RNA viruses." <u>I Virol</u> **80**(10): 5059-5064.
- Weber, M., A. Gawanbacht, M. Habjan, A. Rang, C. Borner, A. M. Schmidt, S. Veitinger, R. Jacob, S. Devignot, G. Kochs, A. Garcia-Sastre and F. Weber (2013). "Incoming RNA virus nucleocapsids containing a 5'-triphosphorylated genome activate RIG-I and antiviral signaling." Cell Host Microbe **13**(3): 336-346.
- Werner, M., E. Purta, K. H. Kaminska, I. A. Cymerman, D. A. Campbell, B. Mittra, J. R. Zamudio, N. R. Sturm, J. Jaworski and J. M. Bujnicki (2011). "2'-O-ribose methylation of cap2 in human: function and evolution in a horizontally mobile family." <u>Nucleic Acids Res</u> **39**(11): 4756-4768.
- Woolford, J. L., Jr. and S. J. Baserga (2013). "Ribosome biogenesis in the yeast Saccharomyces cerevisiae." Genetics **195**(3): 643-681.

References

- Wu, B., A. Peisley, C. Richards, H. Yao, X. Zeng, C. Lin, F. Chu, T. Walz and S. Hur (2013). "Structural basis for dsRNA recognition, filament formation, and antiviral signal activation by MDA5." <u>Cell</u> **152**(1-2): 276-289.
- Wu, J., L. Sun, X. Chen, F. Du, H. Shi, C. Chen and Z. J. Chen (2013). "Cyclic GMP-AMP is an endogenous second messenger in innate immune signaling by cytosolic DNA." <u>Science</u> **339**(6121): 826-830.
- Xing, J., S. Wang, R. Lin, K. L. Mossman and C. Zheng (2012). "Herpes simplex virus 1 tegument protein US11 downmodulates the RLR signaling pathway via direct interaction with RIG-I and MDA-5." <u>I Virol</u> **86**(7): 3528-3540.
- Xu, L. G., Y. Y. Wang, K. J. Han, L. Y. Li, Z. Zhai and H. B. Shu (2005). "VISA is an adapter protein required for virus-triggered IFN-beta signaling." Mol Cell **19**(6): 727-740.
- Yoneyama, M. and T. Fujita (2008). "Structural mechanism of RNA recognition by the RIG-I-like receptors." Immunity **29**(2): 178-181.
- Yoneyama, M. and T. Fujita (2009). "RNA recognition and signal transduction by RIG-I-like receptors." Immunol Rev 227(1): 54-65.
- Yoneyama, M., M. Kikuchi, K. Matsumoto, T. Imaizumi, M. Miyagishi, K. Taira, E. Foy, Y. M. Loo, M. Gale, Jr., S. Akira, S. Yonehara, A. Kato and T. Fujita (2005). "Shared and unique functions of the DExD/H-box helicases RIG-I, MDA5, and LGP2 in antiviral innate immunity." <u>J Immunol</u> **175**(5): 2851-2858.
- Yoneyama, M., M. Kikuchi, T. Natsukawa, N. Shinobu, T. Imaizumi, M. Miyagishi, K. Taira, S. Akira and T. Fujita (2004). "The RNA helicase RIG-I has an essential function in double-stranded RNA-induced innate antiviral responses." Nat Immunol 5(7): 730-737.
- Zampetaki, A., A. Albrecht and K. Steinhofel (2018). "Long Non-coding RNA Structure and Function: Is There a Link?" Front Physiol 9: 1201.
- Zeng, W., L. Sun, X. Jiang, X. Chen, F. Hou, A. Adhikari, M. Xu and Z. J. Chen (2010). "Reconstitution of the RIG-I pathway reveals a signaling role of unanchored polyubiquitin chains in innate immunity." <u>Cell</u> **141**(2): 315-330.
- Zheng, J., H. Y. Yong, N. Panutdaporn, C. Liu, K. Tang and D. Luo (2015). "High-resolution HDX-MS reveals distinct mechanisms of RNA recognition and activation by RIG-I and MDA5." <u>Nucleic Acids Res</u> **43**(2): 1216-1230.
- Zhou, A., B. A. Hassel and R. H. Silverman (1993). "Expression cloning of 2-5A-dependent RNAase: a uniquely regulated mediator of interferon action." <u>Cell</u> **72**(5): 753-765.
- Zhou, Y., D. Ray, Y. Zhao, H. Dong, S. Ren, Z. Li, Y. Guo, K. A. Bernard, P. Y. Shi and H. Li (2007). "Structure and function of flavivirus NS5 methyltransferase." <u>I Virol</u> **81**(8): 3891-3903.
- Zilberstein, A., A. Kimchi, A. Schmidt and M. Revel (1978). "Isolation of two interferon-induced translational inhibitors: a protein kinase and an oligo-isoadenylate synthetase." <u>Proc Natl Acad Sci U S A</u> **75**(10): 4734-4738.
- Zust, R., L. Cervantes-Barragan, M. Habjan, R. Maier, B. W. Neuman, J. Ziebuhr, K. J. Szretter, S. C. Baker, W. Barchet, M. S. Diamond, S. G. Siddell, B. Ludewig and V. Thiel (2011). "Ribose 2'-O-methylation provides a molecular signature for the distinction of self and non-self mRNA dependent on the RNA sensor Mda5." Nat Immunol 12(2): 137-143.

8. Appendix

8.1. RNA Oligonucleotides

Table 8.1: RNA ligands used in Figure 5.3

Name	Sequence (sense)	5´end	Sequence (antisense)	5´end
OH – asOH	ggccgagaccucgaagagaacucu	ОН	agaguucucuucgaggucucggcc	ОН
OH – as3p	ggccgagaccucgaagagaacucu	ОН	agaguucucuucgaggucucggcc	3р
3p – asOH	ggccgagaccucgaagagaacucu	3р	agaguucucuucgaggucucggcc	ОН
3p – as3p	ggccgagaccucgaagagaacucu	3р	agaguucucuucgaggucucggcc	3p

Table 8.2: RNA ligands used in Figure 5.4

Name	Sequence (sense)	5´end	Sequence (antisense)	5'end
3p – as5´-2nt_3´+2AA	ggccgagaccucgaagagaacucu	3p	aguucucuucgaggucucggccaa	ОН
3p – as5'+2AA_3'-1nt	ggccgagaccucgaagagaacucu	3р	aaagaguucucuucgaggucucggc	ОН
3p – as5′+2AA_3′-2nt	ggccgagaccucgaagagaacucu	3р	aaagaguucucuucgaggucucgg	ОН
3p – as5′+2AA_3′-3nt	ggccgagaccucgaagagaacucu	3р	aaagaguucucuucgaggucucg	ОН
3p – as5′+2AA	ggccgagaccucgaagagaacucu	3р	aaagaguucucuucgaggucucggcc	ОН
3p – asOH	ggccgagaccucgaagagaacucu	3р	agaguucucuucgaggucucggcc	ОН
OH – as5′-2nt_3′+2AA	ggccgagaccucgaagagaacucu	ОН	aguucucuucgaggucucggccaa	ОН
OH – as5′+2AA_3′-1nt	ggccgagaccucgaagagaacucu	ОН	aaagaguucucuucgaggucucggc	ОН
OH – as5′+2AA_3′-2nt	ggccgagaccucgaagagaacucu	ОН	aaagaguucucuucgaggucucgg	ОН
OH – as5′+2AA_3′-3nt	ggccgagaccucgaagagaacucu	OH	aaagaguucucuucgaggucucg	ОН
OH – as5´+2AA	ggccgagaccucgaagagaacucu	ОН	aaagaguucucuucgaggucucggcc	ОН
OH – asOH	ggccgagaccucgaagagaacucu	ОН	agaguucucuucgaggucucggcc	ОН

Table 8.3: RNA ligands used in Figure 5.5

Tubic 0.5: Tubic	ingarius uscu ili rigure 5.5			
Name	Sequence (sense)	5´end	Sequence (antisense)	5´end
3p – as5´10nt	ggccgagaccucgaagagaacucu	3p	ggucucggcc	ОН
3p – as5′12nt	ggccgagaccucgaagagaacucu	3p	gaggucucggcc	ОН
3p – as5´-14nt	ggccgagaccucgaagagaacucu	3р	ucgaggucucggcc	ОН
3p – as5′16nt	ggccgagaccucgaagagaacucu	3р	cuucgaggucucggcc	ОН
3p – as5′18nt	ggccgagaccucgaagagaacucu	3р	cucuucgaggucucggcc	ОН
3p – as5′19nt	ggccgagaccucgaagagaacucu	3р	ucucuucgaggucucggcc	ОН
3p – as5´20nt	ggccgagaccucgaagagaacucu	3р	uucucuucgaggucucggcc	ОН
3p – as5´-21nt	ggccgagaccucgaagagaacucu	3p	guucucuucgaggucucggcc	ОН
3p – asOH	ggccgagaccucgaagagaacucu	3р	agaguucucuucgaggucucggcc	ОН
OH – as5′10nt	ggccgagaccucgaagagaacucu	ОН	ggucucggcc	ОН
OH – as5′12nt	ggccgagaccucgaagagaacucu	ОН	gaggucucggcc	ОН
OH – as5′14nt	ggccgagaccucgaagagaacucu	ОН	ucgaggucucggcc	ОН
OH – as5′16nt	ggccgagaccucgaagagaacucu	ОН	cuucgaggucucggcc	ОН
OH – as5′18nt	ggccgagaccucgaagagaacucu	ОН	cucuucgaggucucggcc	ОН
OH – as5´19nt	ggccgagaccucgaagagaacucu	ОН	ucucuucgaggucucggcc	ОН
OH – as5′20nt	ggccgagaccucgaagagaacucu	ОН	uucucuucgaggucucggcc	ОН
OH – as5´21nt	ggccgagaccucgaagagaacucu	ОН	guucucuucgaggucucggcc	ОН
OH – asOH	ggccgagaccucgaagagaacucu	ОН	agaguucucuucgaggucucggcc	ОН

Table 8.4: RNA ligands used in Figure 5.7

Name	Sequence (sense)	5´end	Sequence (antisense)	5'end
OH-dsRNA (24 bp)	ggccgagaccucgaagagaacucu	ОН	agaguucucuucgaggucucggcc	ОН
p-dsRNA (24 bp)	ggccgagaccucgaagagaacucu	р	agaguucucuucgaggucucggcc	р

3p-dsRNA (24 bp)	ggccgagaccucgaagagaacucu	3p	agaguucucuucgaggucucggcc	3p
OH-dsRNA (40 bp)	gggagaugaugcuuucucuuggu ugggccaccuaucuccc	ОН	gggagauagguggcccaaccaagaga aagcaucaucuccc	ОН
p-dsRNA (40 bp)	gggagaugaugcuuucucuuggu ugggccaccuaucuccc	р	gggagauagguggcccaaccaagaga aagcaucaucuccc	р
3p-dsRNA (40 bp)	gggagaugaugcuuucucuuggu ugggccaccuaucuccc	3р	gggagauagguggcccaaccaagaga aagcaucaucuccc	3р

Table 8.5: RNA ligands used in Figure 5.8

Name	Sequence (sense)	5´end	Sequence (antisense)	5'end
1 + 4	aaactgaaagggagaagtgaaagtgag	ОН	ctcactttcacttctccctttcagttt	ОН
2 + 4	aaactgaaagggagaagtgaaagtgag	p (3'end)	ctcactttcacttctccctttcagttt	ОН
6 + 4	aaactgaaagggagaagtgaaagtgag	р	ctcactttcacttctccctttcagttt	ОН
1+7	aaactgaaagggagaagtgaaagtgag	ОН	ctcactttcacttctccctttcagttt	р
2 + 7	aaactgaaagggagaagtgaaagtgag	p (3'end)	ctcactttcacttctccctttcagttt	р
6 + 7	aaactgaaagggagaagtgaaagtgag	р	ctcactttcacttctccctttcagttt	р
1+3	aaactgaaagggagaagtgaaagtgag	ОН	cactttcacttctccctttcagtttat	ОН
2 + 3	aaactgaaagggagaagtgaaagtgag	p (3'end)	cactttcacttctccctttcagtttat	ОН
6 + 3	aaactgaaagggagaagtgaaagtgag	р	cactttcacttctccctttcagtttat	ОН
1+5	aaactgaaagggagaagtgaaagtgag	ОН	tcactttcacttctccctttcagttta	ОН
2 + 5	aaactgaaagggagaagtgaaagtgag	p (3'end)	tcactttcacttctccctttcagttta	ОН
6 + 5	aaactgaaagggagaagtgaaagtgag	р	tcactttcacttctccctttcagttta	ОН

Table 8.6: RNA ligands used in Figure 5.12

Name	Sequence (sense)	5´end	Sequence (antisense)	5'end
P – asP	ggccgagaccucgaagagaacucu	р	agaguucucuucgaggucucggcc	р
OH – asOH	ggccgagaccucgaagagaacucu	ОН	agaguucucuucgaggucucggcc	ОН
P – aOH	ggccgagaccucgaagagaacucu	р	agaguucucuucgaggucucggcc	ОН
OH – asP	ggccgagaccucgaagagaacucu	ОН	agaguucucuucgaggucucggcc	р

Table 8.7: RNA ligands used in Figure 5.13

Name	Sequence (sense)	5´end	Sequence (antisense)	5´end
1	ggccgagaccucgaagagaacucu	3р	aguucucuucgaggucucggccaa	ОН
2	ggccgagaccucgaagagaacucu	3р	aaagaguucucuucgaggucucgg	ОН
3	ggccgagaccucgaagagaacucu	ОН	agaguucucuucgaggucucggcc	ОН
4	ggccgagaccucgaagagaacucu	р	agaguucucuucgaggucucggcc	р
5	ggccgagaccucgaagagaacucu	3р	agaguucucuucgaggucucggcc	3р
6	ggccgagaccucgaagagaacucu	OH	aguucucuucgaggucucggccaa	ОН
7	ggccgagaccucgaagagaacucu	ОН	aaagaguucucuucgaggucucgg	OH
8	ggccgagaccucgaagagaacucu	ОН	agaguucucuucgaggucucggcc	р
9	ggccgagaccucgaagagaacucu	ОН	agaguucucuucgaggucucggcc	ОН
10	ggccgagaccucgaagagaacucu	3р	agaguucucuucgaggucucggcc	3р
11	ggccgagaccucgaagagaacucu	ОН	aguucucuucgaggucucggccaa	ОН
12	ggccgagaccucgaagagaacucu	ОН	aaagaguucucuucgaggucucgg	ОН
13	ggccgagaccucgaagagaacucu	ОН	agaguucucuucgaggucucggcc	р
14	ggccgagaccucgaagagaacucu	ОН	agaguucucuucgaggucucggcc	3р

8.2. List of Figures

Figure 3.1: PRRs and their ligands	7
Figure 3.2: RIG-I signaling pathway	10
Figure 3.3: The optimal RIG-I ligand	12
Figure 3.4: RIG-I structure	19
Figure 3.5: mRNA cap structure	22
Figure 5.1: Knockdown of CMTR1 induces RIG-I-dependent immune activation	56
Figure 5.2: YFV 2'O-methyltransferase prevents immune recognition by RIG-I	58
Figure 5.3: Effect of RIG-I CTD mutations on 3p-dsRNA and OH-dsRNA recognition	59
Figure 5.4: Activation potential of 3p- and OH-dsRNA with overhangs	61
Figure 5.5: Characterization of minimal double-strand stem length of 3p- and OH-ligan	ds 62
Figure 5.6: Viral recognition by RIG-I CTD mutants	63
Figure 5.7: RIG-I activation by RNAs with differing lengths and 5'modifications	65
Figure 5.8: 5'p prevents RIG-I activation in HEK Trex cells and PBMCs	67
Figure 5.9: Effect of 5´p, 3'p, 5´OH and overhangs on RIG-I activation	68
Figure 5.10: 5'p prevents RIG-I CTD binding	69
Figure 5.11: Amino acids in the RIG-I CTD in proximity to the α -phosphate	70
Figure 5.12: RIG-I I875A is activated by 5'p-RNA	72
Figure 5.13: Effect of overhangs on RIG-I I875A activation	73
Figure 5.14: Titration curves of RIG-I WT and RIG-I I875A with different ligands	74
Figure 5.15: Binding studies of RIG-I I875A with different RNA ligands	76
Figure 5.16: Long-term expression of RIG-I I875A causes ISG upregulation without add	ition of
exogenous stimuli	77
Figure 5.17: Long-term expression of RIG-I I875A induces phosphorylation of IRF3 v	vithout
addition of exogenous stimuli	78
Figure 5.18: Whole cell RNA is highly stimulatory for RIG-I I875A	79
Figure 5.19: Effect of heat and enzyme treatment on total RNA extracts	80
Figure 5.20: Immune activation potential of tRNA and rRNA	82
Figure 5.21: polyA RNA is a strong ligand for RIG-I I875A	84
Figure 5.22: XRN1 KD increases immune activation in cells expressing RIG-I I875A	85
Figure 5.23: mtRNA activates RIG-I I875A	87
Figure 5.24: PKR KO rescues immune activation by long RNAs	88

Figure 5.25: Long RNAs activate PKR in A549 and Thp1-Dual™ cells	90
Figure 5.26: Characterization of a new RIG-I ligand	92
Figure 5.27: CL 1 does not activate PKR	93
Figure 6.1: Summary: RNA ligands and their RIG-I activation potential	105
Figure 6.2: Summary: Differentiation between self and non-self by RIG-I	112
Figure 6.3: Summary: RIG-I and PKR interplay	117
8.3. List of Tables	
Table 4.1: Equipment	27
Table 4.2: Chemicals	29
Table 4.3: Enzymes and Biological reagents	30
Table 4.4: Commercial buffer	31
Table 4.5: Antibodies	31
Table 4.6: Kits	31
Table 4.7: Bacteria	32
Table 4.8: Cell culture substances	32
Table 4.9: Cell lines	33
Table 4.10: siRNA sequences	33
Table 4.11: qPCR primer sequences	33
Table 4.12: Plasmid	34
Table 4.13: Phusion PCR program	39
Table 4.14: DreamTaq PCR program	39
Table 4.15: qPCR program	44
Table 4.16: Cell culture media	49
Table 4.17: Cell seeding	49
Table 4.18: CRISPR target sequences	51
Table 6.1: Overview RIG-I ligand detection	101
Table 6.2: Overview RIG-I virus detection	101
Table 8.1: RNA ligands used in Figure 5.3	131
Table 8.2: RNA ligands used in Figure 5.4	131
Table 8.3: RNA ligands used in Figure 5.5	131
Table 8.4: RNA ligands used in Figure 5.7	131
Table 8.5: RNA ligands used in Figure 5.8	132

Table 8.6: RNA ligands used in Figure 5.12	132
Table 8.7: RNA ligands used in Figure 5.13	132

8.4. Abbreviations

(-)ssRNA virus Negative-sense single-stranded RNA virus (+)ssRNA virus Positive-sense single-stranded RNA virus

2´-5´A 2´-5´-oligomers of adenosine

2p Diphosphate3p Triphosphate

3p-RNA RNA with a 5'triphosphate AGS Aicardi-Goutières syndrome

ANOVA Analysis of variance
AP Alkaline Phosphatase

as Antisense

ATP Adenosine triphosphate

bp Base pairs

CARD Caspase activation and recruitment domain

cDNA Complementary RNA
cGAS Cyclic GMP-AMP synthase
CIP Calf intestinal phosphatase

CL Cloverleaf

CLR C-type lectin receptor

CMTR Cap-specific mRNA nucleoside-2´-O- methyltransferase

CTD C-terminal domain

Ctrl Control

DAMP Damage-associated molecular pattern

DAP Diaminopimelic acid
DC Dendritic cells
DENV Dengue virus

DI Defective interfering

DMEM Dulbecco's Modified Eagle's Medium

DMSO Dimethyl sulfoxide
DNA Deoxyribonucleic acid
DNase Deoxyribonuclease
dNTP Nucleotide triphosphate

Dox Doxycycline

dsRNA Double-stranded RNA

DTT Dithiothreitol EBV Epstein-Barr virus

 $\begin{array}{ll} \text{EDTA} & \text{Ethylenediaminetetraacetic acid} \\ \text{eIF2}\alpha & \text{Eukaryotic initiation factor } 2\alpha \\ \text{eIF4} & \text{Eukaryotic initiation factor 4} \end{array}$

ELISA Enzyme-linked immunosorbent assay

EMCV Encephalomyocarditis virus

EMSA Electrophoretic mobility shift assay

EtBr Ethidium bromide F-Luc Firefly Luciferase

FACS Fluorescence-activated cell sorting

FCS Fetal calf serum
G-Luc Gaussia luciferase

GFP Green fluorescent protein

h Hour

HCV Hepatitis C virus
HEG Hexaethylenglycol
HMW High molecular weight
HSV Herpes simplex virus
IAV Influenza A virus

IFIT1 IFN-induced protein with tetratricopeptide repeats 1

IFN Interferon

IFNAR IFN- α/β receptor

IKK IkB kinase

IKK-εI-kappa-B kinase subunit epsilonIP10Interferon gamma-induced protein 10

IRF Interferon regulatory factor ISG Interferon-stimulated gene

ISRE IFN-stimulated response elements

IVT In-vitro transcription

IkB Inhibitor of nuclear factor kappa-B

kb Kilobase KD Knockdown

K_d Dissociation constant

KO Knockout

LACV La Crosse encephalitis virus LDL Low-density lipoprotein

LGP2 Laboratory of Genetics and Physiology 2

LMW Low molecular weight
LPS Lipopolysaccharides
LSU Large ribosomal subunit

MAVS Mitochondrial antiviral-signaling protein

MDA5 Melanoma Differentiation-Associated protein 5

MDP Muramyl dipeptide
MeV Measles morbillivirus

MHC Major histocompatibility complex

MHV Mouse hepatitis virus

min Minute

mRNA Messenger RNA mtDNA Mitochondrial DNA mtRNA Mitochondrial RNA

MTT 3-(4,5-dimethylthiazol-2-yl)-2,5-diphenyltetrazolium bromide

N1 Penultimate nucleotide
N2 Antepenultimate nucleotide

ND Non-defective

ND1 NADH-ubiquinone oxidoreductase chain 1

NDV Newcastle disease virus

NF-kB Nuclear factor kappa-light-chain-enhancer of activated B cells

NK Natural killer cells
NLR NOD-like receptors

NLRP3 NACHT, LRR and PYD domains-containing protein 3

NLS Nuclear localization sequence

NOD Nucleotide-binding domain

ns-NSV (-)ssRNA virus with non-segmented genome

NS1 Non-structural protein 1

NSV (-)ssRNA virus nt Nucleotide

OAS Oligoadenylate synthetase
ODN Oligodesoxyribolucleotide
OH-RNA RNA with a 5'hydroxyl group

PAGE Polyacrylamide gel electrophoresis
PAMP Pathogen-associated molecular pattern
PBMC Peripheral blood mononuclear cell

PBS Phosphate-buffered saline
PCR Polymerase chain reaction
Pen/Strep Penicillin/Streptomycin
PFU Plaque forming units
PKR Protein kinase R

PNPase Polynucleotide phosphorylase polyl:C Polyinosinic:polycytidylic acid

PP Polyphosphatase

PRR Pattern recognition receptors

qPCR Quantitative PCR

rcf Relative centrifugal force
RIG-I Retinoic acid-inducible gene I

RLR RIG-I-like receptors
RNA Ribonucleic acid
RNA Pol RNA polymerase
RNase Ribonuclease

ROS Reactive oxygen species rpm Revolutions per minute

rRNA Ribosomal RNA

RSV Respiratory syncytial virus

RT Room temperature

s-NSV (-)ssRNA virus with segmented genome

SAP Saponin

SDS Sodium dodecyl sulfate

SeV Sendai virus SINV Sindbis virus

siRNA Small interfering RNA

SLE Systemic lupus erythematosus SMS Singleton-Merten syndrome SNP Single-nucleotide polymorphis SPR Surface Plasmon Resonance

ssRNA Single-stranded RNA SSU Small ribosomal subunit

STAT Signal transducer and activator of transcription

TAE Tris-acetic acid-EDTA

TB Terrific broth
TBE Tris-Borat-EDTA

TBK-1 TANK- binding kinase 1
TBS Tris-buffered saline
TE Terminator Exonuclease
TEMED Tetramethylethylenediamine

THOV Thogoto virus

TLR Toll-like receptors (TLRs)

Tris Tris(hydroxymethyl)aminomethane

tRNA Transfer RNA UV Ultraviolet

v/v Volume by volume VACV Vaccinia virus

VpG Viral protein genome-linked VSV Vesicular stomatitis Indiana virus

w/v Weight by volume WNV West Nile virus

XRN1 5'-3'-exoribonuclease 1

YFV Yellow fever virus

9. Acknowledgments

Allen voran bedanke ich mich bei Herrn Prof. Martin Schlee für die finanzielle und strukturelle Förderung, sowie die Begutachtung meiner Arbeit. Viel wichtiger und dankbarer bin ich jedoch für seine hervorragende wissenschaftliche Betreuung, den scheinbar unbegrenzten neuen Ideen und Vorschlägen, seinem Optimismus und den ermutigenden Worten, wenn sie nötig waren. All das hat das Gelingen dieser Arbeit überhaupt erst möglich gemacht. Vielen Dank.

Aufrichtig bedanken möchte ich mich auch bei den weiteren Mitgliedern der Prüfungskommission, Herrn Prof. Sven Burgdorf, Herrn Prof. Matthias Geyer und Herrn Prof. Jochen Dingfelder, die für die Begutachtung dieser Arbeit einen Teil ihrer wertvollen Zeit aufgewendet haben.

Ein weiterer Dank gilt Herrn Prof. Gunther Hartmann für die Möglichkeit in seinem Institut in so einem exzellenten wissenschaftlichen Umfeld zu arbeiten.

Teile dieser Arbeit wären ohne die Zusammenarbeit mit anderen Wissenschaftlern nicht möglich gewesen. Dr. Janos Ludwig möchte ich für seine brillianten Ideen und die unermüdliche Versorgung mit RNAs danken. Ohne Dr. Beate Kümmerer und Janett Wieseler wäre es nicht möglich gewesen das Cap1-Projekt zu einem erfolgreichen Ende zu führen. Prof. Matthias Geyer und den Mitgliedern seiner Arbeitsgruppe, Dr. David Fußhöller, Dr. Kanchan Anand und Dr. Karl Gatterdam, möchte ich für die Zusammenarbeit danken. Die Diskussionen, Vorschläge und die Versorgung mit Protein haben die Projekte entscheidend voran gebracht.

Für die Zusammenarbeit und helfenden Hände möchte ich mich bei allen Mitgliedern des Instituts für Klinische Chemie und Klinische Pharmakologie bedanken. Allen voran den ehemaligen und derzeitigen Mitgliedern der Arbeitsgruppe Schlee. Danke für die Unterstützung, die gute Arbeitsatmosphäre und, dass man sich immer darauf verlassen kann Hilfe zu bekommen. Ein großer Dank gilt Agathe Grünewald, die mich in der Endphase der Doktorarbeit entscheidend unterstützt hat. Bedanken möchte ich mich bei Steven Wolter, der mich seit Anfang meiner Doktorarbeit begleitet, für seine Ideen und seine Hilfe im Labor, aber besonders für alles andere wie die kulturelle Bereicherung (1. Semester). Vielen Dank an Heike Prange dafür das Labor am Laufen zu halten, die immer freundlichen Worte und das offene Ohr. Bei den Kletterern, Doppelkopf-Spielern und allen, die für lustige Stunden im und außerhalb des Labors beigetragen haben, bedanke ich mich herzlich.

Meinen Freunden und Freundinnen möchte ich für den unersetzlichen Ausgleich vom intensiven Laboralltag und die ermutigenden Worte danken. Meiner Familie und besonders meinen Eltern, auf deren Unterstützung ich mich nicht nur während dieser Arbeit sondern während meines ganzen Lebens verlassen konnte, bin ich zutiefst dankbar. Wouter, vielen Dank für deine Hilfe, die Geduld, die aufbauenden Worte, deine Liebe. Danke, dass du immer da bist.